REPUBLIQUE DU CAMEROUN
Paix – Travail – Patrie
****
UNIVERSITE DE YAOUNDE I
FACULTE DES SCIENCES
DEPARTEMENT DE PHYSIQUE
****

REPUBLIC OF CAMEROUN
Peace – Work – Fatherland
****
UNIVERSITY OF YAOUNDE I
FACULTY OF SCIENCE
DEPARTMENT OF PHYSICS
****

ROGUE WAVES IN NONLINEAR SYSTEMS: A CASE STUDY OF BAROTROPIC RELAXING MEDIA

DISSERTATION
Submitted and defended publicly in partial fulfillment of the requirements for the Degree of Doctor/Ph.D.

Par : **MUKAM TAKOUGOUM Serge Paulin**

Sous la direction de
KUETCHE KAMGANG Victor
Associate Professor
University of Yaoundé 1
BOUETOU BOUETOU Thomas
Professor
University of Yaoundé 1

Année Académique : 2020

Rogue waves in nonlinear systems: A case study of barothropic relaxing media

Presented by

Serge Paulin MUKAM TAKOUGOUM

Department of Physics, Faculty of Sciences,

University of Yaounde I, P.O. Box 812, Cameroon

Submitted in Partial Fulfillment of the Requirements

for the Degree of Doctor of Philosophy

at the university of Yaoundé I

May 31, 2020

Dedication

To our almighty God and my whole family.

Acknowledgments

I would like to thank my supervisor Pr Thomas Bouetou Bouetou, Head of Department of computer engineering at the national advanced school of engineering for his constant suggestions.

Thanks to Dr Victor Kuetche Kamgang lecturer of physics at the National Advanced School of Engineering, for his guidance during the achievement of this thesis.

I would like to thank all the members of jury who have accepted to evaluate this work. Besides, I am very grateful to all my teachers from the Master level of Physics, for their effort and determination to carry out competitive students with good background.

Then, I am very thankful to Dr Souleymanou Abbagari, for his help throughout this dissertation.

I am also thankful to the National Advanced School of Engineering (ENSP) for providing me suitable place to prepare this thesis during the last five years.

I am very thankful to the International Center for Theoretical Physics (ICTP) in Italy, for the invitation to the Hands-on research on physics of complex systems 2016. During my stay at the center they gave full access to the library in which I got useful documents for my thesis.

I am thankful to the Institute of Mathematics and Physical Sciences (IMSP) in Benin, for the invitation to the GIRAGA XVI seminar, on 17-22 december 2017.

Thanks to the journals which have accepted to publish my projects.

I would not forget to thank my senior Dr OUANDJI Hermann and my classmates Dr Tchokouansi Hermann, Dr Youssoufa saliou, Dr Francis Nguepjouo and Mr Robert Tamwo for their permanent advices, encouragements and help.

Thanks for others whose names are not here but have been helpful.

Contents

List of Figures

Abstract

Throughout this thesis, we study the dynamics of rogue waves in optical fibers, Bose-Eistein condensates and Plasmas. Since the existence of such waves are proved in these fields, we show that the intrinsic parameters related to these fields namely the nonlinearity and the dispersion, can modify the profiles of these waves during their dynamics. Since the construction of higher-order rogue wave solutions is a great challenge nowadays, we were devoted to construct higher-order rogue wave solutions to the above mentioned fields. We have also shown that rogue like-waves can interact elastically with soliton like-waves in optical fiber. We have also shown the existence of rogue waves in ferrites and barotropic relaxing media. The mathematical tools that we have used throughout this thesis are the generalized Darboux transformation and the homoclinic test approach.

Keywords: Rogue waves; Soliton like-waves; Darboux transformation; Homoclinic approach; Barothropic relaxing media.

Résumé

Tout au long de ce travail, nous étudions la dynamique des ondes célérates dans les milieux physiques tels que la fibre optique, les condensats de Bose-Einstein et les plasmas. La présence de ce type d'onde étant déjà démontrée dans ces milieux, nous démontrons que certains paramètres intrinsèques à ces systèmes tels que la nonlinearité et la dispersion peuvent modifier le profile de ces ondes pendant leur dynamique. La construction des solutions type onde célérate aux ordres supérieurs étant un grand challenge de nos jours, nous nous sommes aussi focalisés sur la construction des solutions type onde célérate jusqu'aux ordres supérieurs dans les systèmes mentionnés ci dessus. Nous avons montré que les ondes célérates peuvent interagir avec les ondes type soliton de façon élastique. Nous avons aussi tout au long de cette thèse montré l'existence des ondes type célérate dans les ferrites et les milieux barotropiques. les méthodes mathématiques utilisées dans nos travaux sont la transformation de Darboux généralisée et la méthode dite homoclinique.

Mots clés: Onde célérate ; Onde type soliton; Transformation de Darboux ; Méthode homoclinique; Système barothropique.

General introduction

Rogue waves are stands for open water phenomenon, in which winds, currents, non-linear phenomena such as solitons, and other circumstances cause a wave to briefly form that is far larger than the "average" large occurring wave of that time and place. The basic underlying physics that makes phenomena such as rogue waves possible is that different waves can travel at different speeds, and so they can "pile up" in certain circumstances. However other situations can also give rise to rogue waves, particularly situations where non-linear effects or instability effects can cause energy to move between waves and be concentrated in one or very few extremely large waves before returning to "normal" conditions.

A rogue wave is a natural ocean phenomenon that is not caused by land movement, only lasts briefly, occurs in a limited location, and most often happens far out at sea. Rogue waves are considered rare but potentially very dangerous, since they can involve the spontaneous formation of massive waves far beyond the usual expectations of ship designers, and can overwhelm the usual capabilities of ocean-going vessels which are not designed for such encounters. Rogue waves are therefore distinct from tsunamis. Tsunamis are caused by massive displacement of water, often resulting from sudden movement of the ocean floor, after which they propagate at high speed over a wide area. They are nearly unnoticeable in deep water and only become dangerous as they approach the shoreline and the ocean floor becomes shallower; therefore tsunamis do not present a threat to shipping at sea (the only ships lost in the 2004 Asian tsunami were in port). They are also distinct from mega-tsunamis, which are single massive waves caused by sudden impact, such as meteor impact or landslides within enclosed or limited bodies of water. In 1826, French scientist and naval officer Captain Jules Dumont d'Urville reported waves as high as 33 meters (108.3 ft) in the Indian Ocean with three colleagues as witnesses, yet he was

publicly ridiculed by fellow scientist François Arago. In that era it was widely held that no wave could exceed 30 feet (9.1 m) [125, 126]. Author Susan Casey wrote that much of that disbelief came because there were very few people who had seen a rogue wave, and until the advent of steel double-hulled ships of the 20th century "people who encountered 100-foot rogue waves generally weren't coming back to tell people about it" [127]. For almost 100 years, oceanographers, meteorologists, engineers and ship designers have used a mathematical system commonly called the Gaussian function (or Gaussian Sea or standard linear model) to predict wave height [128]. This model assumes that waves vary in a regular way around the average (so-called 'significant') wave height. In a storm sea with a significant wave height of 12 metres (39.4 ft), the model suggests there will hardly ever be a wave higher than 15 metres (49.2 ft). One of 30 metres (98.4 ft) could indeed happen but only once in ten thousand years (of wave height of 12 metres [39.4 ft]). This basic assumption was well accepted (and acknowledged to be an approximation). The use of a Gaussian form to model waves has been the sole basis of virtually every text on that topic for the past 100 years [128, 129]. The first known scientific article on "Freak waves" was written by Professor Laurence Draper in 1964. In that paper which has been described as a 'seminal article' he documented the efforts of the National Institute of Oceanography in the early 1960s to record wave height and the highest wave recorded at that time which was about 67 feet (20.4 m). Draper also described freak wave holes [130–132].

Statoil researchers presented a paper in 2000 which collated evidence that freak waves were not the rare realizations of a typical or slightly non-gaussian sea surface population (Classical extreme waves) but rather they were the typical realizations of a rare and strongly non-gaussian sea surface population of waves (Freak extreme waves). A workshop of leading researchers in the world attended the first Rogue Waves 2000 workshop held in Brest in November 2000. In 2000 the British oceanographic vessel discovery recorded a 29-metre (95 ft) wave off the coast of Scotland near Rockall. This was a scientific research vessel and was fitted with high quality instruments. The subsequent analysis determined that under severe gale force conditions with wind speeds averaging 21 metres per second (68.9 ft/s) a ship-borne wave recorder measured individual waves up to 29.1 metres (95.5 ft) from crest to trough, and a maximum significant wave height of 18.5 metres (60.7 ft). These were some of the largest waves recorded by scientific instruments up to that

time. The authors noted that modern wave prediction models are "known" to significantly under-predict extreme sea states for waves with a 'significant' height (Hs) above 12 metres (39.4 ft). The analysis of this event took a number of years, and noted that "none of the state-of-the-art weather forecasts and wave models-the information upon which all ships, oil rigs, fisheries, and passenger boats rely-had predicted these behemoths." Put simply, a scientific model (and also ship design method) to describe the waves encountered did not exist. This finding was widely reported in the press which reported that "according to all of the theoretical models at the time under this particular set of weather conditions waves of this size should not have existed".

It is now proven via satellite radar studies that waves with crest to trough heights of 20 meters (65.6 ft) to 30 meters (98.4 ft), occur far more frequently than previously thought. It is now known that rogue waves occur in all of the world's oceans many times each day. In 2004 the ESA MaxWave project identified more than ten individual giant waves above 25 meters (82 ft) in height during a short survey period of three weeks in a limited area of the South Atlantic. The ESA's ERS satellites have helped to establish the widespread existence of these 'rogue' waves. Thus acknowledgement of the existence of rogue waves (despite the fact that they cannot plausibly be explained by even state-of-the-art wave statistics) is a very modern scientific paradigm. It is now well accepted that rogue waves are a common phenomenon. Professor Akhmediev of the Australian National University, one of the world's leading researchers in this field, has stated that there are about 10 rogue waves in the world's oceans at any moment. Some researchers have speculated that approximately three of every 10,000 waves on the oceans achieve rogue status, yet in certain spots-like coastal inlets and river mouths-these extreme waves can make up three out of every 1,000 waves because wave energy can be focused. Rogue waves may also occur in lakes. A phenomenon known as the "Three Sisters" is said to occur in Lake Superior when a series of three large waves forms. The second wave hits the ship's deck before the first wave clears. The third incoming wave adds to the two accumulated backwashes and suddenly overloads the ship deck with tons of water. The phenomenon was implicated in the sinking of the SS Edmund Fitzgerald on Lake Superior in November 1975.

Because the phenomenon of rogue waves is still a matter of active research, it is

premature to state clearly what the most common causes are or whether they vary from place to place. The areas of highest predictable risk appear to be where a strong current runs counter to the primary direction of travel of the waves; the area near Cape Agulhas off the southern tip of Africa is one such area; the warm Agulhas Current runs to the southwest, while the dominant winds are westerlies. However, since this thesis does not explain the existence of all waves that have been detected, several different mechanisms are likely, with localized variation. Suggested mechanisms for freak waves include the following:

- Diffractive focusing: According to this hypothesis, coast shape or seabed shape directs several small waves to meet in phase. Their crest heights combine to create a freak wave [133].

- Focusing by currents: Waves from one current are driven into an opposing current. This results in shortening of wavelength, causing shoaling (i.e., increase in wave height), and oncoming wave trains to compress together into a rogue wave [133] . This happens off the South African coast, where the Agulhas Current is countered by westerlies [134].

- Nonlinear effects (modulational instability): It seems possible to have a rogue wave occur by natural, nonlinear processes from a random background of smaller waves [135]. In such a case, it is hypothesized, an unusual, unstable wave type may form which 'sucks' energy from other waves, growing to a near-vertical monster itself, before becoming too unstable and collapsing shortly after. One simple model for this is a wave equation known as the nonlinear Schrödinger equation (NLS), in which a normal and perfectly accountable (by the standard linear model) wave begins to 'soak' energy from the waves immediately fore and aft, reducing them to minor ripples compared to other waves. The NLS can be used in deep water conditions. In shallow water, waves are described by the Korteweg-de Vries equation or the Boussinesq equation. These equations also have non-linear contributions and show solitary-wave solutions. A small-scale rogue wave consistent with the nonlinear Schrödinger equation (the Peregrine Solution) was produced in a laboratory water tank in 2011 [136]. In particular, the study of solitons, and especially Peregrine

solitons, have supported the idea that non-linear effects could arise in bodies of water [137].

- Wind wave interactions: While it is unlikely that wind alone can generate a rogue wave, its effect combined with other mechanisms may provide a fuller explanation of freak wave phenomena. As wind blows over the ocean, energy is transferred to the sea surface. When strong winds from a storm happen to blow in the opposing direction of the ocean current the forces might be strong enough to randomly generate rogue waves. Theories of instability mechanisms for the generation and growth of wind waves-although not on the causes of rogue waves-are provided by Phillips [138] and Miles [139].

The possibility of the artificial stimulation of rogue wave phenomena has attracted research funding from DARPA, an agency of the United States Department of Defense. Bahram Jalali and other researchers at UCLA studied microstructured optical fibers near the threshold of soliton supercontinuum generation and observed rogue wave phenomena. After modeling the effect, the researchers announced that they had successfully characterized the proper initial conditions for generating rogue waves in any medium [140]. Additional works carried out in optics have pointed out the role played by a nonlinear structure called Peregrine soliton that may explain those waves that appear and disappear without leaving a trace [141, 142].

The loss of the MS München in 1978 provided some of the first physical evidence of the existence of rogue waves. The MS München was a state-of-the-art cargo ship with multiple water-tight compartments, an expert crew and was considered unsinkable. She was lost with all crew and the wreck has never been found. The only evidence found was the starboard lifeboat which was recovered from floating wreckage some time later. The lifeboats hung from forward and aft blocks 20 metres (65.6 ft) above the waterline. The pins had been bent back from forward to aft, indicating the lifeboat hanging below it had been struck by a wave that had run from fore to aft of the ship which had torn the lifeboat from the ship. To exert such force the wave must have been considerably higher than 20 metres (65.6 ft). At the time of the inquiry, the existence of rogue waves was considered so statistically unlikely as to be near impossible. Consequently, the Maritime Court in-

vestigation concluded that the severe weather had somehow created an 'unusual event' that had led to the sinking of the München [143]. The 1980 loss of the MV Derbyshire during Typhoon Orchid south of Japan with the loss of all crew marked a turning point for ship design. The Derbyshire was an ore-bulk-oil combination carrier built in 1976. At 91,655 gross register tons, she was-and remains-the largest British ship ever to have been lost at sea. The wreck was found in June 1994. The survey team deployed a remotely operated vehicle to photograph the wreck. A private report was published in 1998 which prompted the British government to reopen a formal investigation into the sinking. The British government investigation included a comprehensive survey by the Woods Hole Oceanographic Institution which took 135,774 pictures of the wreck during two surveys. The formal forensic investigation concluded that the ship sank because of structural failure and absolved the crew of any responsibility. Most notably, the report determined the detailed sequence of events that led to the structural failure of the vessel. A third comprehensive analysis was subsequently done by Douglas Faulkner, professor of marine architecture and ocean engineering at the University of Glasgow. His highly analytical and scientific report published in 2001 examined and linked the loss of the MV Derbyshire with what he called the emerging body of scientific evidence regarding the mechanics of freak waves. Professor Faulkner concluded that it was almost certain that Derbyshire would have encountered a wave of sufficient size to destroy her. Faulkner's conclusions have not been refuted in the more than 15 years since they were first presented (as of 2016). Indeed, subsequent analysis by others has corroborated his findings. Faulkner's finding that the Derbyshire was lost because of a rogue wave has had widespread implications on ship design [143]. Faulkner has subsequently proposed the need for a paradigm shift in thinking for the design of ships and offshore installations to include what he calls a Survival Design approach additional to current design requirements. There is however no evidence that his recommendations have yet been adopted (as of 2016) [144,145]. Very few ship-wrecks have ever been fully investigated. The most recent bulk-carrier loss on the open seas to have been subjected to thorough investigation (as at March 2011) was the UK-owned M.V. Derbyshire, which sank in 1980. Its entire crew of forty-four, all British citizens perished. It took 14 years of pressure from the British public and a privately funded expedition to locate the wreck before a formal remote-camera search and inves-

tigation was done by the British government. At least a couple of hundred bulk carriers have been lost since 1980 and none have been properly investigated. A survey of 125 bulk carriers that sank between 1963 and 1996 found that seventy-six probably flooded, another four because of hatch-cover failure, the rest from unidentified causes. Nine other vessels broke completely in two. Causes of the remaining forty losses are unknown [146].

As pointed out by many researchers, rogue waves can appear in the ocean and in optical fibers due to modulation instability (MI) [67]. The latter is widely known as the Benjamin-Feir [36] or Bespalov-Talanov [147] instability. Specifically, a periodic perturbation on the top of a continuous wave exponentially increases its amplitude due to the above instability. Waves in a continuous but limited frequency range are involved in this dynamics. Modulation instability is known for a number of nonlinear equations, with the most important one being the nonlinear Schrödinger equation. (NLSE). For each frequency, the long term dynamics of MI is closely related to the so called Fermi-Pasta-Ulam recurrence [148]. Namely, during the initial stages of the development, each particular frequency mode in a modulation instability phenomenon receives its energy from the central mode, along with the higher harmonics and then returns all the energy back to the central mode [149]. For the particular case of the NLSE, this process can be described by an exact solution that has been referred to as the "Akhmediev Breather" (AB) in a number of earlier works on ocean waves [150]. This solution describes the appearance of a periodic sequence of maxima on the top of a continuous wave and their subsequent disappearance on further evolution [151]. A particular case of modulation instability is the one with a zero frequency (or infinite period) sideband. In this case, the periodic sequence of maxima is reduced to just a single peak which "appears from nowhere and disappears without a trace" [28]. The latter is also described by an exact solution of the NLSE, which has a simple rational representation. The lowest-order solution of this class is known as the Peregrine soliton [54] and can be obtained as a limiting case of an AB with zero frequency of modulation [152]. There is a hierarchy of rational solutions with progressively increasing amplitude [153]. Each of them can be thought of as a rogue wave. Moreover, the high amplitude waves described by the higher-order rational solutions appear naturally in the chaotic wave field as a nonlinear superposition of two or more ABs initiated by modulation instability with nonzero frequency sidebands [154]. Thus, it is

essential to know the structure of rational solutions in order to understand rogue waves in general.

Rational solutions of the nonlinear Schrödinger equation play a major role in the theory of rogue waves [28]. There is a hierarchy of them with progressively increasing central amplitude. The major reason supporting the claim that rational solutions are important in the composition of ocean waves is that, as with waves created by modulation instability, they "appear from nowhere". In other words, the instability induced from a small perturbation on top of a plane wave leads to an increase in the perturbation up to its highest amplitude and then to a decay so that it finally "disappears without a trace". Although for rational solutions the growth rate of the instability is zero, they still develop according to a power law. This may appear to take a very long time, but on the other hand, the ocean is vast and there is enough space for the development of even such slow instabilities. Rational solutions are limiting cases [156] of either periodic "Ma solitons" (MS) [157] or "Akhmediev breathers" (ABs) [151]. MSs have to be created directly from initial conditions consisting of the background plane wave+soliton. In other words, Ma solitons must exist in the wave field right from the very beginning. Only rational solutions and ABs belong to the class of excitations that appear from nowhere [156]. ABs, in particular, arise during evolution due to modulation instability [147]. Once they have appeared, they may collide just as can happen with solitons. Collisions of two or more ABs with transversal frequencies close to zero may create structures similar to higher-order rational solutions [158]. Thus, studies of rational solutions of higher order are of fundamental importance. They may resolve the mystery of rogue waves in the ocean and help in creating useful rogue waves in optical fibers [29].

Recent analysis have shown that the first order effects of dispersion and dissipation in a vast range of physical systems can be described by a few simple nonlinear equations of evolution, such as Burgers equation, sine-Gordon equation, Korteweg-de Vries equation amongst others [1]. And, in such case, these equations have been found to possess stable steady-state solutions with remarkable properties. Hence, it has been seen that the study of nonlinear evolution equations has attracted many mathematicians and theoretical physicists due to its considerable applications in various branches of science [2–7]. As application, it bas been shown that nonlinear integrable evolution equations give rise to

many kind of wave such as soliton, breather, rogue wave and so on [8–13].

A particular kind is the soliton wave. In physics and mathematics, a soliton is a self-reinforcing wave packet, that maintains its shape and its velocity during the propagation. It is a result of cancellation between the nonlinearity and the dispersive effect. solitons are solutions to a widespread class of weakly partial differential equations describing physical systems [14–18]. Soliton seems to be more accurate in the transport of information in nonlinear media.

Another one is called rogue wave. Rogue waves are waves among naturally observed by people on the sea surface that represent an inseparable feature of the ocean. They appear from nowhere, cause danger and disappear without a trace. They occur on the surface of a relatively calm sea and reach very great amplitudes, but still be fatal for ships and crew due to their unexpectedness and abnormal features. Seamen are known to be unsurpassed authors of exciting and horrifying stories about the sea and sea waves. This could explain why, despite the increasing number of documented cases, that sailor's observation of "walls of water" have been considered fictitious for a while. Due to the amount of doubtless evidence of the existence of this mysterious phenomenon, these stories are now addressed again, but still without sufficient information to enable researchers and engineers interested by the phenomenon to completely understand it. The billows appear suddenly, by exceeding two times or more the size of the surrounding waves. This kind of wave have obtained many names such as abnormal, exceptional, extreme, giant, huge, sudden, episodic, freak, monster, killer wave etc. Serious study of the phenomenon have intensified during the recent decade theoretically and experimentally [19–28].

Considerable efforts have been paid in understanding the physics behind this mysterious and destructive event. So D. R. Solli and coworkers [29] studied successfully the rogue waves in optical fiber. They have introduced the concept of optical rogue waves. Using real-time detection technique, they studied a system that possesses extremely steep, large waves as rare outcomes from an almost identically prepared initial population of rogue waves. They modeled the generation of rogue waves using the generalized nonlinear Schrödinger equation and demonstrated that they arise infrequently from initially smooth pulses owing the power transfer seeded by a small noise perturbation.

Originally, the phenomenon of rogue waves refers to a giant ocean wave, responsible

of many marine disasters [30]. Many years after that, more effort have been devoted to the study and the understanding of this mysterious phenomenon in many fields such as hydrodynamics [19–22], plasma physics [87], optics [29,33] and Bose-Einstein condensates [85] just to name a few. From the study of the phenomenon, it resorts that rogue wave appears from nowhere and disappears without a trace [13]; their amplitude is two or three times larger than their surrounding waves [14]. The unpredictability of rogue waves implies that they can be expressed by rational functions localized both in space and time [13,15]. The simplest rogue wave solution was firstly obtained by Peregrin [54]; more after, Akhmediev and coworkers have calculated the first-order rogue wave solution for the nonlinear Schrödinger equation(NLSE) [28]. Analytical rogue wave solution has been also obtained for various physical models [95, 99–101, 104, 106]. The results obtained in these works remain insufficient to understand the phenomenon. Nowadays, the physics behind the rogue wave phenomenon in nonlinear systems remains unclear. If rogue waves exist in such systems and since they are known to be dangerous for mariners, what is their effect on the other existing waves? What is their behavior in a system with higher-order nonlinearity? Can this kind of wave also exist in other nonlinear systems as the known ones?

In view to generate rogue wave solutions to physical models, many mathematical tools have used such as similarity transformation [94], Darboux transformation (DT) [95] just to name a few. The traditional DT was developed in reference [92], but that one is not appropriated to construct higher-order rogue wave solution to nonlinear physical systems. So Guo and coworkers [94] have modified it to derive the generalized DT. This one is the tool used in this work to construct rogue wave solutions. The generalized DT is the essential used in this dissertation to derive rogue wave solution to many physical systems.

The goals of this dissertation are

- to study the behavior of rogue waves in nonlinear systems,
- to determine new rogue wave solutions in some fields,
- to calculate higher-order rogue wave solutions to some equations
- and to prove the existence of such in the barotropic relaxing media.

Then, the organization of this thesis is scheduled as follows:

- In chapter one, we present a literature review on rogue wave phenomenon in the nature, starting from their effects in the ocean. We present some testimonials of mariners according to the destruction of their equipments by such a mysterious like rogue wave. Some real awesome pictures are presented to illustrate their comments. We show that the rogue wave do not exist not only in the oceanic condition, but also in the physical systems such as the fiber optics, the Bose Einstein condensates and plasma. These demonstrations are based on the published works.

- The chapter two is devoted to the presentation of the major method of investigation used in this work to derive interesting rogue wave solution to nonlinear physical system, namely the generalized DT.

- In chapter three, we construct rogue wave solutions to some nonlinear physical systems such as the Manakov system, a nonlinear Schrödinger equation with fifth-order nonlinearity, a couple of equations modeling the nonlinear propagation of wave in ferrites, a generalized nonlinear Schrödinger equation possessing higher-order terms which refer to a femto-second pulse propagation in a nonlinear fiber optic. By the use of the traditional DT, we derived the localized waves solutions to a coupled nonlinear Schrödinger system with four wave mixing effects, self-phase modulation and cross-phase modulation effects, in this case we show that the rogue waves and the solitons can interact elastically. The particularity of this dissertation is the rogue wave in the barothropic relaxing media.

- The last section is devoted to the general conclusion in which we give some perspectives.

Chapter 1

Literature review on rogue waves

Introduction

There are many personal descriptions of unexpectedly high waves collected in the literature by now. Some of them will be discussed hereafter. The sudden formation of spectacular waves in the ocean is well reported and no longer doubted in the scientific community [30–36]. One possible mechanism explaining the formation of rogue waves characterized by strongly localized, is the modulation instability of weakly nonlinear monochromatic waves discovered in water wave [37], aside from the trivial linear superposition of waves. This instability can be modeled through the framework of the nonlinear Schrödinger equation [38, 39] which is an evolution equation that describe the dynamics in space and time of wave trains in water of finite and infinite depth [31]. Rogue waves are waves occasionally appearing in the ocean that can reach the amplitudes more than twice the value of those in the surrounding chaotic wave field. Above description can roughly be taken as the definition although variety of interpretations is still possible .Being considered initially for ocean waves, nowadays the concept is shifted to other fields of physics, that can be modeled by similar nonlinear wave equations. Once the equations describing the phenomenon are established, understanding the features of rogue waves comes through finding special solutions that have the properties of having high amplitudes and are localized in space and in time. From the experimental point of view it is much easier and safer to deal with rogue waves in a laboratory than in the open ocean.

Figure 1: Sinking of Wold Glory tanker in 1968.

In addition to oceanic ones, rogue waves can be observed in variety of physical systems: optical fibers [29] and Bose-Einstein condensates (BEC) [85] just to name a few . The latter system has the advantage that it admits variety of experimental conditions thus allowing for several types of rogue waves.

1.1 Historical review and testimonies about rogue wave behavior in deep or shallow water

Personalities make history human. Our story is created by accidents. The freak wave phenomenon could remain marine folklore if there were no crashes that shake people's minds. Notorious casualties attract attention to the existence of abnormally huge waves, and evidence makes us believe the reports. A long but obviously incomplete list of accidents starting from the time of Christopher Columbus has been collected in [40]. Many other descriptions are available in various publications [41–46]. The stories are sometimes

very similar, but frequently they show distinctive differences and may be useful for the comprehension of the phenomenon. We represent below some stories describing different kinds of rogue wave accidents. The most striking cases of rogue waves correspond to **strongly localized high waves**.

This is the beginning of the history of the tanker "World Glory," announced by a newspaper in 1954 [47]. Its end is not so enthusiastic. On June 13, 1968, traveling along the South African coast under the Liberian flag, World Glory encountered a freak wave, which broke the tanker into two pieces and led to the death of 22 crew members [48] Figure 1. It happened in the Indian Ocean, 105 km east of Durban. As a result, about 14 million gallons of oil spilt into the Ocean.

The tanker Prestige (42,000 gross tons, and about 250 m in length) went down similarly off the Spanish coast in 2002 Figure 34. Estimations of the amount of spilt oil are different, but they are roughly about 20 million gallons. Some people connected with the accident think that the damage that led to its sinking might have been caused by a freak wave. Anyway, it is more or less obvious that the hull was unable to bear the wave force. The Prestige was built more than 20 years after World Glory. The vessel met all American Bureau of Shipping Rule structural requirements and International Association of Classification Societies Rule hull girder strength requirements. The vessel was properly loaded and had adequate hull strength for the reported conditions at the time of the casualty [49]. The number of accidents that occurred with wavelengths less than half the ship's length is small [50], so we could suppose that the damage in both cases was probably caused by intense long waves causing unexpected nonuniform loads on the hulls.

The cruise liner Queen Elizabeth II encountered a rogue wave in the North Atlantic about 30 m height during a storm in 1995. The ship master referred to a particular episode where they had been looking at a **wall of water** from the bridge for a couple of minutes before it hit the ship well above the waterline: "*a great wall of water - it looked as if we were going into the White Cliffs of Dover.*" A similar description was given by one of the crew members of the Statoil floating rig Veslefrikk B (it was hit the same year by a wave that resulted in significant damage) [43]. The first mate of the oil tanker Esso Languedoc described the wall of water in the photo in Figure 3: "*We were in a storm and*

Figure 2: Sinking of tanker prestige in 2002.

the tanker was running before the sea. This amazing wave came from the aft and broke over the deck. I didn't see it until it was alongside the vessel but it was special, much bigger than the others." [44].

Freak events represented by several successive very high waves in wave groups are also well known. A collision of the naval ship Jeanne d'Arc with the Glorious Three in 1963 was described in Ref. [51].

"At about 09:47 a group of large breaking waves was sighted straight ahead, just beyond an area of relative calm water (4-5 m wave height). The first wave heaved the ship; its height was estimated about 15 m. During the interval of about 100 meters in-between the first and the second wave the "Jeanne d'Arc" had time to return approximately to its waterline, but she was soon heeled over to starboard by the second wave, until the heel angle reached about 35^0*. During clearance of those two waves, the freeboard deck and the quarterdeck were submerged in turn, the sea covered the catwalks of the first deck, water reaching the top of the bulkheads at the time of maximum heel. The third wave was cleared in similar conditions, but with not as large amplitude motions, its height being slightly less than that of the two first ones."*

Figure 3: Picture taken on the oil freighter Esso Languedoc outside the coast of Durban, South Africa 1980.

Two unexpectedly large successive waves shattered windows 28 m above the waterline of the cruise liner Queen Elizabeth in 1943; two other waves capsized the trawler Kotuku in 2006; and three large waves hit and threw the fishing boat Starrigavan onto a jetty in 2007 [44]. In the past, seamen of different nationalities mention monstrous wave groups. It is interesting to note that the number of individual waves that supposedly forms a rogue wave packet is different: three sisters or the ninth billow. Surfers sometimes wait for the largest, or seventh, wave. In Ref. [52] it is noted that successive large single-wave crests or deep troughs can cause severe damage due to their impact, or may excite the resonant frequencies of the structures. The Soviet refrigerator tanker Taganrogsky Zaliv was subjected to an abnormal wave, **a hole in the sea**, in 1985 (see Figure 4 Figure 5) and [48].

"Wave height did not exceed 5 m and the length was 40-45 m. The speed of the ship was diminished to a minimum in order to make a safer control of the ship's movement. The ship rode well on the waves. The fore and main deck were not flooded with water. At one o'clock the front part of the ship suddenly dipped, and the crest of a very large wave

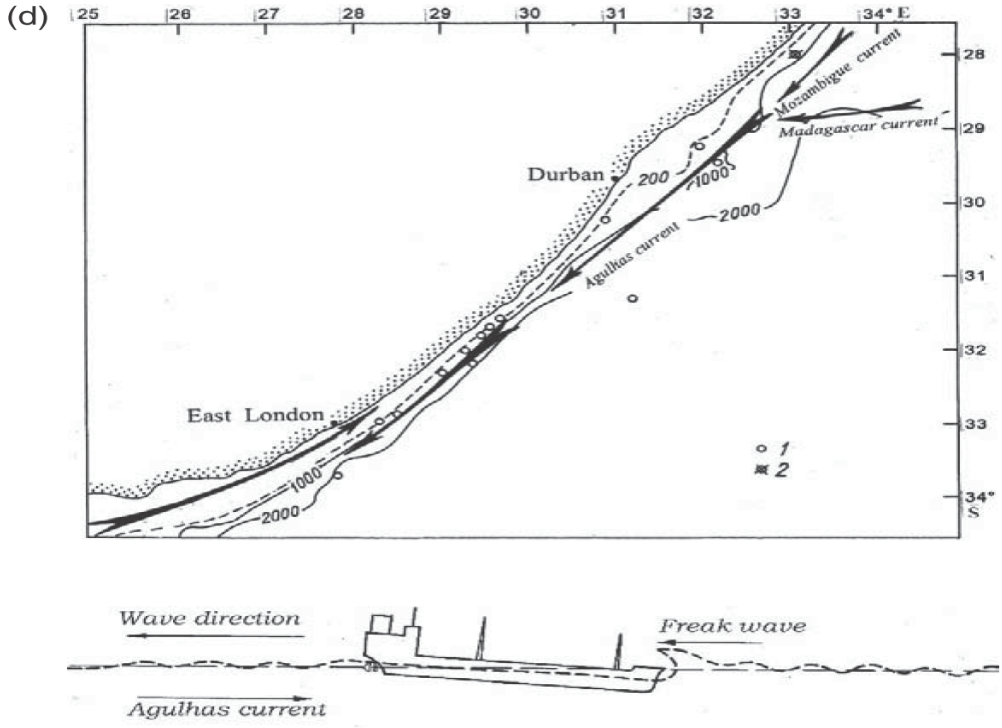

Figure 4: The map of the incidents off the Southeast coast of Africa and the scheme of the collision of tanker Taganrogsky Zaliv with a rogue wave [48].

appeared close to the foredeck. It was 5-6 m higher over the foredeck. The wave crest fell down on the ship. One of the seamen was killed and washed overboard. Nobody was able to foresee the appearance of such a wave. When the ship went down, riding on the wave, and its frontal part was stuck into water, nobody felt the wave's impact. The wave easily rolled over the foredeck, covering it with more than two meters of water. The length of the wave crest was not more than 20 m".

Very similar descriptions are related to accidents with the cruiser Birmingham in 1944 and some other vessels [43] They report sighting a long trough followed by a steep crest, or a "hole" in the sea. There is a viewpoint that a "hole" in the sea is more dangerous for a boat than a crest, since it is less noticeable among the sea waves than huge crests, and the shipmaster cannot change course and prepare the ship in advance. The NOAA's 56-foot research vessel Ballena capsized in an **individual rogue wave** south of Point Arguello, California in 2000. The weather was good, with clear skies and glassy swells (1.5-2 m). At approximately 11:30, the crew observed a 4.5 m swell beginning to break about 30 m from the vessel. The wave crested and broke above the vessel, caught the

Figure 5: A "diving" into a boat. The case looks similar to the descriptions of the accident with the Taganrogsky Zaliv [53].

Ballena broadside, and quickly overturned it [46].

Russian kayakers were lucky to observe and make photos of strange waves 25 km from Cape Olga, Kronotsky Peninsula, about 1-1.5 km offshore Figure 6. They reported that the weather was calm with only very long gently sloping surge waves coming from the open ocean every 15-20 s. About 10 strange waves were observed in the same area with irregular lengths. Freak waves arose, propagated, and collapsed during tens of seconds and ran for about 50 m within this time. Wave heights were about 2-4 m, and typically their length along the front was about 70 m. The first photo in Figure 6 is quite challenging, although the second one (taken from another aspect) looks more ordinary.

These descriptions are in some sense similar to the first kind of observations (i.e., strongly localized high waves), but the reports emphasize individual waves that propagate for some distance and are actually not surrounded by other considerable waves.

Extreme **coastal wave phenomena** similar to the ocean rogue waves have been noted recently. Typically, such accidents are described as a sudden brief coastal flooding or as huge waves rushing coastal structures (raised embankment or breakwaters). These waves

Figure 6: Waves observed in 2006 near Kamchatka [53]

have not been related with tsunamis; although it is more difficult to ascertain whether they are not caused by storm surges.

A very high (25 m) wave splash presented in Figure 7 occurred suddenly and was absolutely unexpected by the students (who made the photos) after they had spent about 45 min observing swell waves that followed a severe storm that had happened one day before.

It was already pointed out that wave height, in addition to its shape and surrounding waves may define the strength of wave impact. Unusual wavelength or small crest length(like in Figure 8) may lead to an inadmissible load distribution that may damage the hull. The most striking examples of rogue waves in the recent literature are unusually asymmetrical with high crests compared to the depth of their troughs. Presumably enormous huge-wave impacts have been already registered [54]. Ships usually travel perpendicular to the crests with low forward speed. A particular traveling direction of a wave group results in complicated wave motion that makes the ship list and makes it difficult to safely overpass the waves. Steep waves (like in Figure 9) may yield dangerous dynamic effects due to ship motion (slamming), even though the significant wave height is

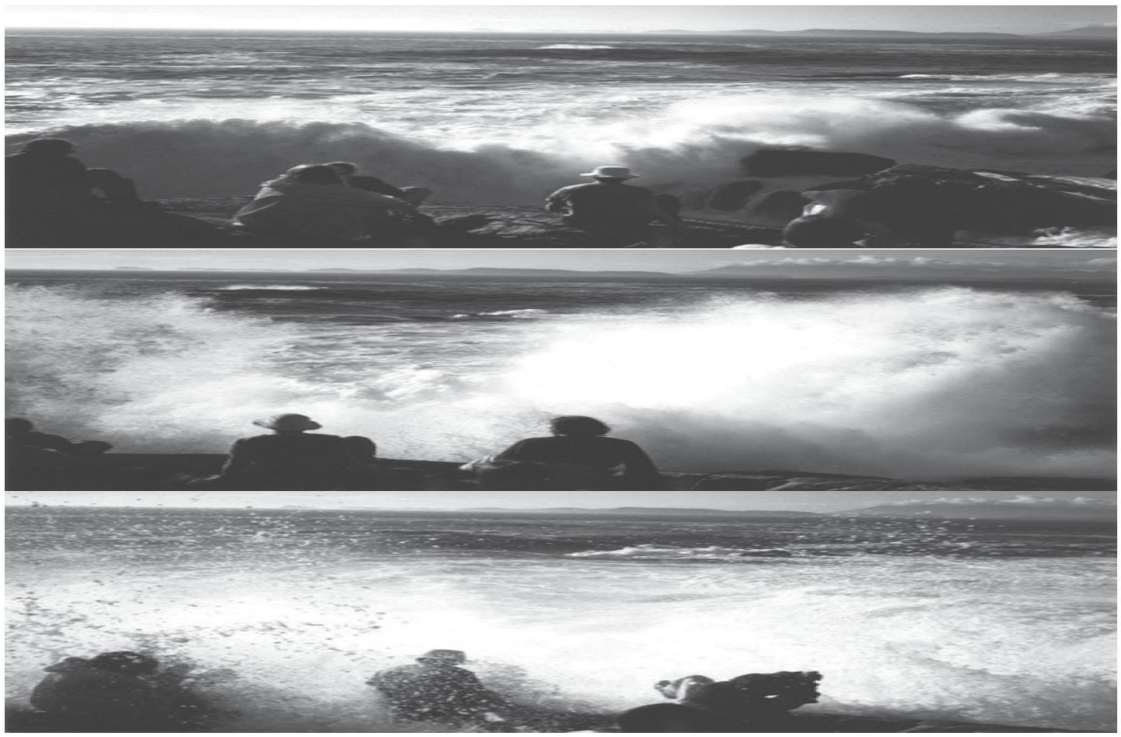

Figure 7: A 2-s photo image sequence taken on the Dianna Island (Canada) [55].

not particularly large. A breaking rogue wave could potentially cause more damage than a nonbreaking wave of the same dimension. These points should be taken into account when studying the wave impact and designing a safe construction.

Due to the relatively large number of registered collisions of ships with abnormal waves, a statistical analysis of the events was performed by Toffoli et al. [50] on the basis of 270 documented accidents selected among a total of 650 that occurred over about four years and collected by the Lloyd's Marine Information Service. Toffoli et al. [50] emphasized that accidents occurred often in the presence of crossing seas: wind waves and swell. They claim that any significant correlation between the main surface wave parameters and ship weight were not found, although more than 90 percent of the incidents occurred in water depths of more than 50 m. It is suggested that different kinds of ships should be subjected to different freak-wave warning criteria. The current state of affairs, however, is obviously not acceptable. Casualties happen too frequently and are too dramatic. Hundreds of vessels sink and hundreds of people perish annually see Figure 10, although the situation has taken a turn for the better over the last few years. The list of accidents related to the attacks of huge waves contains many recent dates. Twenty-two (22) super carriers were

Figure 8: Pyramidal wave off south Japan

lost or severely damaged between 1969 and 1994 due to the occurrence of sudden rogue waves; a total of 542 lives were lost as a result [44]. About 650 incidents are counted during the period from 1995 to 1999 due to bad weather, including total losses of all propelled sea-going merchant ships in the world weighing 100 gross tons or more see Figure 11.

We now go further will presenting significant results obtained for rogue waves in physical systems

1.2 Physical results obtained

It has been shown that rogue waves appear not only in oceanic condition, but also in nonlinear physical systems. In the following, we present results obtained in nonlinear physical systems as nonlinear fiber optics, Bose-Einstein condensates and plasmas.

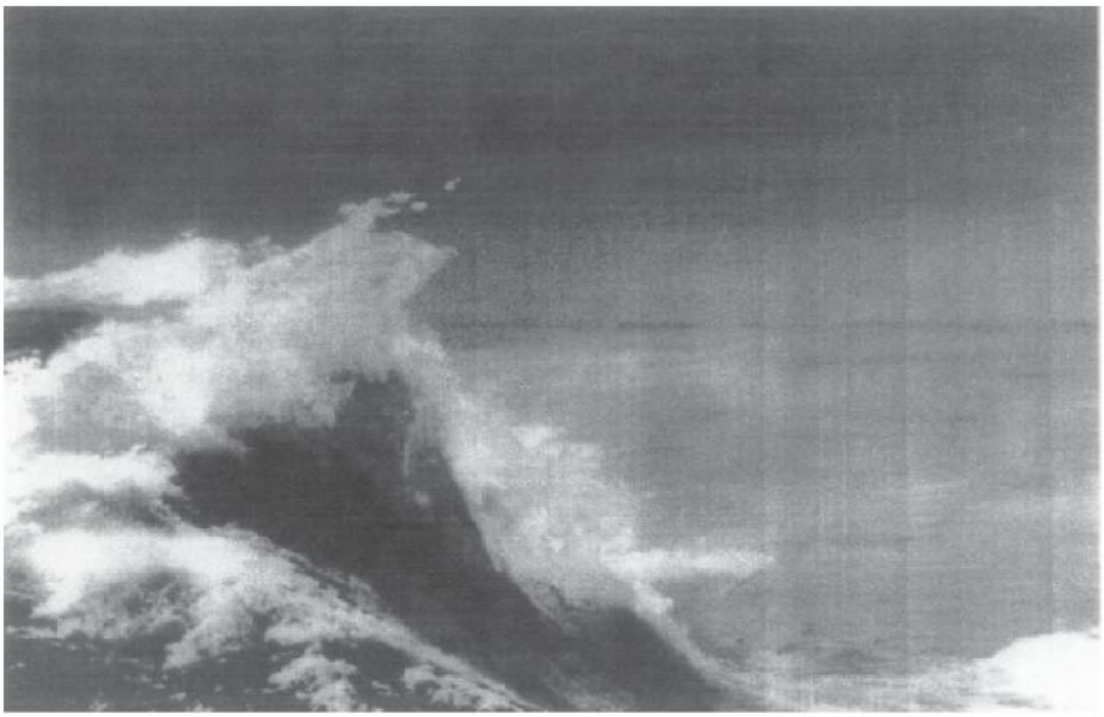

Figure 9: A very steep breaking wave crest [56]

1.2.1 Rogue waves in optical fiber

The results presented in this section have been obtain by Solli and coworkers in Ref. [29].

For centuries, seafarers have told tales of giant waves that can appear without warning on the high seas. These mountainous waves were said to be capable of destroying a vessel or swallowing it beneath the surface, and then disappearing without the slightest trace. Until recently, these tales were thought to be mythical. In the mid-1990s, however, freak waves proved very real when recorded for the first time by scientific measurements during an encounter at the Draupner oil platform in the North Sea [57]. Although they are elusive and intrinsically difficult to monitor because of their fleeting existences, satellite surveillance has confirmed that rogue waves roam the open oceans, occasionally encountering a ship or sea platform, sometimes with devastating results [58]. It is now believed that a number of infamous maritime disasters were caused by such encounters [59]. The unusual statistics of rogue waves represent one of their defining characteristics. Conventional models of ocean waves indicate that the probability of observing large waves should

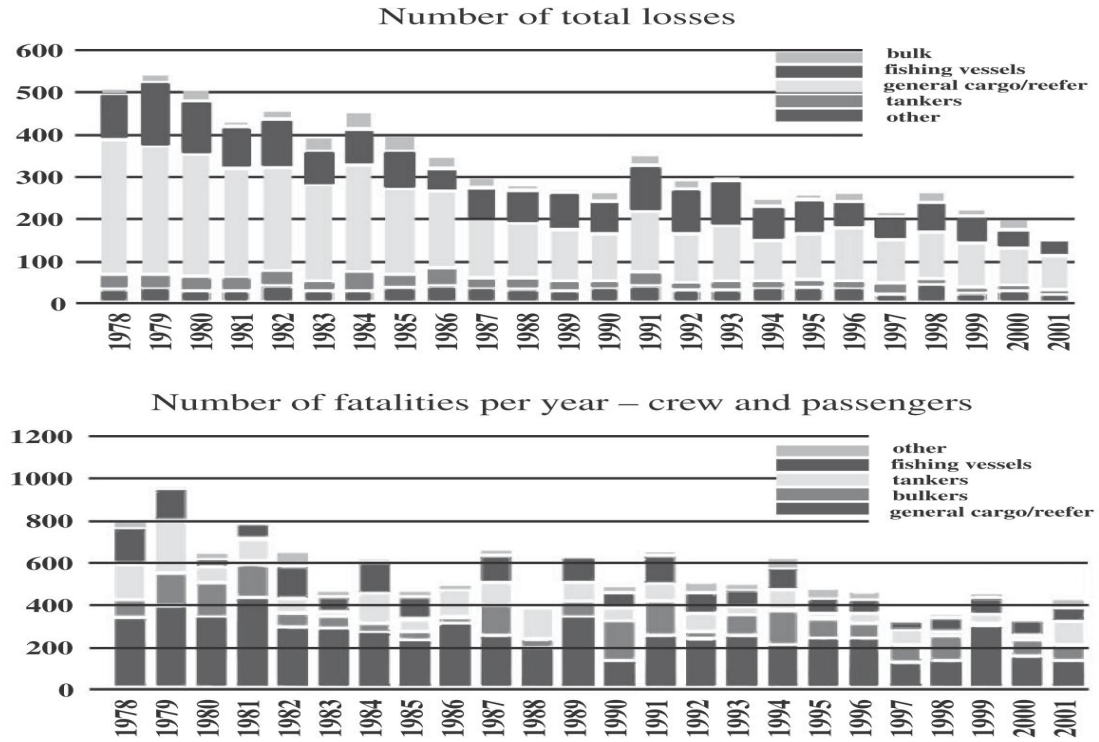

Figure 10: Number of total losses and number of fatalities per year of crew and passenger during 1978-2001 (Source: Det Norske Veritas, http://www.dnv.com/)

diminish extremely rapidly with wave height, suggesting that the likelihood of observing even a single freak wave in hundreds of years should be essentially non-existent. In reality, however, ocean waves appear to follow "L-shaped" statistics: most waves have small amplitudes, but extreme outliers also occur much more frequently than expected in ordinary (for example, gaussian or Rayleigh) wave statistics [60–62]. It is likely that more than one process can produce occasional extreme waves with small but non-negligible probability [63, 64]. Possible mechanisms that have been suggested to explain oceanic rogue waves include effects such as nonlinear focusing via modulation instability in one dimension [65, 66] and in two-dimensional crossings [67, 68], nonlinear spectral instability [69], focusing with caustic currents [70] and anomalous wind excitation. Nonlinear mechanisms have attracted particular attention because they possess the requisite extreme sensitivity to initial conditions. Although the physics behind rogue waves is still under investigation, observations indicate that they have unusually steep, solitary or tightly grouped profiles, which appear like "walls of water" [59]. These features imply that rogue waves have relatively broadband frequency content compared with normal waves, and also sug-

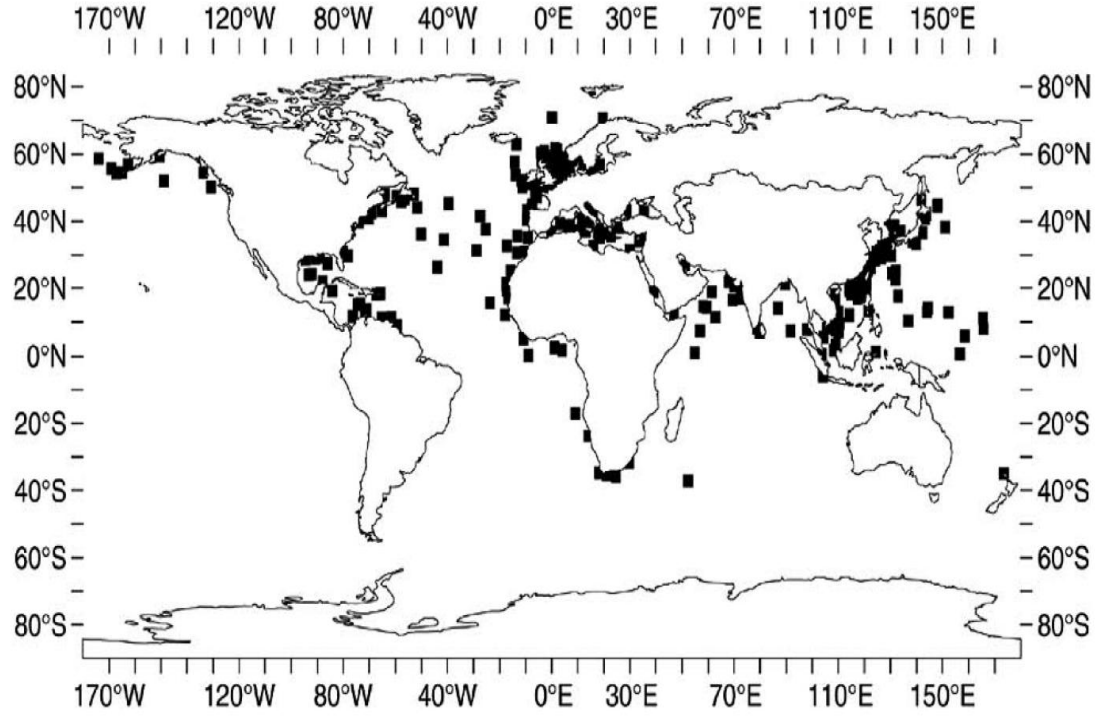

Figure 11: Distribution of shipping accidents from 1995-1999 [50].

gest a possible connection with solitons-solitary waves, first observed by J. S. Russell in the nineteenth century, that propagate without spreading in water because of a balance between dispersion and nonlinearity. As rogue waves are exceedingly difficult to study directly, the relationship between rogue waves and solitons has not yet been definitively established, but it is believed that they are connected.

So far, the study of rogue waves in the scientific literature has focused on hydrodynamic studies and experiments. Intriguingly, there are other physical systems that possess similar nonlinear characteristics and may also support rogue waves. Here the observation and numerical modelling of optical rogue waves in a system based on probabilistic supercontinuum generation in a highly nonlinear microstructured optical fibre is reported. The term "optical rogue waves" is coined, based on striking phenomenological and physical similarities between the extreme events of this optical system and oceanic rogue waves.

Supercontinuum generation has received a great deal of attention in recent years for its complex physics and wealth of potential applications [71]. An extremely broadband supercontinuum source can be created by launching intense seed pulses into a nonlinear fibre at or near its zero-dispersion wavelength [72]. In this situation, supercontinuum

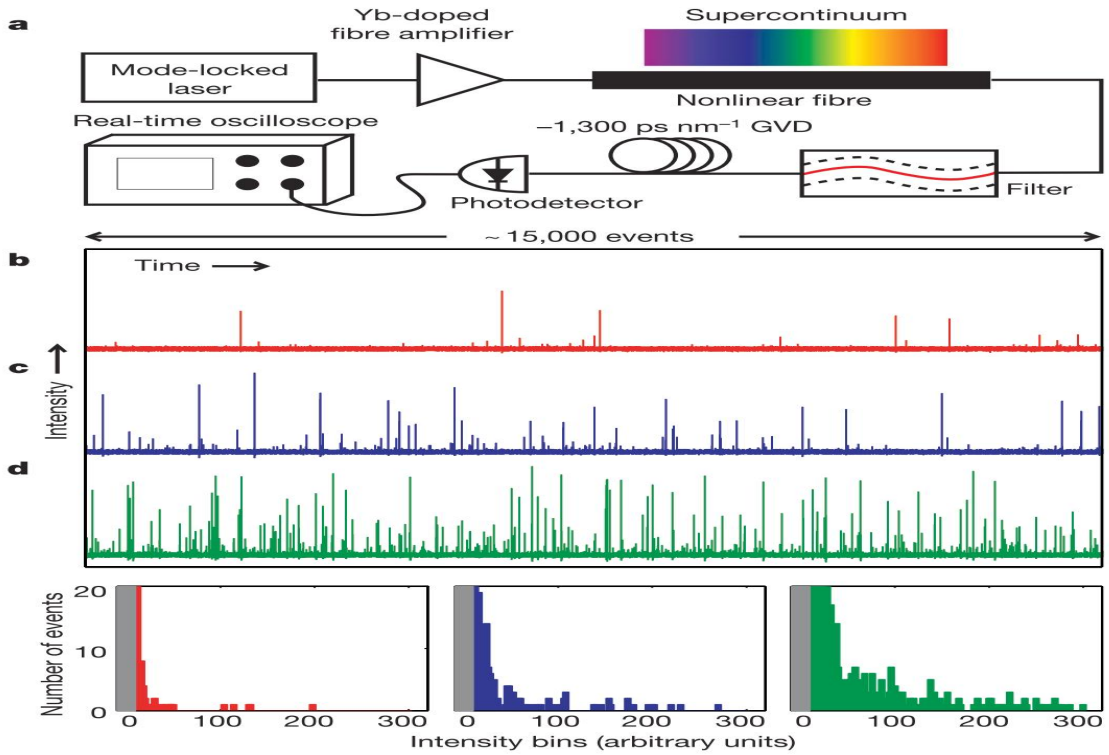

Figure 12: Experimental observation of optical rogue waves. a) Schematic of experimental apparatus. b-d) Single-shot time traces containing roughly 15,000 pulses each and associated histograms (bottom of figure: left, b; middle, c; right, d) for average power levels 0.8 mW (red), 3.2 mW (blue) and 12.8 mW (green), respectively. The grey shaded area in each histogram demarcates the noise floor of the measurement process. In each measurement, the vast majority of events are buried in this low intensity range, and the rogue events reach intensities of at least 30-40 times the average value. These distributions are very different from those encountered in most stochastic processes [29].

production involves generation of high-order solitons-the optical counterparts of Russell's solitary water waves-which fission into redshifted solitonic and blueshifted non-solitonic components at different frequencies [71, 73]. The solitonic pulses shift further towards the red as they propagate through the nonlinear medium because of the Raman-induced self-frequency shift [74]. Interestingly, frequency downshifting effects are also known to occur in water wave propagation. It has been noted that the aforementioned Raman self-frequency shift represents an analogous effect in optics [75]. The nonlinear processes responsible for supercontinuum generation amplify the noise present in the initial laser pulse [76,77] . Especially for long pulses and continuous-wave input radiation, modulation

instability (an incoherent nonlinear wave-mixing process) broadens the spectrum from seed noise in the initial stages of propagation and, as a result, the output spectrum is highly sensitive to the initial conditions [78, 79]. A critical challenge in observing optical rogue waves is the lack of real-time instruments that can capture a large number of very short random events in a single shot. To solve this problem, the of use a wavelength-to-time transformation technique inspired by the concept of photonic time-stretch analog-to-digital conversion [80] is required. In the present technique, group-velocity dispersion (GVD) is used to stretch the waves temporally so that many thousands of random ultra-short events can be captured in real time. A different single-shot technique has been used to study isolated supercontinuum pulses [81]; however, the real-time capture of a large number of random events has not been reported. Using the present method, a small but statistically significant fraction of extreme waves can be discerned from a large number of ordinary events, permitting the first observation of optical rogue waves. The supercontinuum radiation used in this experiments is generated by sending picosecond seed pulses at 1,064 nm through a length of highly nonlinear microstructured optical fibre with matched zero-dispersion wavelength. The output is red-pass filtered at 1,450 nm and stretched as described above so that many thousands of events can be captured with high resolution in a single-shot measurement. A schematic of the experimental apparatus is displayed in Figure 12.

Using this setup, large sets of pulses in real time for very low seed pulse power levels-power levels below the threshold required to produce appreciable supercontinuum are acquired. It is found that the pulse-height distributions are sharply peaked with a well-defined mean, but contrary to expectation, rare events with far greater intensities also appear. In Figure 12, it is shown a representative single-shot time traces and histograms for three different low power levels. In these traces, the vast majority of events are concentrated in a small number of bins and are so weak that they are buried beneath the noise floor of the measurement process; however, the most extreme ones reach intensities at least 30-40 times the average. The histograms display a clear L-shaped profile, with extreme events occurring rarely, yet much more frequently than expected based on the relatively narrow distribution of typical events. Because the red-pass filter transmits only a spectral region that is nearly dark in the vast majority of events, the rare events clearly

have extremely broadband, frequency-downshifted spectral content. The data also show that the frequency of occurrence of the rogue events increases with the average power, but the maximum height of a freak pulse remains relatively constant. These features indicate that the extreme events are sporadic, single solitons.

The nonlinear Schrödinger equation (NLSE) (1.1) models soliton dynamics and has also been used to study hydrodynamic rogue waves generated by nonlinear energy transfer in the open ocean [65–68].

$$iu_t + u_{xx} + 2|u|^2 u = 0. \tag{1.1}$$

Where the quantities u, x and t scale a complex varying envelop, the distance and the time respectively.

As the NLSE also describes optical pulse propagation in nonlinear media, it is certainly plausible that this equation could predict optical rogue waves. The numerical investigation of this is made using the generalized NLSE (neglecting absorption), which is widely used for broadband optical pulse propagation in nonlinear fibres [74] . The generalized NLSE incorporates dispersion and the Kerr nonlinearity, as well as approximations for self-steepening and the vibrational Raman response of the medium. This equation has been successfully used to model supercontinuum generation in the presence of noise [82, 83] and, as demonstrated here, is capable of qualitatively explaining our experimental results. In anticipation of broadband application, it is included several higher orders of dispersion in the nonlinear fibre, which is calculated from the manufacturer's test data. Similarly, higher-order dispersion has also been used to extend the validity of the NLSE for broadband calculations in hydrodynamics [84]. As expected, the present model shows that a high-power, smooth input pulse ejects multiple redshifted solitons and blueshifted non- solitonic components, and a tiny amount of input noise varies their spectral content [71, 79] . On the other hand, for low power levels, the spectral content of the pulse broadens, but no sharp soliton is shed. In this case, the situation changes markedly when a tiny amount of noise is added. This perturbation is amplified by nonlinear interactions including modulation instability, which dramatically lowers the soliton-fission threshold and permits unpredictable freak events to develop. Interestingly, the hydrodynamic equivalent-the Benjamin-Feir modulation instability is also thought to initiate hydrodynamic rogue waves [65–68]. This instability spreads spectral content from a nar-

row bandwidth to a broader range in the initial stages of water wave propagation, just as it does in this optical system.

It is included a stochastic perturbation in the simulations by adding to the initial pulse envelope a small amount of bandwidth-restricted random noise with amplitude proportional to the instantaneous field strength. The NLSE is then solved repeatedly for a large number of independent events. For a small fraction of events, the spectrum becomes exceptionally broad with a clear redshifted solitonic shoulder.

Figure 13a shows the time trace and histogram of peak heights for a trial of 1,000 events after red-pass filtering each output pulse at the start of the solitonic shoulder illustrated in Figure 13b. Clearly, the histogram of heights is sharply peaked but has extended tails, as observed in the experiment, and the distribution contains rogue events more than 50 times as large as the mean. The same rogue events are identified regardless of where the filter is located within the smooth solitonic shoulder and can also be identified from the complementary non-solitonic blue side of the spectrum. The rogue pulses have exceptionally steep leading and trailing edges compared with the initial pulses and the typical events, as shown in Figure 13c. The wide bandwidth and abrupt temporal profile of an optical rogue wave is also highlighted in Figure 14 where the power is displayed as a function of both wavelength and time using a short-time Fourier transform. Because there are no apparent features in the perturbations that lead to the development of the rogue events, their appearance seems unpredictable.

To pinpoint the underlying feature of the noise that produces rogue waves, it is closely analysed the temporal and spectral properties of the initial conditions. Examining the correlations between the initial conditions and their respective output waveforms, it is found that if the random noise happens to contain energy with a frequency shift of about 8 THz within a 0.5-ps window centred about 1.4 ps before the pulse peak (Figure 13c), a rogue wave is born. Noise at this particular frequency shift and on a leading portion of the pulse envelope efficiently seeds modulation instability, reshaping the pulse to hasten its breakup. The output wave height correlates in a highly nonlinear way with this specific aspect of the initial conditions. Thus, the normal statistics of the input noise are transformed into an extremely skewed, L-shaped distribution of output wave heights. Further study is needed to explain precisely why the pulse is so highly sensitive to these

particular noise parameters. Nevertheless, the specific feature we have identified in the initial conditions offers some predictive power for optical rogue waves, and may offer clues to the oceanic phenomenon.

The rogue waves have a number of other intriguing properties warranting further study. For example, they propagate without noticeable broadening for some time, but have a finite, seemingly unpredictable lifetime before they suddenly collapse owing to cumulative effects of Raman scattering. This scattering seeded by noise dissipates energy or otherwise perturbs the soliton pulse beyond the critical threshold for its survival [79] . The decay parallels the unpredictable lifetimes of oceanic rogue waves. The rogue optical solitons are also able to absorb energy from other wavepackets they pass through, which causes them to grow in amplitude, but appears to reduce their lifetime. A similar effect may help to explain the development of especially large rogues in the ocean. In conclusion, it have been observed extreme soliton-like pulses that are the optical equivalent of oceanic rogue waves. These rare optical events possess the hallmark phenomenological features of oceanic rogue waves-they are extremely large and seemingly unpredictable, follow unusual L-shaped statistics, occur in a nonlinear medium, and are broadband and temporally steep compared with typical events.

On a physical level, the similarities also abound, with modulation instability, solitons, frequency downshifting and higher-order dispersion as striking points of connection. Intriguingly, the rogue waves of both systems can be modeled with the nonlinear Schrödinger equation. Although the parameters that characterize this optical system are of course very different from those describing waves on the open ocean, the rogue waves generated in the two cases bear some remarkable similarities.

1.2.2 Rogue waves in the Bose-Einstein condensates

Rogue wave in homogeneous Bose-Einstein condensates

There are at least two fundamental reasons for great interest in generating rogue waves in laboratory conditions. First, this opens possibilities for detailed studies of their properties as well as testing applicability of the mathematical models developed for their descriptions (something unthink- able in the natural conditions). Second, being an es-

sentially nonlinear phenomenon, rogue waves allow us to understand deeply the nature and the dynamics of instabilities in nonlinear systems. Thus, the natural question that appears is whether the rogue waves can be observed in other (than ocean or optical fibers) physical media. The goal here is to give the positive answer to this question by showing that rogue waves are also rather natural in the microworld. Namely, they can be observed in Bose-Einstein condensates (BECs). The physical reasons for this are twofold. First, BEC represents a fluid, which in the mean-field approximation is accurately described by the Gross-Pitaevskii (GP), i.e., by the NLS equation. Second, due to the two-body interactions, BEC is intrinsically a nonlinear system. Moreover, a BEC has great advantages compared to other nonlinear systems. Indeed, the nonlinear interactions can be experimentally managed by means of the Feshbach resonance [159], while the effective atomic mass and the stability properties can be varied with help of the optical lattice [160]. The suitable initial conditions can be created using phase and density engineering. In other words, rogue waves in BECs appear to be well controllable objects.

The existence of rogue waves in the Bose Einsten Condensates (BEC) was predicted in [85] by Bludov and comorkers. The model equation used is the Gross-Pitaevskii (GP) equation given ass follows

$$i\psi_t = -\psi_{xx} + \sigma|\psi|^2\psi - ig|\psi|^4\psi, \tag{1.2}$$

where $\sigma = sgn(a_s)$ and a_s is scattering length. The quantity ψ scale a complex varying envelop while x and t stand for the normalized and distance and time respectively; the subscript means partial derivative. In this equation, the dissipative term has been explicitly included due to inelastic three-body interaction whose strength is characterized by $g > 0$ [86]. This last point is of special relevance as the rogue waves correspond to a giant increase in the local density when the impact of the three-body collisions can become dominant.

Besides the inelastic three-body interactions in a real experimental situation relevant for the BEC applications, trap potential can be taken into account. This makes the problem very different from the analytically solvable nonlinear Schrödinger (NLS) equation. Nevertheless, it is natural to expect that using the exact solution for the NLS rogue wave, one can guess the proper initial conditions, giving rise for the giant density enhancement

in a realistic mean-field model of a BEC. Therefore when scaling $\sigma = -1$ and $g = 0$, equation (1.2) possesses an exact analytical solution [54]

$$\psi_0(x,t) = \rho(x,t)e^{i\theta(x,t)} = \left(1 - 4\frac{1+2it}{1+2x^2+4t^4}\right)e^{it}, \tag{1.3}$$

with the density ρ^2 and the phase distribution θ at each instant of time determined from this formula. Equation (1.3) gives rise to the Figure (15).

To conclude, it is reported that it is possible to observe the rogue waves in BECs. While the fact that the existence of such waves is somehow evident, it follows from the fact that the mean-field dynamics of a BEC is described by the Gross-Pitaevskii equation; there exists several features of the phenomenon observed in a condensed atomic gas. First, condensates are created in the presence of an external potential, which is typically parabolic one. Second, the three-body interactions are expected to become a significant factor in the course of the evolution of the rogue waves. Third, the rogue waves can be generated in a controlled manner by phase and amplitude engineering.

Vector rogue waves in binary mixtures of Bose-Einstein condensates

This work was done and published by Bludov and coworkers [161]. In this work,they studied numerically the rogue waves in the two-component BECs which are described by the coupled set of two Gross-Pitaevskii (GP) equations with variable scattering lengths, i.e. coefficients of nonlinearity. Specifically, they presented the rogue wave solutions for various combinations of these coefficients that admit such solutions. Among their major results we can mention:

- Non trivial relation between the existence of vector Peregrine solutions and the characteristics of the modulational instability of the system.
- Inhibition of the rogue waves due modulational stability induced by inter-atomic interaction
- Rogue waves induced by interatomic interactions in the mixture of condensates with positive scattering lengths (i.e.positive intra-atomic interactions)
- Rogue waves that are accompanied by the exchange of particles between the two components

- Possibility of existence of dark rogue waves.

To be specific, the authors have considered a spinor BEC composed of two hyperfine states,say of the states of ^{87}Rb atoms [162] confined at different vertical positions by parabolic traps and coupled by a time-dependent coupling field. Then, in the mean-field approximation the system is described by the GP equations [163].

$$\begin{aligned} i\psi_{1t} &= -\psi_{xx} + (g_1|\psi_1|^2 + g|\psi_2|^2) + \beta(t)\psi_2 \\ i\psi_{2t} &= -\psi_{xx} + (g|\psi_1|^2 + g_2|\psi_2|^2) + \beta(t)\psi_1. \end{aligned} \tag{1.4}$$

This equation is written on a dimensionless form where the quantity x and t scale the coordinates and the time respectively. The coefficient of proportionality here depends on a particular choice of the transverse trap, and generally is either one or of the order of one. The last terms in Equation (1.4) describes the possibility of conversion between the two hyperfine states, which can be originated by the external magnetic field. In this case, the factor β can be expressed in terms of such field. The authors emphasized that the results are not restricted to the described case.

To limit the number of possibilities, in the present work the authors deal only with the case where the intra-species interactions have the same signs of the scattering length, i.e. when $g_1 g_2 > 0$. They have started some preliminary comments on the system (1.4), mentioning that an important parameter of the theory is the determinant of the nonlinear coefficients: $\Delta = g_1 g_2 - g^2$. Which is known to determine the thermodynamic or modulation instability. The authors have chosen the solution in the form of the one-component rogue wave, namely

$$\Psi(x,t) = \frac{1}{\sqrt{-g}}\left(1 - 4\frac{1+2it}{1+2x^2+4t^2}\right), \tag{1.5}$$

which is valid for $g < 0$. For the system under consideration, the solutions are

$$\psi_1(x,t) = a_1\Psi(x,t), \qquad \psi_2(x,t) = a_2\Psi(x,t)e^{i\delta}, \tag{1.6}$$

where $a_1 = \frac{g-g_2}{\Delta}$ and $a_2 = \frac{g-g_1}{\Delta}$.
The system (1.6) describes a synchronized evolution of the two components, so they should be called *vector rogue waves.* The depictions are shown in Figure (21).

The system becomes physically significantly different when the linear coupling is taken into account i.e $\beta(t) \neq 0$. The number of particles in the first and the second components

relative to the total number of particles can be expressed using equation (1.6) as

$$\frac{\int |\psi_{1,2}(x)|^2 dx}{\int |\Psi(x)|^2 dx} = -\frac{1}{2g}[1 \pm \sin(2\alpha)\cos(2B(t))],$$

where the signs + and - in the right hand side correspond to the first and the second components, respectively. Choosing

$$B(t) = \frac{\pi}{4}\left(1 - b\frac{t - t_0}{t_0}\right),$$

the particles are periodically swapped between the two components. The Figure (22) show the results of numerical simulation of vector rogue waves in the Bose-Einstein condensates with linear coupling.

In the first case, $b = 1$, shown in Figure (22a), the maximum of the rogue wave is located at the maximum of the oscillating background. All particles at $t = 0$ are concentrated in the second component. In the second case, $b = 2$, shown in Figure (22b), the maximum of the rogue wave is located at the slope of the oscillating background. There is an equal number of particles in the two components. Finally, when the frequency of the oscillation of the particles between the two components is high ($b = 15$), the background becomes fast oscillating as can be seen in Figure (22c).

We go forward while presenting other interesting results in physics.

1.2.3 Rogue wave in plasma

The existence of rogue wave dynamics in plasmas was reported by Bailung and coworkers in Ref. [87].

The experimental observation of Peregrine solitons in a multicomponent plasma with the critical concentration of negative ions was reported. A slowly amplitude modulated perturbation undergoes self-modulation and gives rise to a high amplitude localized pulse. The measured amplitude of the Peregrine soliton is 3 times the nearby carrier wave amplitude, which agrees with the theory. The numerical solution of the nonlinear Schrödinger equation is compared with the experimental results.

In a multicomponent plasma with the critical density of negative ions, the NLSE describing the evolution of ion-acoustic wave with weak nonlinearity is given by [88, 89]

$$i\frac{\partial\psi}{\partial\tau} + p\frac{\partial^2\psi}{\partial^2\xi} + \frac{q}{4}|\psi|^2\psi = 0, \tag{1.7}$$

where ψ is the wave amplitude normalized by the electron temperature (T_e), the time τ and the distance ξ in the wave frame are normalized, respectively by the ion plasma period $\omega_{pi}^{-1} = (\varepsilon_0 m_i/ne^2)^{1/2}$ and the electron debye length $\lambda_D = (\varepsilon_0 \kappa T_e/ne^2)^{1/2}$, where m_i is the positive ion mass and n is the unperturbed electron density. The group velocity V_g of the propagating wave normalized by $(\kappa T_e/m_i)^{1/2}$ is given by

$$V_g = \frac{\omega^3}{d\kappa}\left(\frac{1-r}{1+r/\mu}\right) \equiv \frac{d\omega}{d\kappa}.$$

Here, r and μ represent the density ration and the mass ration, respectively, of the negative ions to that of the positive ions. The angular frequency ω and the wave number κ are related with the following dispersion relation:

$$\omega^2 = \frac{\kappa^2}{1+\kappa^2}\left(\frac{1+r/\mu}{1-r}\right).$$

The dispersion coefficient p is given by

$$p = -\frac{3}{2}\frac{\omega^5}{\kappa^4}\left(\frac{1-r}{1+r/\mu}\right)^2 \equiv \frac{1}{2}\frac{d^2\omega}{d\kappa^2},$$

with the nonlinear coefficient $q = -\frac{d\omega}{d|\omega|^2}$.

As the dispersion relation coefficient p is always negative, a finite amplitude sinusoidal wave is modulationally unstable for $q < 0$ [90]. The NLSE 1.7 has a rational solution of the form [54]

$$\psi(\xi,\tau) = \frac{2}{\sqrt{q}}\left[\frac{4(1+i\tau)}{1+4\tau^2+2\xi^2/p} - 1\right] exp(i\tau). \tag{1.8}$$

The development of the initial amplitude modulated wave packet is then given by

$$\eta(x,t) = Re\psi(x,t)exp[i(\kappa x - \omega t)], \tag{1.9}$$

where $\psi(x,t)$ is dimension form of equation 1.8 which can be obtained by using the transformation $\xi \to a_0\kappa_D(x - V_g t)$ and $\tau \to a_0^2\omega_{pi}t$, where a_0 represents the initial wave amplitude of the background carrier wave. The Figures 16, 17, 18, 19 and 20 show the rogue wave dynamics in a multicompent plasma.

Rogue waves have been shown to exist in nonlinear physical systems. Many mathematical tools have been used to construct analytical rational rogue wave solutions to the nonlinear Schrödinger equation and its extensions , the complex modified Kdv equation,

the Hirota equation, the AB system, the Sasa Satuma equation, the Maxwell-Bloch equation, just to name a few. The Darboux matrix method is among other tools used to derive rogue wave solution the nonlinear physical wave equations. In the following we present in detail the procedure on how this powerful technic is used to derive rogue wave solution, through a typical example.

1.2.4 Extreme waves that appear from nowhere: On the nature of rogue waves

This work was reported in reference [158]. It was done by Akhmediev and coworkers. They have numerically calculated chaotic waves of the focusing nonlinear Schrödinger equation (NLSE) starting with a plane wave modulated by relatively weak random waves. They have shown that the peaks with highest amplitude of the resulting wave composition (rogue wave) can be described in terms of exact solutions of the NLSE in the form of the collision of Akhmediev breathers.

In the normalized form, the popular NLSE is written as

$$i\frac{\partial\psi}{\partial x} + \frac{1}{2}\frac{\partial^2\psi}{\partial t^2} + |\psi|^2\psi = 0, \tag{1.10}$$

where x is the propagation distance and t is the transverse variable. This notation is standard both in nonlinear fiber optics and in the theory of ocean waves. Note that ψ represents the envelope of a physical solution, and, in optics, its squared modulus represents a measurable quantity, viz. intensity. The authors used as the initial condition when solving equation (1.10) a plane wave solution with a random noise superimposed on it,

$$\psi(x = 0, t) = [1 + \mu f(t)] \tag{1.11}$$

where $f(t)$ is a normalized complex random function whose standard deviation is $\sigma = 1/\sqrt{3}$. A typical example of the initial condition (1.11) is shown in Figure (23)

The authors were interested in the highest amplitudes of the resulting ocean surface. In each numerical run, they singled out the maximum values of the field which can potentially be rogue waves. Namely, at each x, they found the absolute maximum of the function $|\psi(x = const, t)|$ and plotted it against the x value. The corresponding plot for the initial condition presented in Figure (23) is shown in Figure (24).

The highest amplitude that appears in this numerical run is close to 5. This amplitude cannot be associated with any of the first-order solutions since the maximum amplitude in that case is 3. The latter is attributed to the first-order rational solution (Peregrine soliton):

$$\psi = \left(1 - 4\frac{1+2ix}{1+4x^2+4t^2}\right)e^{ix}. \tag{1.12}$$

This solution is shown in Figure (25)

It is worth noting that 5 is exactly the amplitude of the second-order rational solution of the NLSE [164], given as

$$\psi = \left(1 - \frac{G+iH}{D}\right)e^{ix}, \tag{1.13}$$

where the quantities G, H and D are given by

$G = -\frac{3}{16} + \frac{3}{2}t^2 + t^4 + \frac{9}{2}x^2 + 6t^2x^2 + 5x^4,$

$H = x\left(-\frac{15}{8} - 3t^2 + 2t^4 + x^2 + 4t^2x^2 + 2x^4\right),$

$D = \frac{3}{64} + \frac{9}{16}t^2 + \frac{1}{4}t^4 + \frac{33}{16}x^2 - \frac{3}{2}t^2x^2 + t^4x^2 + \frac{9}{4}x^4 + t^2x^4 + \frac{1}{3}x^6.$

This solution is shown in Figure (26)

Because its maximum amplitude is equal to 5, it can, in principle, explain the high amplitudes that the authors observed in the numerical simulations. However, it is useful to take into account that this solution is a nonlinear superposition of two rational solutions of first-order. As each of them is localized both in x and t directions, their appearance at the same position simultaneously would be an extremely rare event.

Akhmediev breathers and their collisions

As an alternative, the authors considered the collision of two breather waves known as akhmediev breathers (ABs). These are extended in the t direction, so such a collision would have higher chance of occurring in a chaotic field. In order to construct these solutions, they used the Darboux transformation.

The condition of integrability of the NLSE is the compatibility of the two following linear equations:

$$R_t = (lJ + U)R, \qquad R_t = (l^2J + lU + \frac{1}{2}V)R. \tag{1.14}$$

Where U, J and V are matrices given as follows

$$U = \begin{pmatrix} 0 & i\psi^* \\ i\psi & 0 \end{pmatrix}, \quad J = \begin{pmatrix} i & 0 \\ 0 & -i \end{pmatrix}, \quad V = \begin{pmatrix} -i|\psi|^2 & \psi_t^* \\ -\psi_t & i|\psi|^2 \end{pmatrix},$$

while R is a column matrix written as $R = \begin{pmatrix} r \\ s \end{pmatrix}$ and l is a complex eigenvalue.

The eigenvalue l in equation (1.14) is practically an arbitrary complex number that appears as the parameter of the family of solutions that are going to be constructed. In the case of solutions related to modulation instability, the real part of l is the velocity of the solution, while the imaginary part characterizes the frequency of the periodic modulation.

In view to construct solution that is a collision of two first-order breathers, the authors selected two eigenvalues l_1 and l_2, that have to be different for higher-order solution to exist.

Following the procedure given in reference [165], They have assumed that the seeding solution of the NLSE is a plane wave of amplitude 1, given as

$$\psi_0 = e^{ix}.$$

The two linear solutions compatible with the system (2.40) are

$$\begin{aligned} r &= A\exp[i(2\chi + kt + lkx)/2] - B\exp[-i(2\chi + kt + lkx)/2]e^{-\frac{x}{2}}, \\ s &= A\exp[i(-2\chi + kt + lkx)/2] + B\exp[-i(-2\chi + kt + lkx)/2]e^{\frac{x}{2}}, \end{aligned} \tag{1.15}$$

where $\chi = \frac{1}{2}\arccos(\frac{k}{2})$, $k = 2\sqrt{1+l^2}$, A and B are constants of integration given as follows

$$\begin{aligned} A &= \exp[(ilkx_0 - ikt_0 - i\pi/2)/2] \\ B &= \exp[(-ilkx_0 + ikt_0 + i\pi/2)/2] \end{aligned}, \tag{1.16}$$

Substituting (1.16) into (1.15) yields

$$\begin{aligned} r_1 &= \exp[(2i\chi_1 + ik_1t - i\pi/2 + il_1k_1x)/2] - \exp[(-2i\chi_1 - ik_1t + i\pi/2 - l_1k_1x)/2]e^{-\frac{x}{2}}, \\ s_1 &= \exp[(-2i\chi_1 + ik_1t - i\pi/2 + il_1k_1x)/2] - \exp[(2i\chi_1 - ik_1t + i\pi/2 - l_1k_1x)/2]e^{\frac{x}{2}}, \end{aligned} \tag{1.17}$$

where $k_1 = 2\sqrt{1+l_1^2}$ and $\chi_1 = \frac{1}{2}\arccos(k_1/2)$. Here $x_0 = 0$ and $t_0 = 0$, without lost of generality. The subscripts 1 has been added to refer to the eigenvalue l_1.

The nontrivial solution that is found at the first step of the Darboux scheme is given by

$$\psi_1 = \psi_0 + 2\frac{(l_1^* - l_1)s_1 r_1^*}{|r_1|^2 + |s_1|^2}. \tag{1.18}$$

Inserting s_1 and r_1 into (1.18), the first-order breather solution or AB is obtained. The corresponding plots are given in Figures (27) and (28).

The higher-order solution that combines two independent frequencies of modulation k_1 and k_2, can be found using the next step of the Darboux transformation. For this end, the authors used a different eigenvalue, namely, $l = l_2$.

$$r_2 = \exp[(2i\chi_2 + ik_2t - i\pi/2 + il_2k_2x)/2] - \exp[(-2i\chi_2 - ik_2t + i\pi/2 - l_2k_2x)/2]e^{-\frac{x}{2}}, \tag{1.19}$$
$$s_2 = \exp[(-2i\chi_2 + ik_2t - i\pi/2 + il_2k_2x)/2] - \exp[(2i\chi_2 - ik_2t + i\pi/2 - l_2k_2x)/2]e^{\frac{x}{2}}.$$

The solution of the linear set which corresponds to the higher-order NLSE solution can be written in term of r_1, s_1, r_2 and s_2, namely

$$r_{12} = \frac{(l_1^* - l_1)s_1^* r_1 s_2 + (l_2 - l_1)|r_1|^2 r_2 + (l_2 - l_1^*)|s_1|^2 r_2}{|r_1|^2 + |s_1|^2}, \tag{1.20}$$
$$s_{12} = \frac{(l_1^* - l_1)s_1 r_1^* r_2 + (l_2 - l_1)|s_1|^2 s_2 + (l_2 - l_1^*)|r_1|^2 s_2}{|r_1|^2 + |s_1|^2}.$$

The higher-order solution of the NLSE then is

$$\psi_{12} = \psi_1 + 2\frac{(l_2^* - l_2)s_{12} r_{12}^*}{|r_{12}|^2 + |s_{12}|^2}. \tag{1.21}$$

This solutions are shown in figures (29) and (30). The frequencies are $k_1 = 1.6$ and $k_2 = 1.43$. These frequencies are incommensurate. Thus, the superposition has one absolute maximum. With the choice of the integration constants, it is located at the origin. Even in this case, the central maximum of the solution is relatively high. It is certainly higher than the crests of other wavelets in the solution. This maximum will reach the value 5 when both k's approach 1.

Qualitatively, the central part of the profile in each case looks very similar to the higher-order rational solution. This is not unusual because the rational solutions are limiting cases of the ABs in the infinite period limit. However, the probability of the overlapping in the two-dimensional space of the high-order rational solutions is very low, while ABs will necessarily collide, at least at one point. If they are moving with finite velocities, then their collision is very similar to the collision of two solitons, except for the direction of the localization and the periodicity of each breather.

Comparison of numerical simulations with the exact solutions

The above results show that it is indeed possible that rogue waves can be attributed to higher-order solutions. In order to confirm this conclusion, the authors made a detailed comparison of the wave profile that appears in the simulations using random initial conditions with the exact profiles defined by the analytic solutions. These plots are presented in Figures (31) and (32) along the t and x directions, respectively. In each plot, the dashed blue line is taken from the numerical simulations. The exact rational solution is shown by the dotted red line, while the collision of two Akhmediev breathers is shown by the green solid line.

The conclusion is that the amplitude profile around the peaks indeed closely resembles both the second-order rational solution and the result of the collision of two ABs. The central part of the peak accurately follows each of the exact profiles. The discrepancy in the tails of the peak are due to random smaller amplitude waves surrounding the peak.

Conclusion

Throughout this chapter, we have presented the effects of the rogue wave on the marine liners. We have presented some historical testimonies of that phenomenon. It is important to notice that the end of these histories is not enthusiastic. It has been proved that rogue waves appear not only in oceanic condition but also in physical systems. So we have presented some interesting results obtained in the literature in some fields such as optics, plasma and Bose-Einstein condensates. These results have been obtained numerically, not analytically; So Akhmediev and coworkers have derived the rogue waves solution of the nonlinear Schrödinger equation and have compared the results with those obtained numerical. They have also shown that a rogue wave can appear as a collision of two breather wave called Akhmediev breather. We now go further while presenting the methodologies employed in this work to derive rogue wave solutions.

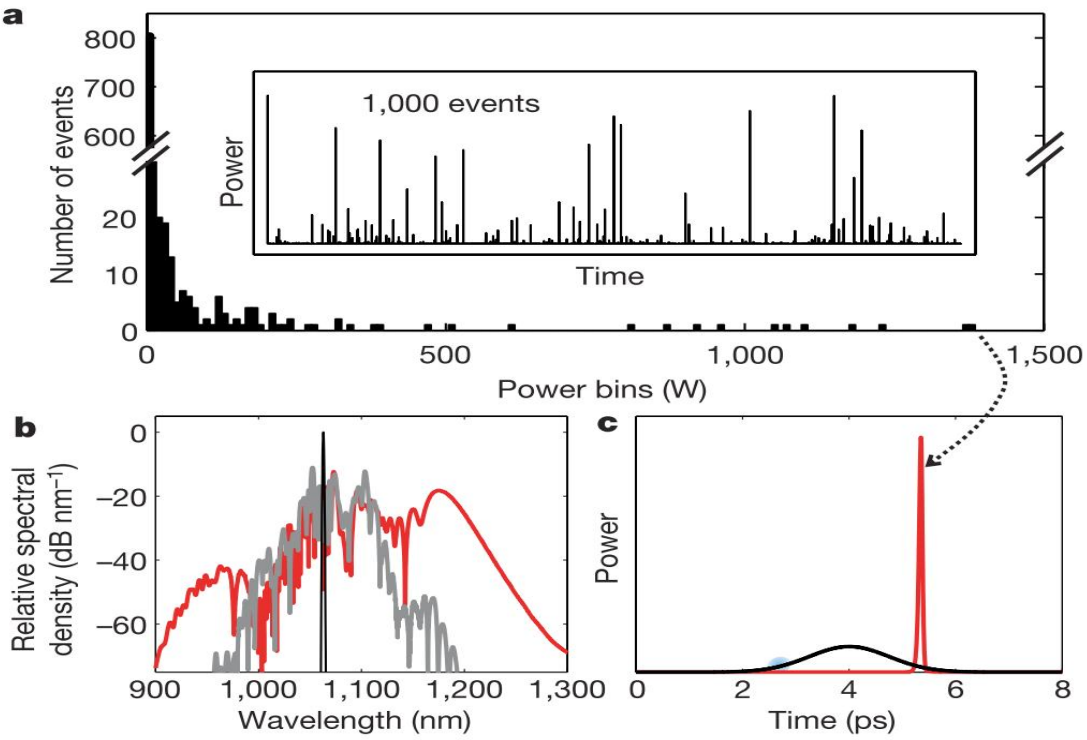

Figure 13: Simulation of optical rogue waves using the generalized nonlinear Schrödinger equation. a) The time trace and histogram of 1,000 events with red-pass filtering from 1,155 nm. The initial (seed) pulses have width 3 ps, peak power 150 W, fractional noise 0.1 percent, and noise bandwidth 50 THz. The vertical axis of the histogram contains a scale break to make it easier to see the disparity between the most common events at low peak power and the rogue events at high peak power. b, The complete relative spectral densities of the initial pulse (black line), a typical event (grey line) and the rare event shown in c (red line). c, The markedly different temporal profiles of the seed pulse and the rare event indicated in the histogram. The typical events from the histogram are so tiny that they are not visible on this linear power scale. The shaded blue region on the seed pulse delineates the time window that is highly sensitive to perturbation [29].

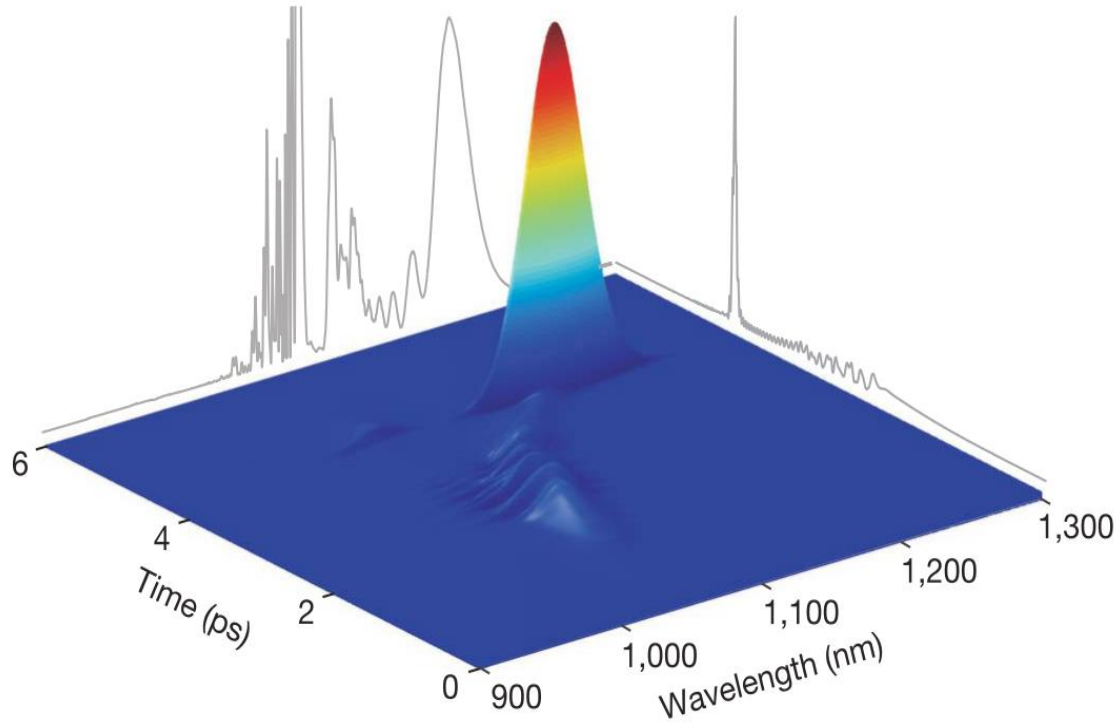

Figure 14: Time-wavelength profile of an optical rogue wave obtained from a short-time Fourier transform. The optical wave has broad bandwidth and has extremely steep slopes in the time domain compared with the typical events. It appears as a 'wall of light' analogous to the "wall of water" description of oceanic rogue waves. The rogue wave travels a curved path in time-wavelength space because of the Raman self-frequency shift and group velocity dispersion, separating from non-solitonic fragments and remnants of the seed pulse at shorter wavelengths. The grey traces show the full time structure and spectrum of the rogue wave. The spectrum contains sharp spectral features that are temporally broad and, thus, do not reach large peak power levels and do not appear prominently in the short-time Fourier transform [29].

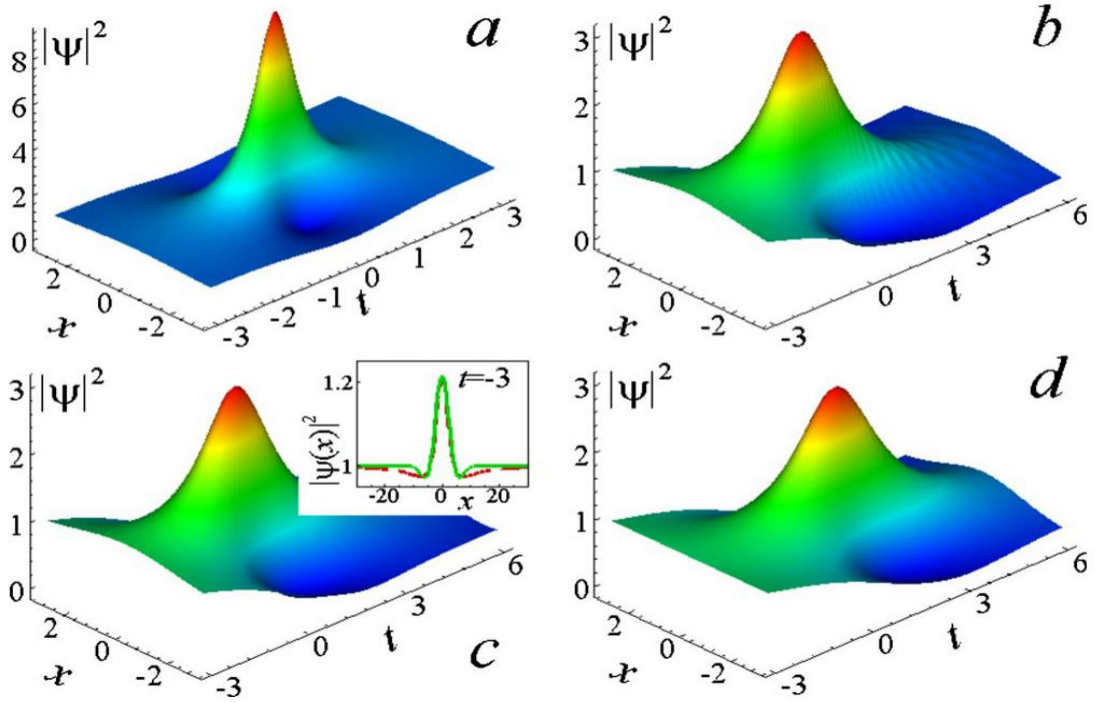

Figure 15: Evolution of the atomic density according to (a) the exact solution 1.3 , (b) TF approximation with i =0.02, (c) Mexican hat, and (d) uniform $\rho_i^2 = 1$ initial conditions. In (b) , (c) , and (d), the initial phase distribution θ_i is taken from Eq.(1.7) . The initial time is $t_i = -3$. The inset in (c) shows the initial densities obtained from Eq. (1.2) (dashed line) and from the Mexican hat approximation ψ_{MH} (solid line). In (b) ,(c) and (d), we used $g = 0.05$ [85].

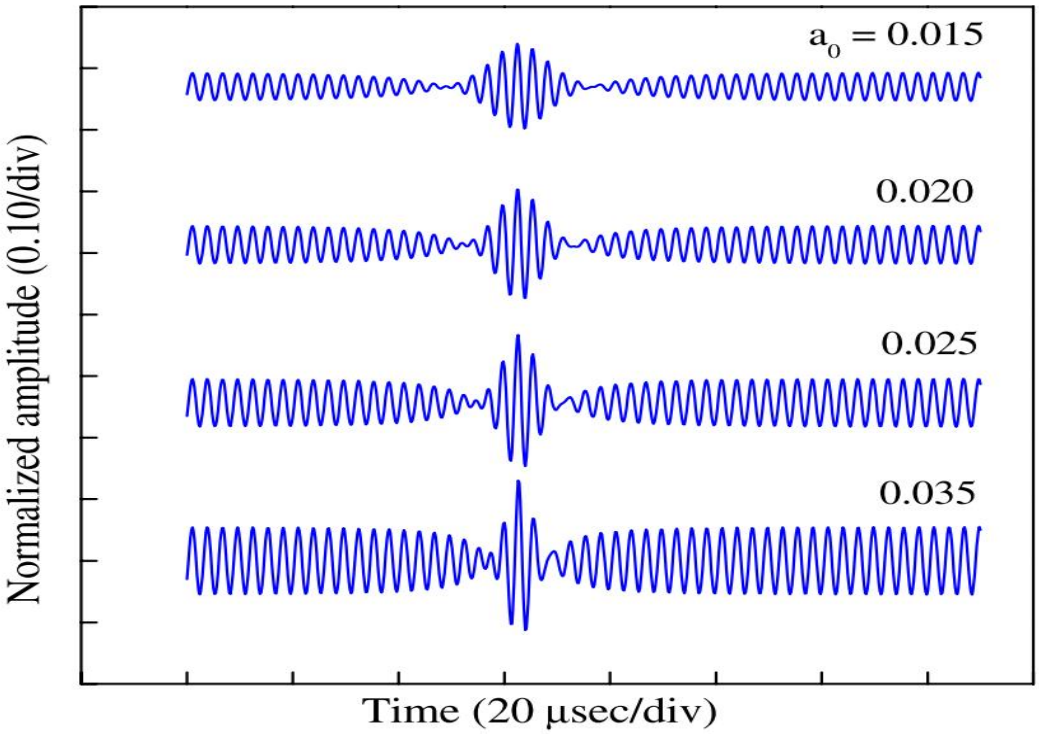

Figure 16: Numerical result of equation 1.9 for different values of a_0. Parameters used are $\omega = 0.7\omega_{pi}$,$(\omega_{pi} = 492kHz)$, $k = 0.74k_D = 1/\lambda_D = 20.0cm^{-1}$, $x = 13.0cm$ [87].

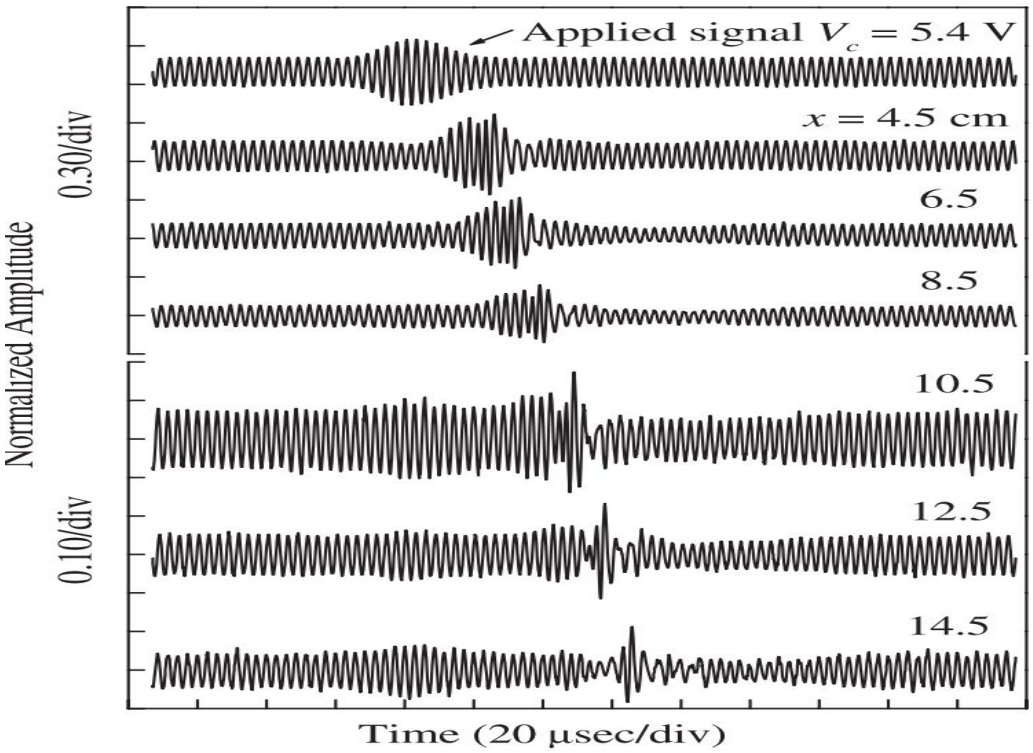

Figure 17: Observed signals of the electron density perturbation at different probe positions from the separation grid. The top trace is the applied signal with carrier and modulation frequencies 350 and 31 kHz, respectively. Peak to peak amplitude of the applied carrier wave (V_c) is fixed at 5.4 V. Signals observed at 10.5 to 14.5 cm are shown with different amplitude scale (0.10/div) for better resolution [87].

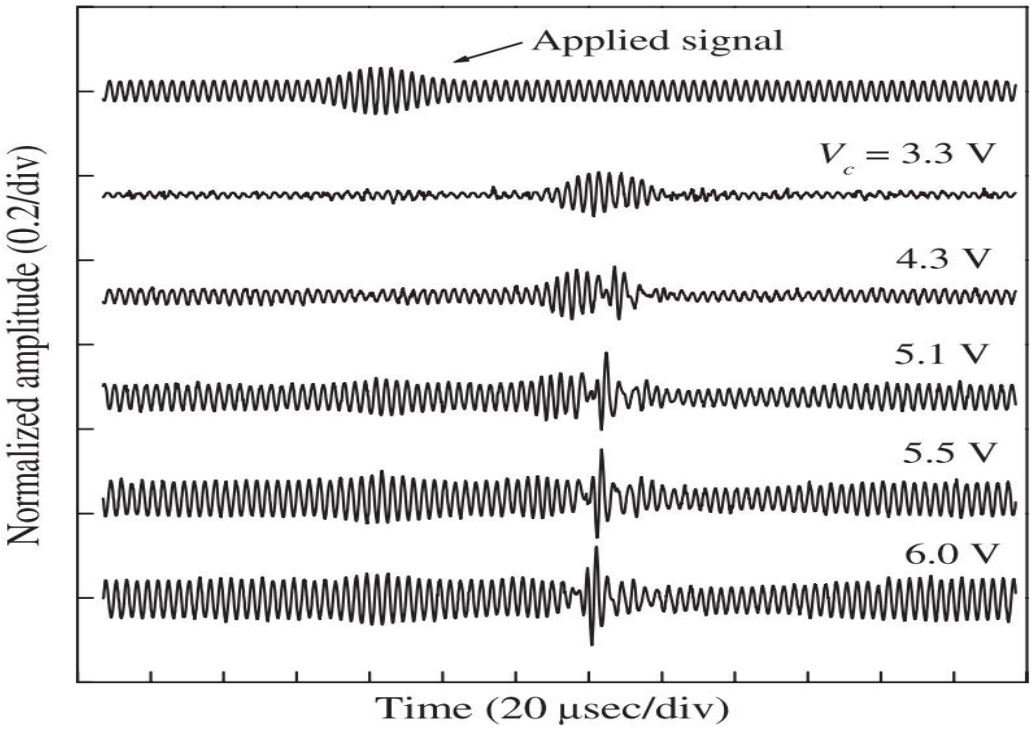

Figure 18: Signals recorded for different excitation amplitudes of the carrier wave. The probe is fixed at 13.6 cm from the separation grid. Top trace represents the applied signal with carrier and modulation frequencies 350 and 31 kHz, respectively. [87].

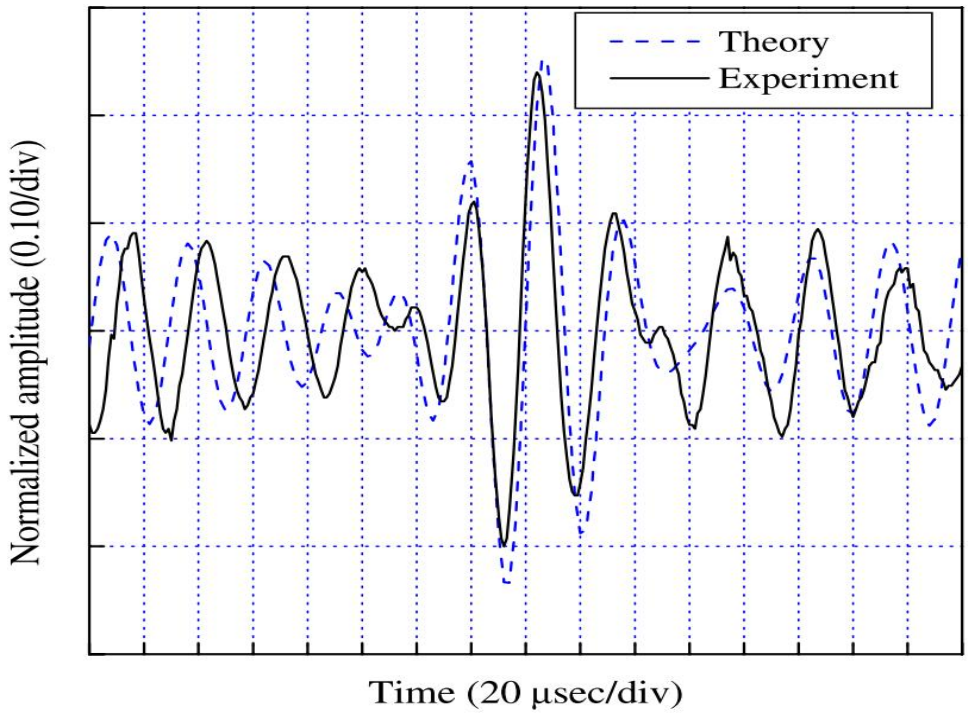

Figure 19: Comparison of the time series signal (solid line) observed at 13.6 cm with the theoretical Peregrine soliton (dashed line) obtained by using Eq. (3). The applied carrier and modulation frequencies are 350 and 31 kHz, respectively. Vc = 5.9 V. The parameters used for numerical are $\omega = 0.7\omega_{pi}$, $(\omega_{pi} = 492kHz)$, $k = 0.74k_D$, $K_D = 1/\lambda_D = 20.0cm^{-1}$ [87].

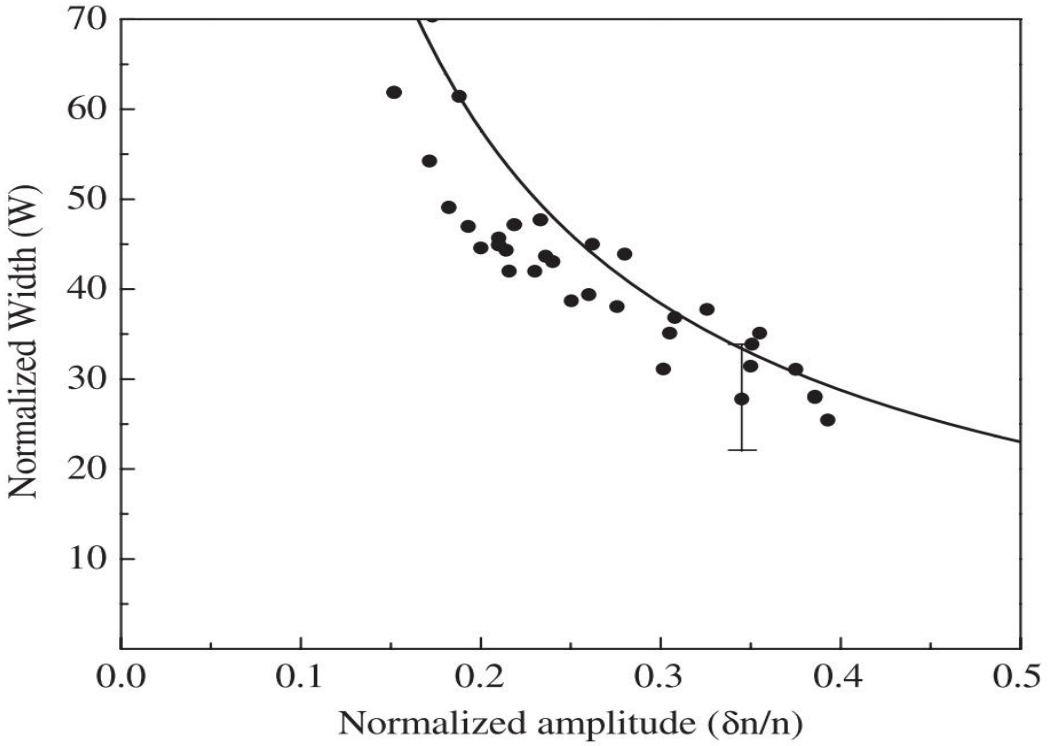

Figure 20: Measured widths W normalized with the electron Debye length λ_D as a function of amplitude δn (peak to peak)/n, where δn is the perturbed electron density. The solid curve is the theoretical width estimated from the wave signals as shown in Fig. 16 [87].

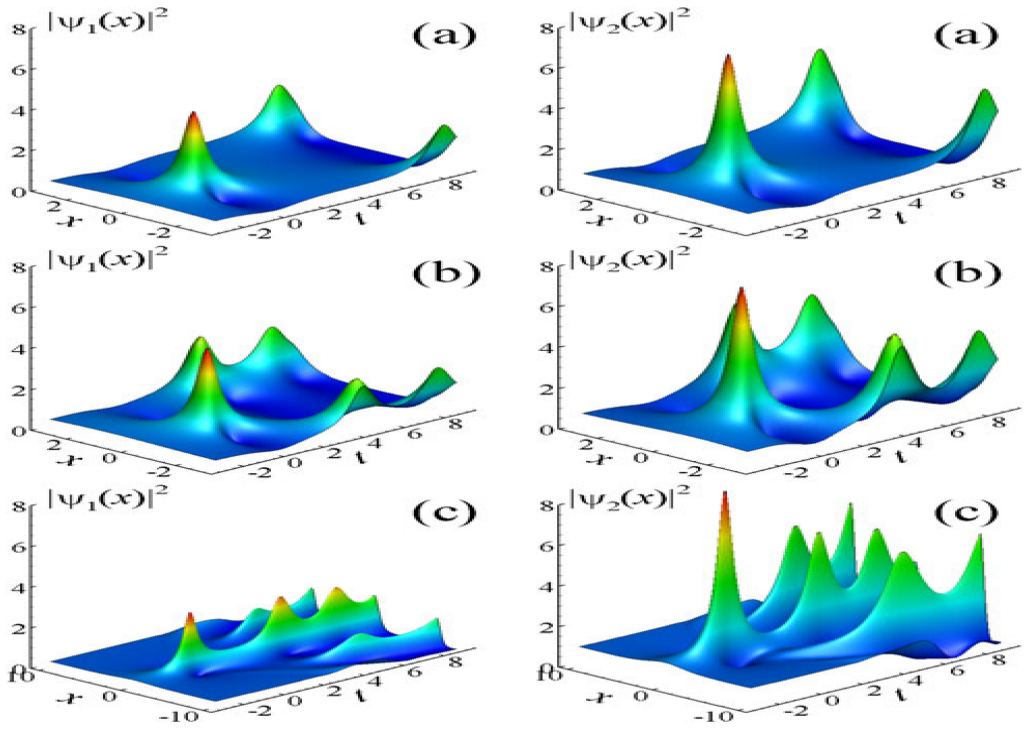

Figure 21: Rogue waves in binary mixtures without linear coupling. Vector rogue waves for the case when the parameters are $g_1 = 0.5$, $g_2 = -0.7$, $g = 1$ ($\Delta < 0$). The numerical results are made for the initial conditions given by the equation (1.6) with $\delta = 0$ at $t = -3$ (panel a); with shifted maxima of the component along the x-axis (panel b); with deturned amplitudes of the coefficients (panel c). [161].

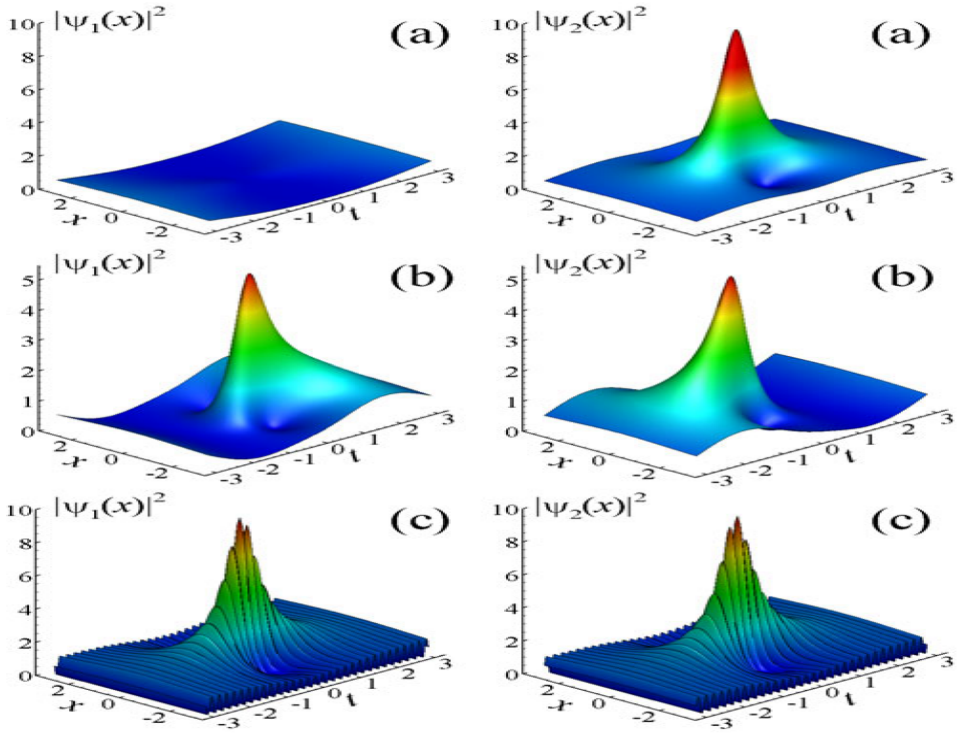

Figure 22: Rogue waves in binary mixtures with linear coupling. Vector rogue waves profile for $g_{1,2} = g = -1$, $\alpha = \pi/4$, $t_0 = -3$ and linear coupling with (a) $b = 1$, (b) $b = 2$ and (c) $b = 15$ [161].

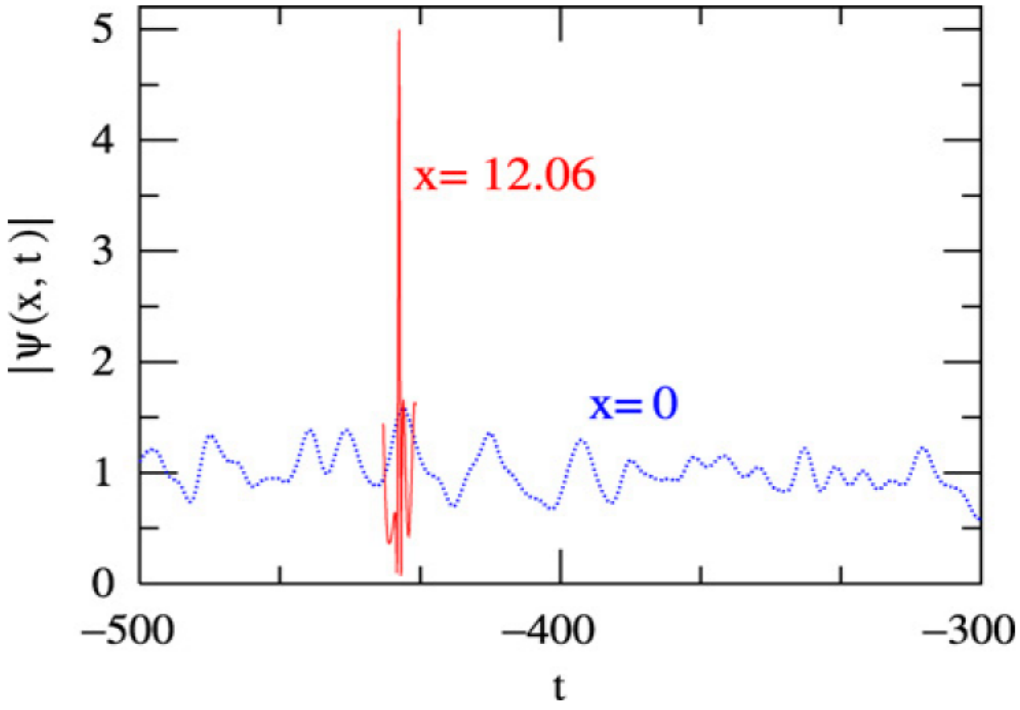

Figure 23: Typical example of a small fraction of the initial condition in the form of a plane wave perturbed by a random function $f(t)$ (dotted blue line) with an amplitude of $\mu = 0.6$, where the mean width of the irregularities is $t = 3.9$. The full temporal interval is much wider and extends from $t = -1000$ to $t = 1000$. The red solid curve shows part of the field modulus, $|\psi|$, at $x = 12.06$ where it reaches its highest value, viz. 5 [158].

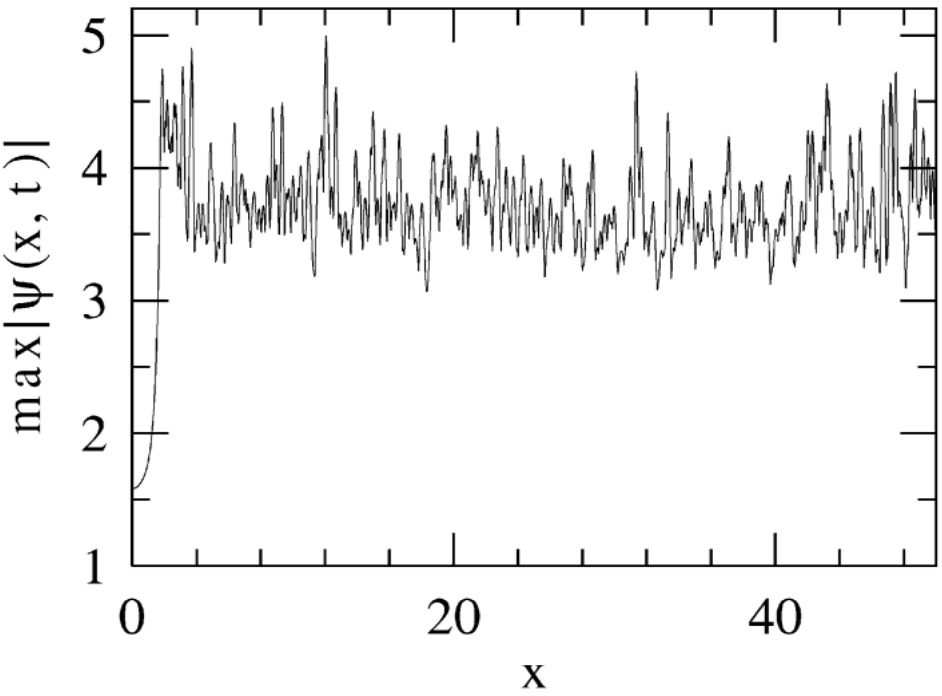

Figure 24: The maximum of the chaotic field $f(t) = |\psi(x = const, t)|$ vs. propagation distance, x, for the case of the initial condition partially represented in Figure (23). Note that the average amplitude of the two-dimensional field, $|\psi(x, t)|$, is around 1, i.e. it is much lower. The highest maximum in this simulation is 5. It appears at $x = 12.06$ [158].

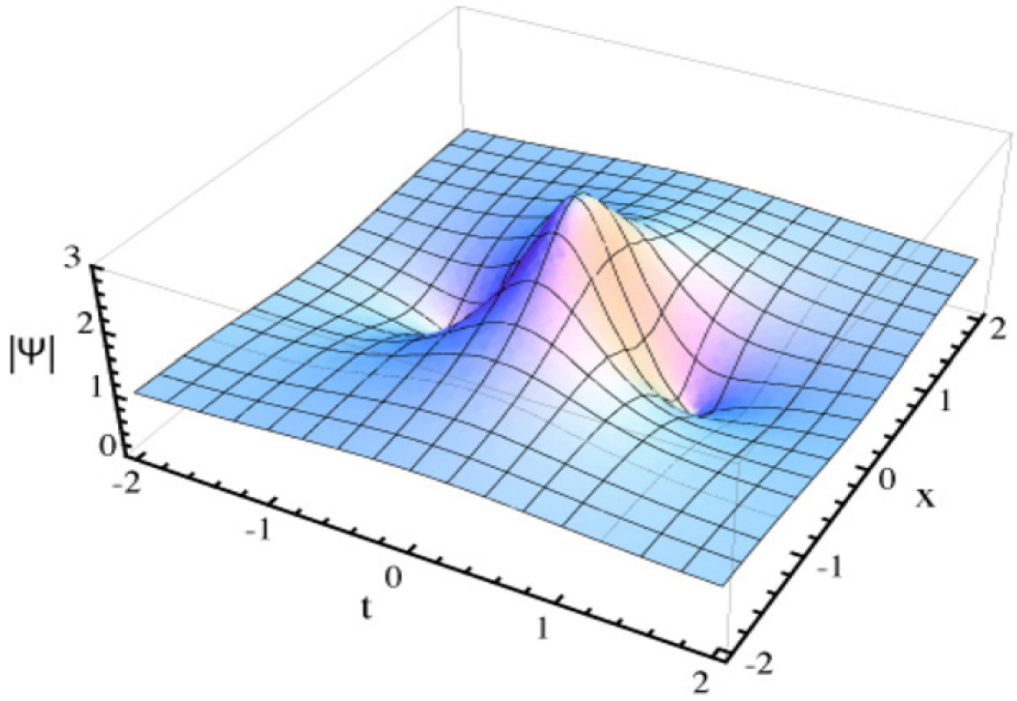

Figure 25: First-order rational solution to the NLSE. [158].

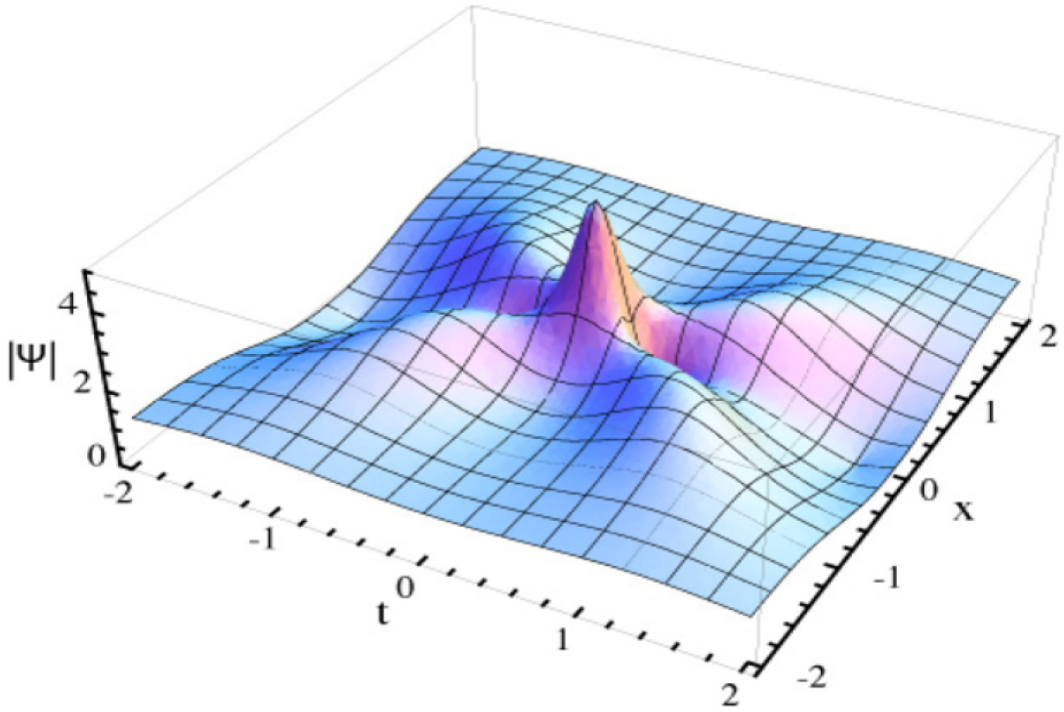

Figure 26: Higher-order rational solution to the NLSE. [158].

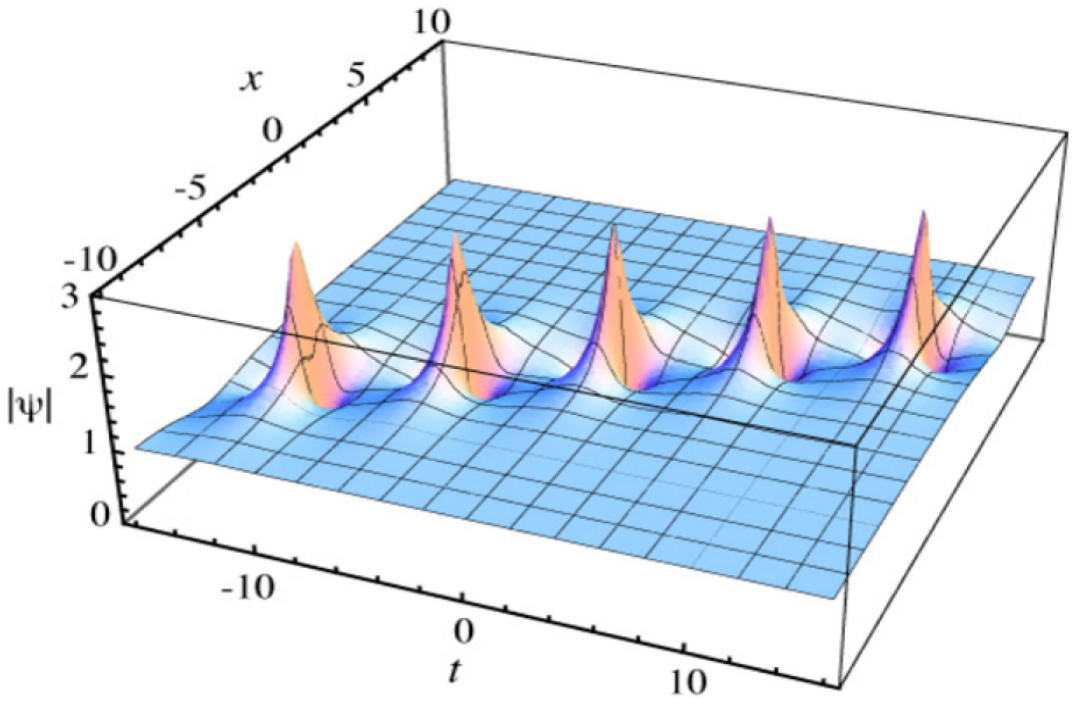

Figure 27: Single Akhmediev breather with nonzero velocity. The eigenvalue is: $l_1 = 0.08 + i0.9$ [158].

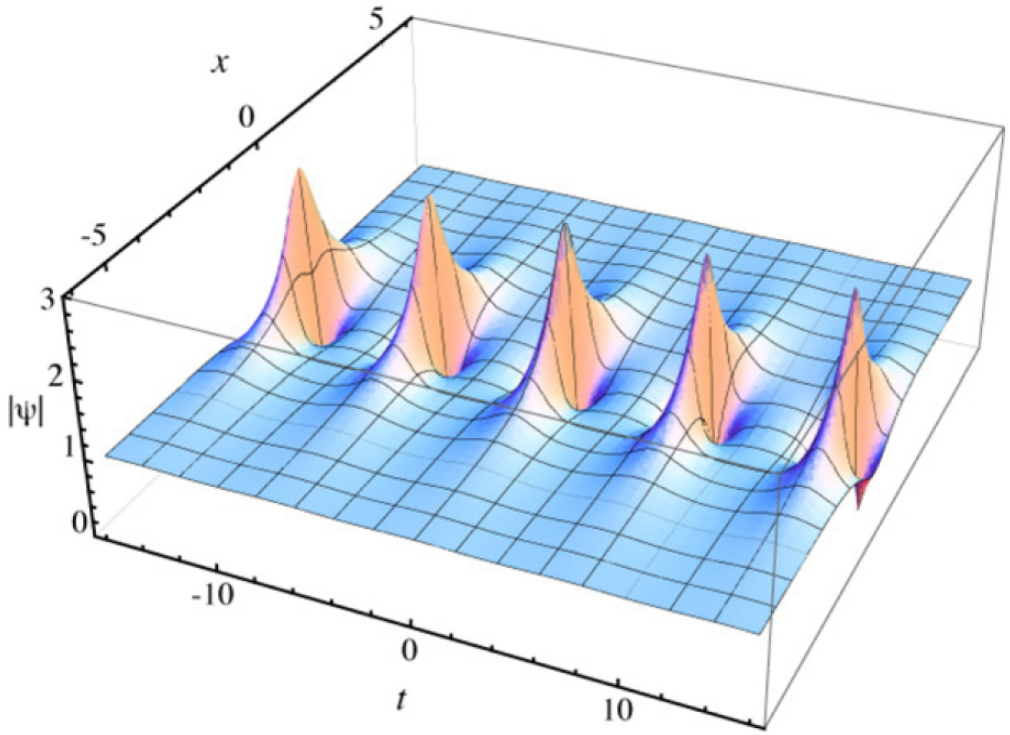

Figure 28: Single Akhmediev breather with zero velocity. It corresponds to the eigenvalue $l_1 = i0.9$ [158].

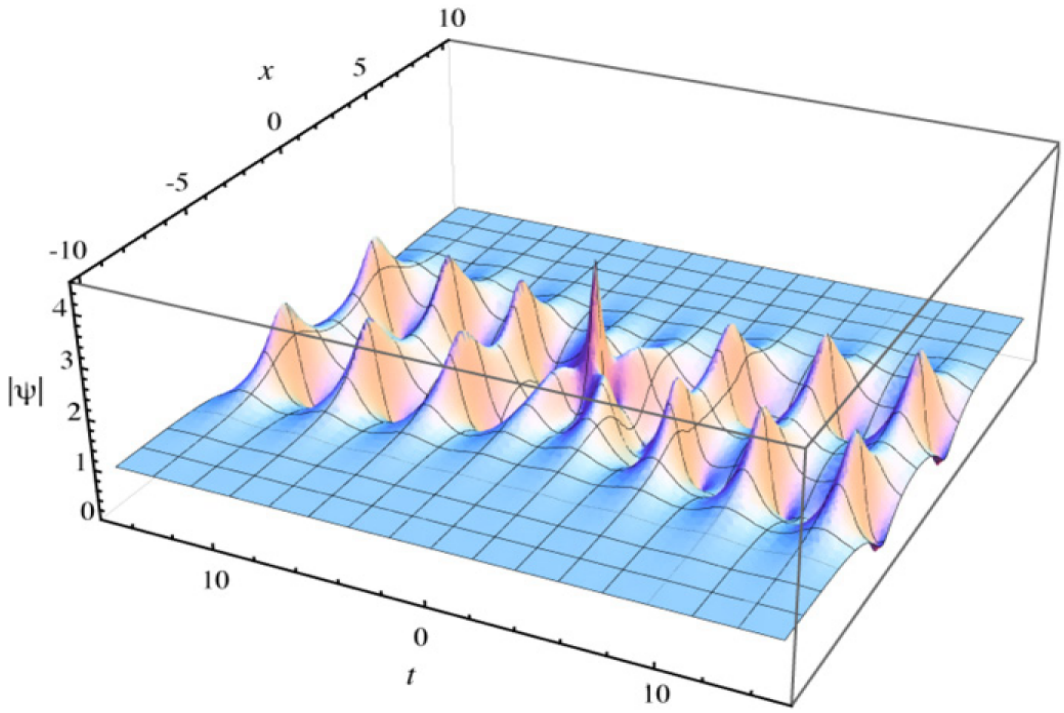

Figure 29: Collision of two Akhmediev breathers with zero velocities. The eigenvalues are: $l_1 = i0.6$ and $l_2 = -i0.7$ [158].

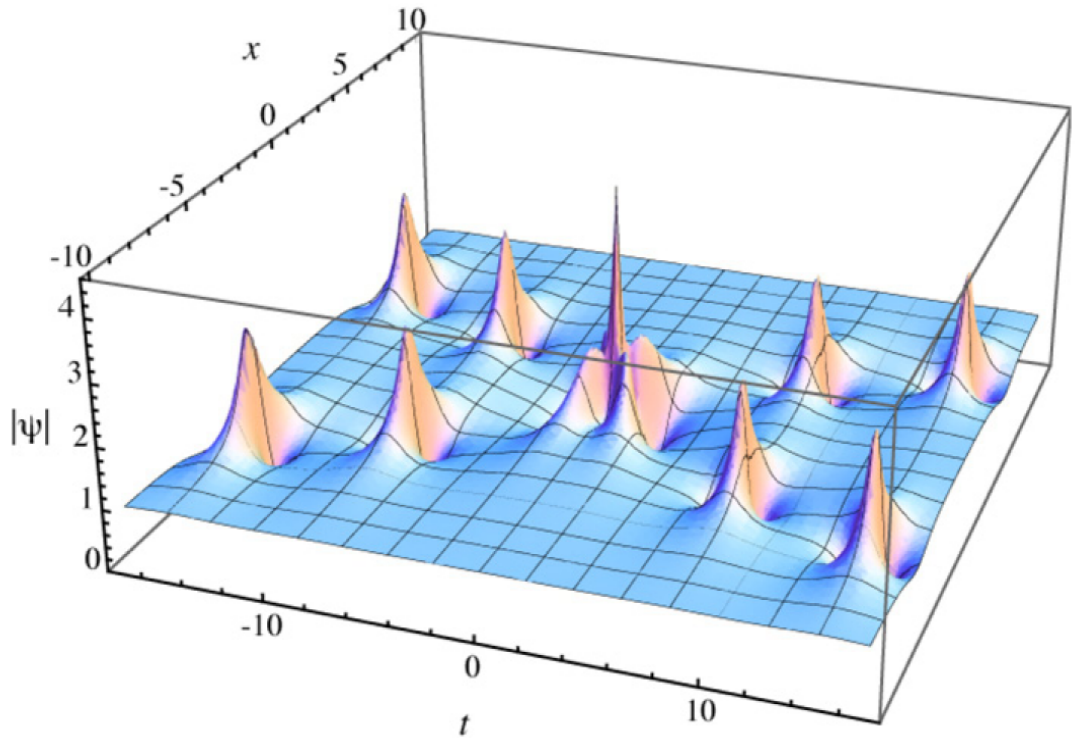

Figure 30: Collision of two Akhmediev breathers with nonzero velocities. The eigenvalues are: $l_1 = 0.05 + i0.9$ and $l_2 = -0.05 + i0.9$ [158].

Chapter 2

Methodologies of investigation: The Darboux matrix method an the homoclinic test approach .

Introduction

The general scheme for solving the NLSE from given initial conditions is the inverse scattering technique [91]. Certain classes of solutions can also be constructed with the use of dressing methods. A particular case of the latter is the so-called *Darboux transformation* (DT) [92]. The DT can be used to construct multisoliton solutions. Solutions of each class consist of corresponding hierarchy of solutions. rational solution belong to a special class and generally cannot be constructed using the traditional DT technique. The lowest-order rational solution or Peregrine soliton can be obtained either as a limiting case of an Akhmediev breather. Obtaining higher-order rational solutions in a similar procedure would be highly involved although not completely impossible. Thus the traditional DT has been modified such a way that limits are taken in the intermediate calculations. This modification allows to find a way to construct the whole hierarchy of rational solutions. A new method, homoclinic breather limit method (HBLM), for seeking rogue wave solution of nonlinear evolution equation is proposed. A new family of homoclinic breather wave solution, and rational homoclinic solution (homoclinic rogue wave) for the Davey-Stewartson I (DSI) and DSII equations are obtained using the extended homoclinic test method and

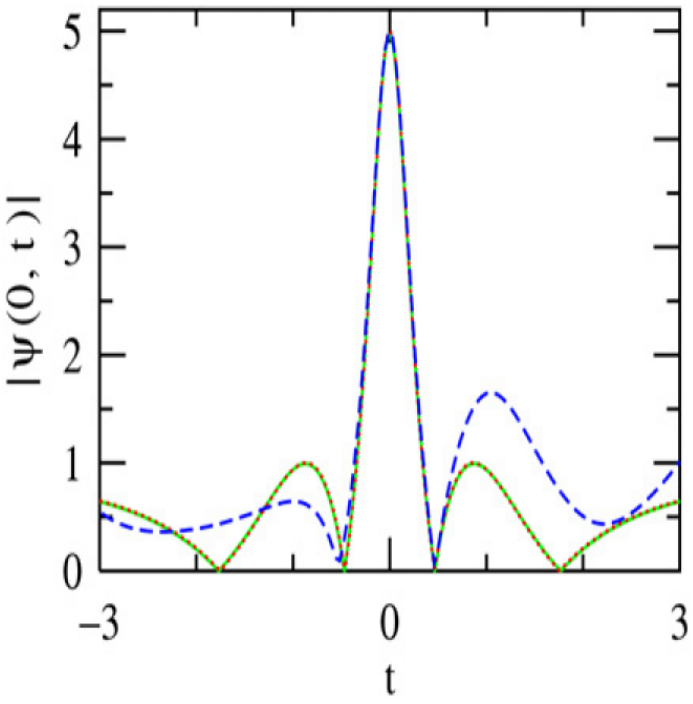

Figure 31: (Dashed blue line) Amplitude profile of the chaotic wave along t around the point of the highest maximum amplitude in Figure (24). It is compared with (dotted red line) the higher-order rational solution of the NLSE and (green solid line) with the collision of two ABs with $l_{1,2} = \pm 0.05 + 0.99$ [158].

homoclinic breather limit method (HBLM), respectively. Moreover, rogue wave solution is exhibited as period of periodic wave in homoclinic breather wave approaches to infinite.This result shows that rogue wave can be generated by extreme behavior of homoclinic breather wave for higher dimensional nonlinear wave fields.

2.1 Original Darboux transformation

In 1882, G. Darboux [93] studied the eigenvalue problem of a linear partial differential equation of second order (now called the one- dimensional Schrödinger equation)

$$-\phi_{xx} - u(x)\phi = \lambda\phi \tag{2.1}$$

Here $u(x)$ is a given function, called potential function; λ is a constant, called spectral parameter. He found out the following fact. If $u(x)$ and $\phi(x, \lambda)$ are two functions satisfying

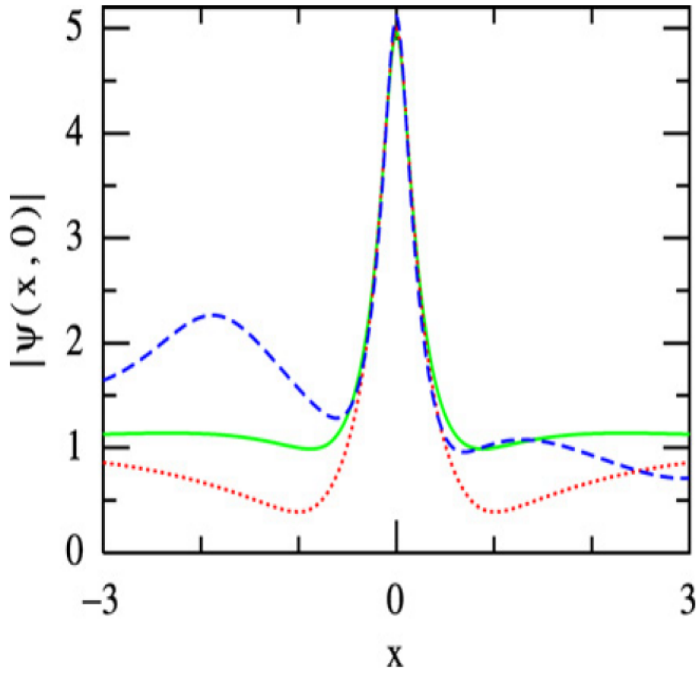

Figure 32: Amplitude profiles around the highest maximum along the x-direction. The notations are the same as in Figure (31) [158].

2.1 and $f(x) = \phi(x, \lambda_0)$ is a solution of the equation 2.1, for $\lambda = \lambda_0$ where λ_0 is a fixed constant, then the functions u' and ϕ' defined by

$$u' = u + 2(\ln f)_{xx}, \qquad \phi'(x, \lambda) = \phi_x(x, \lambda) - \frac{f_x}{f}\phi(x, \lambda), \tag{2.2}$$

satisfy

$$-\phi'_{xx} - u(x)\phi' = \lambda\phi', \tag{2.3}$$

which is of the same form as 2.1. Therefore, the transformation 2.2 transforms the functions (u, ϕ) to (u', ϕ') which satisfy the same equations. This transformation (u, ϕ) $\rightarrow$ (u', ϕ') is the original Darboux transformation, which is valid for $f \neq 0$.

Then explicit calculation from 2.2 gives new special solutions of 2.1. Since ϕ' is known, it is not necessary to solve any linear differential equations again to obtain (u'', ϕ''). That is, we only need algebraic calculation to get (u'', ϕ'')etc.: $(u, \phi) \rightarrow (u', \phi') \rightarrow (u'', \phi'') \rightarrow \cdots (u^n, \phi^n) \rightarrow$. Here the superscripts denote the order of the solution to the system.

2.1.1 Darboux transformation of the modified KdV equation.

The method of Darboux transformation can be applied to many equations such as the modified KdV equation (MKdVE). the sine-Gordon equation etc. The MKdVE is given as follows

$$u_t + 6u^2u_x + u_{xxx} = 0. \tag{2.4}$$

Its integrability is ensured by the following over-determined linear system [166]

$$\Phi_x = U\Phi, \qquad \Phi_t = V\Phi, \tag{2.5}$$

where $U = \begin{pmatrix} \lambda & u \\ -u & -\lambda \end{pmatrix}$ and $V = \begin{pmatrix} -4\lambda^3 - 2u^2\lambda & -4u\lambda^2 - 2u_x\lambda - 2u^3 - u_{xx} \\ 4u\lambda^2 - 2u_x\lambda + 2u^3 + u_{xx} & 4\lambda^3 + 2u^2\lambda \end{pmatrix}$
,

that is, (2.4) is the necessary and sufficient condition for $\Phi_{xt} = \Phi_{tx}$ being an identity. The system (2.5) is called a Lax pair of (2.4) and λ a spectral parameter. Here Φ may be regarded as a column solution or a 22 matrix solution of (2.5)

For a given solution u of the MKdVE, suppose we know a fundamental solution of (2.5)

$$\Phi(x,t,\lambda) = \begin{pmatrix} \Phi_{11} & \Phi_{12} \\ \Phi_{21} & \Phi_{22} \end{pmatrix} \tag{2.6}$$

which composes two linearly independent column solutions of (2.5).

Let λ_1 , μ_1 be arbitrary real numbers and

$$\sigma = \frac{\Phi_{22} + \mu_1\Phi_{21}}{\Phi_{12} + \mu_1\Phi_{11}} \tag{2.7}$$

be the ratio of the two entries of a column solution of the Lax pairs given in (2.5).

Construct the matrix

$$D(x,t,\lambda) = \lambda I - \frac{\lambda_1}{1+\sigma^2}\begin{pmatrix} 1-\sigma^2 & 2\sigma \\ 2\sigma & \sigma^2 - 1 \end{pmatrix} \tag{2.8}$$

and let $\Phi^{'}(x,t,\lambda) = D(x,t,\lambda)\Phi(x,t,\lambda)$. Then it is easily verified that $\Phi^{'}(x,t,\lambda)$ satisfies

$$\Phi^{'}_x = U^{'}\Phi^{'}, \qquad \Phi^{'}_t = V^{'}\Phi^{'}, \tag{2.9}$$

where $U^{'} = \begin{pmatrix} \lambda & u^{'} \\ -u^{'} & -\lambda \end{pmatrix}$ and $V^{'} = \begin{pmatrix} -4\lambda^3 - 2u^{'2}\lambda & -4u^{'}\lambda^2 - 2u^{'}_{x}\lambda - 2u^{'3} - u^{'}_{xx} \\ 4u^{'}\lambda^2 - 2u^{'}_{x}\lambda + 2u^{'3} + u_{xx} & 4\lambda^3 + 2u^{'2}\lambda \end{pmatrix}$ with

$$u^{'} = u + \frac{4\lambda_1\sigma}{1+\sigma^2} \tag{2.10}$$

equation (2.9) is similar to (2.5). The only difference is that u is replaced by $u^{'}$ given in equation (2.10). For any solution Φ of (2.5), $D\Phi$ is a solution of (2.9), hence (2.9) is solvable for any given initial data (the value of Φ at some point (x_0, t_0)). In other words, (2.9) is integrable. The integrability condition of (2.9) implies that u is also a solution of the MKdVE. Using this method, we obtain a new solution of the MKdVE together with the corresponding fundamental solution of its Lax pair from a known one.

The above conclusions can be summarized as follows. Let u be a solution of the MKdVE and Φ be a fundamental solution of its Lax pairs. Take λ_1 , μ_1 to be two arbitrary real constants, and let σ be defined by (2.7), then (2.10) gives a new solution u of the MKdVE, and the corresponding solution to the Lax pair can be taken as $D\Phi$. The transformation $(u, \Phi) \rightarrow (u^{'}, \Phi^{'})$ is the Darboux transformation for the MKdVE. This Darboux transformation in matrix form can be done successively and purely algebraically as $(u, \Phi) \rightarrow (u^{'}, \Phi^{'}) \rightarrow (u^{''}, \Phi^{''}) \cdots$

Single and double soliton solution to the MKdVE

Starting with the trivial solution $u = 0$ of the MKdVE, one can use the Darboux transformation to obtain the soliton solutions. For $u = 0$, the fundamental solution of the Lax pair can be obtained as

$$\Phi(x, t, \lambda) = \begin{pmatrix} \exp(\lambda x - 4\lambda^3 t) & 0 \\ 0 & \exp(-\lambda x + 4\lambda^3 t) \end{pmatrix} \tag{2.11}$$

by integrating (2.5). Taking $\lambda_1 \neq 0$ and $\mu_1 = \exp(2\alpha_1) > 0$, then (2.7) is reduced to

$$\sigma = \sigma_1 = \exp(-2\lambda_1 x + 8\lambda_1^3 t - 2\alpha_1), \tag{2.12}$$

hence

$$D = \lambda I - \frac{\lambda_1}{\cosh v_1} \begin{pmatrix} \sinh v_1 & 1 \\ 1 & -\sinh v_1 \end{pmatrix}, \tag{2.13}$$

where $v_1 = 2\lambda_1 x + 8\lambda_1^3 t - 2\alpha_1$. Then equation (2.10) gives the single soliton solution to the MKdVE written as follows

$$u^{'} = 2\lambda_1 sech(v_1). \tag{2.14}$$

If we take $u^{'}$ as a seed solution, a new Darboux matrix can be constructed from $\Phi^{'}$ and a series of new solutions of the MKdVE can be obtained.

We write down the second Darboux transformation explicitly. Suppose u is a solution of the MKdVE (2.4) , Φ is a fundamental solution of the corresponding Lax pair (2.5). Construct the Darboux matrix $D = (D_{ij})$ according to (2.7) and (2.9) and let $\sigma = \sigma_1$. Moreover, take constants $\lambda_2 \neq 0$ ($\lambda_2 \neq \lambda_1$) and $\mu_2 = \exp(2\alpha_2)$. According to equation (2.7)

$$\sigma_2^{'}(x,t,\lambda_2) = \frac{\Phi_{22}^{'} + \mu_2 \Phi_{21}^{'}}{\Phi_{12}^{'} + \mu_2 \Phi_{11}^{'}}. \tag{2.15}$$

Substituting $\Phi^{'} = D\Phi$ into it we obtain

$$\sigma_2^{'}(x,t,\lambda_2) = \frac{D_{21} + D_{22}\sigma_2}{D_{11} + D_{12}\sigma_2}, \tag{2.16}$$

where $\sigma_2 = \sigma_2(\lambda_2) = \frac{\Phi_{22} + \mu_2 \Phi_{21}}{\Phi_{12} + \mu_2 \Phi_{11}}$.

Using the expression of D given in (2.13), we have

$$\Phi^{'}(x,t,\lambda) = \begin{pmatrix} (\lambda - \lambda_1 \tanh v_1) e^{\lambda x - 4\lambda^3 t} - \lambda_1 sech v_1 e^{-\lambda x + 4\lambda^3 t} \\ -\lambda_1 sech v_1 e^{\lambda x - 4\lambda^3 t} (\lambda + \lambda_1 \tanh v_1) e^{-\lambda x + 4\lambda^3 t} \end{pmatrix}, \tag{2.17}$$

hence

$$\sigma_2^{'} = \frac{-\lambda_1 sech v_1 + (\lambda_2 + \lambda_1 \tanh v_1) e^{-v_2}}{\lambda_2 - \lambda_1 \tanh v_1 - \lambda_1 sech v_1 e^{-v_2}}, \tag{2.18}$$

where $v_2 = 2\lambda_2 x - 8\lambda_2^3 t + 2\alpha_2$. According to the single soliton solution, we obtain the following

$$u^{''} = \frac{2(\lambda_2^2 - \lambda_1^2)(\lambda_2 \cosh v_1 - \lambda_1 \cosh v_2)}{(\lambda_2^2 + \lambda_1^2)\cosh v_1 \cosh v_2 - 2\lambda_1 \lambda_2 (1 + \sinh v_1 \sinh v_2)}. \tag{2.19}$$

This is called the double soliton solution of the MKdVE.

Thus, the original Darboux transformation is not sufficient to derive higher-order wave solution. Then Guo and coworkers [94] have introduced the so called generalized Darboux transformation. That is what we are going to discuss in the next section.

2.2 Generalized Darboux transformation

2.2.1 Generalized Darboux transformation of the KdV equation

This work was reported in reference [94]. First of all, let us present the well-known classical Darboux transformation (DT) KdV equation.

Considering the Sturm-Liouvile equation

$$-\Phi_{xx} + u\Phi = \lambda\Phi \tag{2.20}$$

and introduicing the following first-order operator

$$T[1] = \partial_x - \frac{\Phi_{1x}}{\Phi_1},$$

where Φ_1 is the fixed solution of (2.20) with $\lambda = \lambda_1$, then the DT

$$\Phi[1] = T[1]\Phi = \frac{Wr(\Phi_1, \Phi)}{\Phi_1} \tag{2.21}$$

converts equation (2.20) into

$$-\Phi[1]_{xx} + u[1]\Phi[1] = \lambda\Phi[1], \tag{2.22}$$

where $u[1] = u - 2(\ln\Phi_1)_{xx}$ and $Wr(\Phi_1\Phi) = \Phi_1\Phi_x - \Phi_{1x}\Phi$ is the standard Wronskian determinant.

The N-times iterated or n-fold DT yields the Crum theorem

$$-\Phi[N]_{xx} + u[N]\Phi[B] = \lambda\Phi[N], \qquad u[N] = u - 2(\ln\Phi_1)_{xx} \tag{2.23}$$

where $\Phi[N] = \frac{Wr(\Phi_1,\cdots,\Phi_N,\Phi)}{Wr(\Phi_1,\cdots,\Phi_N)}$ and $\Phi_1, \cdots, \Phi_N$ are solution of (2.20) at $\lambda = \lambda, \cdots, \lambda_N$.

It is obvious that $\Phi_1[1] = T[1]\Phi_1 = 0$, namely Φ_1 is mapped to a trivial solution. This fact implies that a seed solution may not be used more than once when considering the iterations for the DT. However, as pointed out in reference [92], a generalized DT does exist. Then this result have to be derived in a way which may be readily generalized. We start with the assumption that

$$\Phi_2 = \Phi_1(k_1 + \varepsilon), \tag{2.24}$$

where $k_1 = f(\lambda_1)$ is a monotonic function and ε is a small parameter. Expanding Φ_2 in a series in ε, we get

$$\Phi_2 = \Phi_1 + \Phi_1^{[1]}\varepsilon + \Phi_1^{[2]}\varepsilon^2 + \cdots,$$

where $\Phi_1^{[i]} = \frac{1}{i!}\frac{\partial^i \Phi_1(k)}{\partial k^i}|_{k=k_1}$. Since $\Phi_2[1] = T_1[1]\Phi_1$ is a solution to equation (2.21), so is $\frac{\Phi_2[1]}{\varepsilon}$. Taking the limit $\varepsilon \to 0$for this solution, we find

$$\Phi_1[1] = \lim_{\varepsilon\to 0}\frac{T[1]\Phi_1(k_1+\varepsilon)}{\varepsilon} = T[1]\Phi_1^{[1]}, \tag{2.25}$$

which is a nontrivial solution for (2.21) at $\lambda = \lambda_1$. This solution may be adopted to do the second-step DT, that is,

$$T[2] = \partial - \frac{\Phi_{1,x}[1]}{\Phi_1[1]}, \qquad u[2] = u - 2(\ln Wr(\Phi_1, \Phi_1^{[1]}))_{xx}. \tag{2.26}$$

Combining these two DT, we obtain

$$-\Phi[2]_{xx} + u[2]\Phi[2] = \lambda\Phi[2], \qquad \Phi[2] = \frac{Wr(\Phi_1, \Phi_1^{[1]}, \Phi)}{Wr(\Phi_1, \Phi_1^{[1]})}.$$

This process may be continued and results in the so called generalized DT for the system (2.20). Indeed, let $\Phi_1, \Phi_2, \cdots \Phi_N$ n different solution for (2.20) at $\lambda_1, \lambda_2, \cdots, \lambda_n$, and consider the expansions

$$\Phi_i(k_i+\varepsilon) = \Phi_1(k_i) + \Phi_1^{[1]}\varepsilon + \cdots + \Phi_i^{[m_i]} + \cdots,$$

with $k_i = f(\lambda_i) \quad (i = 1, 2, \cdots, n)$ then we have the following

$$u[N] = u - 2(\ln(W1))_{xx}, \qquad \Phi[N] = \frac{W_2}{W_1}, \tag{2.27}$$

with $W_1 = Wr(\Phi_1, \cdots, \Phi_1^{[m_1]}, \Phi_2, \cdots, \Phi^{[m_2]}, \cdots, \Phi_n, \cdots, \Phi_2^{[m_n]})$ and

$W_2 = Wr(\Phi_1, \cdots, \Phi_1^{[m_1]}, \Phi_2, \cdots, \Phi^{[m_2]}, \cdots, \Phi_n, \cdots, \Phi_2^{[m_n]}, \Phi)$

solve

$-\Phi[N]_{xx} + u[N]\Phi[N] = \lambda\Phi[n]$, where $m_1 + m_2 + \cdots m_n = N - n$, $m_i \geq 0$, $m_i \in Z$.

The generalized Darboux transformation (GDT) presented above may be used to generate both solitons and rational solutions for the KdV equation. Let us illustrate this with the following examples. It is well known that the KdV equation,

$$u_t - 6uu_x + u_{xx} = 0, \tag{2.28}$$

takes (2.20) as its spatial part of the spectral problem and the corresponding temporal part reads

$$\Psi_t = -4\Psi_{xxx} + 6u\Psi_x + 3u_x\Psi.$$

In the case of N distinct spectral parameters, we will have the Wronskian representation for the N-soliton solution. To get rational solutions, one starts with the seed solution $u = c$, where c is a real constant and $\Psi_1 = \sin[k_1(x + (4k_1^2 + 6c)t) + p(k_1)]$, $k_1 = \sqrt{\lambda_1 - c}$ and $p(k_1)$ is a polynomial of k_1. Now expanding the function Ψ_1 at $k_1 = 0$ and taking $p(k_1) = 0$ for convenience, we have

$$\Psi_1 = (x+6ct)k_1+[-1/6(x+6ct)^3+4t]k_1^3+[1/120(x+6ct)^5-2t(x+6ct)^5-2t(x+6ct)^2]k_1^5+\cdots,$$

therefore, $\Psi_1^{[0]} = x + 6ct$, $\Psi_1^{[1]} = -1/6(x + 6ct)^3 + 4t$, $\Psi_1^{[2]} = 1/120(x + 6ct)^5 - 2t(x + 6ct)^5 - 2t(x + 6ct)^2$.

Then the generalized Darboux transformation provides us the rational solution for the KdV equation. Namely,

$$u[3] = c + \frac{G}{H^2},$$

where $G = 12[279936c^5t^5(216c^5t^5 + 360c^4xt^4 + 270c^3x^2t^3 + 120c^2x^3t^2 + 35cx^4t + 7x^5) + 38880c^4t^4(180t^2 + 7x^6) + 25920c^3xt^3(x^6 + 180t^2) + 1620c^2x^2t^2(x^6 + 720t^2) + 60ct(x^9 + 2160t^2x^3 + 4320t^3) + 43200t^3x + x^{10} + 5400x^4t^2]$,

$H = 3888c^4t^4(12c^2t^2+12cxt+5x^2)+4320c^3t^3(x^3+3t)+540c^2xt^2(x^3+12t)+36cx^2t(x^3+30t) + x^6 - 720t^2 + 60x^3t$.

The positon solutions for the KdV equation may be found in this way, according to the work done in reference [167].

2.2.2 Generalized Darboux transformation and rogue wave solution to the nonlinear Schrödinger equation

In this section, we extend the idea discussed in the previous section to the nonlinear Schrödinger (NLS) equation and construct a generalized Darboux transformation for it. Furthermore, we show that this Darboux transformation enables one to obtain, apart from the soliton solutions, rational solutions including multi-rogue-wave solutions.

The focusing NLS equation

$$iq_t + \frac{1}{2}q_{xx} + |q|^2 q = 0,$$

is the compatibility condition of the linear spectral problems,

$$\begin{aligned} \Psi_x &= [i\zeta\sigma_1 + iQ]\Phi, \\ \Psi_t &= [i\zeta^2\sigma_1 + i\zeta Q + \tfrac{1}{2}\sigma_1(Q_x - iQ^2)]\Psi, \end{aligned} \tag{2.29}$$

where $\sigma_1 = \begin{pmatrix} 1 & 0 \\ 0 & -1 \end{pmatrix}$, $Q = \begin{pmatrix} 0 & q^* \\ q & 0 \end{pmatrix}$.

Now we manage to find a generalized Darboux transformation. As in the last section, suppose that $\Psi_2 = \Psi_1(\zeta_1 + \delta)$ is a special solution for system, then after transformation we have $\Psi_2[1] = T_1[1]\Psi_2$. Expanding Ψ_2 at ζ_1, we have

$$\Psi = \Psi_1^{[0]} + \Psi_1^{[1]}\delta + \Psi_1^{[2]}\delta^2 + ... + \Psi_1^{[N]}\delta^N, \tag{2.30}$$

where $\Psi_1^{[k]} = \frac{1}{k!}\frac{\partial^k}{\partial\zeta^k}\Psi_1(\zeta)|_{\zeta=\zeta_1}$.

Through the limit process

$$\lim_{\delta\to 0}\frac{T[1]|_{\zeta=\zeta_1+\delta}\Psi_2}{\delta} = \lim_{\delta\to 0}\frac{(\delta + T_1[1])\Psi_2}{\delta} = \Psi_1^{[0]} + T_1[1]\Psi_1^{[1]} \equiv \Psi_1[1], \tag{2.31}$$

we find a solution to the linear system given in (2.29) with $q[1]$ and $\zeta = \zeta_1$. This allows us to go to the next step of the Darboux transformation, namely,

$$\begin{aligned} T_1[2] &= \zeta - \zeta_1^* + (\zeta_1^* - \zeta_1)P_1[2], \\ q[2] &= q[1] + 2(\zeta_1^* - \zeta_1)(P_1[2])_{21}, \end{aligned} \tag{2.32}$$

where $P_1[2] = \frac{\Psi_1[1]\Phi_1[1]^\dagger}{\Psi_1[1]^\dagger\Phi_1[1]}$.

Similarly, the limit

$$\begin{aligned} \lim_{\delta\to 0}\frac{[T[2]T[1]]|_{\zeta=\zeta_1+\delta}\Psi_2}{\delta^2} &= \lim_{\delta\to 0}\frac{(\delta + T_1[2])(\delta + T_1[1])\Psi_1}{\delta^2} \\ &= \Psi_1^{[0]} + (T_1[2] + T_1[1])\Psi_1^{[1]} \\ &\quad + T_1[2]T_1[1]\Psi_1^{[2]} \equiv \Psi_1[2], \end{aligned} \tag{2.33}$$

provides us a nontrivial solution for the linear spectral problem with $q = q[2]$ and $\zeta = \zeta_1$. Thus we may do the third-step iteration of the Darboux transformation, which is the following

$$\begin{aligned} T_1[3] &= \zeta - \zeta_1^* + (\zeta_1^* - \zeta_1)P_1[3], \\ q[3] &= q[2] + 2(\zeta_1^* - \zeta_1)(P_1[3])_{21}, \end{aligned} \tag{2.34}$$

where $P_1[3] = \frac{\Psi_1[2]\Phi_1[2]^\dagger}{\Psi_1[2]^\dagger\Phi_1[2]}$.

Continuing the above process and combining all the Darboux transformation, a generalized Darboux transformation is constructed.

Let us consider an example to illustrate the application of the above formulas to the construction of higher rogue wave solutions. To this end, we start with the seed solution $q[0] = e^{it}$. The corresponding solution for the linear spectral problem at $\zeta = ih$ is

$$\Psi_1(f) = \begin{pmatrix} i(C_1e^A - C_2e^{-A})e^{-\frac{i}{2}t} \\ (C_2e^A - C_1e^{-A})e^{\frac{i}{2}t} \end{pmatrix} \tag{2.35}$$

with $C_1 = \frac{(h-\sqrt{h^2-1})^{1/2}}{\sqrt{h^2-1}}$, $C_2 = \frac{(h+\sqrt{h^2-1})^{1/2}}{\sqrt{h^2-1}}$ and $A = \sqrt{h^2-1}(x+iht)$.

Let $h = 1 + f^2$ expanding the vector function $\Psi_1(f)$ at $f = 0$, we have

$$\Psi_1(f) = \Psi(0) + \Psi_1^{[1]}f^2 + \cdots, \tag{2.36}$$

where $\Psi_1(0) = \begin{pmatrix} (-2t + 2ix - i)e^{-\frac{1}{2}it} \\ (2it + 2x + 1)e^{\frac{1}{2}it} \end{pmatrix}$,

$$\Psi_1^{[1]} = \begin{pmatrix} (\frac{i}{2}x - \frac{5}{2}t + \frac{i}{4} - 2tx^2 + \frac{2}{3}ix^3 - \frac{2}{3}t^3 - 2ixt^2 - ix^2 + 2tx + it^2)e^{-\frac{1}{2}t} \\ (\frac{1}{2}x + \frac{5}{2}it - \frac{1}{4} - 2itx^2 + \frac{2}{3}x^3 - \frac{2i}{3}t^3 - 2xt^2 + x^2 + 2itx - t^2)e^{\frac{1}{2}t} \end{pmatrix}.$$

It is clear that $\Psi_1(0)$ is a solution for (2.29) at $\zeta = i$. By means of the formula given in equation (2.31), we obtain

$$\Psi_1[1] = \lim_{f\to 0}\frac{[if^2 + T_1[1]]\Psi_1(f)}{f^2} = T_1[1]\Psi_1^{[1]} + i\Psi_1(0), \quad T_1[1] = 2i\left(I - \frac{\Psi_1(0)\Psi_1(0)^\dagger}{\Psi_1(0)^\dagger\Psi_1(0)}\right). \tag{2.37}$$

The above formulae yield the second-order rogue wave solution to the NLS equation. Namely,

$$q[2] = \left(1 + \frac{G_1 + itG_2}{H}\right)e^{it}, \tag{2.38}$$

with $G_1 = 36 - 288x^2 - 192x^4 - 1152t^2x^2 - 864t^2 - 960t^4$, $G_2 = 360 + 576x^2 - 192t^2 - 384x^4 - 768x^2t^2 - 384t^4$,

$H = 64t^6 + 192t^4x^2 + 432t^4 + 396t^2 + 192t^2x^4 - 288t^2x^2 + 9 + 108x^2 + 64x^6 + 48x^4$.

The corresponding plot in shown in Figure (33).

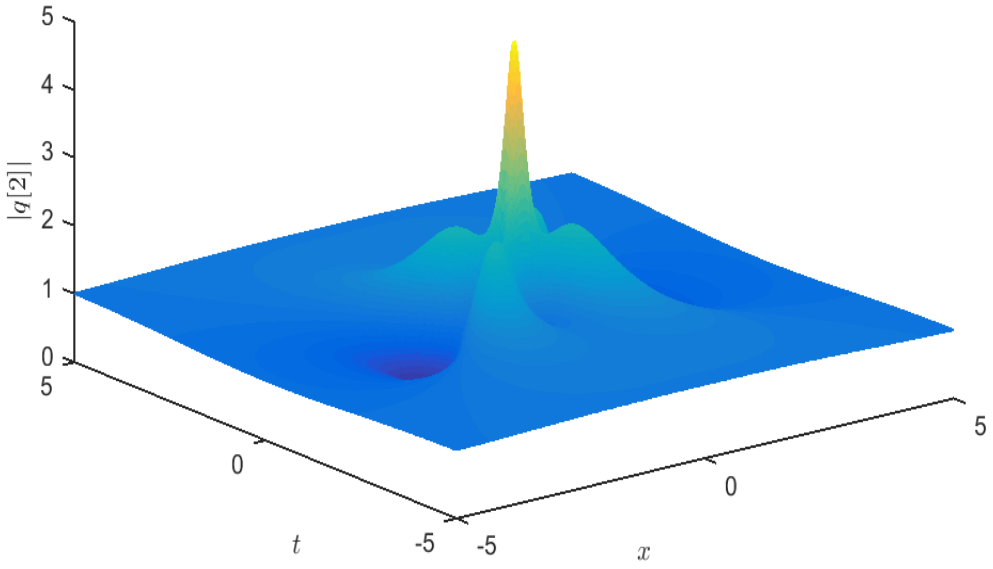

Figure 33: Second-order rogue wave solution the nonlinear Schrödinger equation (2.38).

2.2.3 Generalized Darboux transformation and rogue wave solution to the complex modified KdV equation.

We illustrate the generalized DT by showing its application in the work done by Zhaqilao [95].

In this work, the author have considered the complex modified Kdv equation given as follows

$$u_t + \frac{1}{2}u_{xxx} + 3|u|^2 u_x = 0, \tag{2.39}$$

which has many physical applications [96] including electrodynamics, electromagnetic wave in size-quantized films, internal waves for certain special density stratifications, elastic media and traffic flow. The Lax-pair ensure the total integrability of a nonlinear wave equation. Those of the equation 2.39 are given as

$$\Phi_x = U\Phi, \qquad \Phi_t = V\Phi, \tag{2.40}$$

with $U = \begin{pmatrix} \lambda & u \\ -u^* & -\lambda \end{pmatrix}$

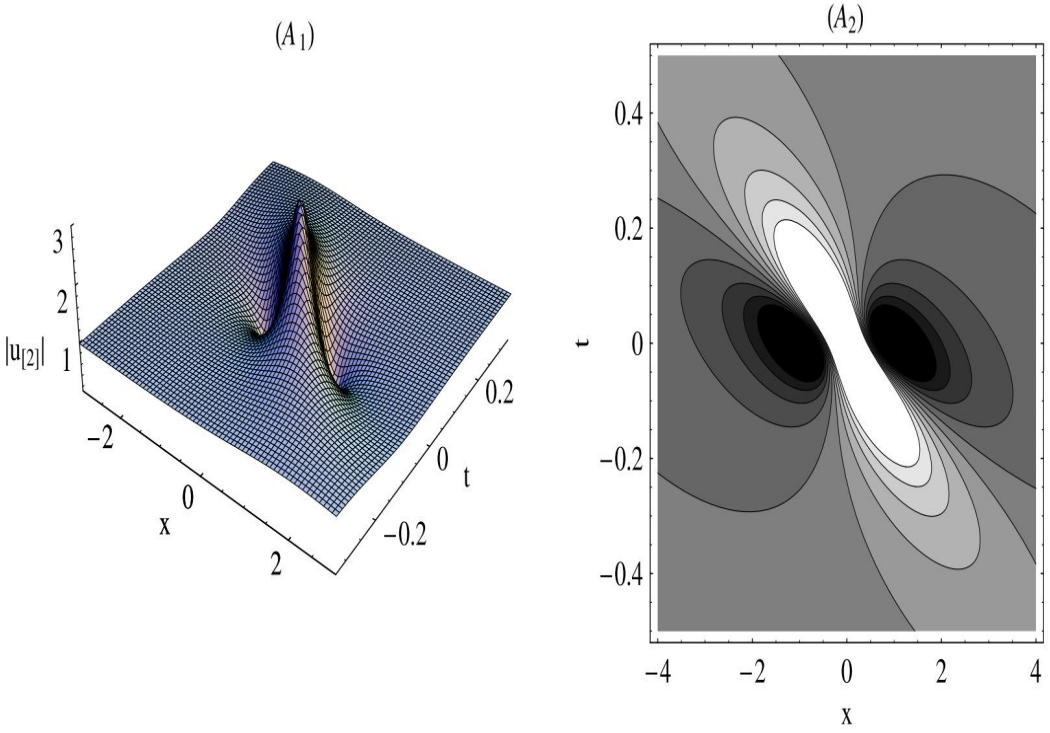

Figure 34: A_1 and A_2 express the first-order rogue wave to equation (2.39) [95]

and $V = \begin{pmatrix} -2\lambda^3 - \lambda|u|^2 + \frac{1}{2}(-u^*u_x + uu_x^*) & -2\lambda^2 u - \lambda u_x + \frac{1}{2}(-2|u|^2 u - u_{xx}) \\ 2\lambda^2 u^* - \lambda u_x^* + \frac{1}{2}(2|u|^2 u^* + u_{xx}^*) & 2\lambda^3 + \lambda|u|^2 - \frac{1}{2}(-u^*u_x + uu_x^*) \end{pmatrix}$, where $\Phi = (\psi(x,t), \phi(x,t))^T$, λ is the spectral parameter, u^* is the complex conjugate of the potential u. The equation 2.39 can be easily obtained by the zero curvature equation $U_t - V_x + [U, V] = 0$.

A DT is actually a special gauge transformation

$$\Phi[1] = T\Phi, \tag{2.41}$$

of solutions of the Lax-pairs given in equation 2.40. T is the Darboux matrix. It change the Lax-pairs of equation 2.40 into a new one, by on the same form, namely,

$$\Phi[1]_x = U[1]\Phi[1], \qquad \Phi[1]_t = V[1]\Phi[1], \tag{2.42}$$

where the matrices $U[1]$ and $V[1]$ have the same form as U and V, but have the new potential $u[1]$ therein.

Combining equation 2.41 and 2.42, we obtain the following,

$$U[1] = (T_x + TU)T^{-1}, \qquad V[1] = (T_t + TV)T^{-1}. \tag{2.43}$$

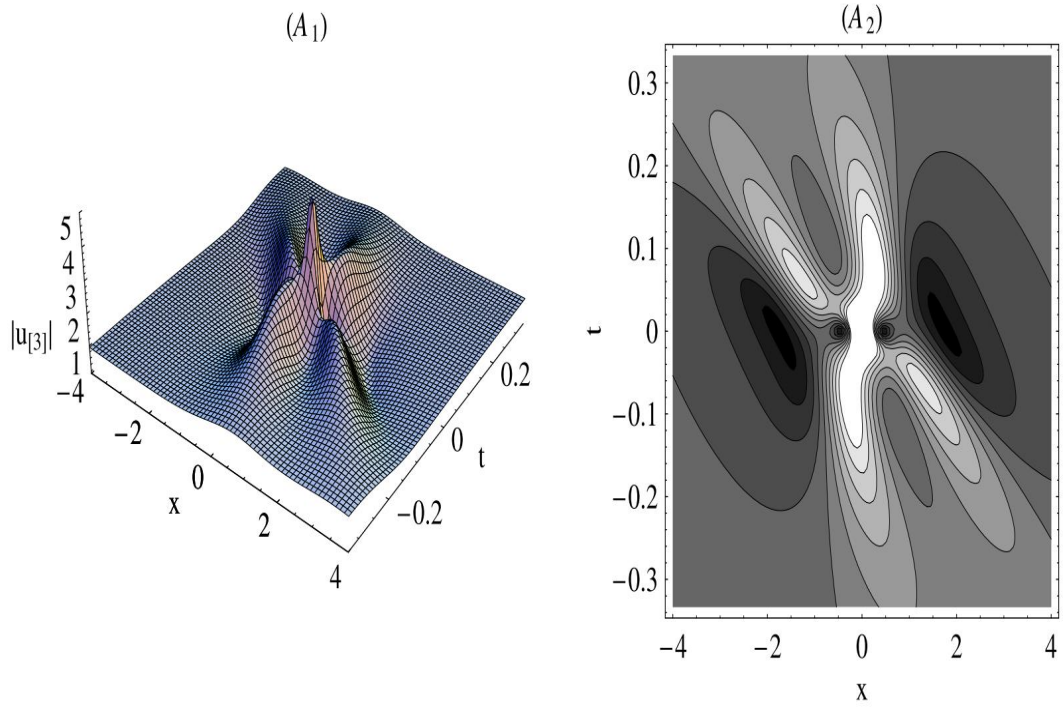

Figure 35: A_1 and A_2 show the second-order rogue wave solution to equation (2.39) [95]

From equation 2.43, it is possible to establish a relationship between the new potential $u[1]$ and the old one u. To this purpose, the Darboux matrix T is defined as

$$T = \lambda I - H\Lambda H^{-1}, \tag{2.44}$$

where $I = \begin{pmatrix} 1 & 0 \\ 0 & 1 \end{pmatrix}$, $H = \begin{pmatrix} \psi_1 & -\phi_1^* \\ \phi_1 & \psi_1^* \end{pmatrix}$, $\Lambda = \begin{pmatrix} \lambda_1 & 0 \\ 0 & -\lambda_1^* \end{pmatrix}$ and $\Phi_1 = (\psi_1, \phi_1)^T$ is a particular solution of the Lax-pairs given in equation 2.40 at $u = u[0]$, $\lambda = \lambda_1$. Therefore, after the action of the Darboux matrix T in equation 2.43, the elementary DT of the complex modified KdV equation 2.39 could be given by

$$\Phi_1[0] = T[0]\Phi_1, \quad u[1] = u[0] + 2\frac{(\lambda_1 + \lambda_1^*)\psi_1[0]\phi_1^*[0]}{|\psi_1[0]|^2 + |\phi_1[0]|^2} \tag{2.45}$$

and $T[1] = \lambda_2 I - H[0]\Lambda[1]H[0]^{-1}$,

where $T[0] = I$, $H[0] = \begin{pmatrix} \psi_1[0] & -\phi_1^*[0] \\ \phi_1[0] & \psi_1^*[0] \end{pmatrix}$, $\Lambda[1] = \begin{pmatrix} \lambda_1 & 0 \\ 0 & -\lambda_1^* \end{pmatrix}$, $\Phi_1[0] = (\psi_1[0], \phi_1[0])^T = (\psi_1, \phi_1)^T = \Phi_1$ and $u[0] = u$.

If N distinct basic solutions $\Phi_k = (\psi_k, \phi_k)^T$ $(k = 1, 2, ..., N)$ of the Lax-pairs at

$\lambda = \lambda_k$ $(k = 1, 2, ..., N)$ are given, the elementary DT can be repeated N times; then the $(N-1)$th-step DT for the complex modified KdV equation is

$$\Phi_N[N-1] = T[N-1]T[N-2]...T[1]T[0]\Phi_N$$

$$u[N] = u[N-1] + 2\sum_{i=1}^{N} \frac{(\lambda_i + \lambda_i^*)\psi_i[i-1]\phi_i^*[i-1]}{|\psi_i[i-1]|^2 + |\phi_i[i-1]|^2} \tag{2.46}$$

and $T[i] = \lambda_{i+1}I - H[i-1]\Lambda[i]H[i-1]^{-1}$ $(i = 1, 2, ..., N)$, where

$H[i-1] = \begin{pmatrix} \psi_1[i-1] & -\phi_i^*[i-1] \\ \phi_i[i-1] & \psi_i^*[i-1] \end{pmatrix}$, $\Lambda[i] = \begin{pmatrix} \lambda_i & 0 \\ 0 & -\lambda_i^* \end{pmatrix}$,

$\Phi_i = (\psi_i, \phi_i)^T$ $(i = 1, 2, ..., N)$ is a solution of the Lax-pairs given in equation 2.40 at $\lambda = \lambda_i$. Here the initial value is $\Phi_1[0] = (\psi_1[0], \phi_1[0])^T = (\psi_1, \phi_1)^T = \Phi_1$.

According to the above elementary DT, we derive a generalized DT for the complex modified KdV equation 2.39. Let us start vith the assumption that

$$\Psi = \Phi_1(\lambda_1, \varepsilon) \tag{2.47}$$

is a special solution of the Lax-pairs. ε is a small parameter in equation (2.47). Expanding Ψ in a Taylor series gives

$$\Psi = \Phi_1^{[0]} + \Phi_1^{[1]}\varepsilon + \Phi_1^{[2]}\varepsilon^2 + ... + \Phi_1^{[N]}\varepsilon^N, \tag{2.48}$$

where $\Phi_1^{[k]} = \frac{1}{k!}\frac{\partial^k}{\partial\lambda^k}\Phi_1(\lambda)|_{\lambda=\lambda_1}$ $(k = 1, 2, ...)$

1. *The zeroth-step generalized* DT. It is easy to show that $\Phi_1[0]$ is a solution to the Lax-pairs given in equation (2.40) with $u = u[0]$ and $\lambda = \lambda_1$. A zeroth-step generalized DT of the complex modified KdV equation (2.39) is given as follows

$$\Phi_1[0] = T[0]\Phi_1, \quad u[1] = u[0] + 2\frac{(\lambda_1 + \lambda_1^*)\psi_1[0]\phi_1^*[0]}{|\psi_1[0]|^2 + |\phi_1[0]|^2} \tag{2.49}$$

and $T[1] = \lambda_2 I - H[0]\Lambda[1]H[0]^{-1}$,

where $H[0] = \begin{pmatrix} \psi_1[0] & -\phi_1^*[0] \\ \phi_1[0] & \psi_1^*[0] \end{pmatrix}$, $\Lambda[1] = \begin{pmatrix} \lambda_1 & 0 \\ 0 & -\lambda_1^* \end{pmatrix}$,

$\Phi_1^{[0]} = \begin{pmatrix} \psi_1^{[0]} \\ \phi_1^{[0]} \end{pmatrix} = \begin{pmatrix} \psi_1[0] \\ \phi_1[0] \end{pmatrix} = \Phi_1[0]$, $u = u[0]$ and $T_1[0]\Phi_1[k] = \Phi_1[k]$ $(k = 1, 2, ...)$.

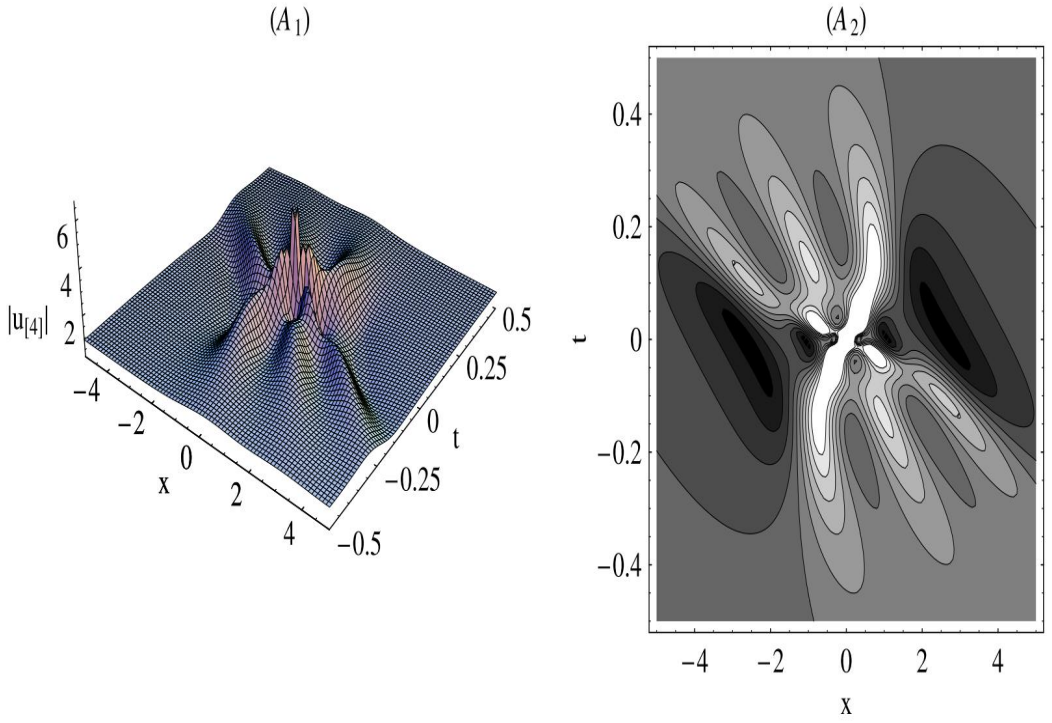

Figure 36: A_1 and A_2 show the third-order rogue wave solution to equation (2.39) [95]

2. *The first-step generalized* DT. Through the limit process

$$\lim_{\varepsilon\to 0}\frac{[T_1[1]|_{\lambda=\lambda_1+\varepsilon}]\Psi}{\varepsilon}=\lim_{\varepsilon\to 0}\frac{\varepsilon+T_1[1]|_{\lambda=\lambda_1}\Psi}{\varepsilon}=\Phi_1^{[0]}+T_1[1](\lambda_1)\Phi_1^{[1]}\equiv\Phi_1[1], \tag{2.50}$$

we find a solution to the Lax-pair with $u[1]$ and $\lambda=\lambda_1$. This allows us to go to a first-step generalized DT, namely,

$$\Phi_1[1]=\Phi_1[0]+T_1[1]\Phi_1^{[1]},\quad u[2]=u[1]+2\frac{(\lambda_1+\lambda_1^*)\psi_1[1]\phi_1^*[1]}{|\psi_1[1]|^2+|\phi_1[1]|^2}, \tag{2.51}$$

and $T_1[2]=\lambda_1 I-H_1[1]\Lambda[1]H_1[1]^{-1}$, where $H_1[1]=\begin{pmatrix}\psi_1[1] & -\phi_1^*[1]\\ \phi_1[1] & \psi_1^*[1]\end{pmatrix}$, $\Phi_1[1]=\begin{pmatrix}\psi_1[1]\\ \phi_1[1]\end{pmatrix}$.

3. *The second-step generalized* DT. Similarly, the limit

$$\lim_{\varepsilon\to 0}\frac{[\varepsilon+T_1[2]][\varepsilon+T_1[1]]\Psi}{\varepsilon^2}=\Phi_1^{[0]}+[T_1[1]+T_1[2]]\Phi_1^{[1]}+T_1[2]T_1[1]\Phi_1^{[2]}\equiv\Phi_1[2] \tag{2.52}$$

provide us with a non-trivial solution for the Lax-pairs with $u[2]$ and $\lambda = \lambda_1$. Thus we may do the second-step iteration of the DT, which is the following:

$$\Phi_1[2] = \Phi_1^{[0]} + [T_1[1] + T_1[2]]\Phi_1^{[1]} + T_1[2]T_1[1]\Phi_1^{[2]}, \tag{2.53}$$

$$u[3] = u[2] + 2\frac{(\lambda_1 + \lambda_1^*)\psi_1[2]\phi_1^*[2]}{|\psi_1[2]|^2 + |\phi_1[2]|^2}, \tag{2.54}$$

and $T_1[2] = \lambda_1 I - H_1[1]\Lambda[1]H_1[1]^{-1}$,

where $H_1[2] = \begin{pmatrix} \psi_1[2] & -\phi_1^*[2] \\ \phi_1[2] & \psi_1^*[2] \end{pmatrix}$, $\Phi_1[2] = \begin{pmatrix} \psi_1[2] \\ \phi_1[2] \end{pmatrix}$.

4. *The (N-1)th-step generalized* DT. Continuing the above process and combining all the Darboux matrices, an (N-1)th-step generalized DT is constructed as follows:

$$\begin{aligned}\Phi_1[N-1] = \Phi_1^{[0]} + \left[\sum_{l=1}^{N-1} T_1[l]\right]\Phi_1^{[1]} + \left[\sum_{l=1}^{k}\sum_{l<k}^{N-1} T_{[1]}[k]T_1[l]\right]\Phi_1^{[2]} \\ +... + [T_1[N-1]T_1[N-2] \times ... \times T_1[1]]\Phi_1^{[N-1]}\end{aligned} \tag{2.55}$$

$$u[N] = u[N-1] + 2\frac{(\lambda_1 + \lambda_1^*)\psi_1[N-1]\phi_1^*[N-1]}{|\psi_1[N-1]|^2 + |\phi_1[N-1]|^2}, \tag{2.56}$$

and $T_1[k] = \lambda_1 I - H_1[k-1]\Lambda[1]H_1[k-1]^{-1}$,

where

$$H_1[k-1] = \begin{pmatrix} \psi_1[k-1] & -\phi_1^*[k-1] \\ \phi_1[k-1] & \psi_1^*[k-1] \end{pmatrix}, \quad \Phi_1[k-1] = \begin{pmatrix} \psi_1[k-1] \\ \phi_1[k-1] \end{pmatrix} \quad (k = 1, 2, ...) \tag{2.57}$$

The formulae (2.55)-(2.57) are a recursive formulae of the (N-1)th-step generalized DT for the complex modified KdV equation. Although it is not difficult to give the $2n \times 2n$ determinant representation of the (N-1)th-step generalized DT, we prefer the form of a recursive formula, because it is very easy to construct higher-order rogue wave solutions in the computer.

2.2.4 Rogue wave solutions.

In order to obtain the rogue wave solution, we start with the non-zero seed solution $u[0] = e^{i\sqrt{6}x}$. Then, the corresponding solution for the Lax-pairs given in equation (2.40) at $\lambda = \varepsilon^2 + \frac{i\sqrt{6}}{2} - 1$ is

$$\Phi_1(\varepsilon) = \begin{pmatrix} (K_1 e^{\eta} + K_2 e^{-\eta}) e^{\frac{i\sqrt{6}}{2}} \\ (K_2 e^{\eta} + K_1 e^{-\eta}) e^{-\frac{i\sqrt{6}}{2}} \end{pmatrix} \tag{2.58}$$

where $\eta = \mu(x + wt + \sum_{j=1}^{N}(b_j + ic_j)\varepsilon^{2j})$ $(b_j, c_j \in \Re)$,

$K_1 = \sqrt{i\frac{\sqrt{6}}{2} - \lambda - \mu}$, $K_2 = \sqrt{i\frac{\sqrt{6}}{2} - \lambda + \mu}$, $\mu = \frac{\sqrt{2}}{2}\sqrt{2\lambda^2 - 2i\sqrt{6}\lambda - 5}$,

$w = 2 - i\sqrt{6}\lambda - 2\lambda^2$, the quantities b_j, c_j and ε are free parameters.

Expanding the vector function $\Phi_1(\varepsilon)$ given in (2.58) at $\varepsilon = 0$, we obtain

$$\Phi_1(\varepsilon) = \Phi_1^{[0]} + \Phi_1^{[1]}\varepsilon^2 + \Phi_1^{[2]}\varepsilon^4 + \Phi_1^{[3]}\varepsilon^6 + ..., \tag{2.59}$$

where

$$\Phi_1^{[0]} = \begin{pmatrix} \psi_1^{[0]} \\ \phi_1^{[0]} \end{pmatrix}, \quad \Phi_1^{[1]} = \begin{pmatrix} \psi_1^{[1]} \\ \phi_1^{[1]} \end{pmatrix}, \quad \Phi_1^{[2]} = \begin{pmatrix} \psi_1^{[2]} \\ \phi_1^{[2]} \end{pmatrix}, \quad \Phi_1^{[3]} = \begin{pmatrix} \psi_1^{[3]} \\ \phi_1^{[3]} \end{pmatrix} ... \tag{2.60}$$

with $\psi_1^{[0]} = 2e^{i\sqrt{\frac{3}{2}}x}$, $\phi_1^{[0]} = 2e^{-i\sqrt{\frac{3}{2}}x}$,

$\psi_1^{[1]} = -\frac{1}{2}e^{i\sqrt{\frac{3}{2}}x}(72i(i + 2\sqrt{6})t^2 + (1 - 2x)^2 + 12(2 + i\sqrt{6})t(-1 + 2x))$,

and $\phi_1^{[1]} = \frac{1}{2}e^{-i\sqrt{\frac{3}{2}}x}(72(1 - 2i\sqrt{6})t^2 - (1 + 2x)^2 - 12i(-2i + \sqrt{6})t(1 + 2x))$.

The analytical expressions of $(\psi_1^{[i]}, \phi_1^{[i]})$ $(i = 2, 3)$ are rather cumbersome to be written down here, there can be found in Ref. [95].

It is clear that $\Phi_1^{[0]}$ is a solution for the Lax-pairs given in equation (2.40) at $u[0] = e^{i\sqrt{6}x}$ and $\lambda_1 = i\frac{\sqrt{6}}{2}$ Substituting $u[0]$, λ_1 and $\Phi_1^{[0]}$ into equation (2.49), we obtain a trivial solution, namely

$$u[1] = -e^{i\sqrt{6}x}, \tag{2.61}$$

to the complex modified KdV equation (2.39) and

$$T_1[1] = \begin{pmatrix} -1 & e^{i\sqrt{6}x} \\ e^{i\sqrt{6}x} & -1 \end{pmatrix}. \tag{2.62}$$

Substituting the expressions given in (2.61) and (2.62) and those of $\Phi_1^{[0]}$, $\Phi_1^{[1]}$ into equation (2.51), we obtain the first-order rogue wave solution to the system under consideration, given as follows

$$u[2] = \left(1 + \frac{-4 + 24i\sqrt{6}t}{1 + 360t^2 + 48tx + 4x^2}\right) e^{i\sqrt{6}x}. \tag{2.63}$$

The corresponding depiction is shown in 34. Following the procedure given above, the higher-order rogue wave solutions to the system under consideration can be obtained. The awesome features corresponding to the second and third-order rogue wave to the complex modified KdV equation are shown in figures (35) and (36), respectively.

2.3 The homoclinic test approach

The homoclinic test approach or breather limit method was recently applied on some nonlinear wave equation [167] to derive rogue wave solution. In the following, we present in detail how the procedure works and illustrate it through some examples.

The homoclinic test approach works in four steps:

Step 1 : By Painleve analysis, a transformation $u = T(f)$ is made for some new and unknown function f.

Step 2 : By using the transformation in step 1, original equation can be converted into Hirota's bilinear form $G(D_t, D_x, f) = 0$. Where the $D-$operator is defined by

$$D_t^m D_x^n f(t,x).g(t,x) = \left(\frac{\partial}{\partial t} - \frac{\partial}{\partial t'}\right)^m \left(\frac{\partial}{\partial x} - \frac{\partial}{\partial x'}\right)^n f(t,x)g(t',x')|_{t'=t,x'=x}.$$

Step 3 Solve the above equation to get homoclinic (heteroclinic) breather wave solution by using extended homoclinic test approach.

Step 4 Let the period of periodic wave go to infinite in homoclinic breather wave solution, we can Obtain a rational homoclinic wave and this wave is just a rouge wave.

Now we illustrate this approach through an example. The results shown here was obtained recently in reference [168]. In this work the authors considered the so-called Benjamin Ono (BO) equation given as follows

$$u_{tt} + \beta(u^2)_{xx} + \gamma u_{xxx} = 0, \tag{2.64}$$

where β and γ are nonzero constants.

By Painlevé analysis, let

$$u = u_0 + \frac{6\gamma}{\beta}(\ln f)_{xx}, \tag{2.65}$$

where $f(x,t)$ is a real unknown function and u_0 is a small perturbation parameter. Substituting (2.65) into (2.64), we obtain the following

$$\frac{6\gamma}{\beta}(\ln f)_{tt} + 12\gamma u_0(\ln f)_{xx} + \frac{36\gamma^2}{\beta}((\ln f)_{xx})^2 + \frac{6\gamma^2}{\beta}(\ln t)_{xxxx} = 0. \tag{2.66}$$

By mean of the Hirota operator given above, the bilinear form of the BO equation is obtained as

$$(D_t^2 + \beta u_0 D_x^2 + \gamma D_x^4) f.f = 0.$$

The test function is chosen to be

$$f(x,t) = e^{p_1(x-w_1 t)} + c_1 \cos(p_2(x+w_2 t)) + c_2 e^{p_1(x-w_1 t)}. \tag{2.67}$$

Inserting this test function into the bilinear form, collecting different terms and solving the resulting equations, the coefficients of the test function (2.67) are obtained and given as follows

$$c_1 = \pm 2\sqrt{\frac{(2\gamma p_1^2 w_2^2 + 2\beta^2 u_0^2 + \beta u_0 w_2^2)c_2}{-4\gamma p_1^2 w_2^2 + 2\beta^2 u_0^2 + \beta u_0 w_2^2}}, \qquad w_1 w_2 = 2\beta u_0, \qquad p_1^2 = \frac{1}{4\gamma}(w_1^2 - w_2^2), \qquad p_1 = p_2.$$

Hence, we obtain two forms of the test function, depending on the sign of the coefficient c_1 as follows

$$\begin{aligned} f_1 &= 2\sqrt{c_2} cosh(p_1(x - 2\tfrac{\beta u_0}{w_2}) + \ln\sqrt{c_2}) + h_1 \cos(p_2(x + w_2 t)), \\ f_2 &= 2\sqrt{c_2} cosh(p_1(x - 2\tfrac{\beta u_0}{w_2}) + \ln\sqrt{c_2}) - h_1 \cos(p_2(x + w_2 t)), \end{aligned} \tag{2.68}$$

with $h_1 = 2\sqrt{\frac{(2\gamma p_1^2 w_2^2 + 2\beta^2 u_0^2 + \beta u_0 w_2^2)c_2}{-4\gamma p_1^2 w_2^2 + 2\beta^2 u_0^2 + \beta u_0 w_2^2}}$. Taking into account the above expressions of the test function, the expressions of the quantity u come from the equation (2.65) as

$$\begin{aligned} u_1 &= u_0 + \frac{6\gamma}{\beta} \frac{-4h_1 p_1^2 2\sqrt{c_2} sinh\left(p_1\left(x - \frac{2\beta u_0}{w_2}\right) + \ln\sqrt{c_2}\right) \sin(p_2(x+w_2 t)) - h_1^2 p_1^2 + 4c_2 p_1^2}{\left(2\sqrt{c_2} cosh\left(p_1(x - \frac{2\beta u_0}{w_2} t) + \ln\sqrt{c_2}\right) + h_1 \cos(p_2(x+w_2 t))\right)^2}, \\ u_1 &= u_0 + \frac{6\gamma}{\beta} \frac{-4h_1 p_1^2 2\sqrt{c_2} sinh\left(p_1\left(x - \frac{2\beta u_0}{w_2}\right) + \ln\sqrt{c_2}\right) \sin(p_2(x+w_2 t)) - h_1^2 p_1^2 + 4c_2 p_1^2}{\left(2\sqrt{c_2} cosh\left(p_1(x - \frac{2\beta u_0}{w_2} t) + \ln\sqrt{c_2}\right) - h_1 \cos(p_2(x+w_2 t))\right)^2}. \end{aligned} \tag{2.69}$$

The solution $u_1(x;t)$ (or $u_2(x,t)$) shows a new family of two-wave, breather solitary wave, which is a solitary wave and also is a periodic wave. The corresponding plot is shown in Figure (37).

Now considering a limit behavior of u_2 as the period $\frac{2\Pi}{p_1}$ of periodic wave $\cos(p_1(x+w_2 t))$ goes to infinite, i.e. $p_1 \to 0$. After computation, the following result is obtained

$$U = u_0 + \frac{24\gamma\left(R - 2\left(x - \frac{2\beta u_0}{w_2}\right)t\right)(x + w_2 t)}{\beta\left(\left(x - \frac{2\beta u_0}{w_2}\right)^2 + (x + w_2 t)^2 + R\right)^2}, \tag{2.70}$$

with $R = \frac{-6\gamma w_2^2}{2\beta^2 u_0^2 + \beta u_0 w_2^2}$. The corresponding plot is shown in figure (38).

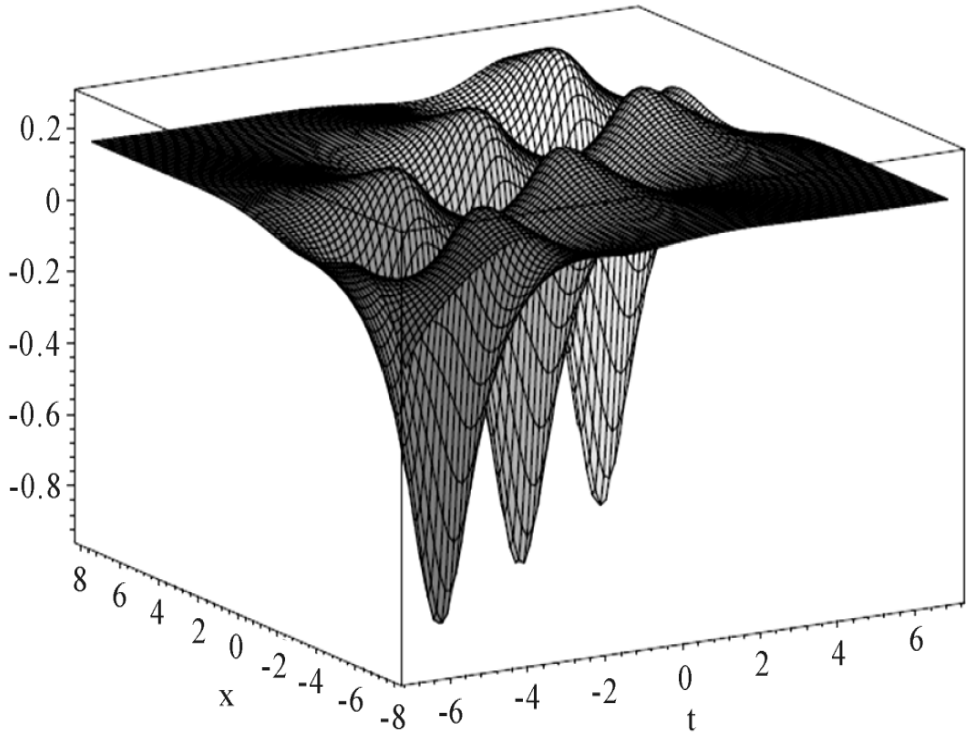

Figure 37: The figure of u_2 with $c_2 = 1$, $u_0 = \frac{1}{6}$, $\beta = 6$ and $\gamma = -1$ [168].

Conclusion

In this chapter, we have presented the methodology of our investigation, starting from the Darboux transformation, passing through the generalized one to the homoclinic test approach. We have first presented the traditional Darboux transformation by illustrating the process on the modified KdV equation. It has been shown that traditional Darboux transformation is not appropriate to derive higher-order solution to nonlinear systems. So we have presented also the generalized Darboux transformation by applying it on the modified KdV equation, the nonlinear Schrödinger equation and the complex modified KdV equation. We have presented also the homoclinic test appraoch showing the illustration on the Benjamin Ono equation. In the next chapter we will present the results obtained by us by applying the above methods on some nonlinear equations.

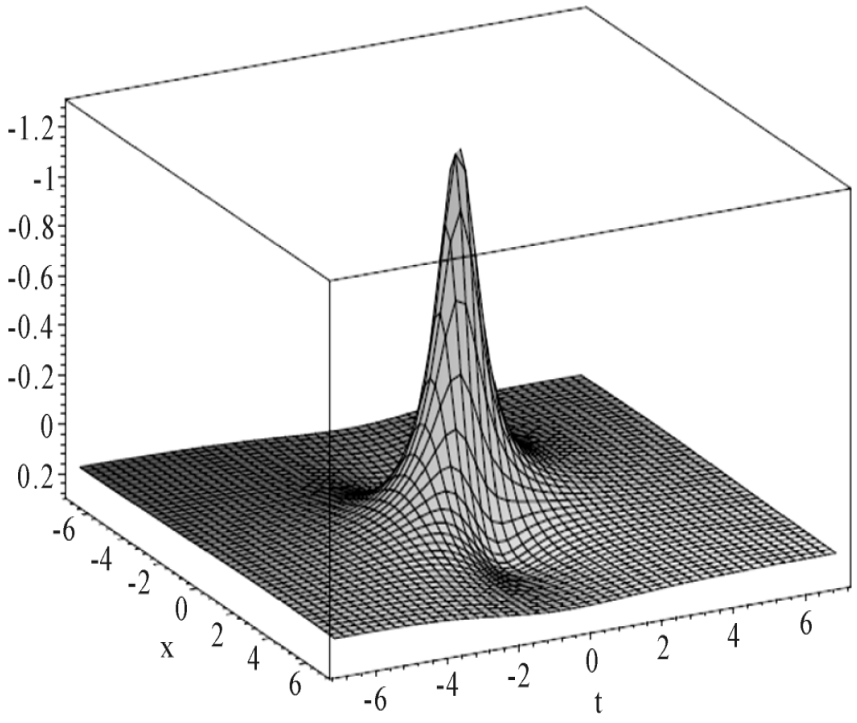

Figure 38: The figure of U with $c_2 = 1$, $u_0 = \frac{1}{6}$, $\beta = 6$ and $\gamma = -1$ [168].

Chapter 3

Results and discussions: Rogue waves of nonlinear systems, a particular case of barothropic relaxing media

Introduction

In physics and mathematics, a soliton is a self-reinforcing solitary wave packet, that maintains its shape while propagating at a constant velocity. It is a result of cancelation between the nonlinearity and the dispersive effect. Solitons are solutions to a widespread class of weakly nonlinear dispersive partial differential equations describing physical systems [14–16, 18, 97]. Soliton seems to be more accurate to the transport of information in nonlinear media. In the past few decades, a new kind of wave has appeared, namely the rogue wave [54]. Originally, the rogue wave appeared as monster wave, responsible of many marine disasters. More after, it has been shown that, rogue wave appears not only in ocean condition but also in physical nonlinear media such as hydrodynamics [32], plasma physics [87], optics [29] just to name a few. Now again, rogue waves are still mysterious so that in any of these disciplines, the new studies enrich the concept and lead to progress toward a comprehensive understanding of this phenomenon. It has been shown that rogue waves are so unpredictable that they appear from nowhere and disappear with-

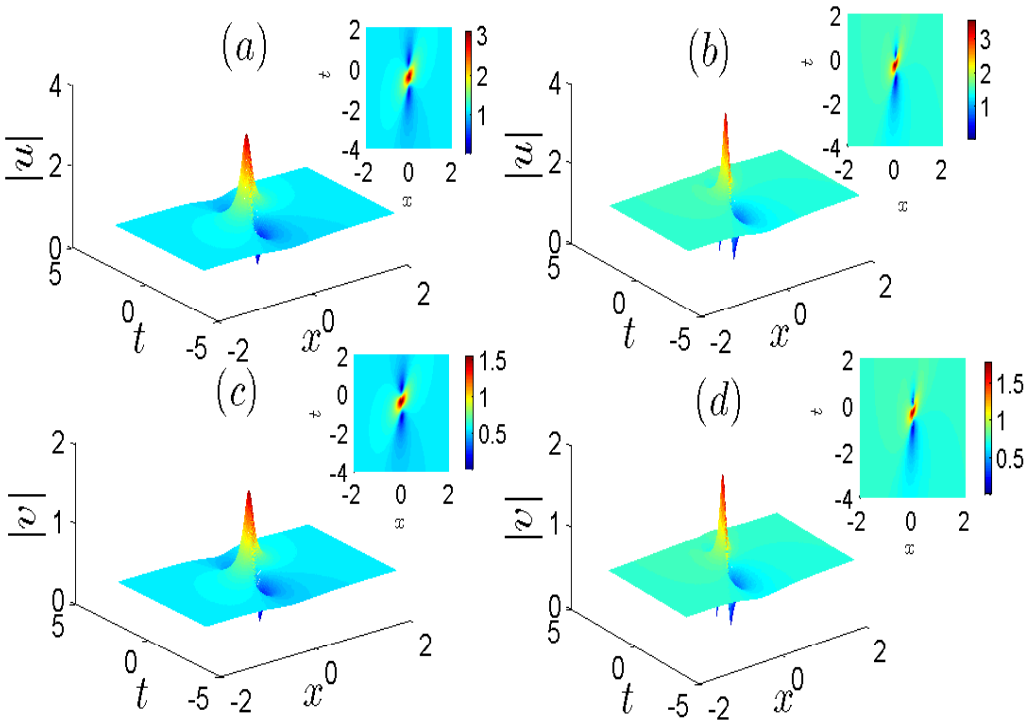

Figure 39: Rogue wave dynamics in the generalized nonlinear Schrödinger equation. The panel (a) and (b) correspond to the u component, depicted with the parameter $\gamma = 0.1+i$ and $\gamma = 0.75+i$, respectively. The panel (c) and (d) correspond to the v component, depicted with the parameter $\gamma = 0.1+i$ and $\gamma = 0.75+i$, respectively. All the depictions are done with $f = 0$, $a_1 = 1$ and $a_2 = 0.5$.

out a trace. The unpredictability of rogue waves implies that they can be expressed by rational functions localized both in space and time. The simplest rogue wave solution was firstly obtained by Peregrine; more after, Akhmediev et al. [28] have calculated the first-order rogue wave solution for the nonlinear Schrödinger equation (NLSE). Different kinds of laboratory experiment and theoretical approaches have been used to study the rogue waves [33]. The aim of this chapter, is to show the different results obtained during our investigation. In section 1, we present the localized waves in a general nonlinear Schrödinger equation, showing the interaction process between rogue wave and soliton, between rogue wave and breather wave. In section 2, using the generalized Darboux transformation, we derive higher-order rogue wave solutions the a nonlinear Schrödinger system named the Manakov system. In section 3, also based on the Darboux matrix technic, we derive rogue wave solutions to a nonlinear wave equation which model the propagation

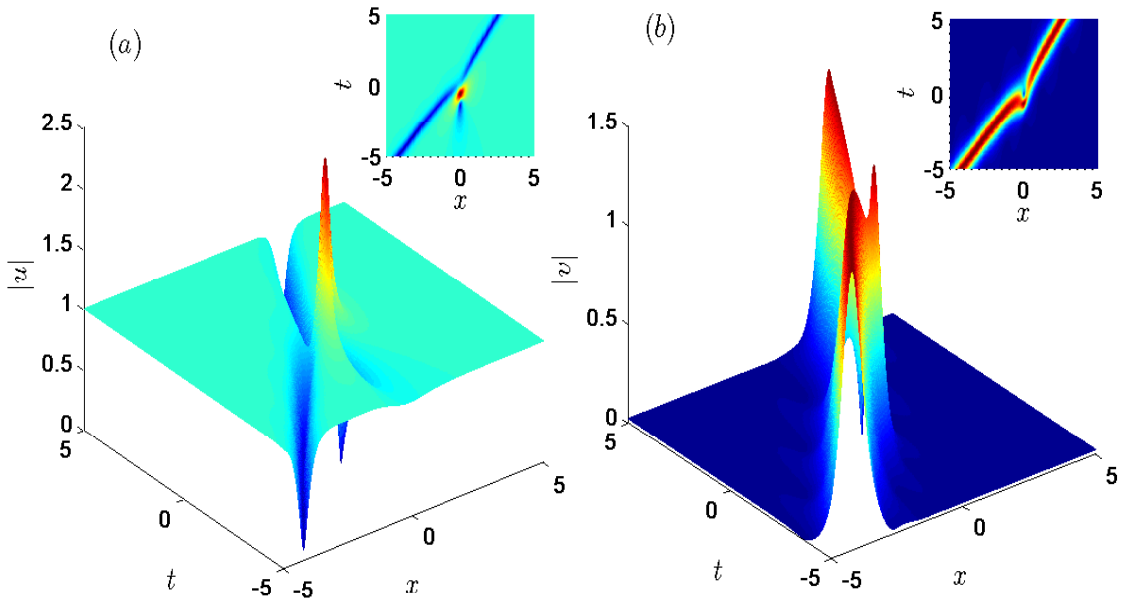

Figure 40: Rogue wave dynamics in the generalized nonlinear Schrödinger equation. In the panel (a) we can observe a rogue wave together with a dark-soliton for the u component; in the panel (b) a rogue wave with a bright soliton for the v component. All the depictions are done with $f = 1$ and $\gamma = 0.5 + i$.

of waves in ferrites. In section 4, we construct the generalized Darboux transformation of a generalized nonlinear Schrödinger equation, we derive rogue waves solutions to this system and show that the rogue waves can be controlled during their propagation. In section 5, we derive rogue wave solutions to a nonlinear Schrödinger equation while showing the effects of nonlinear higher-order terms on their profile. In section 6, based on the extended homoclinic test approach, we construct rogue wave solution to the Boussinesq equation. The last section is devoted to the particular case of this thesis, the rogue waves in a barothropic relaxing media.

3.1 Localized waves in a general coupled nonlinear Schrödinger equation

In a monomode birefringent fiber, the propagation of two polarized waves can be modeled by the coupled NLSE, where the nonlinearity is expressed by coupling terms to the third-order susceptibility [10, 97, 98]. The coupled NLSE under consideration in this section is a general one, given as follows [18]

$$\begin{aligned} iu_t + u_{xx} + 2(\alpha|u|^2 + \beta|v|^2 + \gamma uv^* + \gamma^* vu^*)u = 0, \\ iv_t + v_{xx} + 2(\alpha|u|^2 + \beta|v|^2 + \gamma uv^* + \gamma^* vu^*)v = 0, \end{aligned} \tag{3.1}$$

where u and v stand for slowly varying envelop. The quantities α and β are real constants scaling self-phase modulation and cross-phase modulation effects respectively whereas the complex constant γ denotes the four-wave mixing effects. This system has been studied in Ref. [18] and its soliton solutions have been calculated using the Darboux matrix method. More recently, the generalized Darboux transformation of the above system was given and its higher-order rogue wave solutions were provided [99]. The aim of this work is to show the interaction between rogue wave and dark-bright soliton and the interaction between rogue wave and breather in the above system. We aim also to show the effects of the four waves mixture parameter on the profiles of the localized waves. The results obtained in this work are useful in understanding the interaction process in nonlinear physical systems. In fact, it shows that rogue waves and solitons can coexist in a same medium and the information contained in the soliton cannot be destroyed during the interaction with rogue wave. Thus, the organization of this section is settled as follows. In subsection one we use the Darboux transformation to construct localized wave of the system (3.1) starting from his seed solutions. In subsection 2, we discuss the results obtained.

3.1.1 Localized waves

The system given in Eq. (3.1) can be cast into a 3×3 eigenvalue problem [18], namely,

$$\begin{aligned} R_x = UR = (\lambda J + U_0)R, \\ R_t = VR = (\lambda^2 V_0 + \lambda V_1 + V_2)R, \end{aligned} \tag{3.2}$$

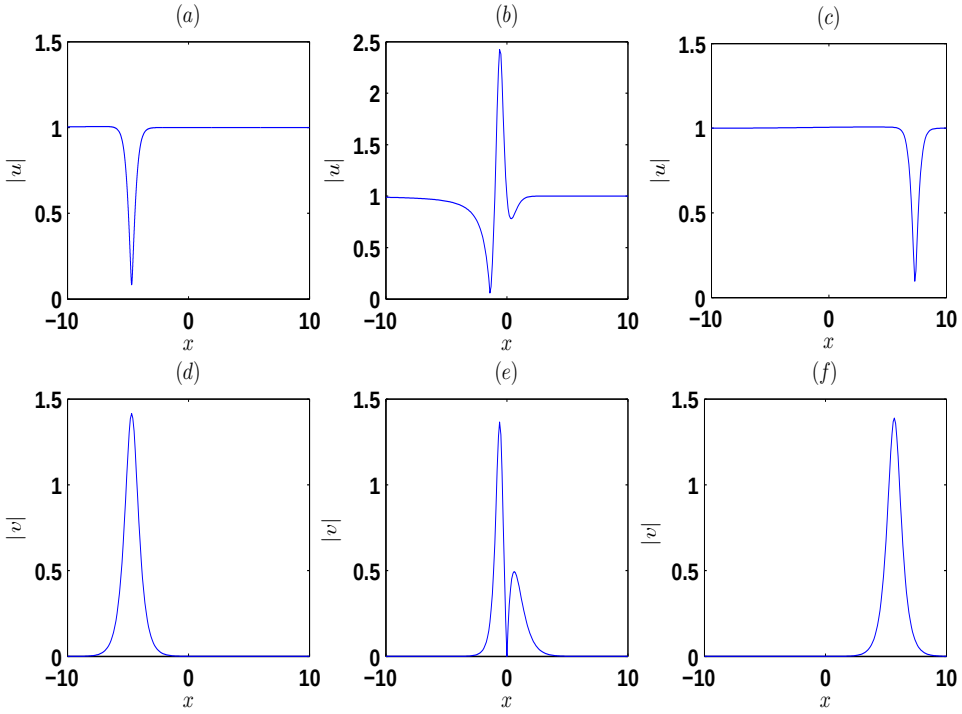

Figure 41: Wave interaction process for the generalized nonlinear Schrödinger equation. The u component is depicted in the panels (a), (b) and (c) at $t=-4$, $t=0$ and $t=4$, respectively. The v component is depicted in the panels (d), (e) and (f) at $t=-4$, $t=0$ and $t=4$, respectively. $f=1$ and $\gamma=0.5+i$.

with $U_0=\begin{pmatrix} 0 & 0 & u \\ 0 & 0 & v \\ r_1 & r_2 & 0 \end{pmatrix}$, $V_0=-2i\begin{pmatrix} 1 & 0 & 0 \\ 0 & 1 & 0 \\ 0 & 0 & -1 \end{pmatrix}$, $V_1=-2\begin{pmatrix} 0 & 0 & u \\ 0 & 0 & v \\ r_1 & r_2 & 0 \end{pmatrix}$,

$$V_2=\begin{pmatrix} -iur_1 & -iur_2 & iu_x \\ -ivr_1 & -ivr_2 & iv_x \\ -ir_{1x} & -ir_{2x} & iur_1+ivr_2 \end{pmatrix}$$

and $J=diag(i,i,-i)$, where $r_1=-(\alpha u^*+\gamma v^*)$ and $r_2=-(\gamma^* u^*+\beta v^*)$. The quantity $R=(r(x,t),s(x,t),w(x,t))^T$ (T means matrix transpose) is the vector eigenfunction, while λ is the spectral parameter. The system (1.1) can be obtained using the zero-curvature equation $U_t-V_x+UV-VU=0$. The Darboux transformation (DT) [92]

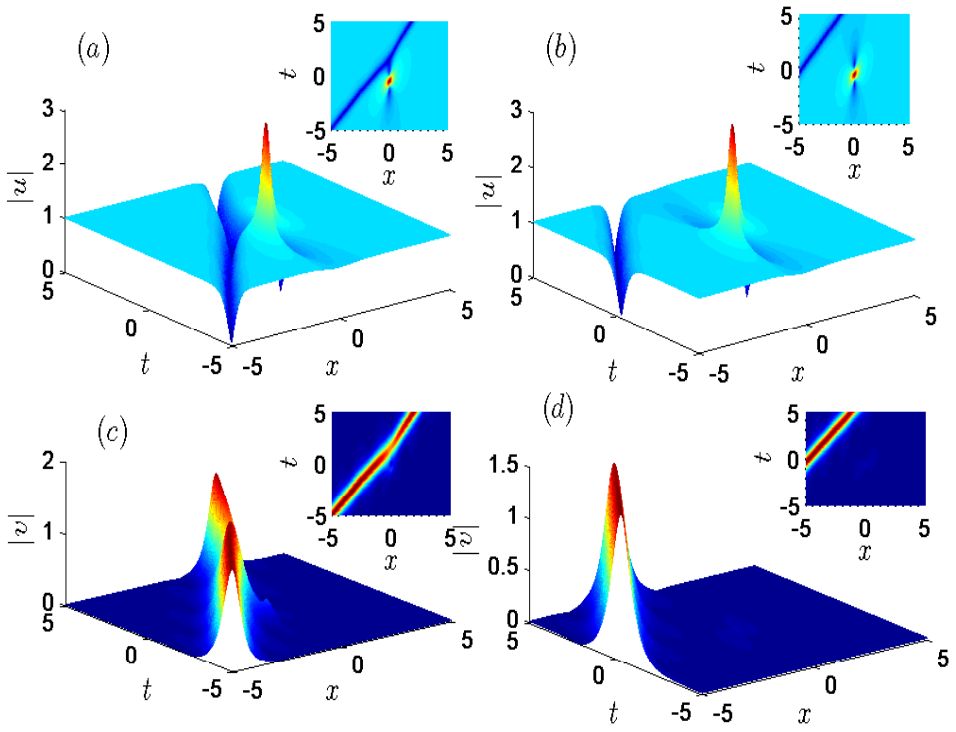

Figure 42: Localized waves dynamics for the generalized nonlinear Schrödinger equation. The panels (a) and (b) correspond to the u component for the values of $f = 1$ and $f = 0.0001$, respectively. The panels (c) and (d) correspond to the v component for the values of $f = 1$ and $f = 0.0001$, respectively. For all the depictions $\gamma = 0.5 + i$.

changes the Lax-pairs given in Eq. (3.2) into a new one as follows,

$$\widetilde{R} = (\lambda I - S)R, \quad \widetilde{u} = u + 2iS_{13}, \quad \widetilde{v} = v + 2iS_{23},$$

$$S = H\Lambda H^{-1} = \begin{pmatrix} S_{11} & S_{12} & S_{13} \\ S_{21} & S_{22} & S_{23} \\ S_{31} & S_{32} & S_{33} \end{pmatrix}, \quad H = \begin{pmatrix} r & w^* & 0 \\ s & 0 & w^* \\ w & -r^* & -w^* \end{pmatrix}, \quad \Lambda = \begin{pmatrix} \lambda & 0 & 0 \\ 0 & \lambda^* & 0 \\ 0 & 0 & \lambda^* \end{pmatrix}, \tag{3.3}$$

where I is the 3×3 unitary matrix. $\widetilde{R}$ satisfies the new Lax-pairs

$$\widetilde{R}_x = \widetilde{U}\widetilde{R}, \qquad \widetilde{R}_t = \widetilde{V}\widetilde{R}, \tag{3.4}$$

where the matrices $\widetilde{U}$ and $\widetilde{V}$ have the same form as U and V with the new potentials $\widetilde{u}$ and $\widetilde{v}$ therein. In view to obtain rational solution to the system (3.1), we start with plane wave solutions as seed solutions as follows

$$u = a_1 e^{iat}, \qquad v = a_2 e^{iat}, \tag{3.5}$$

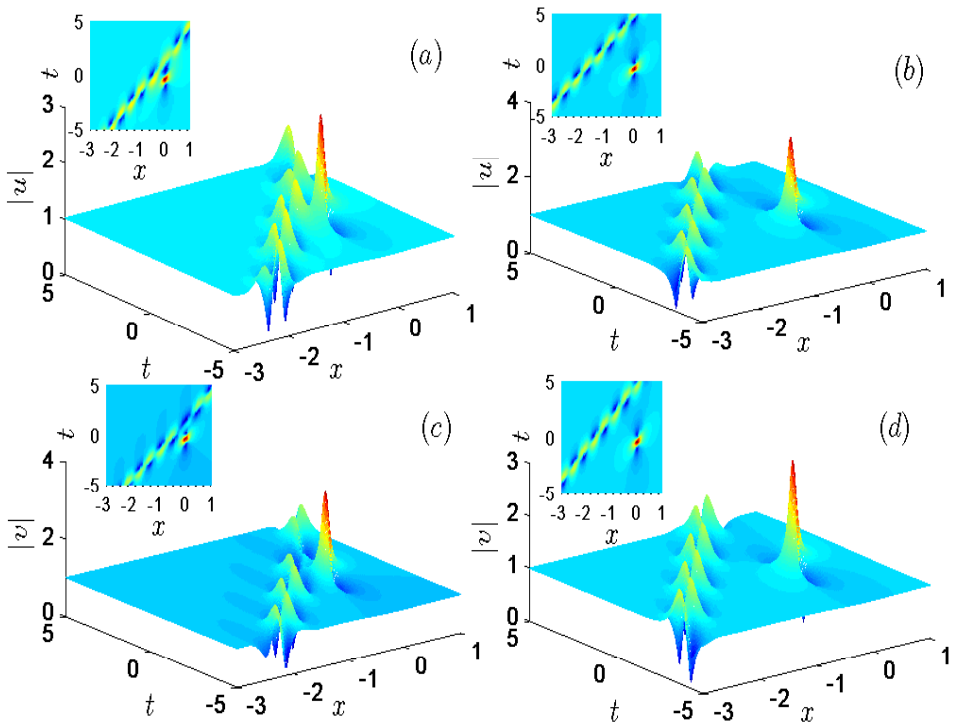

Figure 43: Localized waves dynamics for the generalized nonlinear Schrödinger equation. We can observe in the panels (a) and (b) for the u component a rogue wave merging with a breather wave for $f = 1$ and $f = 0.001$, respectively. In the panels (c) and (d) for the v component, one can observe also a rogue wave merging with a breather wave for the values $f = 1$ and $f = 0.001$, respectively. The depictions are made with $\gamma = i$.

with $a = 2(a_1^2\alpha + a_2^2\beta) + 2a_1a_2(\gamma + \gamma^*)$. The quantities a_1 and a_2 are real-valued constants, with no loss of generality. Next, we derive the eigenfunction compatible with the Lax-pairs given in equation (3.3) and corresponding to the seed solutions to the system (3.1). So we assume the following,

$$r = a_1M_1e^{iat} + a_2C_1e^{-iat}, \quad s = a_2M_2e^{iat} - a_1C_2e^{-iat}, \quad w = M_3, \tag{3.6}$$

where the quantities M_1, M_2, M_3, C_1 and C_2 are to be determined. Inserting the quantities above into the Lax-pairs given in Eq. (3.3) and integrating the corresponding system, one can obtain the following for $\lambda = -i\sqrt{\frac{a}{2}}$,

$$\begin{aligned} r &= [a_1(2a\sqrt{2a}t - 4\sqrt{2a}x + 12iat - 8)e^{\frac{\sqrt{2a}}{2}(-x+2at)}]e^{iat} + a_2fe^{-iat+\frac{\sqrt{2a}}{2}(-2x+at)}, \\ s &= [a_2(2a\sqrt{2a}t - 4\sqrt{2a}x + 12iat - 8)e^{\frac{\sqrt{2a}}{2}(-x+2at)}]e^{iat} - a_1fe^{-iat+\frac{\sqrt{2a}}{2}(-2x+at)}, \\ w &= 2a(-2x + at - 3i\sqrt{2a}t)e^{\frac{\sqrt{2a}}{4}(-2x+at)}, \end{aligned} \tag{3.7}$$

where f is a real parameter.

Substituting the above expressions into equation (3.4), we derive the following rational solutions to the system (3.1) as follows

$$u = a_1 e^{iat} + \frac{a_1(A+iB)e^{iat} + a_2 C e^{\eta_1}}{D + Ee^{\eta_2}}, \qquad v = a_2 e^{iat} + \frac{a_2(A+iB)e^{iat} - a_1 C e^{\eta_1}}{D + Ee^{\eta_2}} \tag{3.8}$$

where

$A = -8a(36a\sqrt{2a}t^2 - 8a\sqrt{2a}tx + 2a^2\sqrt{2a}t^2 + 8\sqrt{2a}x^2 + 16x - 8at)$, $B = +24\sqrt{2a}t$, $C = 2\,af\left(at - 3\,i\sqrt{2a}t - 2\,x\right)$, $D = (a_1^2+a_2^2)(64+144a^2t^2+8a^3t^2+32ax^2+64\sqrt{2a}x-32a\sqrt{2a}t-32tx) - 16a^3xt + 72a^3t^2 + 4a^4t^2 + 16a^2x^2$, $E = f^2\,({a_1}^2 + {a_2}^2)$, $\eta_1 = \frac{3\sqrt{2a}}{4}(2x - at) - iat$ and $\eta_2 = \frac{3\sqrt{2a}}{2}(2x - at)$.

We now go further while discussing three different cases in the waves dynamics.

1. If the parameter $f = 0$, the expression given in equation (3.8) is reduced to the following

$$u = a_1\left(1 + \frac{A+iB}{D}\right)e^{iat}, \qquad v = a_2\left(1 + \frac{A+iB}{D}\right)e^{iat}. \tag{3.9}$$

This solution is merely the first-order vector rogue wave soliton to the system (3.1) [99]. It is easy to remark that the two above solutions are proportional to each other, hence the solution obtained in Eq. (3.9) is a generalization of rogue wave solution to the decoupled system. It is important to remark that, the real part of the four wave mixing parameter γ make the rogue wave more thinner and higher when increasing; this result was also observed in Ref. [100, 101]. Also, one background peak of the rogue wave disappears gradually with high values of the parameter γ (see Figure 39).

2. If $f \neq 0$, $a_1 = 0$, $a_2 = 0$. In this case, nothing occurs, since the numerators of the equations given in 3.8 vanish. We have in this case a trivial solution to the system.

3. If we set $f \neq 0$, $a_1 \neq 0$ and $a_2 = 0$, we observe a rogue wave merging with a dark soliton (see Figure 40a) and a rogue wave interacting with a bright soliton (see Fig. 41a). The Figure 41 shows in details the interaction process between rogue waves and soliton. The four wave mixing parameter has no effect in this case since it is canceled from the dispersion relation with $a_2 = 0$.

4. If $f \neq 0$, $a_1 = 0$, $a_2 \neq 0$. In this case, we observe a bright pulse together with a rogue wave in the v component and dark pulse with a rogue wave for the u component; in contrary of the previous parametric choice($f \neq 0$, $a_1 \neq 0$, $a_2 = 0$).

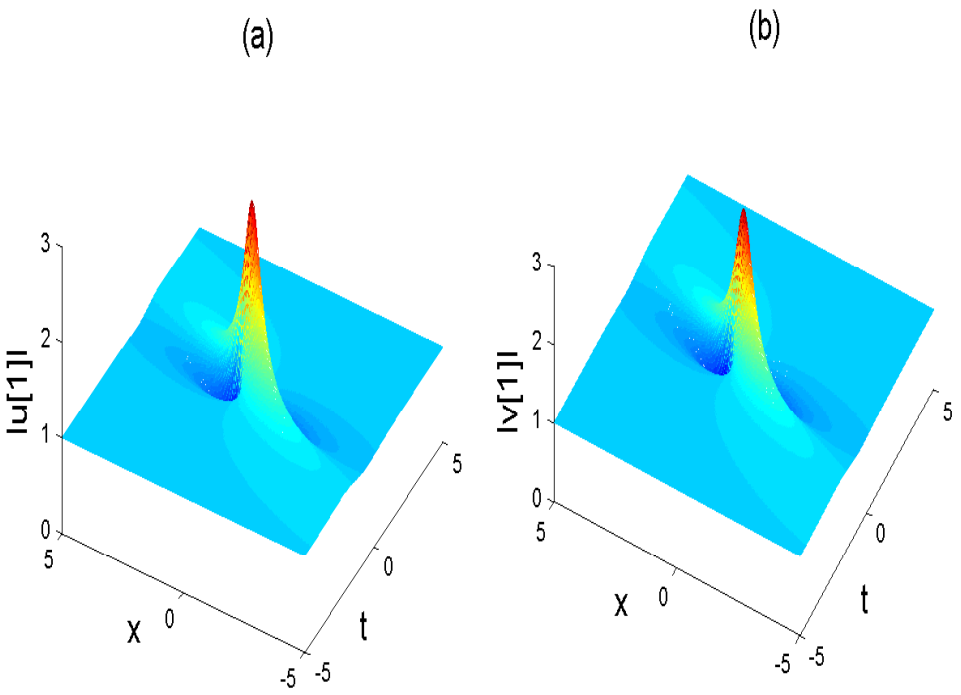

Figure 44: First-order rogue waves $u[1]$ and $v[1]$ depicted with the following parameters (a) $a = 1$, $b = 1/4$, and (b) $a = 1/4$, $b = 1$, $\alpha = 1$.

5. If $f \neq 0$, $a_1 \neq 0$ and $a_2 \neq 0$, we can observe in Figure 43 rogue waves interacting with breather wave. The interaction is possible for the four wave mixing parameter being taken pure imaginary.

3.1.2 Discussion and interpretation

(i) Since the quantities α, β and γ are arbitrary, the coupled system given in the equation (3.1) can describe a wide variety of systems than the well-known standard coupled nonlinear Schrödinger equation. If $\alpha = \beta$ and $\gamma = 0$ the system (3.1) is reduced to the Manakov system [102], localized waves for the late system was predicted in Ref. [103]. Since the system under consideration is a generalization of the nonlinear Schrödinger equation, the results obtained in this work is a generalization of the results obtained in Ref. [102].

(ii) In the Figure. 40, we observe some rogue wave merging with dark-bright soliton. The Figure 41 shows in details the interaction process. The solitons are propagating along

the x axis in the positive direction. It is important to notice that, at time $t = 0$, a rogue wave appears from nowhere and interacts with the soliton, after that, the rogue wave suddenly disappears without a trace since the soliton conserve its shape and its velocity after the interaction process. The interaction is merely elastic. This fact explains the nature of rogue wave as predicted in Ref. [28]. In addition, the results obtained in this work are useful in understanding the interaction process in nonlinear physical systems. In fact, it shows that rogue waves and solitons can coexist in a same medium and the information contained in the soliton cannot be destroyed during the interaction with rogue wave. In the Figure 42d, the rogue wave is separated with the bright soliton and is difficult to be seen due to its zero background amplitude. In the Figure 42, we can remark that for the decreasing values of the parameter f, the soliton and the rogue wave are more distant.

(iii) Observing the Figure 43, one can see some rogue wave brewed with breather wave. For the decreasing values of the parameter f, the rogue wave and the breather are faraway. In this case, the breather wave results from the superposition of the bright and the dark contribution.

(iv) During the interaction process, the fact that the rogue wave appears from nowhere and disappears without a trace can be related to the modulation instability. Indeed, the instability created by the plane wave solution on his top induces an increase of perturbation up to his highest amplitude and a decay [20].

Throughout this section, we have made an investigation on a generalized nonlinear Schrödinger equation, which can describe the wave propagation in a wide variety of physical systems. Using the Darboux transformation on the Lax-pairs of the above system and starting from plane wave solutions as seed solutions, we have constructed analytical rational solution to the system. Giving arbitrary values to the constants α, β and γ contained in the equation, we have observed many behaviors of the localized wave in their dynamics. Particularly for the parameter γ(four wave mixing parameter), we have observed interesting behavior of localized wave during their dynamics. We have seen that the real part of this parameter compresses the rogue wave during his dynamics and increase its shape. We have also remarked that the interaction between a breather wave and a rogue wave is possible if the real part of the four wave mixing parameter is null.

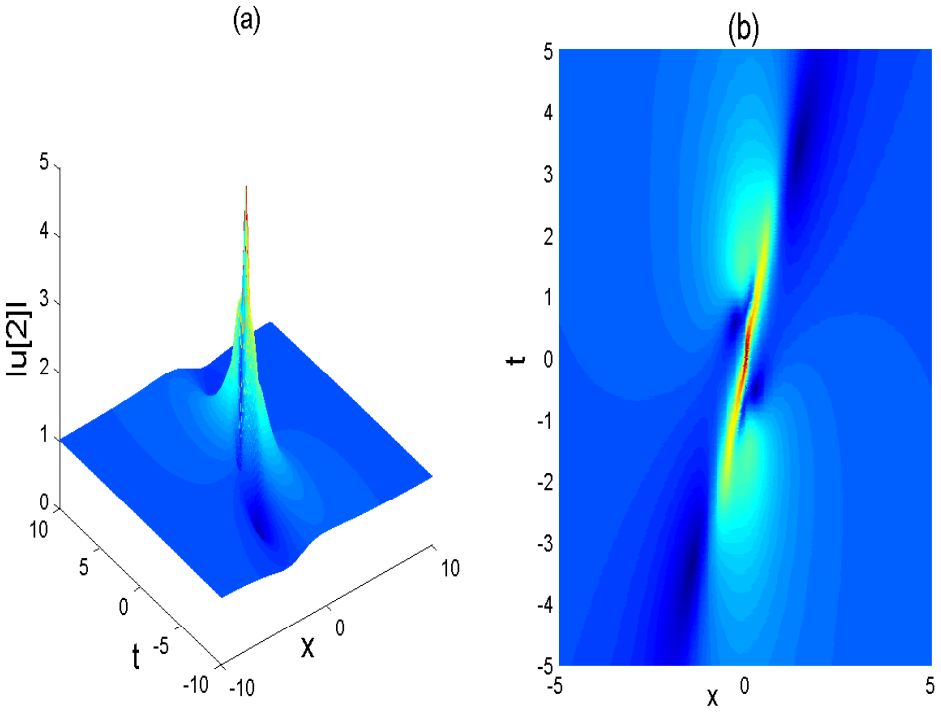

Figure 45: Second-order composite rogue wave $u[2]$ depicted with the following parameters: $a = 1$, $b = 0$, $c_1 = d_1 = 0$ and $\alpha = 1$. Panel (a) represents the 3-D perspective and the panel (b) stands for the density plot of the 3-D representation.

Additionally, for the value of the parameter $f = 0$, the solution obtained is merely the first-order rogue wave generalization of the decoupled system since the two components are proportional to each other. For the values of $f \neq 0$, we observe some rogue wave brewed with dark-bright soliton propagating along the x axis in the positive direction and for other case, rogue wave melted with breather wave for the both component u and v. A possible application of the results obtained in this work, is the explanation of the propagation of rogue light pulses in nonlinear systems interacting with soliton carrying an information which cannot be destroyed during the interaction, such as plasma and optical fiber. This work was published in the European physical Journal Plus [104]. We now go forward while presenting the results obtained for the manakov system.

3.2 Nth-order rogue waves to the Manakov system

Understanding the behavior and the dynamics of natural phenomena stand to be worth fundamental. That is why it has been one of the most challenging aspects of modern science and technology in studying nonlinear nature of system. The importance of nonlinearity has been well-appreciated for many years, because nonlinearity is a fascinating occurrence of nature in the context of large amplitude waves or high-intensity laser pulses observed in various fields. This fascinating subject has branched out in almost all areas of science, and its applications are percolating through the whole science. In general, nonlinear evolution equations exhibiting a wide range of high complexities in terms of different linear and nonlinear effects model nonlinear phenomena. Nonlinear science has experienced an explosive growth by the invention of several exciting and fascinating new concepts in the past few decades, such as solitons, dispersion-managed solitons, dromions, rogue waves, among others [19, 20].

Rogue waves, also called freak waves, giant waves or killer waves have attracted considerable attentions. A rogue wave is a large-amplitude local wave, short-lived wave, meet in an ocean that appears from nowhere and disappears without a trace. Rogue waves appear not only in oceanic conditions, but also in optics, superfluids, Bose-Einstein condensates and in the form of capillary waves. In any of these disciplines, new studies of rogue waves enrich the concept and lead to progress toward a comprehensive understanding of this still mysterious phenomenon. The first-order rational solution for the nonlinear Schrödinger equation (NLSE) was given by Peregrine. Akhmediev and co-workers have calculated the simplest rogue wave solutions for the NLSE. The construction of higher-order analogues is actually a challenging problem. The construction of higher-order rogue wave solutions needs a simple approach which is the generalized Dardoux transformation (DT). This approach was proposed by Guo et al.

The DT, originating from the work of Darboux on the Sturm-Liouville equation, is a powerful method for constructing solutions for integrable systems such as the NLSE, the Korteweg-de Vries (KdV) equation, the Kadomtsev-Petviashvili equation, the Davey-Stewartson equation and the Toda lattice equation just to name a few. But the original DT is not applicable directly to obtain the rogue wave solutions for the nonlinear wave equa-

tions. Matveev introduced the so-called generalized DT and the positon solutions were calculated for the celebrated KdV equation. Recently, Guo and coworkers re-examined Matveev's generalized DT and proposed a new approach to derive the generalized DT for the KdV and the NLS equations.

In this work, we discuss the Guo et al [94]'s approach to a focusing vector NLSE (VNLSE), known as Manakov system given as follows

$$\begin{aligned} iu_t + \frac{1}{2}u_{xx} + u(|u|^2 + |v|^2) = 0, \\ iv_t + \frac{1}{2}v_{xx} + v(|u|^2 + |v|^2) = 0, \end{aligned} \tag{3.10}$$

with x and t being two independent variables, $u(x,t)$ and $v(x,t)$ standing for complex envelop of two field components. This system has many physical significant applications such as the propagation in elliptically birefringent optical fibers [105] and for modeling crossing sea waves [106].

3.2.1 Lax-pairs and Darboux transformation

We consider in this section, the VNLS equations in the anomalous dispersion regime. The aim of this work is to construct Nth-order rogue wave solutions of the previous system. The main tool is the generalized DT. Based on the Darboux matrix method, we iterate the generalized DT of equations (3.10) and work out a formula for generation of higher-order rogue wave solutions. It is worth noting that the rogue wave solutions of this system have early been constructed in ref. [20], using however a non-recursive Darboux transformation up to second-order.

Equation (3.10) can be cast into a 3×3 linear eigenvalue problem due to integrability [107]

$$\mathbf{R}_x = \mathbf{U}\mathbf{R}, \quad \mathbf{R}_t = \mathbf{V}\mathbf{R}, \tag{3.11}$$

where,

$$\mathbf{U} = \lambda\mathbf{E} + \mathbf{Q}, \quad \mathbf{V} = \frac{3}{2}\lambda^2\mathbf{E} + \frac{3}{2}\lambda\mathbf{Q} + \frac{i}{2}\sigma_3(\mathbf{Q}_x - \mathbf{Q}^2), \tag{3.12}$$

$$\mathbf{E} = diag(-2i, i, i),\ \sigma_3 = diag(1, -1, -1),\ \mathbf{Q} = \begin{pmatrix} 0 & -u & -v \\ u^* & 0 & 0 \\ v^* & 0 & 0 \end{pmatrix}.$$

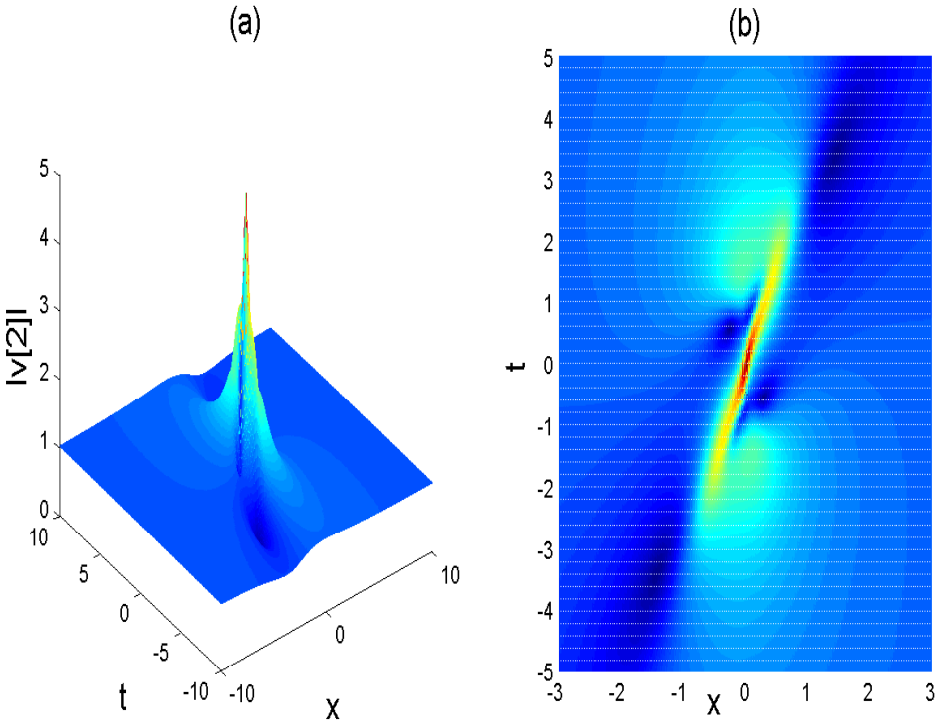

Figure 46: Second-order composite rogue wave $v[2]$ depicted with the following parameters: $a = 0$, $b = 1$, $c_1 = d_1 = 0$ and $\alpha = 1$. Panel (a) represents the 3-D perspective and the panel (b) stands for the density plot of the 3-D representation.

Let $\mathbf{R}_1 = (r_1, s_1, w_1)^T$ be a solution of the Lax-pairs given in equation (3.11) with $u = u[0]$, $v = v[0]$ and $\lambda = \lambda_1$. The classical DT of the Ablowitz-Kaup-Newell-Segur (AKNS) spectral problem allows us to write the following formulas:

$$\mathbf{R}[1] = T[1]\mathbf{R}, \qquad T[1] = \lambda_1 \mathbf{I} - H[0]\Lambda_1 H[0]^{-1}, \tag{3.13}$$

$$u[1] = u[0] + 2i(\lambda - \lambda^*)\frac{r_1[0]s_1[0]^*}{|r_1[0]|^2 + |s_1[0]|^2 + |w_1[0]|^2}, \tag{3.14}$$

$$v[1] = v[0] + 2i(\lambda - \lambda^*)\frac{r_1[0]w_1[0]^*}{|r_1[0]|^2 + |s_1[0]|^2 + |w_1[0]|^2}, \tag{3.15}$$

which satisfy

$$\mathbf{R}[1]_x = \mathbf{U}[1]\mathbf{R}[1], \qquad \mathbf{R}[1]_t = \mathbf{V}[1]\mathbf{R}[1], \tag{3.16}$$

where $\mathbf{R}_1[0] = T[0]\mathbf{R}_1$, $r_1[0] = r_1$, $s_1[0] = r_1$, $r_1[0] = r_1$, $\mathbf{I} = \begin{pmatrix} 1 & 0 & 0 \\ 0 & 1 & 0 \\ 0 & 0 & 1 \end{pmatrix}$, $H[0] =$

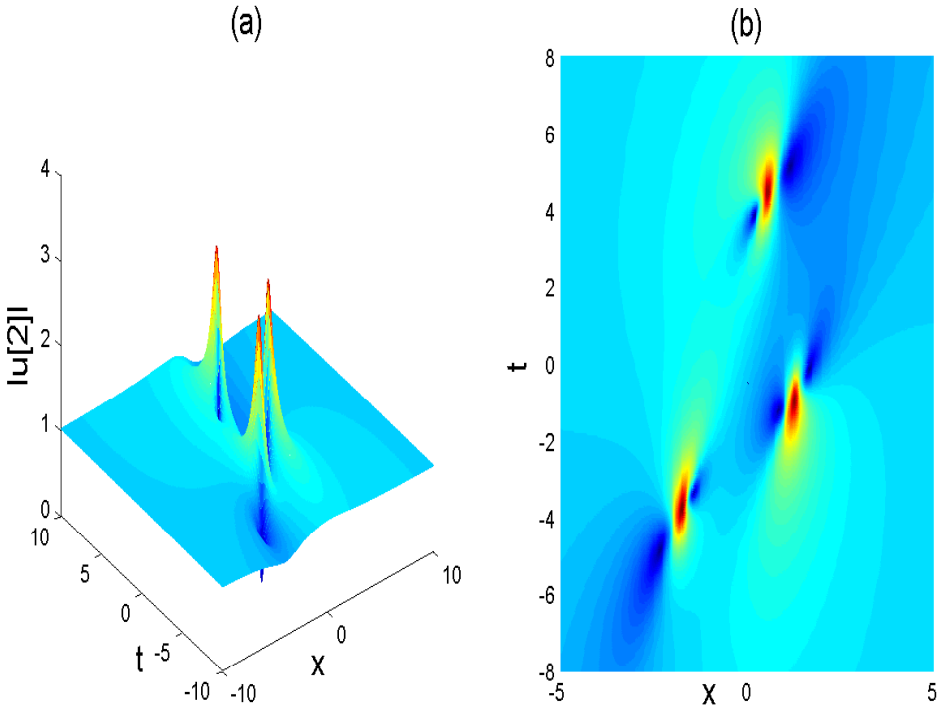

Figure 47: Second-order rogue wave $u[2]$ depicted with the following parameters: $a = 1$, $b = 0$, $c_1 = d_1 = 25$ and $\alpha = 1$. Panel (a) represents the 3-D perspective and the panel (b) stands for the density plot of the 3-D representation.

$$\begin{pmatrix} r_1[0] & s_1[0]^* & w_1[0]^* \\ s_1[0] & -r_1[0]^* & 0 \\ w_1[0] & 0 & -r_1[0]^* \end{pmatrix},$$

and $\Lambda_1 = \begin{pmatrix} \lambda_1 & 0 & 0 \\ 0 & \lambda_1^* & 0 \\ 0 & 0 & \lambda_1^* \end{pmatrix}$. The quantities $\mathbf{U}[1]$ and $\mathbf{V}[1]$ have the same form as $\mathbf{U}$ and $\mathbf{V}$ except that the old potentials u and v are replaced by the new ones $u[1]$ and $v[1]$. The quantity T stands for the Darboux matrix. If N distinct basic solutions $\mathbf{R}_k = (r_k, s_k, w_k)^T$ $(k = 1, 2, 3, ..., N)$ of the Lax-pairs expressed by equation (3.11) at $\lambda = \lambda_k$ $(k = 1, 2, 3, ..., N)$ are given, the DT can be repeated N times. Then, the Nth-step DT for the VNLSE (3.10) is

$$\mathbf{R}[N] = T[N]T[N-1]...T[1]\mathbf{R}, \quad T[k] = \lambda\mathbf{I} - H[k-1]\Lambda_k H[k-1]^{-1}, \tag{3.17}$$

$$u[N] = u[N-1] + 2i(\lambda-\lambda^*)\times \frac{r_N[N-1]s_N[N-1]^*}{|r_N[N-1]|^2+|s_N[N-1]|^2+|w_N[N-1]|^2}, \tag{3.18}$$

$$v[N] = v[N-1] + 2i(\lambda-\lambda^*)\times \frac{r_N[N-1]w_N[N-1]^*}{|r_N[N-1]|^2+|s_N[N-1]|^2+|w_N[N-1]|^2}, \tag{3.19}$$

where

$$H[k-1]=\begin{pmatrix} r_k[k-1] & s_k[k-1]^* & w_k[k-1]^* \\ s_k[k-1] & -r_k[k-1]^* & 0 \\ w_k[k-1] & 0 & -r_k[k-1]^* \end{pmatrix}, \Lambda_k=\begin{pmatrix} \lambda_k & 0 & 0 \\ 0 & \lambda_k^* & 0 \\ 0 & 0 & \lambda_k^* \end{pmatrix},$$

$\mathbf{R}_k[k-1]=(r_k[k-1],s_k[k-1],w_k[k-1])^T=\mathbf{R}_k[k-1]$ and $\mathbf{R}[k-1]=T[k-1]T[k-2]...T[1]\mathbf{R}$.

3.2.2 Generalized Darboux transformation

According to the above classical DT, we derive the generalized DT for the system of equation (3.11). We start with the assumption that

$$R_1 = R_1(\lambda_1+\epsilon), \tag{3.20}$$

is a particular solution of the Lax-pairs of equation (3.11). The constant ϵ being a small parameter. Expanding R_1 in a Taylor series gives

$$R_1 = R_1^{[0]} + R_1^{[1]}\epsilon + R_1^{[2]}\epsilon^2 + ... + R_1^{[N]}\epsilon^N + ..., \tag{3.21}$$

where $R_1^{[k]}=\frac{1}{k!}\frac{\partial^k}{\partial\epsilon^k}R_1|_{\epsilon=0}$ $(k=1,2,3,...)$. 1. *The first-step of the method.*

From the above assumption, it is easy to find that $R_1^{[0]}$ is a solution for the Lax-pairs of equation (3.11) with $u=u[0]$ and $v=v[0]$ at $\lambda=\lambda_1$. The first-step DT for the system (3.10) is expressed as

$$\mathbf{R}[1]=T[1]\mathbf{R}, \qquad T[1]=\lambda_1\mathbf{I}-H[0]\Lambda_1 H[0]^{-1}, \tag{3.22}$$

$$u[1]=u[0]+2i(\lambda-\lambda^*)\frac{r_1[0]s_1[0]^*}{|r_1[0]|^2+|s_1[0]|^2+|w_1[0]|^2}, \tag{3.23}$$

$$v[1]=v[0]+2i(\lambda-\lambda^*)\frac{r_1[0]w_1[0]^*}{|r_1[0]|^2+|s_1[0]|^2+|w_1[0]|^2}, \tag{3.24}$$

where

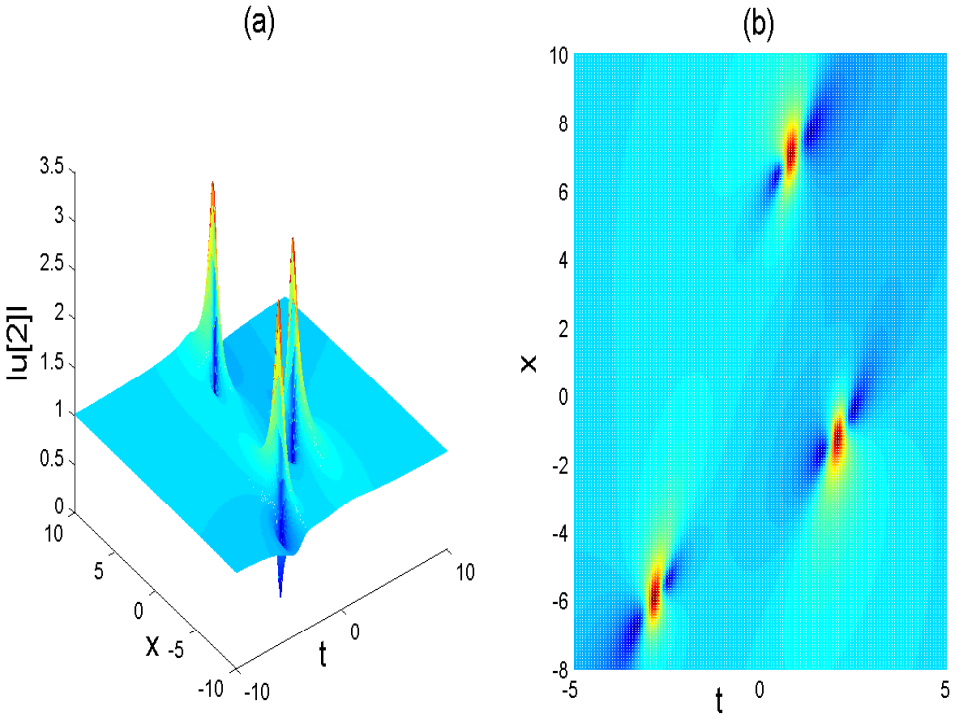

Figure 48: Second-order rogue wave $u[2]$ depicted with the following parameters: $a = 1$, $b = 0$, $c_1 = d_1 = 100$ and $\alpha = 1$. Panel (a) represents the 3-D perspective and the panel (b) stands for the density plot of the 3-D representation.

$\mathbf{R}_1[0] = T[0]\mathbf{R}_1$, $r_1[0] = r_1$, $s_1[0] = r_1$, $r_1[0] = r_1$,

$$\mathbf{I} = \begin{pmatrix} 1 & 0 & 0 \\ 0 & 1 & 0 \\ 0 & 0 & 1 \end{pmatrix}, \; H[0] = \begin{pmatrix} r_1[0] & s_1[0]^* & w_1[0]^* \\ s_1[0] & -r_1[0]^* & 0 \\ w_1[0] & 0 & -r_1[0]^* \end{pmatrix},$$

and $\Lambda_1 = \begin{pmatrix} \lambda_1 & 0 & 0 \\ 0 & \lambda_1^* & 0 \\ 0 & 0 & \lambda_1^* \end{pmatrix}$.

2. *The second-step of the method.*

With

$$\lim_{\epsilon\to 0} \frac{T[1]|_{\lambda=\lambda_1+\epsilon R_1}}{\epsilon} = \lim_{\epsilon\to 0} \frac{(\epsilon + T_1[1])R_1}{\epsilon} = R_1^{[0]} + T_1[1]R_1^{[1]} \equiv R_1[1], \tag{3.25}$$

we find a solution to the Lax-pairs of equation (3.11) with $u[2]$ and $v[2]$ and $\lambda = \lambda_1$.

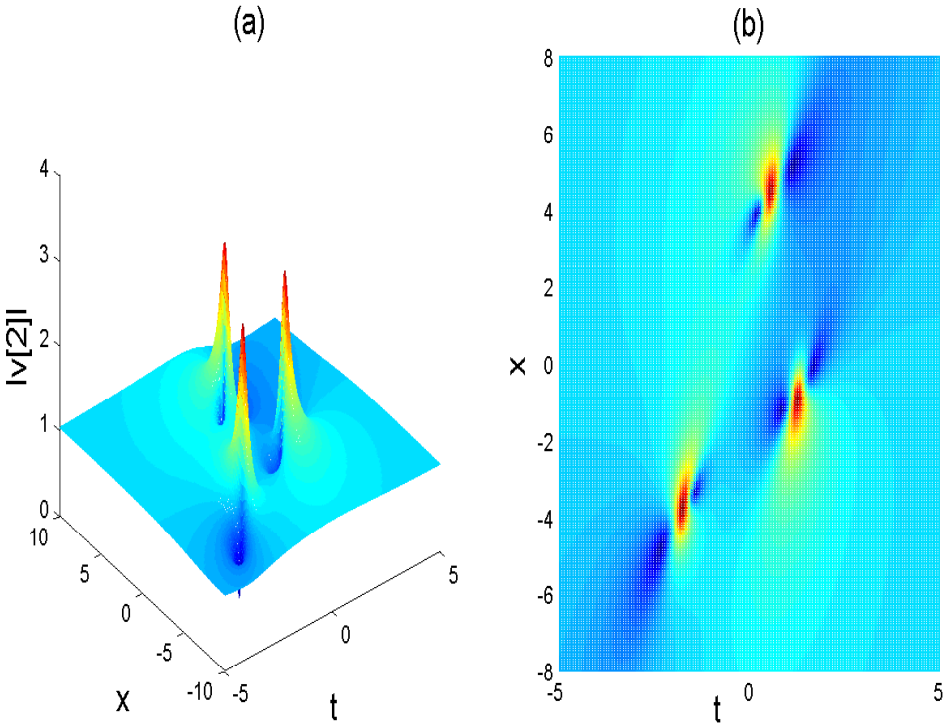

Figure 49: Second-order rogue wave $v[2]$ depicted with the following parameters: $a = 0$, $b = 1$, $c_1 = d_1 = 25$ and $\alpha = 1$. Panel (a) represents the 3-D perspective and the panel (b) stands for the density plot of the 3-D representation.

This allows us to go to the second step DT, namely,

$$R[2] = T[2]T[1]R, \quad T[2] = \lambda_1 \mathbf{I} - H[1]\Lambda_2 H[1]^{-1}, \tag{3.26}$$

$$u[2] = u[1] + 2i(\lambda - \lambda^*)\frac{r_1[1]s_1[1]^*}{|r_1[1]|^2 + |s_1[1]|^2 + |w_1[1]|^2}, \tag{3.27}$$

$$v[2] = v[1] + 2i(\lambda - \lambda^*)\frac{r_1[1]w_1[1]^*}{|r_1[1]|^2 + |s_1[1]|^2 + |w_1[1]|^2}, \tag{3.28}$$

where $(r_1[1], s_1[1], w_1[1])^T = R_1[1]$, $\mathbf{I} = \begin{pmatrix} 1 & 0 & 0 \\ 0 & 1 & 0 \\ 0 & 0 & 1 \end{pmatrix}$, $H[1] = \begin{pmatrix} r_1[1] & s_1[1]^* & w_1[1]^* \\ s_1[1] & -r_1[1]^* & 0 \\ w_1[1] & 0 & -r_1[1]^* \end{pmatrix}$,

and $\Lambda_2 = \begin{pmatrix} \lambda_1 & 0 & 0 \\ 0 & \lambda_1^* & 0 \\ 0 & 0 & \lambda_1^* \end{pmatrix}$.

3. *The third-step of the method.*

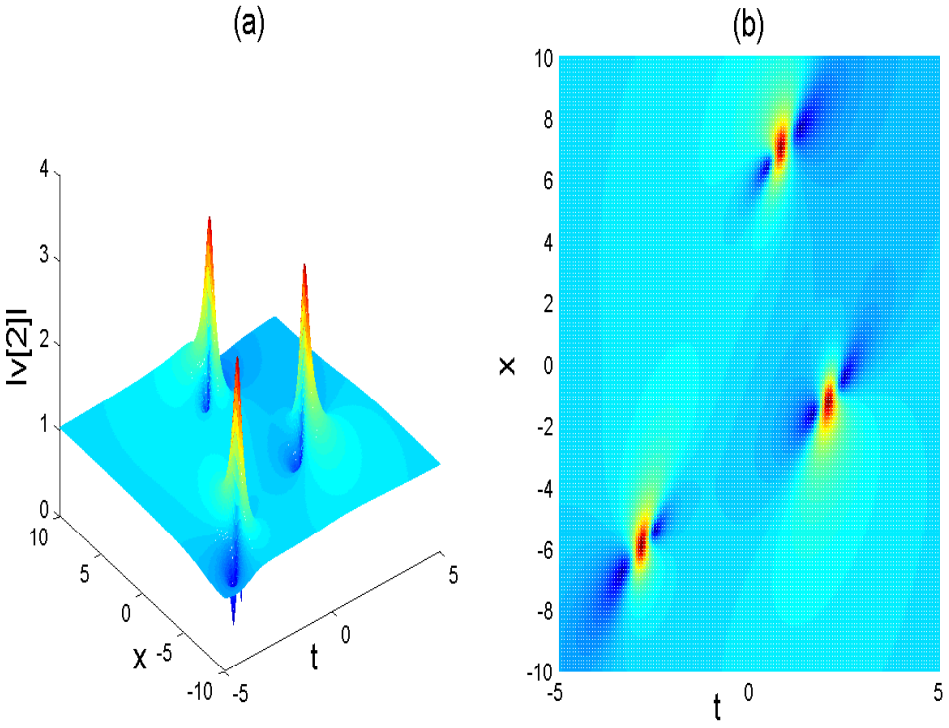

Figure 50: Second-order rogue wave $v[2]$ depicted with the following parameters: $a = 0$, $b = 1$, $c_1 = d_1 = 100$ and $\alpha = 1$. Panel (a) represents the 3-D perspective and the panel (b) stands for the density plot of the 3-D representation.

Similarly, the following limit

$$\begin{aligned}\lim_{\epsilon\to 0}\frac{[T[2]T[1]]|_{\lambda=\lambda_1+\epsilon}R_1}{\epsilon^2} &= \lim_{\epsilon\to 0}\frac{(\epsilon+T_1[2])(\epsilon+T_1[1])R_1}{\epsilon^2}\\ &= R_1^{[0]}+(T_1[2]+T_1[1])R_1^{[1]}\\ &+T_1[2]T_1[1]R_1^{[2]}\equiv R_1[2],\end{aligned}\tag{3.29}$$

provides us with a non-trivial solution for the Lax-pairs of equation (3.11) with $u[3]$, $v[3]$ and $\lambda = \lambda_1$. Then, the third-step generalized DT can be given as follows

$$R[3] = T[3]T[2]T[1]R, \quad T[3] = \lambda_1\mathbf{I} - H[2]\Lambda_3 H[2]^{-1},\tag{3.30}$$

$$u[3] = u[2] + 2i(\lambda-\lambda^*)\frac{r_1[2]s_1[2]^*}{|r_1[2]|^2+|s_1[2]|^2+|w_1[2]|^2},\tag{3.31}$$

$$v[3] = v[2] + 2i(\lambda-\lambda^*)\frac{r_1[2]w_1[2]^*}{|r_1[2]|^2+|s_1[2]|^2+|w_1[2]|^2},\tag{3.32}$$

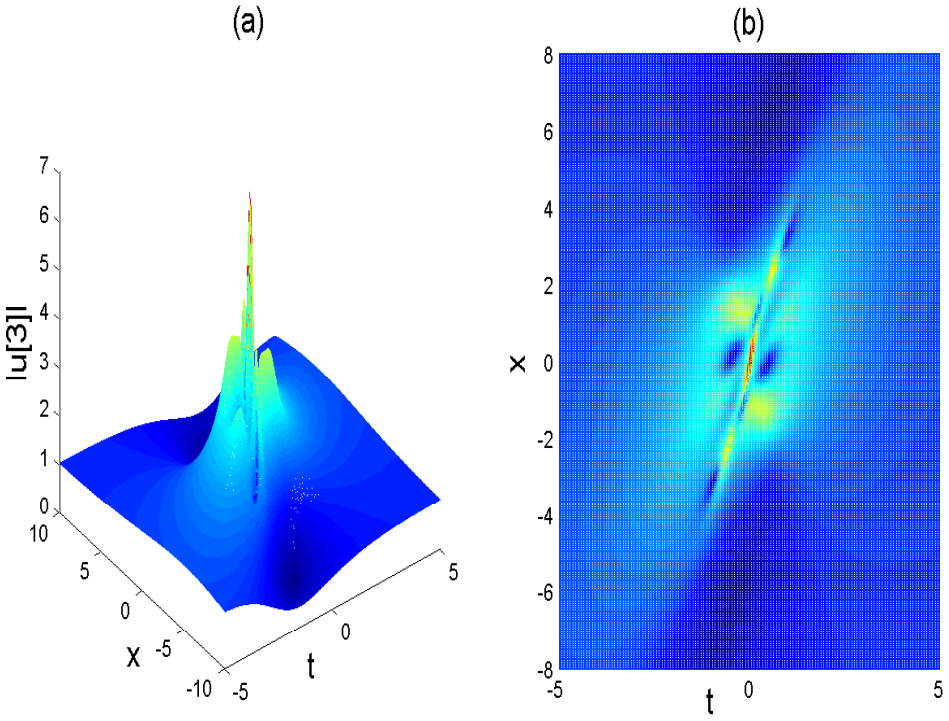

Figure 51: Third-order composite rogue wave $u[3]$ depicted with the following parameters: $a = 1$, $b = 0$, $c_1 = d_1 = c_2 = d_2 = 0$ and $\alpha = 1$. Panel (a) represents the 3-D perspective and the panel (b) stands for the density plot of the 3-D representation.

where $(r_1[2], s_1[2], w_1[2])^T = R_1[2]$, $\mathbf{I} = \begin{pmatrix} 1 & 0 & 0 \\ 0 & 1 & 0 \\ 0 & 0 & 1 \end{pmatrix}$, $H[2] = \begin{pmatrix} r_1[2] & s_1[2]^* & w_1[2]^* \\ s_1[2] & -r_1[2]^* & 0 \\ w_1[2] & 0 & -r_1[2]^* \end{pmatrix}$, and $\Lambda_3 = \begin{pmatrix} \lambda_1 & 0 & 0 \\ 0 & \lambda_1^* & 0 \\ 0 & 0 & \lambda_1^* \end{pmatrix}$. Continuing the above process and combining all the Darboux matrices, an Nth-step generalized DT is considered.

Proposition. *Notation*

$$R_1[N-1] = R_1^{[0]} + \sum_{k=1}^{N-1} T_1[k] R_1^{[1]} + \sum_{k=1}^{N-1} \sum_{l=1}^{k-1} T_1[k] T_1[l] R_1^{[2]} + \ldots + T_1[N-1] T_1[N-2] \ldots T_1[1] R_1^{[N-1]}, \tag{3.33}$$

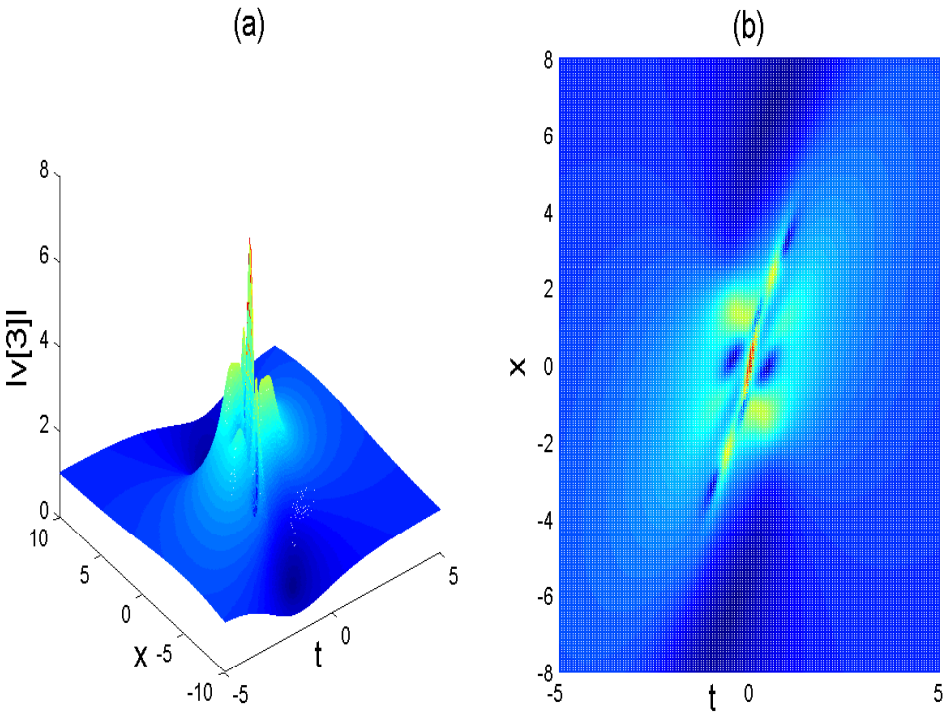

Figure 52: Third-order composite rogue wave $v[3]$ depicted with the following parameters: $a = 0$, $b = 1$, $c_1 = d_1 = c_2 = d_2 = 0$ and $\alpha = 1$. Panel (a) represents the 3-D perspective and the panel (b) stands for the density plot of the 3-D representation.

then the N-step generalized DT is provided

$$R[N] = T[N]T[N-1]...T[1]R, \quad T[k] = \lambda_1 \mathbf{I} \\ -H[k-1]\Lambda_k H[k-1]^{-1}, \tag{3.34}$$

$$u[N] = u[N-1] + 2i(\lambda - \lambda^*) \times \\ \frac{r_1[N-1]s_1[N-1]^*}{|r_1[N-1]|^2 + |s_1[N-1]|^2 + |w_1[N-1]|^2}, \tag{3.35}$$

$$v[N] = v[N-1] + 2i(\lambda - \lambda^*) \times \\ \frac{r_1[N-1]w_1[N-1]^*}{|r_1[N-1]|^2 + |s_1[N-1]|^2 + |w_1[N-1]|^2}, \tag{3.36}$$

where $(r_1[N-1], s_1[N-1], w_1[N-1])^T = R_1[N-1]$

$$H[k-1] = \begin{pmatrix} r_1[k-1] & s_1[k-1]^* & w_1[k-1]^* \\ s_1[k-1] & -r_1[k-1]^* & 0 \\ w_1[k-1] & 0 & -r_1[k-1]^* \end{pmatrix},$$

$$\Lambda_k = \begin{pmatrix} \lambda_1 & 0 & 0 \\ 0 & \lambda_1^* & 0 \\ 0 & 0 & \lambda_1^* \end{pmatrix}, \text{ and } \mathbf{I} = \begin{pmatrix} 1 & 0 & 0 \\ 0 & 1 & 0 \\ 0 & 0 & 1 \end{pmatrix}.$$

The formulae given by equations (3.33)-(3.36) are a recursive formula of the Nth-order generalized DT for the Manakov system (3.10). Although it is possible to give the $(3N) \times (3N)$ determinant representation by using the so-called crum theorem. But we prefer to use a recursive formula, because it is easy to construct higher-order rogue wave solutions with the computer. Some interesting higher-order rogue wave solutions are obtained for the Manakov system in the following section.

3.2.3 Rogue wave solutions

In order to obtain the rogue wave solution, we start with the following seed solutions of the system (3.10) as

$$u[0] = ae^{i\beta t}, \quad v[0] = be^{i\beta t}, \tag{3.37}$$

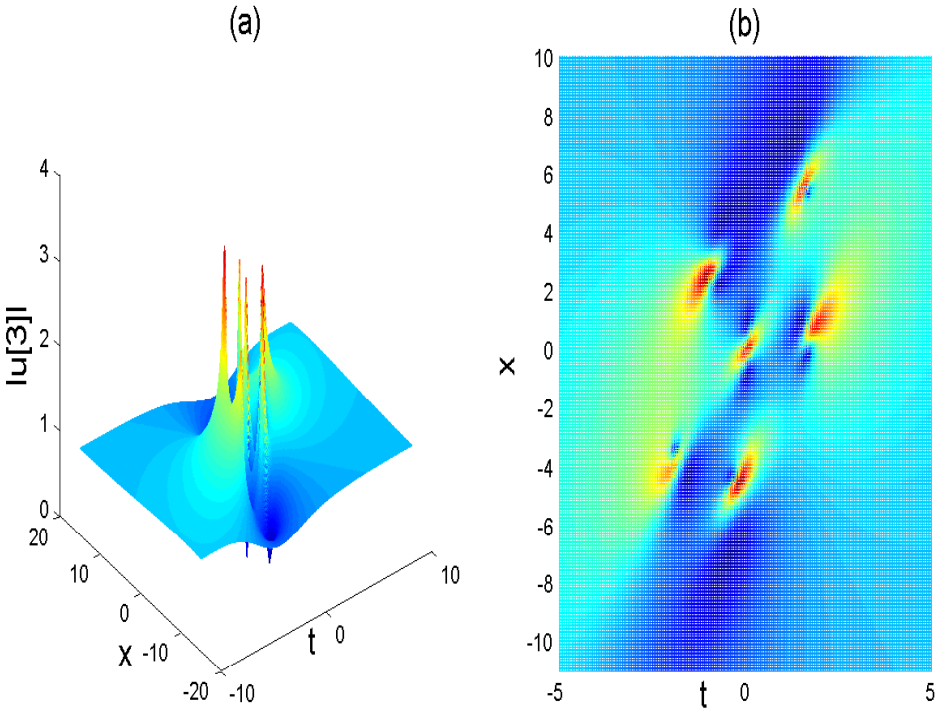

Figure 53: Third-order rogue wave $u[3]$ depicted with the following parameters: $a = 1$, $b = 0$, $c_1 = d_1 = 0$, $c_2 = d_2 = 100$ and $\alpha = 1$. Panel (a) represents the 3-D perspective and the panel (b) stands for the density plot of the 3-D representation

with $\beta = a^2 + b^2$, a and b are real constants. Then the basic solution for the Lax-pairs of equation (3.11) with $u[0]$, $v[0]$ and λ holds

$$R_1 = \begin{pmatrix} (m_1 e^{\eta_1+\eta_2} - m_2 e^{\eta_1-\eta_2}) e^{\frac{i\beta t}{2}} \\ \tau_1 (m_2 e^{\eta_1+\eta_2} - m_1 e^{\eta_1-\eta_2}) e^{-\frac{i\beta t}{2}} \\ \tau_2 (m_2 e^{\eta_1+\eta_2} - m_1 e^{\eta_1-\eta_2}) e^{-\frac{i\beta t}{2}} \end{pmatrix}, \tag{3.38}$$

where $m_1 = \left(\frac{\lambda-\sqrt{\beta+\lambda^2}}{\lambda^2+\beta}\right)^{\frac{1}{2}}$, $m_2 = \left(\frac{\lambda+\sqrt{\beta+\lambda^2}}{\lambda^2+\beta}\right)^{\frac{1}{2}}$,

$\eta_1 = 2i\alpha(\frac{1}{\alpha}x + \lambda(\lambda+2)t)$, $\tau_1 = \frac{a}{\sqrt{\beta}}$, $\tau_2 = \frac{b}{\sqrt{\beta}}$,

$\eta_2 = i\alpha\sqrt{\beta+\lambda^2}\left(\frac{1}{\alpha}x + (\lambda(\lambda+2) - \frac{\beta}{2})t + \Omega_j\right)$,

with $\Omega_j = \sum_{j=1}^{N}(c_j + id_j)\varepsilon^{2j}$.

Here the constant ε is a small parameter.

Let $\lambda = i\sqrt{\beta}(1+\varepsilon^2)$, expanding the vector function $R_1(\varepsilon)$ at $\varepsilon = 0$, we obtain

$$R_1(\varepsilon) = R_1^{[0]} + R_1^{[1]}\varepsilon^2 + R_1^{[2]}\varepsilon^4 + ..., \tag{3.39}$$

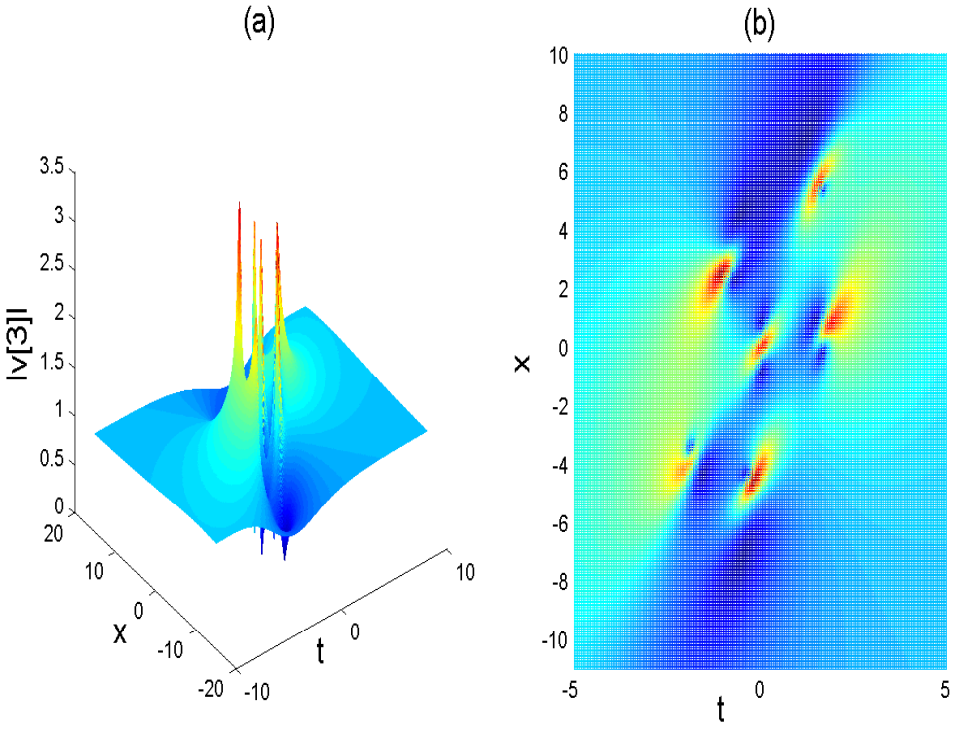

Figure 54: Third-order rogue wave $v[3]$ depicted with the following parameters: $a = 0$, $b = 1$, $c_1 = d_1 = 0$, $c_2 = d_2 = 100$ and $\alpha = 1$. Panel (a) represents the 3-D perspective and the panel (b) stands for the density plot of the 3-D representation

where,

$$R_1^{[0]} = \begin{pmatrix} r_1^0 \\ s_1^0 \\ w_1^0 \end{pmatrix}, \; R_1^{[1]} = \begin{pmatrix} r_1^1 \\ s_1^1 \\ w_1^1 \end{pmatrix}, \; R_1^{[2]} = \begin{pmatrix} r_1^2 \\ s_1^2 \\ w_1^2 \end{pmatrix} \text{...,} \text{ and } (r_1^{[i-1]}, s_1^{[i-1]}, w_1^{[i-1]}) \text{ (i=1,2,3)}$$

are given in appendix.

It is clear that $R_1^{[0]}$ is a solution of the Lax pairs (3.11) at $u[0] = ae^{i\beta t}$, $v[0] = be^{i\beta t}$ and $\lambda = i\sqrt{\beta}(1+\varepsilon^2)$. Hence from the formulae (3.23) and (3.24), we arrive at

$$u[1] = ae^{i\beta t}\left(1 + \frac{F_1 + iH_1}{D_1}\right), \quad v[1] = be^{i\beta t}\left(1 + \frac{F_1 + iH_1}{D_1}\right), \tag{3.40}$$

where

$F_1 = -4\sqrt{\beta}\alpha\,(4\beta x^2 - 12\alpha\beta^2 tx + \alpha^2\beta^2(9\beta + 16)t^2 - 1)$,

$D_1 = \frac{2}{\beta}\,(4\beta x^2 - 12\alpha\beta^2 tx + \alpha^2\beta^2(9\beta + 16)t^2 + 1)\,,$

$H_1 = 32\alpha\sqrt{\beta}t.$

The solutions $u[1]$ and $v[1]$ here stand for the vector generalized first-order rogue wave

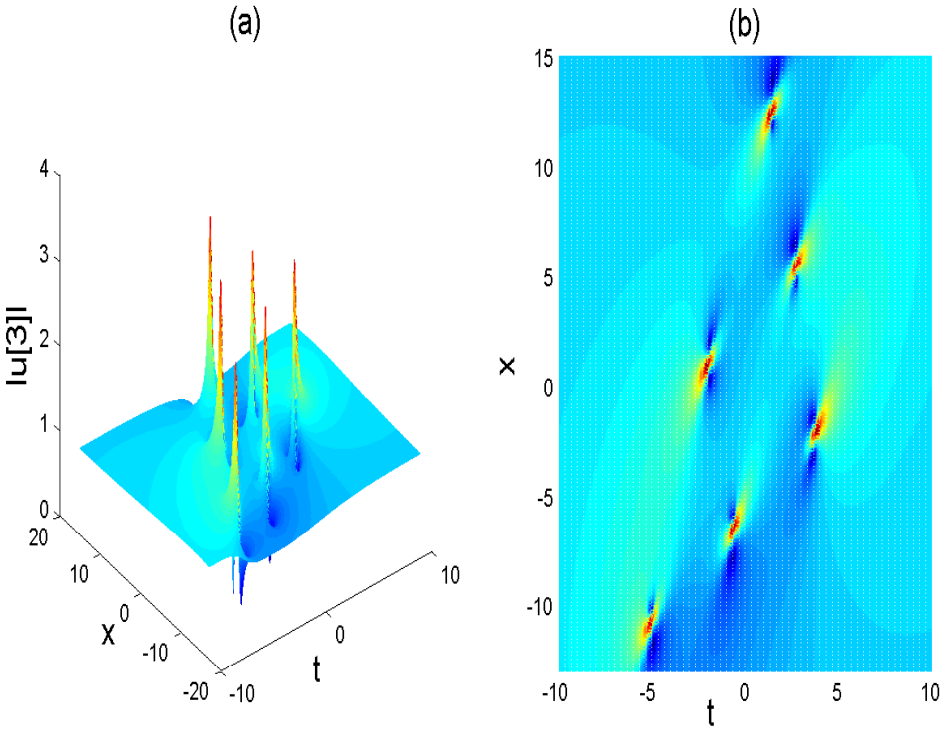

Figure 55: Third-order rogue wave $u[3]$ depicted with the following parameters: $a = 1$, $b = 0$, $c_1 = d_1 = c_2 = d_2 = 100$ and $\alpha = 1$. Panel (a) represents the 3-D perspective and the panel (b) stands for the density plot of the 3-D representation

solutions for the Manakov system (3.11). It is important to remark that, $u[1]$ and $v[1]$ are merely proportional. These solutions are depicted in figure 44. It is also important to note that the solutions obtained here for the Manakov system resemble those obtained in ref [107].

Then, using the matrices $R_1^{[0]}$ and $R_1^{[1]}$ given in appendix A, and substituting them into the expression of equation (3.27), we obtain the matrix $R_1[1]$ which elements are also given in appendix. The matrix elements $r_1[1]$, $s_1[1]$ and $w_1[1]$ are then substituted into equations (3.29) and (3.30), which give rise to the second-order vector generalization rogue wave solutions of the Manakov system (3.10).

The second-order rogue wave solution possesses two free parameters c_1 and d_1. In general, the second-order rogue solution is composed of three first-order rogue waves. For the case where $c_1 = d_1 = 0$, the rogue wave are crowded round the origin (0,0) and the maximum of $u[2]$ and $v[2]$ is 5. For this case we have rogue wave composite (see figures 45 and 46), which resemble those obtained in Ref [107]. When we increase the value of

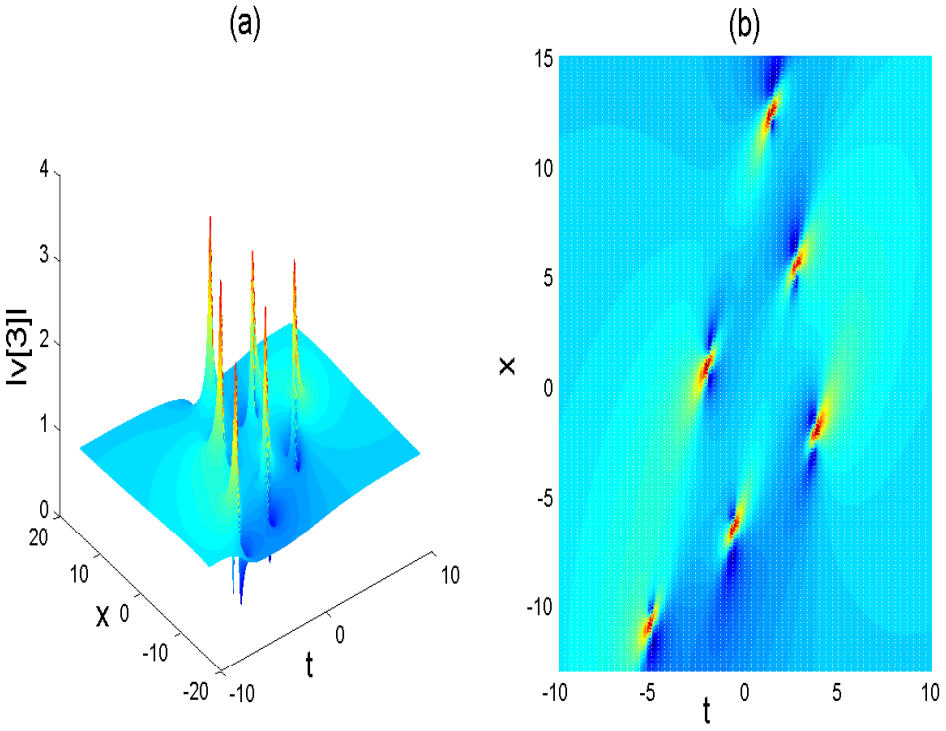

Figure 56: Third-order rogue wave $v[3]$ depicted with the following parameters: $a = 0$, $b = 1$, $c_1 = d_1 = c_2 = d_2 = 100$ and $\alpha = 1$. Panel (a) represents the 3-D perspective and the panel (b) stands for the density plot of the 3-D representation.

$|c_1|$ and $|d_1|$ we observe that three first-order rogue waves are scattered in all direction (see Figures 47-50).

Iterating formulae (3.35)-(3.36) three times (with $N = 3$), we obtain the third-order rogue wave solutions $u[3]$ and $v[3]$. We omit presenting analytical expressions since they are rather cumbersome to be write down here. By means of computer, we give the pictures of these third-order rogue wave solutions in Figures 52 and 53. We know that the third-order rogue wave possesses four free parameters c_1, d_1, c_2 and d_2. The third-order rogue wave solution is composed of six first-order rogue waves. For the case where $c_1 = d_1 = c_2 = d_2 = 0$, we can observe a composite third-order rogue wave solution and the maximum value of $u[3]$ and $v[3]$ is 7 (see Figures 51 and 52). When $c_1 = d_1 = 0$, $c_2 = d_2 = 100$, the six first-order rogue wave array a pentagon; among the six first-order rogue waves, one sits in the center and the rest are located on the vertices of the pentagon (see Figures 53 and 54)

When $c_1 = d_1 = 100$, $c_2 = d_2 = 100$, the corresponding third-order rogue wave is

composed of six first-order rogue waves as well, which array a triangle (see figures 55 and 56). This work can be found in Ref. [124].

3.3 Rogue waves dynamics in ferrites

Solitary wave solutions provide significant physical information in nonlinear science. The electromagnetic wave-propagation plays an important role in ferro- or ferrimagnetic media both from the viewpoint of theoretical perspective and from the viewpoint of practical uses, particularly in connection with the behavior of ferrite devices at microwave frequencies such as ferrite-loaded waveguide [170]. It appears fundamental and more crucial to understand deeply the micromagnetic structures in microsize and nanosize of magnets [171–174] due to the increasing interest in advanced magnetic information storage and data process elements. Indeed, the understanding of the electromagnetic propagation in ferromagnetic materials is actually made possible by the Maxwell's equations in such media. Theses equations are supplemented with a relation between the magnetization and the auxiliary magnetic field in the materials. Such a relation appears as the phenomenological equation of motion for the magnetization.

The genuine motivation of this work stems from the fact that the bulk polaritons propagating through the real ferrite with spatial configuration exhibit different complex features within the propagating directions with varying profiles, amplitudes and speeds in such a way that these features cannot be deeply understood merely by virtue of the one-dimensional configuration system of propagation. The engineering of the magnetic bulk polariton system through the soliton management technique stands to be underlying in the understanding of the fast remagnetization process of data inputs within magnetic memory devices.

Kraenkel et al. [109] reported the following. The ferrite is a ferromagnet of zero conductivity, a ferromagnetic insulator. in this case, it is assumed that it is in presence of external magnetic field and is saturated. Hence in the absence of eddy currents, electromagnetic waves may propagate. The equations that describe this wave propagation are fundamentally nonlinear. In absence of currents and charges, the Maxwell equations are

reduced to

$$-\nabla(\nabla.H) + \nabla^2 H = \frac{1}{c^2}\frac{\partial^2}{\partial^2 t}(H + M), \tag{3.41}$$

where $c = 1/\sqrt{\mu_0 \varepsilon}$ is the speed of light, μ_0 is the magnetic permeability of the vacuum, M and H are respectively the magnetization density and the magnetic induction. The following constitutive relations have been assumed

$$D = \varepsilon E, \qquad B = \mu_0(H + M).$$

A relation between the quantities H and M reads

$$\frac{\partial M}{\partial t} = -\mu_0 \gamma M \times H, \tag{3.42}$$

where γ is the gyromagnetic ratio. It is by means of this equation that the nonlinearity sets in. In view to linearize the above relations, the following perturbation have been adopted

$$M = M_0 + me^{i(kx-wt)}, \qquad H = H_0 + he^{i(kx-wt)},$$

where m and h are real vector of component (m_x, m_y, m_z) and (h_x, h_y, h_z) and k and w are respectively, the wave number and the frequency of the wave. This leads to the following dispersion relation,

$$M_0^2[w^2(1+\alpha) - \alpha k^2][w^2(1+\alpha) - k^2(\alpha + \sin^2\varphi)] - w^2(w^2 - k^2)^2 = 0.$$

It is introduced the following rescaled variables

$$\frac{\partial}{\partial x} = \frac{1}{\varepsilon}\frac{\partial}{\partial \xi}, \qquad \frac{\partial}{\partial t} = -\frac{1}{\varepsilon}\frac{\partial}{\partial \xi} + \varepsilon\frac{\partial}{\partial \tau},$$

and considered the general expressions

$$\begin{aligned} M &= M^{(0)} + \varepsilon M^{(1)} + \varepsilon^2 M^{(2)} + \cdots \\ H &= H^{(0)} + \varepsilon H^{(1)} + \varepsilon^2 H^{(2)} + \cdots . \end{aligned}$$

Introducing these relations into (3.41) and (3.42), the second order equation equation leads to $M_y^{(1)} = M_z^{(1)} = 0$ and the relations $M_x^{(1)} = -H_x^{(1)}$ and $\frac{\partial}{\partial \xi}M_x^{(1)} = M_0 H_z^{(0)}$. The third order reads

$$\begin{array}{c} \frac{\partial}{\partial \tau}H_y^{(0)} = -\frac{1}{2M_0}M_x^{(1)}\frac{\partial}{\partial \xi}M_x^{(1)}, \\ \frac{\partial^2}{\partial \xi \partial \tau}M_x^{(1)} = \frac{M_0}{2}M_x^{(1)}(H_y^{(o)} + M_0). \end{array},$$

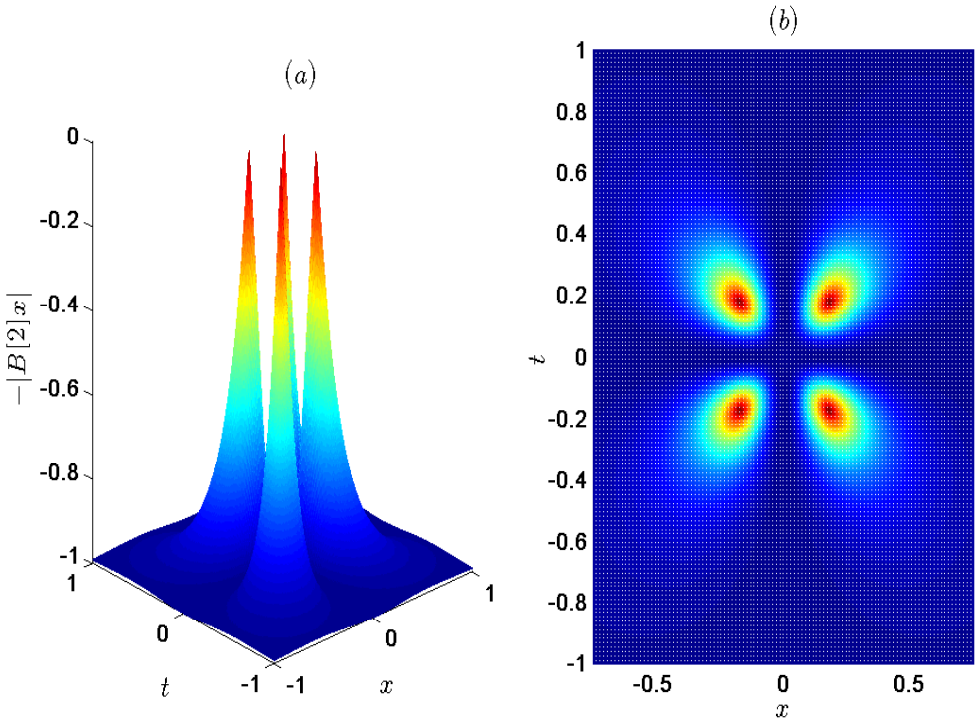

Figure 57: Rogue wave dynamics $B[2]_x$ depicted with the parameters $\alpha = 2$ and $\beta = 0$. Panel (b) is the density plot of panel (a)

These equations are nonlinear ones describing the evolution of the nonlinear terms in the expansion of H and M. Defining $M_x^{(1)} = \pm\Theta$ and $H_y^{(0)} = -M_0 + \frac{4}{M_0}\eta_\xi$, hence the following system is obtained

$$\begin{aligned} \frac{\partial^2\eta}{\partial\xi\partial\tau} &= -2\Theta\frac{\partial\Theta}{\partial\xi}, \\ \frac{\partial^2\Theta}{\partial\xi\partial\tau} &= 2\Theta\frac{\partial\eta}{\partial\xi}. \end{aligned}$$

For convenience, we adopt the following notation:

$$\begin{aligned} B_{xt} &= BC_x \\ C_{xt} &= -BB_x \end{aligned}, \tag{3.43}$$

The variables x and t stand for the space and the time coordinate respectively, while the quantities B and C represent two physical observables related respectively to the magnetization and the external magnetic field to the ferrite. The subscripts to the observables refer to their partial derivatives with respect to the corresponding variables.

Recently, Kuetche et al. [110], investigated the higher-dimensional extension of the above system and soliton solutions were calculated. More after, the above authors investigated the inhomogeneous exchange within ferrites through the phase analysis [111]. More recently, soliton solutions for the system (3.43) has been calculated via the inverse scattering transform [112].

In the past few decades, rogue waves also called freak waves, killer waves or giant waves have attracted particular attentions. A rogue wave is a large-amplitude wave met originally in oceanic conditions. In this work we extend to a complex-valued one the system (3.43) as follows:

$$\begin{aligned} B_{xt} &= BC_x \\ C_{xt} &= -\tfrac{1}{2}(B^*B)_x \end{aligned} . \tag{3.44}$$

We actually want to investigate the rogue waves solution to the above system, with the assumption that the magnetization may be complex-valued. The physical implication is that, we can have rotating waves in the ferrites due to the angular momentum of the magnetization. The main tool used in this work is the generalized Darboux transformation (DT) based on the Darboux matrix method.

3.3.1 Lax-pairs and generalized Darboux transformation

It is well known that, the Lax-pairs ensure the total integrability of nonlinear systems. Those of the system (3.44) can be given as follows

$$y_x = Uy, \quad y_t = Vy, \tag{3.45}$$

For the system (3.44) to be integrable that is U and V well-defined. Hence the system (3.44) becomes

$$\begin{aligned} B_{xt} &= BC_x \\ C_{xt} &= -\tfrac{1}{2}(B^*B)_x \end{aligned} . \tag{3.46}$$

Therefore, we obtain $U = -i\lambda \begin{pmatrix} C_x & B_x^* \\ B_x & -C_x \end{pmatrix}$, $V = \begin{pmatrix} i/4\lambda & -B^*/2 \\ B/2 & -i/4\lambda \end{pmatrix}$,

while using the zero curvature equation $U_t - V_x + [U, V] = 0$. The observable y stands for eigenfunction and is defined as $y = (r(x,t), w(x,t))^T$ (T means matrix transpose) and

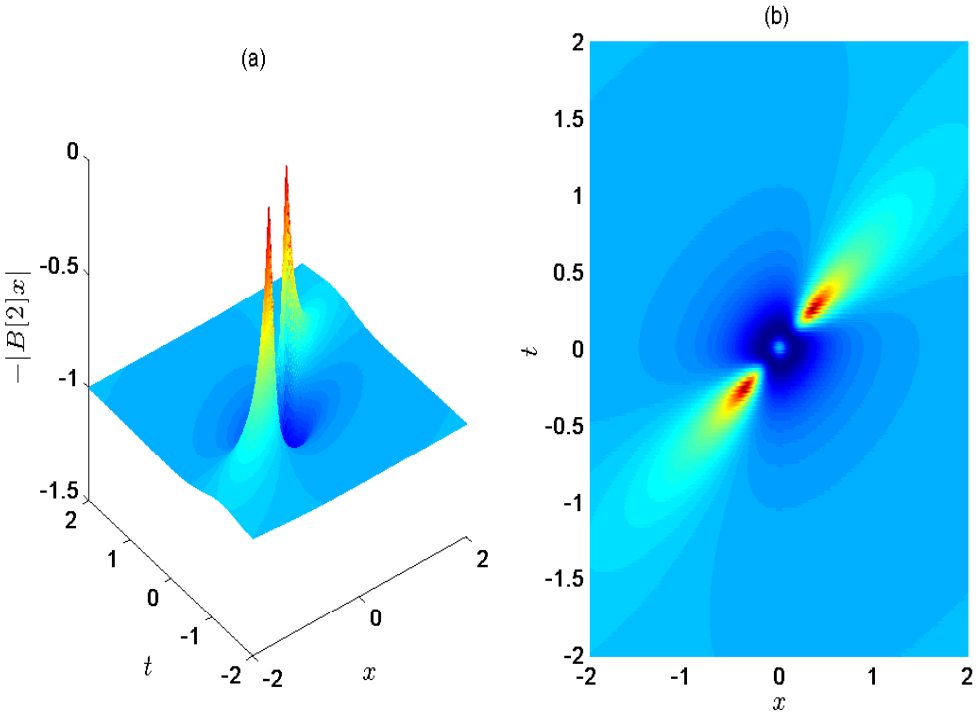

Figure 58: Rogue wave dynamics $B[2]_x$ depicted with the parameters $\alpha = 2$ and $\beta = 1$. Panel (b) is the density plot of panel (a)

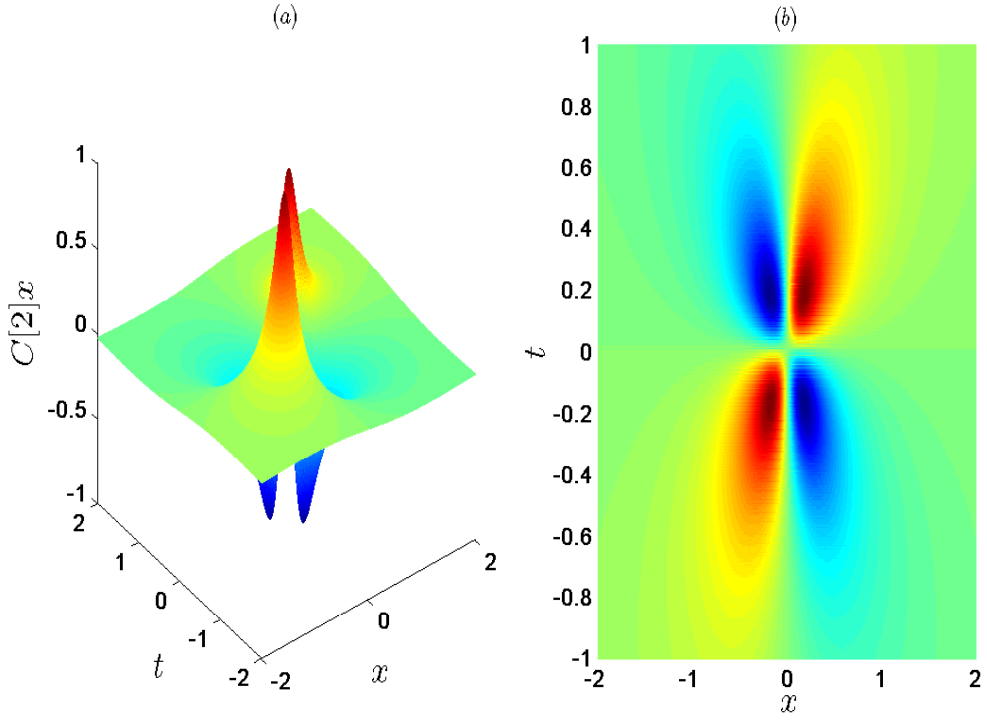

Figure 59: Rogue wave dynamics $C[2]_x$ depicted with the parameters $\alpha = 2$ and $\beta = 0$. Panel (b) is the density plot of panel (a)

λ is a spectral parameter. We start with the assumption that the function $y_1 = (r_1, w_1)^T$ is a particular solution to the Lax-pairs given in equation (3.45) with the spectral parameter λ_1 at $C = C_1[0]$ and $B = B_1[0]$.

We can transform the system (3.45) into a new one,

$$y[1]_x = U[1]y[1], \qquad y[1]_t = V[1]y[1], \tag{3.47}$$

with the following elementary DT:

$$y[1] = T[1]y, \quad T[1] = \frac{1}{\lambda}I - H[0]\Lambda[1]^{-1}H[0]^{-1}, \tag{3.48}$$

$$\begin{aligned} B[1]_x = \tfrac{\lambda_1^*}{\lambda_1}B[0]_x - i\tfrac{(\lambda_1-\lambda_1^*)r[0]^*}{\lambda_1^2\lambda_1^*(|r_1[0]|^2+|w_1[0]|^2)^2}(\lambda_1 r_1[0]^*\times \\ (w_1[0]r_{1x}[0] - r_1[0]w_{1x}[0]) - \lambda_1^*(r_1[0]r_1[0]^*w_{1x}[0] \\ +w_1[0](2w_1[0]^*w_{1x}[0] + r_1[0]^*r_{1x}[0]))), \\ C[1]_x = \tfrac{\lambda_1^*}{\lambda_1}C[0]_x + i\tfrac{\lambda_1-\lambda_1^*}{\lambda_1^2\lambda_1^*(|r_1[0]|^2+|w_1[0]|^2)^2}(\lambda_1 w_1[0]^*\times \\ r_1[0]^*(w_1[0]r_{1x}[0] - r_1[0]w_{1x}[0]) \\ +\lambda_1^*(-w_1[0]w_1[0]^{*^2}w_{1x}[0] + r_1[0]r_1[0]^{*^2}r_{1x}[0])), \end{aligned} \tag{3.49}$$

where $r_1[0] = r_1$, $w_1[0] = w_1$, $I = \begin{pmatrix} 1 & 0 \\ 0 & 1 \end{pmatrix} = T[0]$, $H[0] = \begin{pmatrix} r_1[0] & -w_1[0]^* \\ w_1[0] & r_1[0]^* \end{pmatrix}$

$\Lambda[1] = \begin{pmatrix} \lambda_1 & 0 \\ 0 & \lambda_1^* \end{pmatrix}$.

Here, the matrices U and V are replaced by $U[1]$ and $V[1]$ with the new potentials $B[1]_x$ and $C[1]_x$ therein.

In the following, we use the Guo and coworkers's approach to derive the generalized Darboux transformation for the system (3.46). We note that,

$$y_1 = y_1(\lambda_1 + \varepsilon) \tag{3.50}$$

is a special solution to the Lax-pairs given in equation (3.45) with $B = B[0]$, $C = C[0]$ and $\lambda = \lambda_1 + \varepsilon$. Here ε is a perturbation parameter. Expanding y_1 in a Taylor series in ε, we get

$$y_1(\lambda_1 + \varepsilon) = y_1^{[0]} + y_1^{[1]}\varepsilon + y_1^{[2]}\varepsilon^2 + y_1^{[3]}\varepsilon^3 + ... \tag{3.51}$$

where $y_1^{[j]} = \frac{1}{j!}\frac{\partial^j}{\partial \lambda_1^j} y_1(\lambda_1)$ $(j = 0, 1, 2, 3, ...)$.

It is clear that $y_1^{[0]}$ is a solution to the Lax-pairs of equation (3.45), with the seed solutions $B_x = B[0]_x$, $C_x = C[0]_x$ corresponding to the spectral parameter $\lambda = \lambda_1$. So the first step generalized DT follows,

$$\begin{aligned}
B[1]_x = \tfrac{\lambda_1^*}{\lambda_1} B[0]_x - i\tfrac{(\lambda_1-\lambda_1^*)r[0]^*}{\lambda_1^2\lambda_1^*(|r_1[0]|^2+|w_1[0]|^2)^2}(\lambda_1 r_1[0]^* \times \\
(w_1[0]r_{1x}[0] - r_1[0]w_{1x}[0]) - \lambda_1^*(r_1[0]r_1[0]^* w_{1x}[0] \\
+w_1[0](2w_1[0]^* w_{1x}[0] + r_1[0]^* r_{1x}[0]))), \\
C[1]_x = \tfrac{\lambda_1^*}{\lambda_1} C[0]_x + i\tfrac{\lambda_1-\lambda_1^*}{\lambda_1^2\lambda_1^*(|r_1[0]|^2+|w_1[0]|^2)^2}(\lambda_1 w_1[0]^* \times \\
r_1[0]^*(w_1[0]r_{1x}[0] - r_1[0]w_{1x}[0]) \\
+\lambda_1^*(-w_1[0]w_1[0]^{*^2} w_{1x}[0] + r_1[0]r_1[0]^{*^2} r_{1x}[0])),
\end{aligned} \tag{3.52}$$

and $T[1] = \frac{1}{\lambda} I - H[0]\Lambda[1]^{-1}H[0]^{-1}$, where the quantities I, $H[0]$ and $\Lambda[1]$ are identical as those given above.

Through the following limit process,

$$\begin{aligned}
\lim_{\varepsilon\to 0} \frac{(T[1]|_{\lambda=\lambda_1+\varepsilon})\, y_1}{\varepsilon} &= \lim_{\varepsilon\to 0} \frac{(\varepsilon + T_1[1]|_{\lambda=\lambda_1})y_1}{\varepsilon} \\
&= y_1^{[0]} + T_1[1]y_1^{[1]} \equiv y_1[1],
\end{aligned} \tag{3.53}$$

we get another solution to the Lax-pair of equation (3.45). Then, the second-step generalized DT can be forwarded, namely,

$$\begin{aligned} B[2]_x &= \tfrac{\lambda_1^*}{\lambda_1} B[1]_x - i\tfrac{(\lambda_1-\lambda_1^*)r[0]^*}{\lambda_1^2\lambda_1^*(|r_1[1]|^2+|w_1[1]|^2)^2}(\lambda_1 r_1[1]^*\times \\ &(w_1[1]r_{1x}[1] - r_1[1]w_{1x}[1]) - \lambda_1^*(r_1[1]r_1[1]^* w_{1x}[1] \\ &+w_1[1](2w_1[1]^* w_{1x}[1] + r_1[1]^* r_{1x}[1]))), \\ C[2]_x &= \tfrac{\lambda_1^*}{\lambda_1} C[1]_x + i\tfrac{\lambda_1-\lambda_1^*}{\lambda_1^2\lambda_1^*(|r_1[1]|^2+|w_1[1]|^2)^2}(\lambda_1 w_1[1]^*\times \\ &r_1[1]^*(w_1[1]r_{1x}[1] - r_1[1]w_{1x}[1]) \\ &+\lambda_1^*(-w_1[1]w_1[1]^{*^2} w_{1x}[1] + r_1[1]r_1[1]^{*^2} r_{1x}[1])), \end{aligned} \tag{3.54}$$

and $T[2] = \lambda^{-1}I - H[1]\Lambda[2]^{-1}H[1]^{-1}$, where

$H[1] = \begin{pmatrix} r_1[1] & -w_1[1]^* \\ w_1[1] & r_1[1]^* \end{pmatrix}$, $\Lambda[2] = \begin{pmatrix} \lambda_1 & 0 \\ 0 & \lambda_1^* \end{pmatrix}$, and $y_1[1] = (r_1[1], s_1[1])^T$.

3.3.2 Rogue wave solutions.

In view to obtain rogue wave solutions for the system (3.46), we begin with the seeding ones $B[0]_x = i\alpha e^{i(\alpha x+\beta t)}$ and $C[0]_x = -\alpha\beta$, where the quantities α and β are two real free parameters. The corresponding solution for the Lax-pairs of equation (3.45) at $\lambda = -\frac{1}{2(\beta+i)}(1+\varepsilon^2)$ holds

$$y_1(\varepsilon) = \begin{pmatrix} (M_1 e^{\sigma} + M_2 e^{-\sigma})e^{-\frac{i}{2}\theta} \\ (M_2 e^{\sigma} + M_1 e^{-\sigma})e^{\frac{i}{2}\theta} \end{pmatrix}, \tag{3.55}$$

where $\sigma = \frac{1}{2}\alpha\rho(x+wt)$, $\rho = \sqrt{-4\beta^2\lambda^2 - 4\lambda^2 - 4\beta\lambda - 1}$, $w = \frac{1}{2\alpha\lambda}$,

$M_1 = \sqrt{\frac{\rho+2i\beta+i}{2\lambda}}$, $\quad M_2 = \sqrt{\frac{-\rho+2i\beta\lambda+i}{2\lambda}}$ and $\theta = \alpha x + \beta t$.

Expanding the vector function $y_1(\varepsilon)$ in a Taylor series at $\varepsilon = 0$, we obtain the following expression

$$y_1(\varepsilon) = y_1^{[0]} + y_1^{[1]}\varepsilon^2 + y_1^{[2]}\varepsilon^4 + y_1^{[3]}\varepsilon^6 + ..., \tag{3.56}$$

where $y_1^{[0]} = \begin{pmatrix} r_1^{[0]} \\ w_1^{[0]} \end{pmatrix}$, $\quad y_1^{[1]} = \begin{pmatrix} r_1^{[1]} \\ w_1^{[1]} \end{pmatrix}$...

with $r_1^{[0]} = 2e^{-\frac{i}{2}\theta}$, $w_1^{[0]} = 2e^{\frac{i}{2}\theta}$

$r_1^{[1]} = -2e^{-\frac{i}{2}\theta}(-1 - 4t + 4\beta^2 t - 4i\alpha x + 8it\beta - 4\alpha x\beta)$,

and $w_1^{[1]} = 2e^{\frac{i}{2}\theta}(1 - 4\alpha x\beta - 4i\alpha x + 8it\beta + 4\beta^2 t - 4t)$,

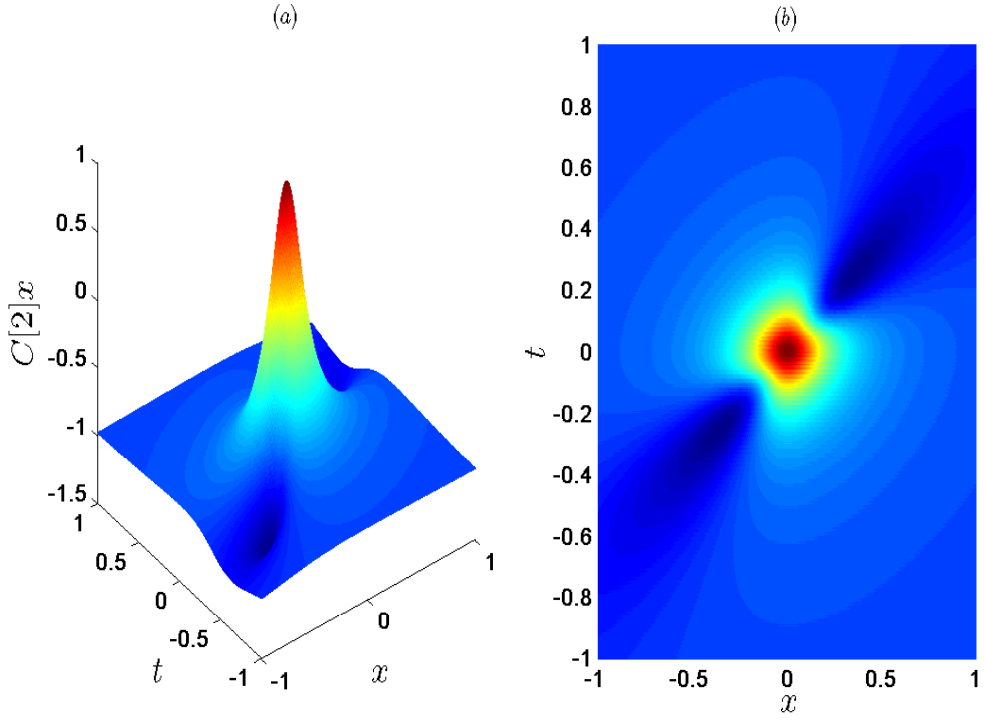

Figure 60: Rogue wave dynamics $C[2]_x$ depicted with the parameters $\alpha = 2$ and $\beta = 1$. Panel (b) is the density plot of panel (a)

It is very important to notify that only the first two terms of the series are taken into account, because it is sufficient to construct the first-order rogue wave solution to the system (3.46). If higher-order rogue wave are targeted, one needs to consider more terms in equation (3.56) to be sure to the accuracy of the results.

Taking into account that the function $y_1^{[0]}$ is a solution to the Lax-pairs (3.45) at $B_x = B[0]_x$, $C_x = C[0]_x$, we substitute the above seed solution into equations (3.51) and we get a trivial solution to the system (3.46) as follows $B[1]_x = -i\alpha e^{i\theta}$ and $C[1]_x = -\alpha\beta$ Using the trivial solutions above and the formulae given in equations (3.53) and (3.54), with the following Darboux matrix $T[1] = \begin{pmatrix} -2i & -2ie^{-i\theta} \\ 2ie^{i\theta} & -2i \end{pmatrix}$, the rogue wave solution for the system (3.46), can be given as follows

$$B[2]_x = \frac{H_1 + iG_1}{D_1}, \qquad C[2]_x = \frac{F_1}{D_1}, \tag{3.57}$$

with $F_1 = -\alpha\,(\beta^3 - 3\,\beta - 64\,\alpha\,\beta^6 tx + 704\,\alpha\,\beta^2 tx - 256\,\alpha\,\beta^4 tx + 6144\,\alpha^2\beta^5 t^2x^2 + 5120\,\alpha^2\beta^7 t^2x^2 + 3072\,\alpha^2\beta^3 t^2x^2 + 512\,\alpha^2\beta\,t^2x^2 - 1024\,\alpha^3\beta^8 tx^3 - 4096\,\alpha\,\beta^8 t^3x - 3072\,\alpha^3\beta^6 tx^3 -$

$6144\,\alpha\,\beta^6t^3x-1024\,\alpha^3\beta^2tx^3-1024\,\alpha\,\beta^2t^3x-3072\,\alpha^3\beta^4tx^3-4096\,\alpha\,\beta^4t^3x+1536\,\alpha^2\beta^6t^2x^2-1024\,\alpha\,\beta^{10}t^3x-128\,xt\alpha+768\,\alpha^4\beta^5x^4+128\,\alpha^2\beta^3x^2-160\,\alpha^2\beta\,x^2+768\,\alpha^4\beta^3x^4+32\,\alpha^2\beta^5x^2+256\,\alpha^4\beta\,x^4+256\,\alpha^4\beta^7x^4+256\,\beta^{11}t^4+2560\,\beta^5t^4-544\,\beta^3t^2+256\,\beta\,t^4+352\,\beta\,t^2+160\,\beta^5t^2+32\,\beta^7t^2+1280\,\beta^6t^4+1280\,\beta^3t^4+2560\,\beta^7t^4)$,

$G_1 = \alpha - 1024\,\alpha^4\beta\,tx^3 - 1024\,\alpha^2\beta\,t^3x - 4096\,\alpha^2\beta^3t^3x + 64\,\alpha^2\beta^5tx - 6144\,\alpha^2\beta^5t^3x - 1024\,\alpha^4\beta^7tx^3-4096\,\alpha^2\beta^7t^3x+1536\,\alpha^3\beta^8t^2x^2-1024\,\alpha^2\beta^9t^3x-384\,\alpha^2\beta^3tx+3072\,\alpha^3\beta^2t^2x^2+6144\,\alpha^3\beta^4t^2x^2-3072\,\alpha^4\beta^5tx^3-3072\,\alpha^4\beta^3tx^3+576\,\alpha^2\beta\,tx+5120\,\beta^6\alpha^3t^2x^2+256\,\alpha^5\beta^6x^4+768\,\alpha^5\beta^4x^4+2560\,\alpha\,\beta^6t^4+1280\,\alpha\,\beta^8t^4+256\,\alpha\,\beta^{10}t^4-32\,\alpha^3\beta^4x^2+512\,\alpha^3t^2x^2+128\,\alpha^3x^2\beta^2-32\,\alpha\,\beta^6t^2+224\,\alpha\,t^2\beta^4+768\,\alpha^5\beta^2x^4+2560\,\alpha\,\beta^4t^4+1280\,\alpha\,\beta^2t^4-736\,\alpha\,t^2\beta^2+32\,\alpha\,t^2-96\,\alpha^3x^2+256\,\alpha\,t^4-3\,\alpha\,\beta^2+256\,\alpha^5x^4$,

$H_1 = 1024\,\alpha^3\beta^5tx^2 + 2048\,\alpha^3\beta^3tx^2 + 1024\,\alpha^3\beta\,tx^2 - 1792\,\alpha^2\beta^2t^2x - 2816\,\alpha^2\beta^4t^2x - 1280\,\alpha^2\beta^6t^2x - 256\,\alpha^4\beta^4x^3 - 256\,\alpha^2t^2x - 512\,\alpha^4\beta^2x^3 - 48\,\alpha^2\beta^2x - 64\,\alpha\,\beta\,t + 512\,\alpha\,\beta\,t^3 + 512\,\alpha\,\beta^7t^3 + 64\,\alpha\,\beta^3t + 1536\,\alpha\,\beta^3t^3 + 1536\,\alpha\,\beta^5t^3 + 16\,\alpha^2x - 256\,\alpha^4x^3$,

and $D_1 = (1+\beta^2)\,(1+16\,t^2+32\,t^2\beta^2+16\,t^2\beta^4-32\,\alpha\,\beta\,tx-32\,\alpha\,\beta^3tx+16\,\alpha^2x^2+16\,\alpha^2x^2\beta^2)^2$.

The depictions corresponding to the rogue wave solution are shown in figures (57), (58), (59) and (60).

In the Figures (57), (58) and (59), the familiar symmetry of the Peregrine soliton is absent, since the place where the usual rogue waves reach their maximum shape moves from the center to the surroundings. Also, in the Figure (57), we observe wave scattered in all direction, while in the Figures (58) and (59), the waves are localized both in the space and time directions. In our knowledge, the rogue wave solution in ferrites has not yet been reported in the literature.

3.4 Generalized Darboux transformation and Parameter-dependent rogue wave solutions to a nonlinear Schrödinger system

Originally, the phenomenon of rogue waves refers to a giant ocean wave, responsible of many marine disasters [1]. Many years after that, more effort have been devoted to the study and the understanding of this mysterious phenomenon in many fields such as hydro-

dynamics, plasma physics, optics, capillary waves and Bose-Einstein codensates just to name a few. From the study of the phenomenon, it resorts that rogue wave appears from nowhere and disappears without a trace [13]; their amplitude is two or three times larger than their surrounding waves. The unpredictability of rogue waves implies that they can be expressed by rational functions localized both in space and time. The simplest rogue wave solution was firstly obtained by Peregrin ; more after, Akhmediev and coworkers have calculated the first-order rogue wave solution for the nonlinear Schrödinger equation(NLSE). Analytical rogue wave solution has been also obtained for various physical models.

In view to generate rogue wave solutions to physical models, many mathematical tools have been used such as similarity transformation, Darboux transformation (DT) just to name a few. The traditional DT was developed in reference [167], but that one is not appropriated to construct higher-order rogue wave solution to nonlinear physical systems. So Guo and coworkers have modified it to derive the generalized DT. This one is the tool used in this work to construct rogue wave solutions.

The system under consideration in this section was derived in reference [113]. His DT was constructed and soliton solutions were provided. This system is a couple of generalized nonlinear Schrödinger equations(GNLSE):

$$\begin{aligned} iu_t + u_{xx} - 2u^2v + 4\beta^2u^3v^2 + 4i\beta(uv)_xu = 0, \\ iv_t - v_{xx} + 2uv^2 - 4\beta^2u^2v^3 + 4i\beta(uv)_xv = 0. \end{aligned} \tag{3.58}$$

The quantities u, v are two polarized varying complex envelopes and β is a constant parameter denoting the strength of higher-order terms. The subscripts mean partial derivative. Setting $v = \epsilon u^*$, the system above is reduced to a GNLSE as follows

$$iu_t + u_{xx} - 2\epsilon|u|^2u + 4\epsilon^2\beta^2|u|^4u + 4i\epsilon\beta(|u|^2)_xu = 0, \quad \epsilon = \pm 1. \tag{3.59}$$

This equation was studied in Ref. [114] by means of the gauge transformation. In equation (3.59), for the value of the parameter $\epsilon = +1$, the system has compact manifold ie admits the $SU(2)$ symmetry; and for the case $\epsilon = -1$ the system has non compact manifold ie admit the $SU(1,1)$ symmetry [114]. In equation (3.59), the third and the fourth terms are cubic and quintic nonlinearity respectively, and they describe the dynamics of two and three body atomic interactions in a Bose Einstein condensates(BECs), while the last one

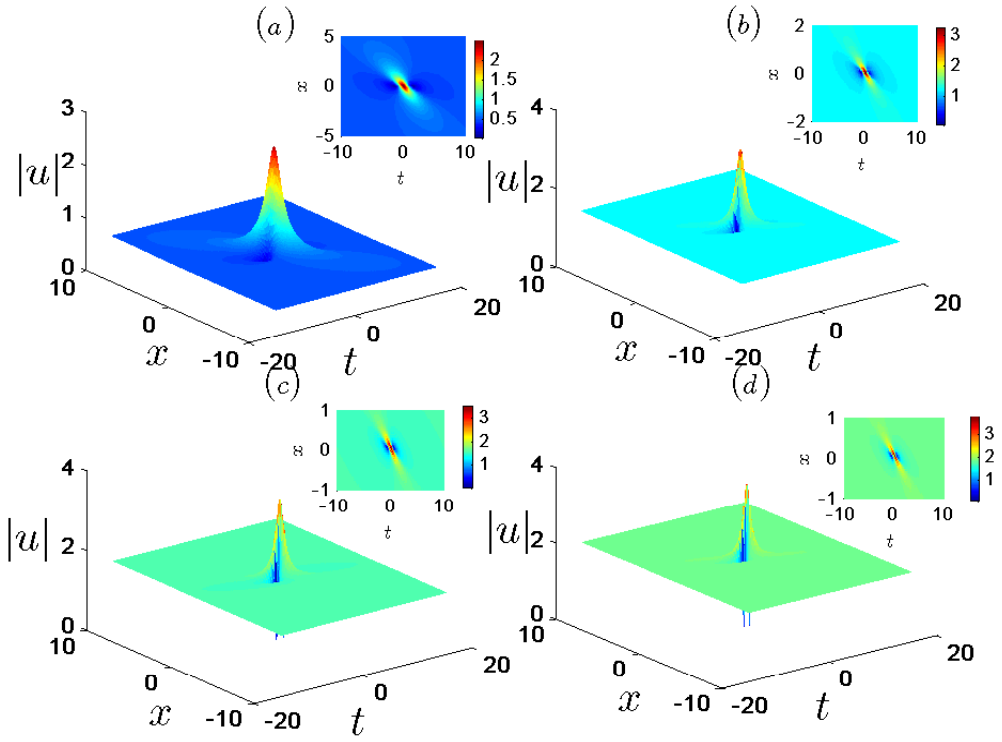

Figure 61: First-order rogue wave solution to system (1.1). The panels (a), (b), (c) and (d) are depicted with the value of $\beta = 0.8$, $\beta = 0.9$, $\beta = 0.95$ and $\beta = 1$, respectively.

scales the delayed nonlinear response of the system which offsets the modulation arising from three-body interactions. In the nonlinear fiber optics, the last term of equation (3.59) stands for self-frequency shift (SFS). The system (3.58) can model the propagation of nonlinear wave in a wide variety of fields such as BECs, plasma, nonlinear optics and the theory of deep water waves.

3.4.1 Lax-pairs and Darboux transformation

Due to integrability, the system (1.1) can be cast into 2×2 eigenvalue problem [113], namely

$$\Phi_x = U\Phi, \qquad \Phi_t = V\Phi, \tag{3.60}$$

with $U = \begin{pmatrix} -i\lambda - i\beta uv & u \\ v & i\lambda + i\beta uv \end{pmatrix}$, $V = \begin{pmatrix} A & B \\ C & -A \end{pmatrix}$,

$A = -2i\lambda^2 + \beta(u_x v - uv_x) + 4i\beta^2 u^2 v^2 - iuv$, $B = 2u\lambda + iu_x - 2\beta u^2 v$, $C = 2v\lambda - iv_x - 2\beta uv^2$.

The quantity λ is the spectral parameter and $\Phi = \begin{pmatrix} \varphi(x,t) \\ \phi(x,t) \end{pmatrix}$ is the vector eigenfunction. Through the zero-curvature equation $U_t - V_x + (UV - VU) = 0$, the system (3.58) can be easily obtained.

(i) First iteration.

A special gauge transformation is now the DT [113],

$$\Phi[1] = T[1]\Phi, \qquad T[1] = \begin{pmatrix} \alpha_1 & 0 \\ 0 & 1/\alpha_1 \end{pmatrix} (I\lambda - S[1]), \tag{3.61}$$

where

$(ln\alpha_1)_x = 4i\beta[|S[1]_{12}|^2 - Im(S[1]_{12}u^*)]$,

$(ln\alpha_1)_t = 4i\beta[4Re(S[1]_{11})|S[1]_{12}|^2 - 2Im(S[1]_{22}S[1]_{21}u) + 2\beta Im(S[1]_{12}v) - iIm(S[1]_{21}u_x)]$,

Φ and $\Phi[1]$ are old and new eigenfunctions respectively, T is the Darboux matrix, I is the identity matrix and S is a non-singular matrix. The DT (1.7) transforms the Lax-pairs given in equation (3.60) into the new ones,

$$\Phi[1]_x = U[1]\Phi[1], \qquad \Phi[1]_t = V[1]\Phi[1], \tag{3.62}$$

where the matrices $U[1]$ and $V[1]$ have same form as U and V with the new potentials $u[1]$ and $v[1]$ therein. Inserting equation (3.61) into equation (3.60), one can easily obtain the following

$$U[1] = (T_x + TU)T^{-1}, \qquad V[1] = (T_t + TV)T^{-1}. \tag{3.63}$$

We assume the matrix S to be on the form

$$S = \begin{pmatrix} S_{11} & S_{12} \\ S_{21} & S_{22} \end{pmatrix} = H_1\Lambda_1 H_1^{-1}, \quad H_1 = \begin{pmatrix} \varphi_1 & -\phi_1^* \\ \phi_1 & \varphi_1^* \end{pmatrix}, \quad \Lambda_1 = \begin{pmatrix} \lambda_1 & 0 \\ 0 & \lambda_1^* \end{pmatrix}. \tag{3.64}$$

The quantities φ_1^*, ϕ_1^* and λ_1^* are complex conjugates of φ_1, ϕ_1 and λ_1 respectively. The elementary DT follows

$$\begin{aligned} u[1] &= \alpha_1^2(u + 2iS_{12}), \\ v[1] &= \tfrac{1}{\alpha_1^2}\,(v - 2iS_{21})\,. \end{aligned} \tag{3.65}$$

$\Phi_1 = (\varphi_1, \phi_1)^T$ is a special solution of the Lax-pairs given in equation (3.60) at $\lambda = \lambda_1$. From the orthogonality condition, it follows that $(-\phi_1^*, \varphi_1^*)^T$ is also a solution to the Lax-pairs given in equation (3.60) at $\lambda = \lambda_1^*$. From the first iteration given by equation (3.61),

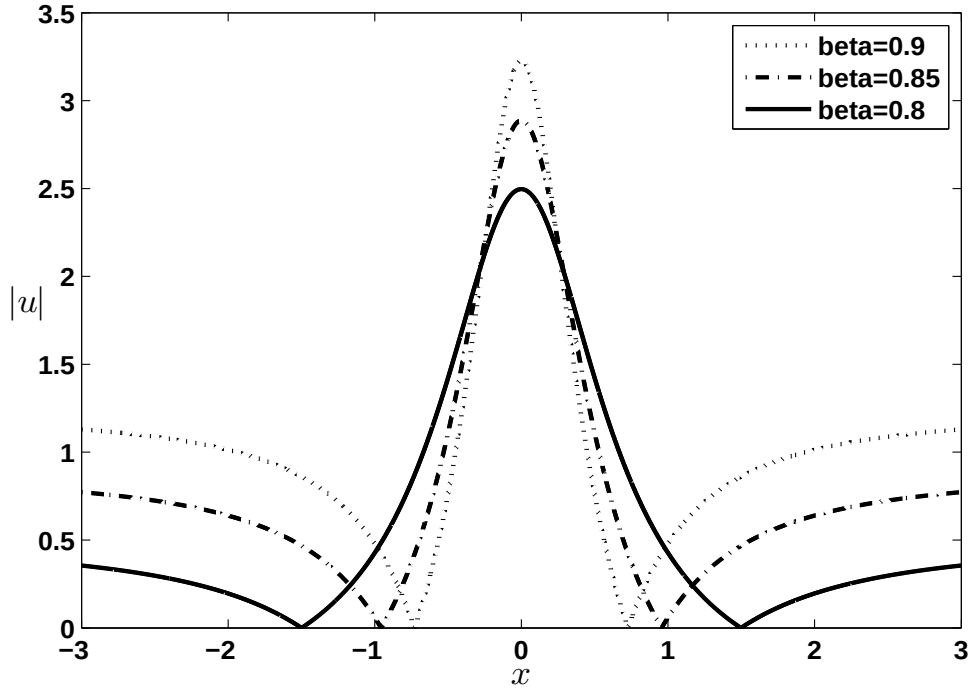

Figure 62: Compression of the wave along the x axis. The continuous line corresponds to the case where $\beta = 0.8$, the small dashed line is for $\beta = 0.85$ and the big dashed line is for the case where $\beta = 0.9$.

it follows that if H_1 is a solution of $\Phi[1]$ for $\Lambda = \Lambda_1$, then

$$H_1\Lambda_1 - S[1]H_1 = 0 \Longrightarrow S[1] = H_1\Lambda_1 H_1^{-1}. \tag{3.66}$$

Such that

$$\begin{pmatrix} S_{11} & S_{12} \\ S_{21} & S_{22} \end{pmatrix} = \begin{pmatrix} \varphi_1 & -\phi_1^* \\ \phi_1 & \varphi_1^* \end{pmatrix} \times \begin{pmatrix} \lambda_1 & 0 \\ 0 & \lambda_1^* \end{pmatrix} \times \begin{pmatrix} \varphi_1 & -\phi_1^* \\ \phi_1 & \varphi_1^* \end{pmatrix}^{-1}. \tag{3.67}$$

From the cramer's rule, the exact forms of the matrix elements S_{12} and S_{21} are expressed as follows

$$S_{12} = \frac{\begin{vmatrix} \lambda_1\varphi_1 & -\lambda_1^*\phi_1^* \\ \varphi_1 & -\phi_1^* \end{vmatrix}}{\begin{vmatrix} \varphi_1 & -\phi_1^* \\ \phi_1 & \varphi_1^* \end{vmatrix}}, \qquad S_{21} = \frac{\begin{vmatrix} \phi_1 & \varphi_1^* \\ \lambda_1\phi_1 & \lambda_1^*\varphi_1^* \end{vmatrix}}{\begin{vmatrix} \varphi_1 & -\phi_1^* \\ \phi_1 & \varphi_1^* \end{vmatrix}}. \tag{3.68}$$

From these determinant forms, the compact forms of S_{12} and S_{21} yield

$$S_{12} = \frac{(\lambda_1^* - \lambda_1)\varphi_1\phi_1^*}{|\varphi_1|^2 + |\phi_1|^2}, \qquad S_{21} = \frac{(\lambda_1^* - \lambda_1)\phi_1\varphi_1^*}{|\varphi_1|^2 + |\phi_1|^2}. \tag{3.69}$$

Knowing the exact expressions of S_{12} and S_{21}, the solutions of the system (3.58) can be given, according to equation (3.65) as follows

$$u[1] = \alpha_1^2\left(u + 2i\frac{(\lambda_1^* - \lambda_1)\varphi_1\phi_1^*}{|\varphi_1|^2 + |\phi_1|^2}\right), \qquad v[1] = \frac{1}{\alpha_1^2}\left(v - 2i\frac{(\lambda_1^* - \lambda_1)\phi_1\varphi_1^*}{|\varphi_1|^2 + |\phi_1|^2}\right). \tag{3.70}$$

The solutions $u[1]$ and $v[1]$ can be expressed in form of determinant as follows

$$u[1] = \alpha_1^2\left(u + 2i\frac{\begin{vmatrix} \lambda_1\varphi_1 & -\lambda_1^*\phi_1^* \\ \varphi_1 & -\phi_1^* \end{vmatrix}}{\begin{vmatrix} \varphi_1 & -\phi_1^* \\ \phi_1 & \varphi_1^* \end{vmatrix}}\right), \qquad v[1] = \frac{1}{\alpha_1^2}\left(v - 2i\frac{\begin{vmatrix} \phi_1 & \varphi_1^* \\ \lambda_1\phi_1 & \lambda_1^*\varphi_1^* \end{vmatrix}}{\begin{vmatrix} \varphi_1 & -\phi_1^* \\ \phi_1 & \varphi_1^* \end{vmatrix}}\right). \tag{3.71}$$

From the above equations, it is possible to generate soliton wave solution, breather wave solution and rogue wave solution to the system under consideration.

(ii) Second iteration

The second step DT begin with

$$\Phi[2] = T[2]\Phi[1], \qquad T[2] = \begin{pmatrix} \alpha_2 & 0 \\ 0 & 1/\alpha_2 \end{pmatrix}(I\lambda - S[2]), \tag{3.72}$$

where

$(ln\alpha_2)_x = 4i\beta[|S[2]_{12}|^2 - Im(S[2]_{12}u[1]^*)]$,

$(ln\alpha_2)_t = 4i\beta[4Re(S[2]_{11})|S[2]_{12}|^2 - 2Im(S[2]_{22}S[2]_{21}u[1]) + 2\beta Im(S[2]_{12}v[1]) - iIm(S[2]_{21}u[1]_x)]$,

$\Phi[2]$ and $\Phi[1]$ stand for the second and the first iteration of the DT respectively, $T[2]$ is the second iterated Darboux matrix. This DT transforms the Lax-pairs obtained in the first iteration into a new one

$$\Phi[2]_x = U[2]\Phi[2], \qquad \Phi[2]_t = V[2]\Phi[2], \tag{3.73}$$

where $U[2]$ and $V[2]$ are matrices as $U[1]$ and $V[1]$ with the new potentials $u[2]$ and $v[2]$ therein. Then, Inserting equation (3.72) into (3.62), one can easily obtain the following

$$U[2] = (T[2]_x + T[2]U[1])\,T[2]^{-1}, \qquad V[2] = (T[2]_t + T[2]V[1])\,T[2]^{-1}. \tag{3.74}$$

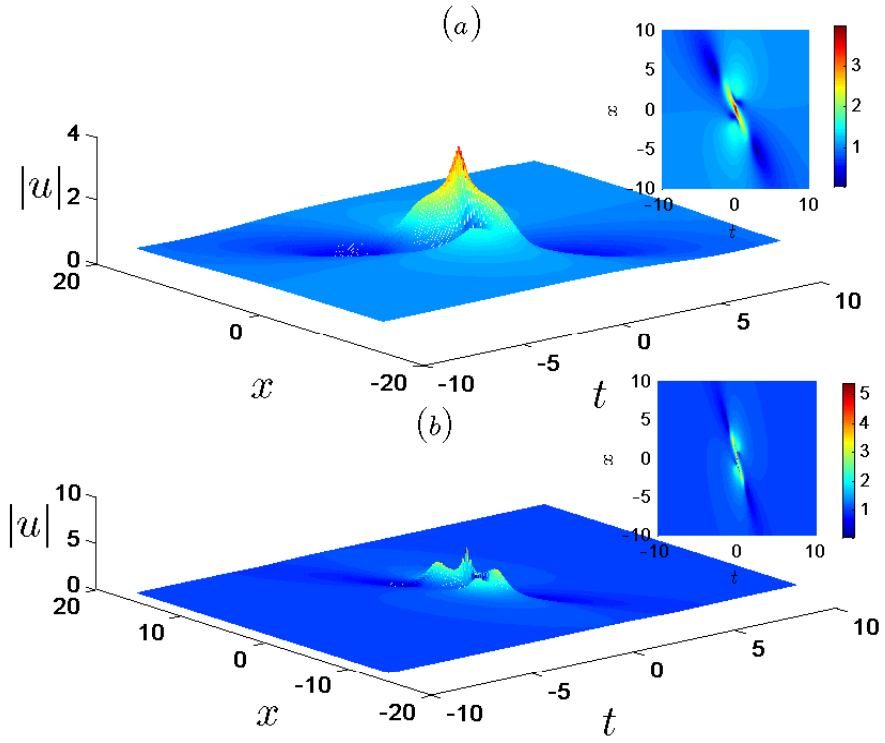

Figure 63: Second-order rogue wave solution to system (1.1). The panels (a) and (b) are depicted with the value of $\beta = 0.8$ and $\beta = 0.95$, respectively. In all the cases $c_1 = d_1 = 0$

We assume the matrix $S[2]$ to be on the form

$$S[2] = \begin{pmatrix} S[2]_{11} & S[2]_{12} \\ S[2]_{21} & S[2]_{22} \end{pmatrix} = H_2[1]\Lambda_2 H_2[1]^{-1}, \quad H_2[1] = \begin{pmatrix} \varphi_1[2] & -\phi_1[2]^* \\ \phi_1[2] & \varphi_1[2]^* \end{pmatrix}, \quad \Lambda_2 = \begin{pmatrix} \lambda_2 & 0 \\ 0 & \lambda_2^* \end{pmatrix}. \tag{3.75}$$

$\Phi_2[1] = (\varphi_1[2], \phi_1[2])^T$ is the vector eigenfunction solution to the new Lax-pairs given in equation (3.73) at $\lambda = \lambda_2$. In this case the elementary DT of the system (3.58) follows

$$u[2] = \alpha_2^2(u[1] + 2iS[2]_{12}), \qquad v[2] = \frac{1}{\alpha_2^2}(v[1] - 2iS[2]_{21}). \tag{3.76}$$

From the orthogonality condition, it follows that $(-\phi_2[1]^*, \varphi_2[1])^T$ is also a solution to the Lax-pairs given in equation (3.73) at $\lambda = \lambda_2^*$. From the second iteration given in equation(3.72) it follows that if $H_2[1]$ is a solution of $\Phi[2]$ for $\Lambda = \Lambda_2$, then

$$H_2[1]\Lambda_2 - S[2]H_2[1] = 0 \Longrightarrow S[2] = H_2[1]\Lambda_2 H_2[1]^{-1}, \tag{3.77}$$

such that

$$\begin{pmatrix} S[2]_{11} & S[2]_{12} \\ S[2]_{21} & S[2]_{22} \end{pmatrix} = \begin{pmatrix} \varphi_2[1] & -\phi_2[1]^* \\ \phi_2[1] & \varphi_2[1]^* \end{pmatrix} \times \begin{pmatrix} \lambda_2 & 0 \\ 0 & \lambda_2^* \end{pmatrix} \times \begin{pmatrix} \varphi_2[1] & -\phi_2[1]^* \\ \phi_2[1] & \varphi_2[1]^* \end{pmatrix}^{-1}. \tag{3.78}$$

Here again, we need to evaluate only the exact expressions of the matrix elements $S[2]_{12}$ and $S[2]_{21}$ using the Cramer's rule. We then obtain

$$S[2]_{12} = \frac{(\lambda_2^* - \lambda_2)\varphi_2[1]\phi_2[1]^*}{|\varphi_2[1]|^2 + |\phi_2[1]|^2}, \qquad S[2]_{21} = \frac{(\lambda_2^* - \lambda_2)\phi_2[1]\varphi_2[1]^*}{|\varphi_2[1]|^2 + |\phi_2[1]|^2}. \tag{3.79}$$

From equation (3.76), we obtain the second iterated solution to the system (3.58) as follows

$$u[2] = \alpha_2^2 \left(u[1] + 2i\frac{(\lambda_2^* - \lambda_2)\varphi_2[1]\phi_2[1]^*}{|\varphi_2[1]|^2 + |\phi_2[1]|^2} \right), \qquad v[2] = \frac{1}{\alpha_2^2} \left(v[1] - 2i\frac{(\lambda_2^* - \lambda_2)\phi_2[1]\varphi_2[1]^*}{|\varphi_2[1]|^2 + |\phi_2[1]|^2} \right). \tag{3.80}$$

From the above equations, two-soliton solution, second-order breather solution and second-order rogue wave solution to the system (3.58) can be provided. The solutions $u[2]$ and $v[2]$ can be rewritten in terms of determinant as follows

$$u[2] = \alpha_2^2 \left(\alpha_1^2 u + 2i\frac{|A_1|}{|B|} \right), \qquad v[2] = \frac{1}{\alpha_2^2} \left(\frac{1}{\alpha_1^2} v - 2i\frac{|A_2|}{|B|} \right), \tag{3.81}$$

where

$$A_1 = \begin{pmatrix} \alpha_1^2\lambda_1\phi_1 & \lambda_2\phi_2[1] & \alpha_1^2\lambda_1^*\varphi_1^* & \lambda_2^*\varphi_2[1]^* \\ \alpha_1^2\varphi_1 & \varphi_2[1] & -\alpha_1^2\phi_1^* & -\phi_2[1]^* \\ \alpha_1^2\lambda_1\phi_1 & \lambda_2\phi_2[1] & \alpha_1^2\lambda_1^*\varphi_1^* & \lambda_2^*\varphi_2[1]^* \\ \alpha_1^2\phi_1 & \phi_2[1] & \alpha_1^2\varphi_1^* & \varphi_2^*[1] \end{pmatrix},$$

$$A_2 = \begin{pmatrix} \alpha_1^{-2}\lambda_1\varphi_1 & \lambda_2\varphi_2[1] & \alpha_1^{-2}\lambda_1^*\phi_1^* & \lambda_2^*\phi_2[1]^* \\ \alpha_1^{-2}\phi_1 & \phi_2[1] & -\alpha_1^{-2}\varphi_1^* & -\varphi_2[1]^* \\ \alpha_1^{-2}\lambda_1\varphi_1 & \lambda_2\varphi_2[1] & \alpha_1^{-2}\lambda_1^*\phi_1^* & \lambda_2^*\phi_2[1]^* \\ \alpha_1^{-2}\varphi_1 & \varphi_2[1] & \alpha_1^{-2}\phi_1^* & \phi_2^*[1] \end{pmatrix}, \tag{3.82}$$

$$B = \begin{pmatrix} \lambda_1\varphi_1 & \lambda_2\varphi_2[1] & -\lambda_1^*\phi_1^* & -\lambda_2^*\phi_2[1]^* \\ \alpha_1^2\varphi_1 & \varphi_2[1] & -\alpha_1^2\phi_1^* & -\phi_2[1]^* \\ \lambda_1\phi_1 & \lambda_2\phi_2[1] & \lambda_1\varphi_1^* & \lambda_2\varphi_2[1]^* \\ \alpha_1^2\phi_1 & \phi_2[1] & \alpha_1^2\varphi_1^* & \varphi_2[1]^* \end{pmatrix}.$$

(iii) N-th iteration

Repeating the above process N-times, The N-th iterated solution $(\varphi_l,\phi_l)^T$ $(l = 1, 2, \ldots, N)$ to the Lax-pairs given in the equation (3.60) for $\lambda = \lambda_l$ $(l = 1, 2, \ldots, N)$, provide the N-th iterated solution to the system (3.58).

Proposition: *Denoting*

$$\begin{aligned} u[N] &= \alpha_N^2 \left(u[N-1] + 2i \tfrac{(\lambda_N^* - \lambda_N)\varphi_N[N-1]\phi_N[N-1]^*}{|\varphi_N[N-1]|^2 + |\phi_N[N-1]|^2} \right), \\ v[N] &= \tfrac{1}{\alpha_N^2} \left(v[N-1] - 2i \tfrac{(\lambda_N^* - \lambda_N)\phi_N[N-1]\varphi_N[N-1]^*}{|\varphi_N[N-1]|^2 + |\phi_N[N-1]|^2} \right). \end{aligned} \tag{3.83}$$

Where

$|\alpha_N| = 1$

$(ln\alpha_N)_x = 4i\beta[|S[N]_{12}|^2 - Im(S[N]_{12}u[N-1]^*)]$,

$(ln\alpha_N)_t = 4i\beta[4Re(S[N]_{11})|S[N]_{12}|^2 - 2Im(S[N]_{22}S[2]_{21}u[N-1]) + 2\beta Im(S[N]_{12}v[N-1]) - iIm(S[N]_{21}u[N-1]_x)]$,

$\Phi[N-1] = T[N-1]T[N-2]\ldots T[1]T[0]\Phi$,

with $T[N] = \begin{pmatrix} \alpha_N & 0 \\ 0 & 1/\alpha_N \end{pmatrix} (I\lambda - S[N])$,

$\Lambda[N] = \begin{pmatrix} \lambda_N & 0 \\ 0 & \lambda_N^* \end{pmatrix}$ and $H_N[N-1] = \begin{pmatrix} \varphi_N[N-1] & -\phi_N[N-1]^* \\ \phi_N[N-1] & -\varphi_N[N-1]^* \end{pmatrix}$.

Then the compact forms of the N-th iterated solution to the system (1.1) is written as follows

$$u[N] = \alpha_N^2 \left(\alpha_1^2 u + 2i \frac{|C_1|}{|D|} \right), \qquad v[N] = \frac{1}{\alpha_N^2} \left(\frac{1}{\alpha_1^2} v - 2i \frac{|C_2|}{|D|} \right), \tag{3.84}$$

where

$$C_1 = \begin{pmatrix} \lambda_1^N\varphi_1 & \cdots & \lambda_N^N\varphi_N & -\lambda_1^{*N}\phi_1^* & \cdots & -\lambda_N^{*N}\phi_N^* \\ \vdots & \cdots & \vdots & \vdots & \cdots & \vdots \\ \alpha_1^2\lambda_1\varphi_1 & \cdots & \lambda_N\varphi_N & -\alpha_1^2\lambda_1^*\phi_1^* & \cdots & -\lambda_N^*\phi_N^* \\ \lambda_1^{N-1}\varphi_1 & \cdots & \lambda_N^{N-1}\varphi_N & -\lambda_1^{N-1}\phi_1^* & \cdots & -\lambda_N^{N-1}\phi_N^* \\ \vdots & \cdots & \vdots & \vdots & \cdots & \vdots \\ \varphi_1 & \cdots & \varphi_N & -\phi_1^* & \cdots & -\phi_N^* \end{pmatrix},$$

$$C_2 = \begin{pmatrix} \lambda_1^{N-1}\phi_1 & \cdots & \lambda_N^{N-1}\phi_N & \lambda_1^{N-1}\varphi_1^* & \cdots & \lambda_N^{N-1}\varphi_N^* \\ \vdots & \cdots & \vdots & \vdots & \cdots & \vdots \\ \alpha_1^{-2}\phi_1 & \cdots & \phi_N & \alpha_1^{-2}\varphi_1^* & \cdots & \varphi_N^* \\ \lambda_1^N\phi_1 & \cdots & \lambda_N^N\phi_N & \lambda_1^{*N}\varphi_1^* & \cdots & \lambda_N^{*N}\varphi_N^* \\ \vdots & \cdots & \vdots & \vdots & \cdots & \vdots \\ \lambda_1\phi_1 & \cdots & \lambda_N\phi_N & \lambda_1^*\varphi_1^* & \cdots & \lambda_N^*\varphi_N^* \end{pmatrix}, \tag{3.85}$$

$$D = \begin{pmatrix} \lambda_1^{N-1}\varphi_1 & \cdots & \lambda_N^{N-1}\varphi_N & -\lambda_1^{N-1}\phi_1^* & \cdots & -\lambda_N^{N-1}\phi_N^* \\ \vdots & \cdots & \vdots & \vdots & \cdots & \vdots \\ \varphi_1 & \cdots & \varphi_N & -\phi_1^* & \cdots & -\phi_N^* \\ \lambda_1^{N-1}\phi_1 & \cdots & \lambda_N^{N-1}\phi_N & \lambda_1^{N-1}\varphi_1^* & \cdots & \lambda_N^{N-1}\varphi_N^* \\ \vdots & \cdots & \vdots & \vdots & \cdots & \vdots \\ \phi_1 & \cdots & \phi_N & \varphi_1^* & \cdots & \varphi_N^* \end{pmatrix}.$$

From equation (3.84), N-soliton solution, N-breather solution and so on can be provided.

The original DT is not applicable directly to obtain the rogue wave solutions for the nonlinear wave equations. We now go forward while constructing generalized DT of the system (3.58).

3.4.2 Generalized Darboux transformation

The N-th iterated DT contains N-eigenfunctions Φ_l associated with N-separate eigenvalues λ_l, but when carrying out the iteration in the original DT scheme, the generating eigenfunction cannot be more than once. In view to obtain higher-order rogue wave solution for a fixed eigenvalue λ_0, we must use repeated DTs. To overcome this problem, we must consider the limit $\lambda_l \to \lambda_1$ in the corresponding eigenvalues found in the DT. Hence,

we adopt the procedure given in [92] to generate the higher-order rogue wave solution to the system (3.58) using only one eigenvalue.

(i) First-step

We start with the assumption that $\Phi_1 = \Phi_1(\lambda_1 + f)$ is a special solution to the Lax-pairs given in equation (3.60), also $\frac{\Phi(\lambda_1+f)}{f}$ solution to these Lax-pairs where f is a perturbation small parameter. We consider the Taylor expansion of the function Φ at λ_1 given as follows

$$\Phi_1 = \Phi_1^{[0]} + \Phi_1^{[1]} f^2 + \Phi_1^{[2]} f^4 + ..., \tag{3.86}$$

where $\Phi_1^{[l]} = \frac{1}{l!}\frac{\partial^l}{\partial\lambda^l}\Phi_1|_{\lambda=\lambda_1}$ (l=0,1,2...). It is clear that the eigenfunction $\Phi_1^{[0]}$ is a solution of the Lax-pairs given in equation (3.60) at $\lambda = \lambda_1$ with the seed solutions u and v. Hence the first-step generalized DT (GDT) follows

$$u[1] = \alpha_1^2\left(u + 2i\frac{(\lambda_1^* - \lambda_1)\varphi_1[0]\phi_1[0]^*}{|\varphi_1[0]|^2 + |\phi_1[0]|^2}\right), \qquad v[1] = \frac{1}{\alpha^2}\left(v - 2i\frac{(\lambda_1^* - \lambda_1)\phi_1[0]\varphi_1[0]^*}{|\varphi_1[0]|^2 + |\phi_1[0]|^2}\right), \tag{3.87}$$

with $\Phi_1^{[0]} = \Phi_1[0] = (\varphi_1[0], \phi_1[0])^T$. The first-order rogue wave solution to the system (3.58) can be derived directly from equation (3.87).

(ii) Second-step

Through the following limit process

$$\lim_{f\to 0}\frac{T[1]|_{\lambda=\lambda_1+f}\Phi}{f} = \lim_{f\to 0}\frac{(f + T[1]|_{\lambda=\lambda_1})\Phi(\lambda_1 + f)}{f} = \Phi_1^{[0]} + T_1[1]\Phi_1^{[1]} \equiv \Phi_1[1], \tag{3.88}$$

we get another solution to the Lax-pair of equation (3.60), namely $\Phi_1[1] = (\varphi_1[1], \phi_1[1])^T$. The quantities $\Phi_1[0]$ and $\Phi_1^{[1]}$ are already calculated in the taylor expansion given in equation (3.86). Then, the second-step GDT forwards, namely,

$$u[2] = \alpha_2^2\left(u[1] + 2i\frac{(\lambda_1 - \lambda_1^*)\varphi_1[1]\phi_1^*[1]}{|\varphi_1[1]|^2 + |\phi_1[1]|^2}\right), \qquad v[2] = \frac{1}{\alpha_2^2}\left(v[1] - 2i\frac{(\lambda_1 - \lambda_1^*)\varphi_1[1]\phi_1^*[1]}{|\varphi_1[1]|^2 + |\phi_1[1]|^2}\right). \tag{3.89}$$

It is important to remark that λ_1 and its associated eigenfunction in equation (2.62) replace the eigenvalue (λ_2) and eigenfunction in equation (2.52). Applying the limit process above on equation (2.53), we obtain the determinant form of equation (3.89) as follows

$$u[2]=\alpha_2^2\left(\alpha_1^2u+2i\lim_{\lambda_2\to\lambda_1}\frac{|E_1[2]|}{|F[2]|}\right),\qquad v[2]=\frac{1}{\alpha_2^2}\left(\frac{1}{\alpha_1^2}v-2i\lim_{\lambda_2\to\lambda_1}\frac{|E_2[2]|}{|F[2]|}\right),\tag{3.90}$$

where

$$\begin{aligned}
E_1[2]&=\begin{pmatrix}\lambda_1\phi_1 & \phi_1[1,1] & \lambda_1^*\varphi_1^* & \varphi_1[1,1]^*\\ \varphi_1 & \alpha_1^2\varphi_1[0,1] & -\phi_1^* & -\alpha_1^2\phi_1[0,1]^*\\ \lambda_1\phi_1 & \phi[1,1] & \lambda_1^*\varphi_1^* & \varphi_1[1,1]^*\\ \phi_1 & \alpha_1^2\phi_1[0,1] & \varphi_1^* & \alpha_1^2\varphi_1[0,1]^*\end{pmatrix},\\
E_2[2]&=\begin{pmatrix}\lambda_1\varphi_1 & \varphi_1[1,1] & \lambda_1^*\phi_1^* & \phi_1[1,1]^*\\ \phi_1 & \alpha_1^{-2}\phi_1[0,1] & -\varphi_1^* & -\alpha_1^{-2}\varphi_1[0,1]^*\\ \lambda_1\varphi_1 & \varphi_1[1,1] & \lambda_1^*\phi_1^* & \phi_1[1,1]^*\\ \varphi_1 & \alpha_1^{-2}\varphi_1[0,1] & \phi_1^* & \alpha_1^{-2}\phi_1^*[0,1]\end{pmatrix},\\
F[2]&=\begin{pmatrix}\lambda_1\varphi_1 & \varphi_1[1,1] & -\lambda_1^*\phi_1^* & -\phi_1[1,1]^*\\ \varphi_1 & \alpha_1^2\varphi_1[0,1] & -\phi_1^* & -\alpha_1^2\phi_1[0,1]^*\\ \lambda_1\phi_1 & \phi_1[1,1] & \lambda_1^*\varphi_1^* & \varphi_1[1,1]^*\\ \phi_1 & \alpha_1^2\phi_1[0,1] & \varphi_1^* & \alpha_1^2\varphi_1[0,1]^*\end{pmatrix},
\end{aligned}\tag{3.91}$$

with $\varphi_1[i,m]=\frac{1}{m!}\frac{\partial^m}{\partial\lambda_1^m}[(\lambda_1+f)^i\varphi_1(\lambda_1+f)]|_{f=0}$ and $\phi_1[i,m]=\frac{1}{m!}\frac{\partial^m}{\partial\lambda_1^m}[(\lambda_1+f)^i\phi_1(\lambda_1+f)]|_{f=0}$ $(i.m=0,1.)$.

Using the above determinant form given in equation (3.90), one can easily derive the second-order rogue wave solution to the system (3.58).

(iii) Nth-step

Repeating the above process N times and combining all the Darboux matrices, the Nth iterated GDT for the system (3.58) is defined as follows

$$\begin{aligned}
u[N]&=\alpha_N^2\left(u[N-1]+2i\tfrac{(\lambda_1^*-\lambda_1)\varphi_1[N-1]\phi_1[N-1]^*}{|\varphi_1[N-1]|^2+|\phi_1[N-1]|^2}\right),\\
v[N]&=\tfrac{1}{\alpha_N^2}\left(v[N-1]-2i\tfrac{(\lambda_1^*-\lambda_1)\phi_1[N-1]\varphi_1[N-1]^*}{|\varphi_1[N-1]|^2+|\phi_1[N-1]|^2}\right),
\end{aligned}\tag{3.92}$$

where

$|\alpha_k|=1$

$(ln\alpha_k)_x=4i\beta[|S[k]_{12}|^2-Im(S[k]_{12}u[k-1]^*)]$,

$(ln\alpha_k)_t=4i\beta[4Re(S[k]_{11})|S[k]_{12}|^2-2Im(S[k]_{22}S[2]_{21}u[k-1])+2\beta Im(S[k]_{12}v[k-1])-iIm(S[k]_{21}u[k-1]_x)]$,

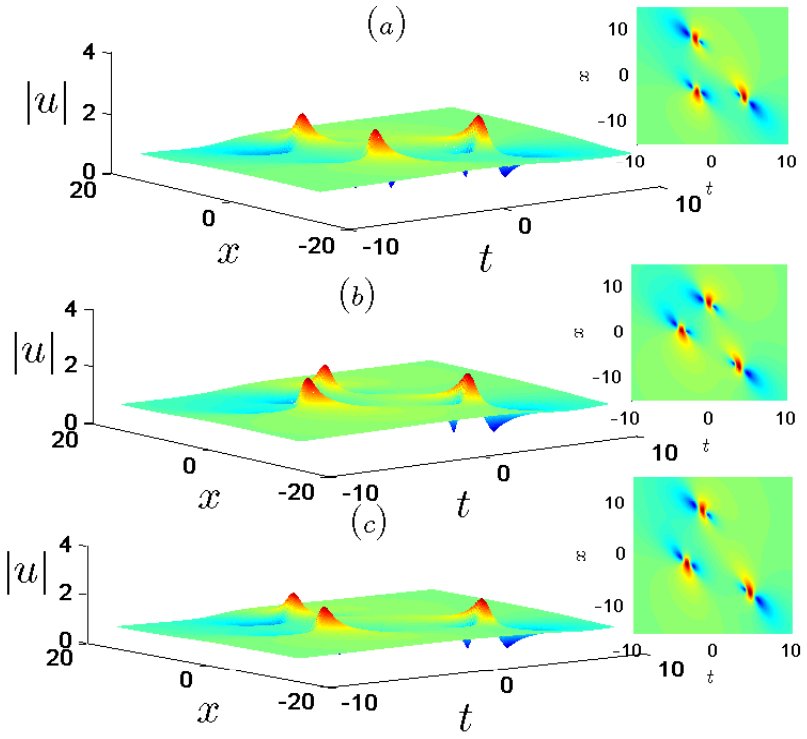

Figure 64: Second-order rogue wave solution to system (1.1). The panels (a), (b) and (c) are depicted with the parametric choices $(c_1 = 100, \quad d_1 = 0)$, $(c_1 = 0, \quad d_1 = 100)$ and $(c_1 = d_1 = 100)$, respectively. In all the cases $\beta = 0.8$.

with $T[k] = \begin{pmatrix} \alpha_k & 0 \\ 0 & 1/\alpha_k \end{pmatrix} (I\lambda - S[N])$,

$\Lambda[k] = \begin{pmatrix} \lambda_k & 0 \\ 0 & \lambda_k^* \end{pmatrix}$ and $H_N[N-1] = \begin{pmatrix} \varphi_N[N-1] & -\phi_N[N-1]^* \\ \phi_N[N-1] & -\varphi_N[N-1]^* \end{pmatrix}$.

$\Phi_1[N-1] = \Phi_1^{[0]} + \sum_{k=1}^{N-1} T_1[k]\Phi_1^{[1]} + \sum_{k=1}^{N-1}\sum_{l=1}^{k-1} T_1[k]T_1[l]\Phi_1^{[2]} + ... + T_1[N-1]T_1[N-2]...T_1[1]\Phi_1^{[N-1]}$.

Applying the limit process on the determinant given in equation (3.84), we obtain the following compact form of the Nth iterated GDT of the system (3.58)

$$u[N] = \alpha_N^2 \left(\alpha_1^2 u + \lim_{\lambda_N \to \lambda_1} 2i \frac{|G_1[N]|}{|H[N]|} \right), \qquad v[N] = \frac{1}{\alpha_N^2} \left(\frac{1}{\alpha_1^2} v - \lim_{\lambda_N \to \lambda_1} 2i \frac{|G_2[N]|}{|H[N]|} \right), \tag{3.93}$$

where

$$G_1[N]=\begin{pmatrix} \lambda_1^N\varphi_1 & \cdots & \lambda_1^N\varphi_1[N,N-1] & -\lambda_1^{*N}\phi_1^* & \cdots & -\lambda_1^{*N}\phi_1^*[N,N-1] \\ \vdots & \cdots & \vdots & \vdots & \cdots & \vdots \\ \alpha_1^2\lambda_1\varphi_1 & \cdots & \lambda_1\varphi_1[1,N-1] & -\alpha_1^2\lambda_1^*\phi_1^* & \cdots & -\lambda_1^*\phi_1^*[1,N-1] \\ \lambda_1^{N-1}\varphi_1 & \cdots & \lambda_1^{N-1}\varphi_1[N-1,N-1] & -\lambda_1^{N-1}\phi_1^* & \cdots & -\lambda_1^{N-1}\phi_1^*[N-1,N-1] \\ \vdots & \cdots & \vdots & \vdots & \cdots & \vdots \\ \varphi_1 & \cdots & \varphi_1[0,N-1] & -\phi_1^* & \cdots & -\phi_1^*[0,N-1] \end{pmatrix},$$

$$G_2[N]=\begin{pmatrix} \lambda_1^{N-1}\phi_1 & \cdots & \lambda_1^{N-1}\phi_1[N-1,N-1] & \lambda_1^{N-1}\varphi_1^* & \cdots & \lambda_1^{N-1}\varphi_1^*[N-1,N-1] \\ \vdots & \cdots & \vdots & \vdots & \cdots & \vdots \\ \alpha_1^{-2}\phi_1 & \cdots & \phi_1[0,N-1] & \alpha_1^{-2}\varphi_1^* & \cdots & \varphi_1^*[0,N-1] \\ \lambda_1^N\phi_1 & \cdots & \lambda_1^N\phi_1[N,N-1] & \lambda_1^{*N}\varphi_1^* & \cdots & \lambda_1^{*N}\varphi_1^*[N,N-1] \\ \vdots & \cdots & \vdots & \vdots & \cdots & \vdots \\ \lambda_1\phi_1 & \cdots & \lambda_1\phi_1[1,N-1] & \lambda_1^*\varphi_1^* & \cdots & \lambda_1^*\varphi_1^*[1,N-1] \end{pmatrix},$$

$$J[N]=\begin{pmatrix} \lambda_1^{N-1}\varphi_1 & \cdots & \lambda_1^{N-1}\varphi_1[N-1,N-1] & -\lambda_1^{N-1}\phi_1^* & \cdots & -\lambda_1^{N-1}\phi_1^*[N-1,N-1] \\ \vdots & \cdots & \vdots & \vdots & \cdots & \vdots \\ \varphi_1 & \cdots & \varphi_1[0,N-1] & -\phi_1^* & \cdots & -\phi_1^*[0,N-1] \\ \lambda_1^{N-1}\phi_1 & \cdots & \lambda_1^{N-1}\phi_1[N-1,N-1] & \lambda_1^{N-1}\varphi_1^* & \cdots & \lambda_1^{N-1}\varphi_1^*[N-1,N-1] \\ \vdots & \cdots & \vdots & \vdots & \cdots & \vdots \\ \phi_1 & \cdots & \phi_1[0,N-1] & \varphi_1^* & \cdots & \varphi_1^*[0,N-1] \end{pmatrix}. \tag{3.94}$$

Where

$\varphi_1[i,m]=\frac{1}{m!}\frac{\partial^m}{\partial\lambda_1^m}[(\lambda_1+f)^i\varphi_1(\lambda_1+f)]|_{f=0}$ and $\phi_1[i,m]=\frac{1}{m!}\frac{\partial^m}{\partial\lambda_1^m}[(\lambda_1+f)^i\phi_1(\lambda_1+f)]|_{f=0}$ $(i.m=0,1,2\ldots N)$.

The determinant form given in equation (3.93) is useful for determining the N-order rogue wave solution to the system (3.58), using the generalized Darboux transformation and a seed solution.

3.4.3 Rogue wave dynamics

In order to obtain the rogue wave solution to the system (3.58), we start with the following plane wave solutions as seed solutions to the system

$$u[0]=e^{ia_1t}, \qquad v[0]=e^{-ia_2t}, \tag{3.95}$$

where the quantities a_1 and a_2 are real constants. Inserting the above seed solutions into the system (3.58) and making the restriction $a_1 = a_2 = a$, we obtain a dispersion relation in the form $a = 4\beta^2 - 2$. Then the basic solution to the Lax-pairs given in equation (3.60) with $u[0]$, $v[0]$ and λ_1 holds

$$\Phi_1 = \begin{pmatrix} i(M_1 e^{\mu} - M_2 e^{-\mu}) e^{i\frac{\theta}{2}} \\ (M_2 e^{\mu} - M_1 e^{-\mu}) e^{-i\frac{\theta}{2}} \end{pmatrix}, \tag{3.96}$$

with $\theta = 2(2\beta^2 - 1)t$, $M_1 = \left(\frac{\lambda_1 - \sqrt{\lambda_1^2 + a}}{\lambda_1^2 + a}\right)^{1/2}$, $M_2 = \left(\frac{\lambda_1 + \sqrt{\lambda_1^2 + a}}{\lambda_1^2 + a}\right)^{1/2}$.

The quantity μ reads $\mu = i\sqrt{\lambda_1^2 + a}(x - 2\lambda_1(\lambda_1 + 1) + \sum_{j=1}^{N}(c_j + id_j)\delta^{2j})$; c_j and d_j are constant real free parameters which will be responsible to the triplet and triangular arrangement on rogue wave structure.

In view to obtain rogue wave solution to the system under consideration, we fix the eigenvalue to be $\lambda = i\sqrt{a}(1 + \delta^2)$, where the quantity δ is a small perturbation parameter. We expand the vector eigenfunction at $\delta = 0$ and we get the following

$$\Phi_1 = \Phi_1^{[0]} + \Phi_1^{[1]}\delta^2 + \Phi_1^{[2]}\delta^4 + ..., \tag{3.97}$$

where,

$\Phi_1^{[0]} = \begin{pmatrix} \varphi_1^{[0]} \\ \phi_1^{[0]} \end{pmatrix}$, $\Phi_1^{[1]} = \begin{pmatrix} \varphi_1^{[1]} \\ \phi_1^{[1]} \end{pmatrix}$, $\Phi_1^{[2]} = \begin{pmatrix} \varphi_1^{[2]} \\ \phi_1^{[2]} \end{pmatrix}$...

with

$\varphi_1^{[0]} = -\frac{1}{\sqrt{a}}(2\sqrt{a}x + 4a^{3/2}t - 4iat + 1)e^{i\frac{\theta}{2}}$,

$\phi_1^{[0]} = -\frac{i}{\sqrt{a}}\left(-2\sqrt{a}x - 4a^{3/2}t + 4iat + 1\right)e^{-i\frac{\theta}{2}}$,

$\varphi_1^{[1]} = e^{i\frac{\theta}{2}}(8a^{5/2}xt^2 - 16/3\,a^{9/2}t^3 - 16/3\,ia^3t^3 - 4a^3t^2 + 16ia^4t^3 - 4a^2xt - 2/3\,a^{3/2}x^3 + 4a^2t^2 + 4ia^2x^2t - 2\sqrt{a}c_1 - 9a^{3/2}t + 5iat + 16a^{7/2}t^3 + 16ia^3xt^2 - 2i\sqrt{a}d_1 - 8a^{7/2}t^2x - 1/2\sqrt{a}x + 4ia^{3/2}xt - ax^2 + 8ia^{5/2}t^2 - 4a^{5/2}x^2t + 1/4)$,

$\phi_1^{[1]} = e^{-i\frac{\theta}{2}}(-16ia^{7/2}t^3 + 4ia^{5/2}x^2t + 5at + 8ia^{7/2}t^2x - 2\sqrt{a}d_1 - 4ia^2xt - 4ia^3t^2 - 8ia^{5/2}xt^2 + 4a^2x^2t + 2/3\,ia^{3/2}x^3 + 9ia^{3/2}t + 16a^3xt^2 + 1/2\,i\sqrt{a}x + 16a^4t^3 - 16/3\,a^3t^3 + 16/3\,ia^{9/2}t^3 + 4ia^2t^2 - 4a^{3/2}xt + 2i\sqrt{a}c_1 - 8a^{5/2}t^2 - iax^2 + 1/4\,i)$.

It is important to note that only the two first terms in equation (3.97) are taken into account, because it is sufficient for us to construct up to second-order rogue wave solution to the system (3.58). If higher-order are targeted, one must consider more terms to be sure to the accuracy of the results.

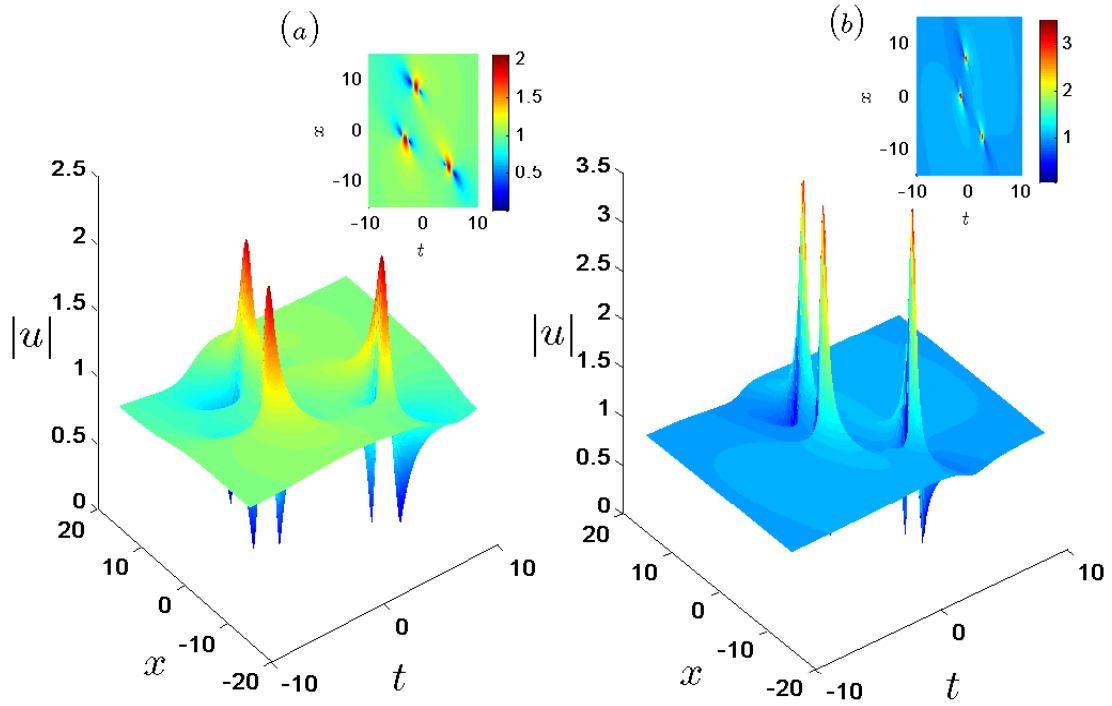

Figure 65: Second-order rogue wave solution to system (1.1). The panels (a) and (b) are depicted with the values $\beta = 0.8$ and $\beta = 0.95$, respectively. In all the cases $c_1 = d_1 = 100$.

(i) First-order rogue wave dynamics

Taking into account that $\Phi_1^{[0]}$ is a solution to the Lax-pairs given in equation (3.60), we insert it into equation (3.87) and the first-order rogue wave solution to the system under consideration yields

$$\begin{aligned} u[1] &= \left[1 + 4\sqrt{a}\tfrac{F+iG}{D}\right] e^{i\theta}, \\ v[1] &= \left[1 + 4\sqrt{a}\tfrac{F+iG}{D}\right] e^{-i\theta}, \end{aligned} \tag{3.98}$$

where,

$\alpha_1 = 1$, $F = 1 - 4a^2x - 16a^2xt - 16a^2(a+1)t^2$, $G = -8at$ and $D = 8ax^2 + 32xt + 32a^2(a+1)t^2$.

The first-order rogue wave solution corresponding to equation (3.98) is depicted in figure (61). The same feature is observed for the $v[1]$ component since the components u and v are proportional.

(ii) Second-order rogue wave dynamics

Next, considering the expressions of $\Phi_1^{[0]}$ and $\Phi_1^{[1]}$ and using equation (3.88), one can obtain the analytical expressions of $\varphi_1[1]$ and $\phi_1[1]$ as

$\varphi_1[1] = \frac{-e^{i\frac{\theta}{2}}}{3\Delta}(3 + 6\sqrt{a}x - 12\,ad_1 + 64\,a^3x^3t + 96\,a^{5/2}xt^2 + 96\,a^{7/2}t^2x + 96\,a^{5/2}x^2t + 384\,a^4t^2x^2 + 768\,a^5t^3x + 256\,a^4xt^3 + 48\,a^2tc_1 + 48\,a^{5/2}td_1 + 24\,a^{3/2}xd_1 - 12\,iac_1 + 512\,a^6t^4 + 512\,a^5t^4 + 24\,a^{3/2}x^3 + 256\,a^{7/2}t^3 + 12\,ax^2 + 144\,a^3t^2 + 48\,a^2t^2 + 48\,ia^2tx^2 + 96\,ia^3t^2x + 48\,ia^3x^2t + 96\,ia^4t^2x + 144\,ia^{5/2}xt + 144\,ia^{5/2}t^2 + 256\,ia^{9/2}t^4 + 240\,ia^{7/2}t^2 + 12\,ia^{3/2}x^2 + 192\,ia^3t^3 + 8\,ia^2x^3 + 64\,ia^5t^3 + 12\,iat - 512\,ia^{11/2}xt^3 - 128\,ia^{7/2}x^3t - 384\,ia^{9/2}x^2t^2 - 60\,ia^2t - 256\,ia^{13/2}t^4 - 16\,ia^{5/2}x^4 - 6\,iax + 48\,a^{3/2}t + 48\,ia^{5/2}tc_1 + 24\,ia^{3/2}xc_1 - 48\,ia^2td_1)$,

$\phi_1[1] = \frac{-ie^{-i\frac{\theta}{2}}}{\Delta}(3 - 6\sqrt{a}x + 12\,ad_1 - 48\,ia^{5/2}tc_1 - 24\,ia^{3/2}xc_1 - 144\,ia^{5/2}xt - 144\,ia^{5/2}t^2 - 12\,ia^{3/2}x^2 - 256\,ia^{9/2}t^4 + 64\,a^3x^3t - 96\,a^{5/2}xt^2 - 96\,a^{7/2}t^2x - 96\,a^{5/2}x^2t + 384\,a^4t^2x^2 + 768\,a^5t^3x + 256\,a^4xt^3 + 48\,a^2tc_1 + 48\,a^{5/2}td_1 + 24\,a^{3/2}xd_1 - 12\,iac_1 + 512\,a^6t^4 + 512\,a^5t^4 - 24\,a^{3/2}x^3 - 256\,a^{7/2}t^3 + 12\,ax^2 + 144\,a^3t^2 + 48\,a^2t^2 + 48\,ia^2tx^2 + 96\,ia^3t^2x + 48\,ia^3x^2t + 96\,ia^4t^2x + 512\,ia^{11/2}xt^3 + 128\,ia^{7/2}x^3t + 384\,ia^{9/2}x^2t^2 + 256\,ia^{13/2}t^4 + 16\,ia^{5/2}x^4 + 192\,ia^3t^3 + 8\,ia^2x^3 + 64\,ia^5t^3 + 12\,iat - 60\,ia^2t - 6\,iax - 48\,a^{3/2}t - 240\,ia^{7/2}t^2 + 48\,ia^2td_1)$, with $\Delta = 4ax^2 + 16xt + 16a^2(a+1)t^2$.

Inserting the expressions of $\varphi_1[1]$ and $\phi_1[1]$ into equation (3.89) or in its determinant form given in equation (3.90) starting from the seed solutions, the second-order rogue wave solution to the system (3.58) is provided; the corresponding depiction is shown in figure (63). The same feature occurs for the $v[2]$ component.

3.4.4 Discussion and interpretation of the results

1. The solution obtained in equation (3.98) is the first-order vector rogue wave solution to the system (3.58). It is easy to remark that the two above solutions are merely proportional to each other, hence the solution obtained is a generalization of the rogue wave solution to the decoupled system. A similar case has been obtained in our previous work [104]. One can remark in the figure (61) that for the increasing values of the parameter β, the wave is compressed along the x and the t axis and the amplitude of the wave increases. Great appreciation of the effects of the parameter β on the structure of the rogue wave is shown in the Figure (62).

2. The second-order rogue wave solution possesses two free parameters c_1 and d_1. For the case where $c_1 = d_1 = 0$, the rogue wave is crowded round the origin (0,0) and the maximum of the $u[2]$ and $v[2]$ is 4, for this case we have rogue wave composite as the one obtained in Ref. [107] (see Figure 63). When we increase the value of c_1 and d_1 we observe

three first-order rogue waves scattered in all direction arraying a triangular arrangement (see Figure64). If we increase the values of the parameters c_1 and d_1 the distances between the rogue waves increase also. If we interchange the values of the parameters c_1 and d_1 for example ($c_1 = 100$, $d_1 = 0$) and ($c_1 = 0$, $d_1 = 100$), the triangular arrangement of the rogue waves persists but with different orientations (see Figure64a and Figure64b). If we give the same values to c_1 and d_1 for example ($c_1 = d_1 = 100$), we obtain the same triangular arrangement but in a different orientation (see Figure64c).

3. In the Figure (65), one can also remark the compression of the rogue wave along both x and t axis and the increase of the amplitude for different increasing values of the parameter β. The parameter β in the system (3.58) is close to the higher-order terms representing higher-order nonlinearity. Hence the effects of this term on the dynamics of the rogue waves express the increase of the nonlinearity of the waves in the medium.

4. The results obtained in this work show that the profile of the rogue wave can be modified so that it can propagate in sophisticated nonlinear physical systems such as Spin chain. The rogue wave can also be controlled during its propagation by changing the values of the parameter β [115, 116].

5. Rogue waves are short live waves which appear from nowhere and disappear without a trace due to modulation instability. The effects of the parameter β on the rogue wave can be that, for the small values of β the modulation instability can be modified so that the wave lives very shortly and for the big values the wave lives more longer due the increase of his amplitude.

3.5 Controllable rogue waves in nonlinear optical fibers

Generally, nonlinear phenomena are modeled by nonlinear evolution equations such as the Korteweg de-Vries equation , the NLS equation and its extensions , the Schäfer-wayne short pulse equation just to name a few. The nonlinearity have attracted particular attention of scientists for many years, because nonlinearity is a fascinating subject which have many applications in modern science. As an illustration, soliton solutions to the aforementioned equations have been calculated, since soliton solutions arise from the combination of the nonlinearity and the dispersion.

During the past few decades, another kind of solutions to the nonlinear evolution equations have been calculated, namely the rogue wave solutions. The rogue waves are currently called freak waves, monster waves, killer waves because there are often responsible of the destruction of large ships in the ocean. Rogue waves are not only met in the ocean but also in physical conditions in the following fields: optics, superfluids [9], Bose-Einstein condensates and in the form of capillary waves. Now, rogue waves still mysterious so that in any of this discipline, the new studies enrich the concept and lead to progress toward a comprehensive understanding of this phenomenon. The first-order rational solution to the NLS equation was first calculated by Peregrine. More after, the simplest rogue wave solutions for the NLSE was calculated by Akhmediev et al. The construction of higher-order analogues is actually a challenging problem. In our recent work, we have studied the interaction between the rogue wave and soliton wave, from the investigation it resorts that the both kind of wave can interact elastically.

In this section, we consider a generalized nonlinear schrödinger equation (GNLSE) given as follows [117],

$$iu_t + u_{xx} + 2u|u|^2 + \gamma(u_{xxxx} + 6u_x^2u^* + 4u|u_x|^2 + 8|u|^2u_{xx} + 2u^2u_{xx}^* + 6|u|^4u) = 0. \quad (3.99)$$

The quantities u is the complex envelope, u^* its complex conjugate and γ stands for a parameter scaling the effects of higher-order linear and nonlinear terms. The integrability of this equation has been shown and its soliton solutions have been calculated. It gauge equivalent to Heisenberg spin chain has been established [118, 119]. We derive the higher-order rogue wave solutions to equation (3.99), using the generalized Darboux transformation (DT) based on the Darboux matrix method. The generalized DT for equation (3.99) is iterated and a formula for generating the higher-order rogue wave solutions is given. We also show the impact of the parameter γ on the dynamic of rogue wave solution to equation (3.99).

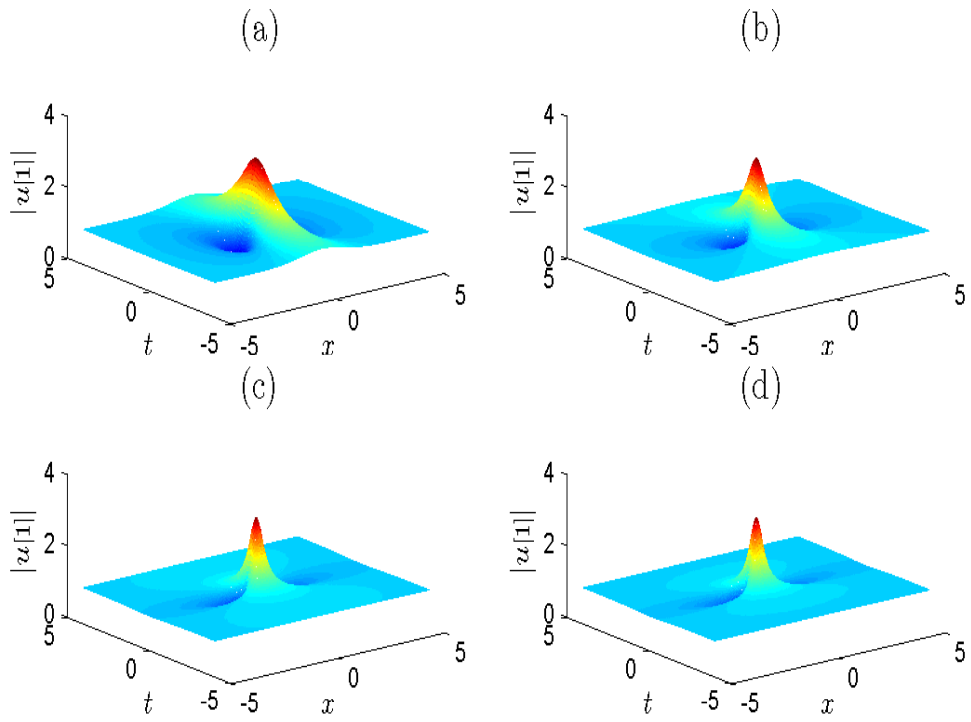

Figure 66: First-order rogue wave solution to equation (1.1) depicted in panel (a) with $\gamma = 1/2$, in panel (b) with $\gamma = 1$, in panel (c) with $\gamma = 2$ and in panel (d) with $\gamma = 5/2$.

3.5.1 Lax-pairs and generalized Darboux transformation

Equation (3.99) can be cast into a 2×2 linear eigenvalue problem due to integrability [117]

$$y_x = My, \qquad y_t = Ny, \tag{3.100}$$

where $M = \begin{pmatrix} -i\lambda & u \\ -u^* & i\lambda \end{pmatrix}$ and $N = 8i\gamma N_4 - 2iN_2$ with

$$
\begin{aligned}
N_2 &= \begin{pmatrix} \lambda^2 - \frac{1}{2}|u|^2 & iu\lambda - \frac{1}{2}u_x \\ -iu^*\lambda - \frac{1}{2}u_x^* & -\lambda^2 + \frac{1}{2}|u|^2 \end{pmatrix}, \\
N_4 &= \begin{pmatrix} A & B \\ C & -A \end{pmatrix}, \\
A &= \lambda^4 - \frac{1}{2}|u|^2\lambda^2 + \frac{1}{4}(uu_x^* - u_xu^*)\lambda + \frac{1}{8}(3|u|^4 + u^*u_{xx} + uu_{xx}^* - u_xu_x^*), \\
B &= iu\lambda^3 - \frac{1}{2}u_x\lambda^2 - \frac{i}{4}(u_{xx} + 2u|u|^2)\lambda + \frac{1}{8}(u_{xxx} + 6|u|^2u_x), \\
C &= -iu^*\lambda^3 - \frac{1}{2}u_x^*\lambda^2 + \frac{i}{4}(u_{xx}^* + 2u^*|u|^2)\lambda + \frac{1}{8}(u_{xxx}^* + 6|u|^2u_x^*).
\end{aligned}
$$

Here $y = (r(x,t), w(x,t))^T$ (the superscript T means transpose), λ is the spectral parameter. Through direct calculation, one can get equation (3.99) by the use of the zero curvature equation $U_t - V_x + [U,V] = 0$.

We start with the assumption that the function $y_1 = (r_1, w_1)^T$ is a particular solution to the Lax-pairs given in equation (3.100) with the spectral parameter λ_1 at $u = u[0]$.

We can transform the system (3.100) into a new one,

$$y[1]_x = M[1]y[1], \qquad y[1]_t = N[1]y[1], \tag{3.101}$$

with the following elementary DT:

$$y[1] = T[1]y, \quad T[1] = \lambda I - H[0]\Lambda[1]H[0]^{-1}, \tag{3.102}$$

$$u[1] = u[0] + 2(\lambda - \lambda^*)\frac{r_1[0]w_1[0]^*}{|r_1[0]|^2 + |w_1[0]|^2}, \tag{3.103}$$

where $r_1[0] = r_1$, $w_1[0] = w_1$, $I = \begin{pmatrix} 1 & 0 \\ 0 & 1 \end{pmatrix} = T[0]$, $H[0] = \begin{pmatrix} r_1[0] & -w_1[0]^* \\ w_1[0] & r_1[0]^* \end{pmatrix}$, $\Lambda[1] = \begin{pmatrix} \lambda_1 & 0 \\ 0 & \lambda_1^* \end{pmatrix}$.

Here, the matrices M and N are replaced by $M[1]$ and $N[1]$ with the new potential $u[1]$ therein. Then, making use of the above DT N times, we get the N-fold DT of system (3.99),

$$
\begin{aligned}
y[N] = T[N]T[N-1]...T[1]y, \quad T[j] = \lambda I \\
-H[j-1]\Lambda[j]H[j-1]^{-1},
\end{aligned} \tag{3.104}
$$

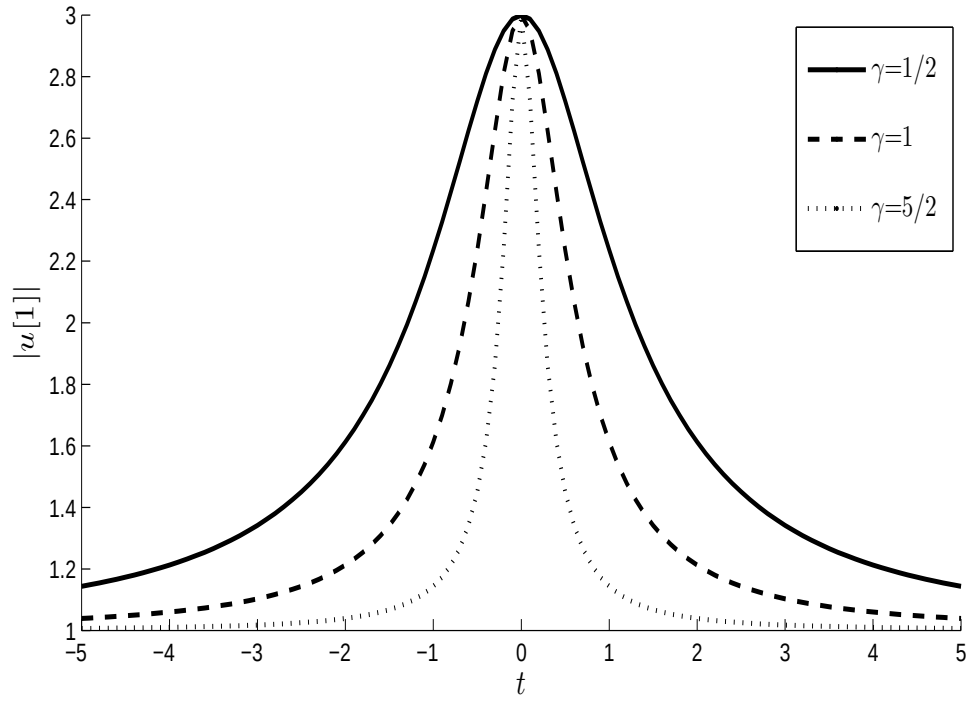

Figure 67: Compression of the rogue wave along the time coordinate. The feature in continue line correspond to the value of $\gamma = 1/2$, in small dashed line for $\gamma = 1$ and in big dashed line for $\gamma = 5/2$.

$$u[N] = u[N-1] + 2(\lambda - \lambda^*)\frac{r_1[N-1]w_1[N-1]^*}{|r_1[N-1]|^2 + |w_1[N-1]|^2}, \tag{3.105}$$

$$H[j-1] = \begin{pmatrix} r_1[j-1] & -w_1[j-1]^* \\ w_1[j-1] & r_1[j-1]^* \end{pmatrix}, \quad \Lambda[j] = \begin{pmatrix} \lambda_j & 0 \\ 0 & \lambda_j^* \end{pmatrix}.$$

with $(r_j[j-1], w_j[j-1])^T = y_j[j-1]$, $T_j[l] = T[l]|_{\lambda=\lambda_j}$, $1 \leq j \leq N$, $1 \leq l \leq j-1$

The original DT is not applicable directly to obtain the rogue wave solutions for the nonlinear wave equations. Matveev constructed the so-called generalized DT and the positon solutions were calculated for the KdV equation [92]. Recently, Guo and coworkers [94] re-examined Matveev's generalized DT and introduced a new method to get the generalized DT for the KdV and the NLS equations. In the following, we use the Guo and coworkers's approach to derive the generalized Darboux transformation for the equation (3.99). We note that ,

$$y_1 = y_1(\varepsilon) \tag{3.106}$$

is a special solution to the Lax-pairs given in equation (3.100) with $u = u[0]$ and $\lambda = \lambda_1 + \varepsilon$.

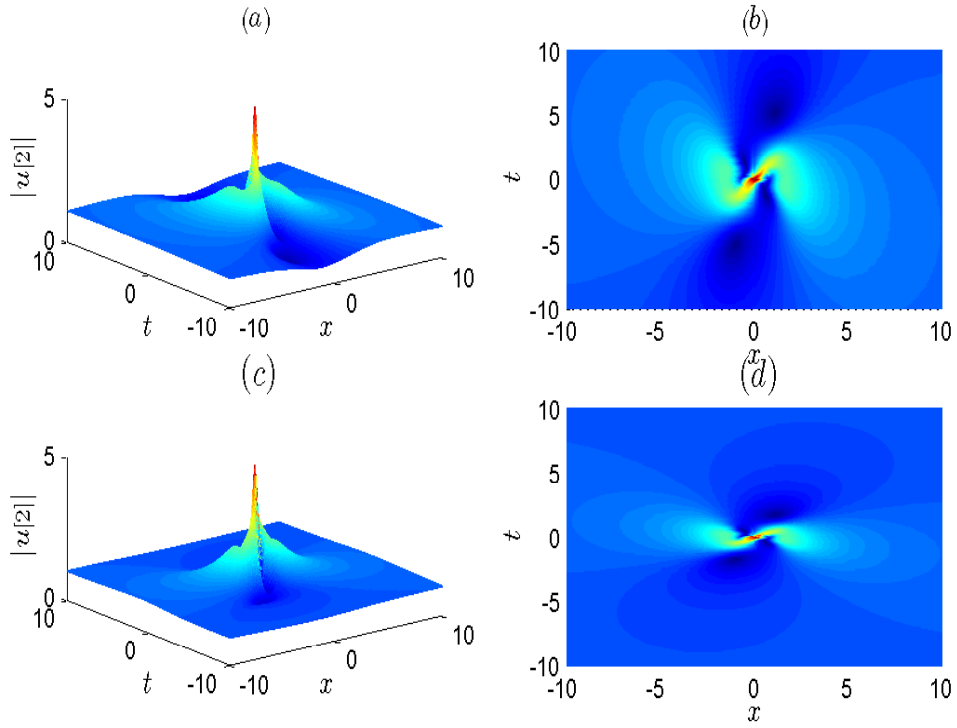

Figure 68: Second-order rogue wave solution to equation (1.1) depicted in panel (a) with $\gamma = 1/2$, the panel (b) stands for the density plot of panel (a); the panel (c) corresponds to the depiction with $\gamma = 3/2$ and the panel (d) is the corresponding density plot. All the depictions are made for $c_1 = d_1 = 0$.

Here ε is a perturbation parameter. Expanding y_1 in a taylor series in ε, we get

$$y_1 = y_1^{[0]} + y_1^{[1]}\varepsilon + y_1^{[2]}\varepsilon^2 + y_1^{[3]}\varepsilon^3 + ... + y_1^{[N]}\varepsilon^N + ... \tag{3.107}$$

where $y_1^{[j]} = \frac{1}{j!}\frac{\partial^j y_1(\lambda)}{\partial \lambda^j}|_{\lambda=\lambda_1}$ $(l = 0, 1, 2, 3, ...)$.

It is clear that $y_1^{[0]}$ is a solution to the Lax-pairs of equation (3.100), with the seed solution $u = u[0]$ corresponding to the spectral parameter $\lambda = \lambda_1$. So the first step generalized DT follows,

$$u[1] = u[0] + 2(\lambda - \lambda^*)\frac{r_1[0]w_1[0]^*}{|r_1[0]|^2 + |w_1[0]|^2}, \tag{3.108}$$

and $T[1] = \lambda I - H[0]\Lambda[1]H[0]^{-1}$, where the quantities I, $H[0]$ and $\Lambda[1]$ are identical as those given above. Through the following limit process,

$$\lim_{\varepsilon\to 0}\frac{T[1]|_{\lambda=\lambda_1+\varepsilon y_1}}{\varepsilon} = \lim_{\varepsilon\to 0}\frac{(\varepsilon + T_1[1])y_1}{\varepsilon} = y_1^{[0]} + T_1[1]y_1^{[1]} \equiv y_1[1], \tag{3.109}$$

we get another solution to the Lax-pair of equation (3.100). Then, the second-step generalized DT can be forwarded, namely,

$$u[2] = u[1] + 2(\lambda - \lambda^*)\frac{r_1[1]w_1[1]^*}{|r_1[1]|^2 + |w_1[1]|^2}, \tag{3.110}$$

and $T[2] = \lambda I - H[1]\Lambda[1]H[1]^{-1}$,

$$H[1] = \begin{pmatrix} r_1[1] & -w_1[1]^* \\ w_1[1] & r_1[1]^* \end{pmatrix}, \quad \Lambda[2] = \begin{pmatrix} \lambda_1 & 0 \\ 0 & \lambda_1^* \end{pmatrix}.$$

Similarly, the following limit

$$\begin{aligned} \lim_{\epsilon\to 0}\frac{[T[2]T[1]]|_{\lambda=\lambda_1+\epsilon}y_1}{\epsilon^2} &= \lim_{\epsilon\to 0}\frac{(\epsilon + T_1[2])(\epsilon + T_1[1])y_1}{\epsilon^2} \\ &= y_1^{[0]} + (T_1[2] + T_1[1])y_1^{[1]} \\ &+T_1[2]T_1[1]y_1^{[2]} \equiv y_1[2], \end{aligned} \tag{3.111}$$

provides us with a solution for the Lax-pairs of equation (3.100) with $u[3]$ and $\lambda = \lambda_1$. Then, the third-step generalized DT can be expressed as follows

$$u[3] = u[2] + 2(\lambda - \lambda^*)\frac{r_1[2]w_1[2]^*}{|r_1[2]|^2 + |w_1[2]|^2}, \tag{3.112}$$

$T[3] = \lambda I - H[2]\Lambda_3 H[2]^{-1}$,

$$H[2] = \begin{pmatrix} r_1[2] & -w_1[2]^* \\ w_1[2] & r_1[2]^* \end{pmatrix}, \quad \Lambda[3] = \begin{pmatrix} \lambda_1 & 0 \\ 0 & \lambda_1^* \end{pmatrix}.$$

Repeating the above process N times, an Nth-step generalized DT can be considered.

Proposition. *Notation*

$$\begin{aligned} y_1[N-1] &= y_1^{[0]} + \sum_{k=1}^{N-1} T_1[k]y_1^{[1]} + \sum_{k=1}^{N-1}\sum_{l=1}^{k-1} T_1[k]T_1[l]y_1^{[2]} + ... \\ &+T_1[N-1]T_1[N-2]...T_1[1]y_1^{[N-1]}, \end{aligned} \tag{3.113}$$

then, the N-step generalized DT is provided, namely,

$$u[N] = u[N-1] + 2(\lambda - \lambda^*)\frac{r_1[N-1]w_1[N-1]^*}{|r_1[N-1]|^2 + |w_1[N-1]|^2}, \tag{3.114}$$

A recursive formula of the Nth-order generalized DT for the equation (3.99) is given by the equations (3.113) and (3.114). As an application, the above formulae are used to derive rogue wave solutions to equation (3.99) in the following and some depictions are presented.

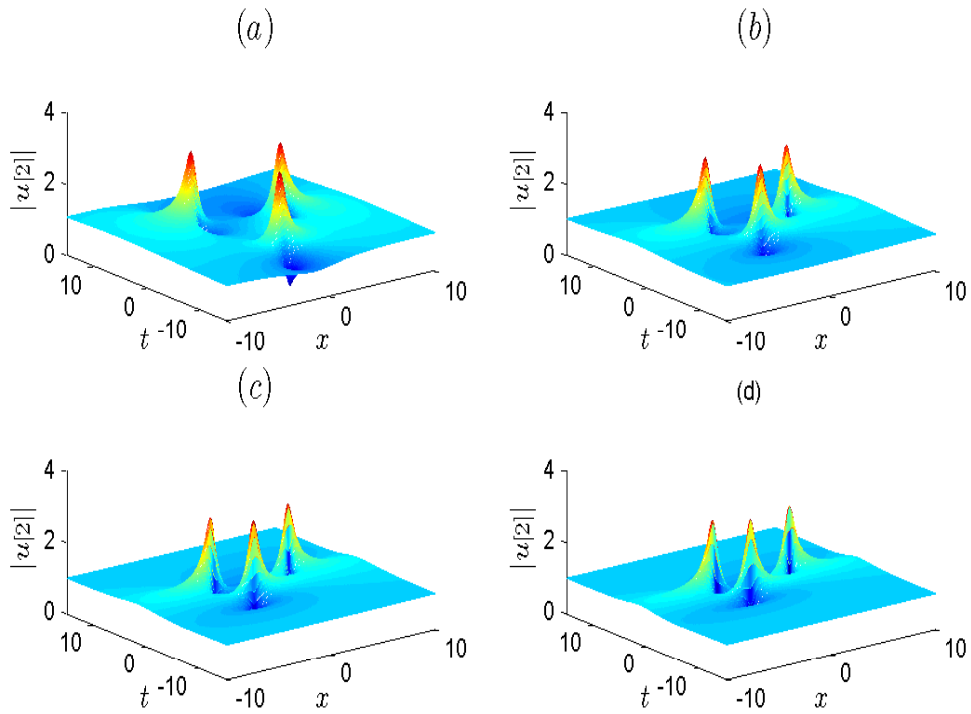

Figure 69: Second-order rogue wave solution to equation (1.1) depicted in panel (a) with $\gamma = 1/2$, in the panel (b) with $\gamma = 1$, in the panel (c) with $\gamma = 3/2$ and in the panel (d) with $\gamma = 2$. All the depictions are made for $c_1 = d_1 = 30$.

3.5.2 Rogue wave solutions

In view to obtain rogue wave solutions to equation (3.99), we begin with the seeding one $u[0] = e^{i(2+6\gamma)t}$. The corresponding solution for the Lax-pairs of equation (3.100) at $\lambda = i(1+\delta^2)$ can be given as follows

$$y_1(\delta) = \begin{pmatrix} i(M_1 e^{\eta} - M_2 e^{-\eta}) e^{-\frac{1}{2}i(2+6\gamma)t} \\ (M_2 e^{\eta} - M_1 e^{-\eta}) e^{\frac{1}{2}i(2+6\gamma)t} \end{pmatrix}, \tag{3.115}$$

with

$$M_1 = \left(\frac{1+\delta^2 - \sqrt{(1+\delta^2)^2 - 1}}{(1+\delta^2)^2 - 1} \right)^{1/2}, \quad M_2 = \left(\frac{1+\delta^2 + \sqrt{(1+\delta^2)^2 - 1}}{(1+\delta^2)^2 - 1} \right)^{1/2},$$

and

$$\eta = \sqrt{(1+\delta^2)^2 - 1} \left(x + i\gamma(1+\delta^2)t + \sum_{j=1}^{N} (c_j + i d_j)\delta^{2j} \right),$$

the quantities c_j and d_j are free real parameters. Expanding the vector function $y_1(\delta)$ in

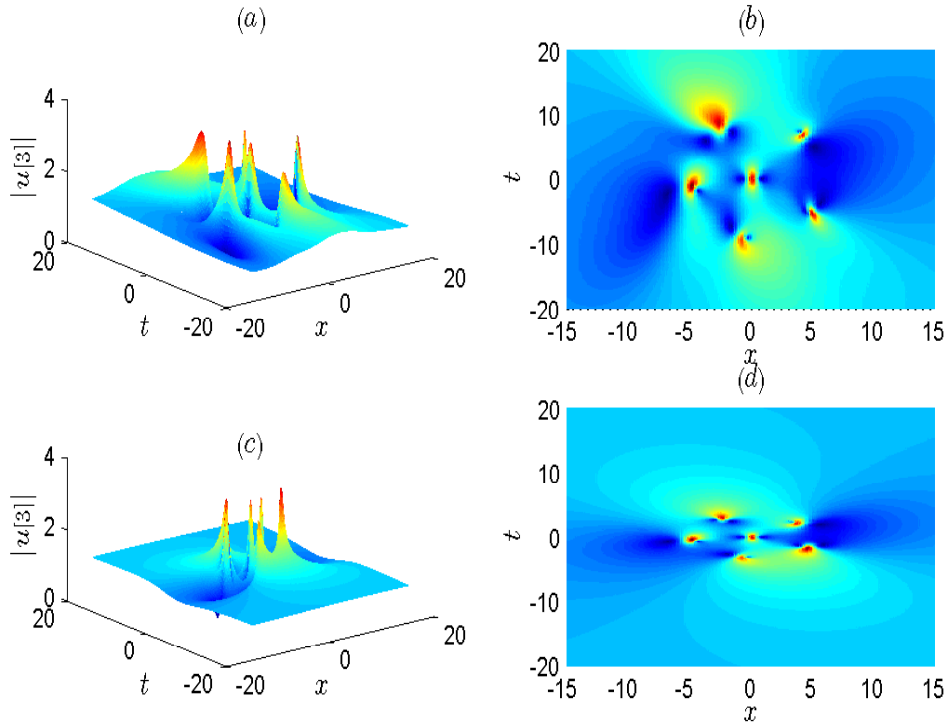

Figure 70: Third-order rogue wave solution to equation (1.1) depicted in panel (a) with $\gamma = 1/2$, the panel (b) is the density plot of the panel (a), the panel (c) show the depiction with $\gamma = 3/2$ and the panel (d) is its density plot. All the depictions are made for $c_1 = d_1 = 0$ and $c_2 = d_2 = 100$.

a Taylor series at $\delta = 0$, we obtain the following expression

$$y_1(\delta) = y_1^{[0]} + y_1^{[1]}\delta^2 + y_1^{[2]}\delta^4 + y_1^{[3]}\delta^6 + ..., \tag{3.116}$$

$$y_1^{[0]} = \begin{pmatrix} r_1^{[0]} \\ w_1^{[0]} \end{pmatrix}, \quad y_1^{[1]} = \begin{pmatrix} r_1^{[1]} \\ w_1^{[1]} \end{pmatrix}, \quad y_1^{[2]} = \begin{pmatrix} r_1^{[2]} \\ w_1^{[2]} \end{pmatrix}, \quad y_1^{[3]} = \begin{pmatrix} r_1^{[3]} \\ w_1^{[3]} \end{pmatrix} ...$$

The analytical expressions of the quantities $r_1^{[j]}$ and $w_1^{[j]}$ $(j = 0, 1, 2)$ are given in the following with the help of the maple 13 software:

$r_1^{[0]} = i(2\,x + 2\,i\gamma\,t - 1)\mathrm{e}^{-i(1+3\,\gamma)t}$, $w_1^{[0]} = (2\,x + 2\,i\gamma\,t + 1)\mathrm{e}^{i(1+3\,\gamma)t}$.

$r_1^{[1]} = (-1/12)\,i(-30\,i\gamma\,t - 24\,c_1 - 24\,id_1 - 6\,x - 8\,x^3 - 24\,ix^2\gamma\,t + 24\,x\gamma^2t^2 + 8\,i\gamma^3t^3 + 12\,x^2 + 24\,ix\gamma\,t - 12\,\gamma^2t^2 - 3)\mathrm{e}^{-i(1+3\,\gamma)t}$,

$w_1^{[1]} = (-1/12)\,(-30\,i\gamma\,t - 24\,c_1 - 24\,id_1 - 6\,x - 8\,x^3 - 24\,ix^2\gamma\,t + 24\,x\gamma^2t^2 + 8\,i\gamma^3t^3 - 12\,x^2 - 24\,ix\gamma\,t + 12\,\gamma^2t^2 + 3)\mathrm{e}^{i(1+3\,\gamma t)t}$.

$r_1^{[2]} = \frac{1}{480}\,i(-45 + 240\,c_1 - 30\,x + 960\,id_2 - 120\,x^2 + 240\,x^3 - 80\,x^4 + 32\,x^5 - 80\,\gamma^4t^4 +$

$480\,x^2\gamma^2t^2 + 160\,ix^4\gamma\,t - 320\,ix^2\gamma^3t^3 + 1680\,ix^2\gamma\,t - 320\,ix^3\gamma\,t + 320\,ix\gamma^3t^3 - 1200\,ix\gamma\,t + 1080\,\gamma^2t^2 + 960\,ix^2d_1 + 960\,\gamma\,td_1 - 960\,\gamma^2t^2c_1 - 960\,ixd_1 + 1920\,ix\gamma\,tc_1 - 1920\,\gamma\,td_1x - 960\,i\gamma^2t^2d_1 - 960\,i\gamma\,tc_1 - 960\,xc_1 + 960\,x^2c_1 + 240\,id_1 + 160\,\gamma^4t^4x - 320\,x^3\gamma^2t^2 - 1200\,i\gamma^3t^3 + 210\,i\gamma\,t + 32\,i\gamma^5t^5 + 960\,c_2 - 2640\,x\gamma^2t^2)\mathrm{e}^{-i(1+3\,\gamma)t}$,

$w_1^{[2]} = \frac{1}{480}\,(45 + 240\,c_1 - 30\,x + 960\,id_2 + 120\,x^2 + 240\,x^3 + 80\,x^4 + 32\,x^5 + 80\,\gamma^4t^4 - 480\,x^2\gamma^2t^2 + 160\,ix^4\gamma\,t - 320\,ix^2\gamma^3t^3 + 1680\,ix^2\gamma\,t + 1200\,ix\gamma\,t - 320\,ix\gamma^3t^3 + 320\,ix^3\gamma\,t - 1080\,\gamma^2t^2 + 960\,ixd_1 + 960\,ix^2d_1 - 960\,\gamma\,td_1 - 960\,\gamma^2t^2c_1 + 1920\,ix\gamma\,tc_1 + 960\,i\gamma\,tc_1 - 1920\,\gamma\,td_1x - 960\,i\gamma^2t^2d_1 + 960\,xc_1 + 960\,x^2c_1 + 240\,id_1 + 160\,\gamma^4t^4x - 320\,x^3\gamma^2t^2 - 1200\,i\gamma^3t^3 + 210\,i\gamma\,t + 32\,i\gamma^5t^5 + 960\,c_2 - 2640\,x\gamma^2t^2)\mathrm{e}^{i(1+3\,\gamma)t}$.

It is important to notify that only the first three terms of the series are taken into account, because it is sufficient to construct up to third-order rogue wave solution for the equation (3.99). If higher-order rogue wave are targeted, one needs to consider more terms in equation (3.113) to be sure to the accuracy of the results.

Taking into account that the function $y_1^{[0]}$ is a solution to the Lax-pairs (3.100) at $u = u[0]$, we substitute the above seed solution into equation (2.39) and we get the first-order rogue wave solution to equation (3.99) as follows

$$u[1] = \left(1 + \frac{-8\,x^2 - 8\,\gamma^2t^2 + 2 - 8\,i\gamma\,t}{4\,x^2 + 4\,\gamma^2t^2 + 1}\right) e^{i(2+6\gamma)t}. \tag{3.117}$$

The dynamics of this first-order rogue wave is depicted in figure (66)

It is easy here to observe that, when increasing the values of the parameter γ, the wave in compressed along the time coordinate. This implies the effect of the linear and nonlinear additional terms close to the parameter γ. The Figure (67) show us the compression in the time direction as well.

Using formula (3.109) and substituting equation (3.115) into (3.110), the second-order rogue wave solution to equation (3.99) can be obtained in the following form:

$$u[2] = \left(1 + \frac{F_2 + iG_2}{H_2}\right) e^{i(2+6\gamma)t}, \tag{3.118}$$

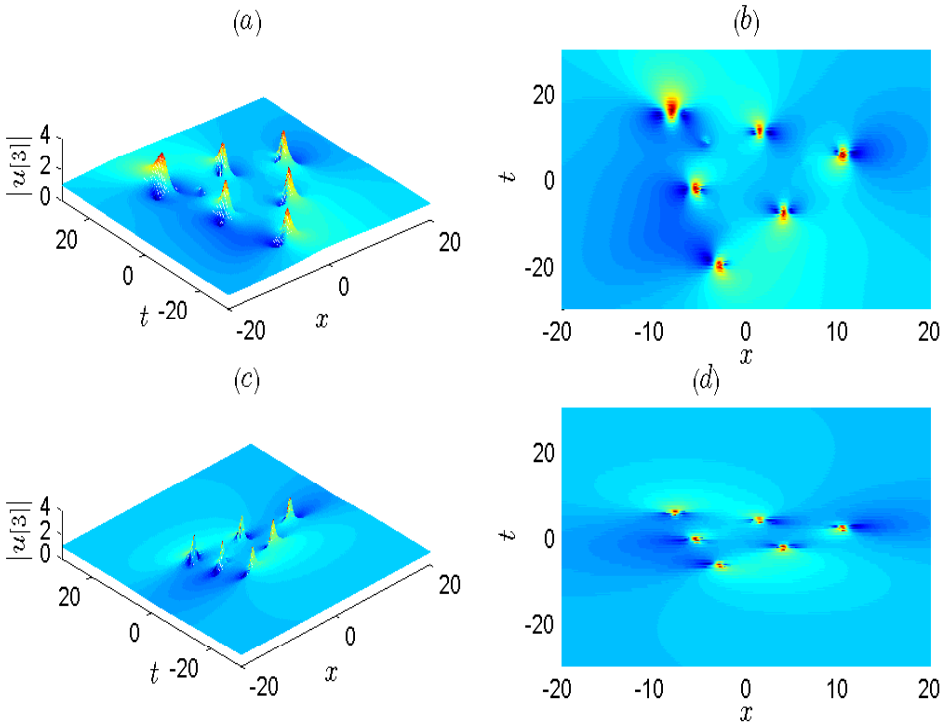

Figure 71: Third-order rogue wave solution to equation (1.1) depicted in panel (a) with $\gamma = 1/2$, the panel (b) is the density plot of the panel (a), the panel (c) show the depiction with $\gamma = 3/2$ and the panel (d) is its density plot. All the depictions are made for $c_1 = d_1 = 100$ and $c_2 = d_2 = 100$.

with

$$F_2 = -9 - 3072\,x^3 c_1 \gamma^2 t^2 - 4608\,\gamma^4 t^4 c_1 x + 4608\,x^4 d_1 \gamma\, t + 3072\,x^2 d_1 \gamma^3 t^3 + 72\,x^2$$
$$+1152\,c_1 \gamma^2 t^2 x + 5760\,d_1 x^2 \gamma\, t + 256\,x^8 + 384\,x^6 - 72\,\gamma^2 t^2 + 1024\,x^2 \gamma^6 t^6$$
$$+1024\,x^6 \gamma^2 t^2 + 1536\,x^4 \gamma^4 t^4 - 1536\,\gamma^5 t^5 d_1 + 2304\,\gamma^2 t^2 {c_1}^2$$
$$+2304\,\gamma^2 t^2 {d_1}^2 + 1536\,x^5 c_1 + 2304\,x^2 {d_1}^2 + 2304\,x^2 {c_1}^2 + 1152\,c_1 x^3 + 4992\,x^4 \gamma^2 t^2$$
$$+2688\,x^2 \gamma^4 t^4 + 3456\,\gamma^2 t^2 x^2 - 1920\,\gamma^6 t^6 + 3456\,\gamma^4 t^4 + 5760\,d_1 \gamma^3 t^3 + 256\,\gamma^8 t^8,$$
$$G_2 = -72\,\gamma\, t - 1920\,\gamma^5 t^5 + 1152\,d_1 x^4 + 512\,\gamma^7 t^7 + 1248\,\gamma^3 t^3 - 288\,x^2 \gamma\, t + 1152\,\gamma\, t {d_1}^2$$
$$+1152\,\gamma\, t {c_1}^2 + 512\,\gamma\, t x^6 - 1920\,\gamma^4 t^4 d_1 + 1536\,\gamma^3 t^3 x^4 + 1536\,\gamma^5 t^5 x^2 + 2304\,x^2 \gamma^3 t^3$$
$$+2304\,d_1 \gamma^2 t^2 + 1152\,x^4 \gamma\, t - 72\,d_1 + 2304\,\gamma^2 t^2 d_1 x^2 - 4608\,\gamma^3 t^3 c_1 x - 1536\,\gamma\, t c_1 x^3,$$
$$H_2 = 16\,d_1 x^2 \gamma\, t + (8/3)\,x^2 \gamma^4 t^4 + (8/3)\,x^4 \gamma^2 t^2 - (16/3)\,d_1 \gamma^3 t^3 - 16\,c_1 \gamma^2 t^2 x$$
$$+20\,\gamma^2 t^2 x^2 + 20\,\gamma\, t d_1 + 1/8 + (10/3)\,x^4 + \frac{8}{9}\,x^6 + \frac{27}{2}\,\gamma^2 t^2 - (14/3)\,\gamma^4 t^4$$
$$+\frac{8}{9}\,\gamma^6 t^6 - 1/2\,x^2 + 8\,{c_1}^2 + 4\,c_1 x + (16/3)\,c_1 x^3 + 8\,{d_1}^2.$$

The depiction of the second-order rogue wave is shown in figure (68)

In the Figure (68), we observe also that the wave is compressed in the time direction. This kind of rogue reassemble those obtained in Ref [107] called composite rogue for the vector nonlinear Schrödinger equation II.

In the Figure (69), we see second-order rogue wave divided in three individual first-order rogue waves. The three waves are scattered in all directions for the values of free parameters c_1 and d_1 different from zero. The three rogue waves array a triangle in which every wave sit on a vertices. Every wave is compressed along the time coordinate in his dynamics for the increasing values of the parameter γ.

Using formulae (3.111) and (3.112), one can get the third-order rogue wave solution to equation (3.99). The analytical expression for $u[3]$ is rather cumbersome to be written down here. Thus, the dynamics of the third-order are shown in Figures (70) and (71).

In the Figures (70) and (71), we see particular rogue waves scattered in all directions depending from the values of parameters c_1, c_2, d_1 and d_2. In the Figure (70), we observe five first-order rogue waves arraying a pentagon in which we have one in the center and the others sit on vertices. We also see the compression of the wave in the time direction. In Figure (71), we see six first-order rogue waves as well arraying a triangle. They are also compressed in time direction.

The Figure 71 shows us the compression in the time direction as well.

3.6 Homoclinic rogue waves to the Boussinesq equation

The rogue waves have been intensively studied in recent years, experimentally and theoretically. So far there have been a variety of approaches in the studies, starting from linear wave analysis, which can explain some of the phenomena that involve high amplitudes. In particular, for the deep ocean waves described by the nonlinear Schrödinger equation (NLSE), the localization is exemplified by the Peregrine soliton. Rogue waves always have two to three times amplitude higher than its surrounding waves and generally form in a short time for which people think that their come from nowhere.Besides the NLSE, rogue waves have also been explored in some other wave equations such as the(Dysthe equation, Zakharov equation), the Davey-Stewartson equation, just to name a

few .

In this section, we use a homoclinic (heteroclinic) breather limit method for seeking rogue wave solution to nonlinear evolution equation, Which is divided up in four steps:

Step 1

By painleve analysis, a transformation $u = T(f)$ is made for some new and unknown function f.

Step 2

By using the transformation in step 1, original equation can be converted into Hirota's bilinear form

$G(D_t, D_x; f) = 0,$

where the D-operator [121] is defined by

$$D_t^m D_x^n f(t,x).g(t,x) = \left(\frac{\partial}{\partial t} - \frac{\partial}{\partial t'}\right)^m \left(\frac{\partial}{\partial x} - \frac{\partial}{\partial x'}\right)^n f(t,x)g(t',x')|_{t'=t,x'=x}.$$

Step 3

Solve the above equation to get homoclinic (heteroclinic) breather wave solution by using extended homoclinic test approach (EHTA) [120] .

Step 4

Let the period of periodic wave go to infinite in homoclinic (heteroclinic) breather wave solution, we can obtain a rational homoclinic (heteroclinic) wave and this wave is just a rogue wave.

We consider in this work the Boussinesq equation,

$$u_{tt} - u_{xx} - 3(u^2)_{xx} - u_{xxxx} = 0,$$

Which is a good candidate to study water waves, since it finds applications in fluid dynamics. The Boussinesq equation,

$$u_{tt} - u_{xx} - 3(u^2)_{xx} - u_{xxxx} = 0, \tag{3.119}$$

By painlevé analysis, let

$$u = u_0 + 2(logf)_{xx} \tag{3.120}$$

Where, $f(x,t)$ is a real and unknown function to be determined, and u_0 is a small pertur-

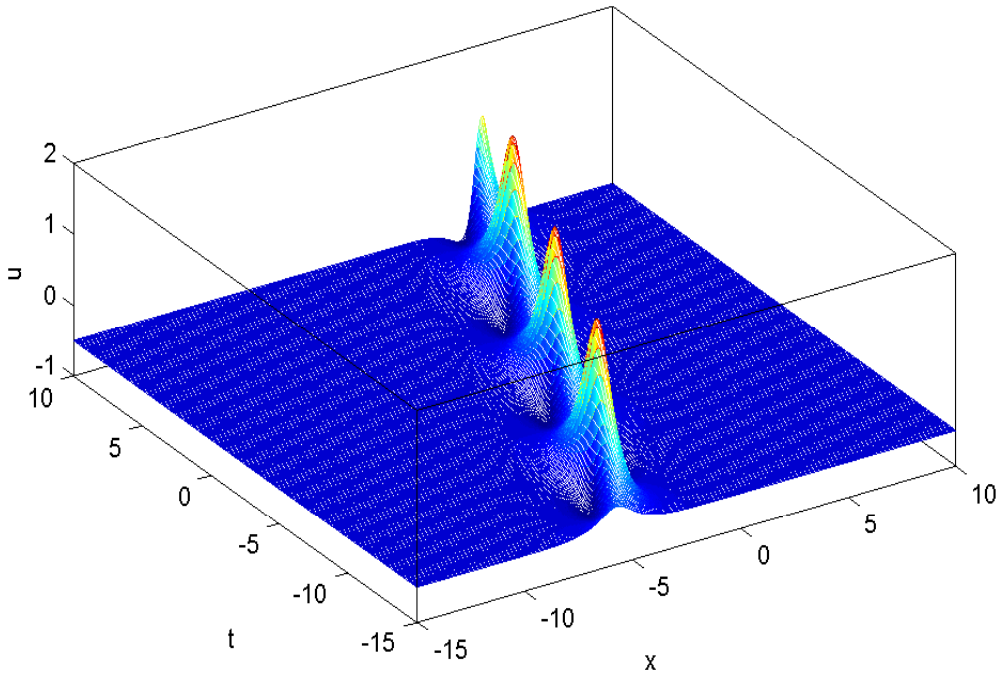

Figure 72: The figure of u(x,t) as $u_0 = -1/2$

$w_2 = 3/4$

bation parameter. Substituting (3.120) into (3.119), we get the following bilinear equation:

$$[D_t^2 - (1+6u_0)D_x^2 - D_x^4 - (3u_0^2 + A)]f.f = 0, \tag{3.121}$$

where, A is constant of integration, $D_x^4(f.f) = 2(f_{xxxx}f - 4f_{xxx}f_x + 3f_{xx}^2)$ and $D_x^2 = 2(f_{xx}f - f_x^2)$. In this case, we choose extended homoclinic test function

$$f(x,t) = e^{-p_1(x-w_1t)} + a_1 cos\,(p_2(x+w_2t)) + a_2 e^{p_1(x-w_1t)} \tag{3.122}$$

where p, p_1, w_1, w_2, a_1 and a_2 are constants to be determined.

Substituting equation (3.122) into equation (3.121), we can get algebraic equation of $e^{p_1(x-w_1t)}$. Then equating the coefficients of all powers of $e^{jp_1(x-w_1t)}$ $(j = -2, -1, 0, 1, 2)$ to zero, we get

$$\begin{cases} -a_1a_2(3u_0^2 + A) - a_1a_2(p_2^4 + p_1^4 - 6p_1^2p_2^2) + a_1a_2(p_1^2w_1^2 - p_2^2w_2^2) - 2a_1a_2(1+6u_0)(p_1^2 - p_2^2) = 0, \\ a_1p_1p_2w_1w_2 + a_1(1+6u_0)p_1p_2 + 2a_1p_1p_2(p_1^2 - p_2^2) = 0, \\ 4(p_1^2w_1^2a_2 - a_1^2p_2^2w_2^2) + 2(1+6u_0)(4p_1^2a_2 - a_1^2p_2^2) - 2(3u_0^2 + A)a_2 - 8(4p_1^4a_2 + a_1^2p_2^4) = 0, \\ 3u_0^2 + A = 0. \end{cases} \tag{3.123}$$

Setting $p_1 = p_2$ and making any simplifications, equation (3.123) is then reduced as follows,

$$\begin{cases} 4p_1^2 a_1 a_2 + a_1 a_2 (w_1^2 - w_2^2) = 0, \\ w_1 w_2 a_1 + a_1(1 + 6u_0) = 0, \\ 2(a_2 w_1^2 - a_1^2 w_2^2) + (1 + 6u_0)(2a_2 - a_1^2) - 2p_1^2(4a_2 + a_1^2) = 0. \end{cases} \tag{3.124}$$

Solving equation (3.124) yields

$$a_1 = \pm\sqrt{\frac{2w_1^2 + \beta - 4p_1^2}{2w_2^2 + \beta + 2p_1^2} a_2}, \qquad w_1 w_2 = -\beta, \qquad p_1^2 = \frac{1}{4}(w_2^2 - w_1^2), \tag{3.125}$$

with $\beta = 1 + 6u_0$. choosing $u_0 \neq -\frac{1}{6}$ and $a_2 > 0$, from (3.125) we find that

$$|w_2| > |w_1|, \quad w_1 = \beta/w_2 \quad and \quad w_1^2 > \beta \quad or \quad w_1^2 < \beta \quad (u_0 < -1/6 \quad or \quad u_0 > -1/6) \tag{3.126}$$

Substituting (3.126) into (3.122), we get the following solutions,

$$\begin{aligned} f_1(x,t) &= 2\sqrt{a_2}\cosh\left(p_1\left(x + \frac{\beta}{w_2}t\right) + \frac{1}{2}\ln(a_2)\right) + b_1\cos\left(p_1(x + w_2 t)\right) \\ f_2(x,t) &= 2\sqrt{a_2}\cosh\left(p_1\left(x + \frac{\beta}{w_2}t\right) + \frac{1}{2}\ln(a_2)\right) - b_1\cos\left(p_1(x + w_2 t)\right) \end{aligned} \tag{3.127}$$

Where, $b_1 = \sqrt{\frac{2w_1^2+\beta-4p_1^2}{2w_2^2+\beta+2p_1^2} a_2}$, $p_1 = \pm\frac{\sqrt{w_2^2 - w_1^2}}{2}$. Equation (3.127) into (3.120) provides us solutions of (3.119) as follows respectively

$$\begin{aligned} u_1 &= u_0 + 2p_1^2 \frac{a_2 - b_1^2 + 2b_1\sqrt{a_2}\sinh\left(p_1\left(x + \frac{\beta}{w_2}t\right) + \frac{1}{2}\ln(a_2)\right)\sin(p_1(x + w_2 t))}{\left(2\sqrt{a_2}\cosh\left(p_1\left(x + \frac{\beta}{w_2}t + \frac{1}{2}\ln(a_2)\right)\right) + b_1\cos(p_1(x + w_2 t))\right)^2} \\ u_2 &= u_0 + 2p_1^2 \frac{a_2 - b_1^2 - 2b_1\sqrt{a_2}\sinh\left(p_1\left(x + \frac{\beta}{w_2}t\right) + \frac{1}{2}\ln(a_2)\right)\sin(p_1(x + w_2 t))}{\left(2\sqrt{a_2}\cosh\left(p_1\left(x + \frac{\beta}{w_2}t + \frac{1}{2}\ln(a_2)\right)\right) - b_1\cos(p_1(x + w_2 t))\right)^2} \end{aligned} \tag{3.128}$$

The solution $u_1(x,t)$ (respectively $u_2(x,t)$) shows a new family of two-waves, breather solitary wave, which is a solitary wave and meanwhile is a periodic wave whose amplitude periodically oscillates with the evolution of time Figure72. It shows elastic interaction between a left-propagation(backward-direction) periodic wave with speed w_2 and homoclinic of different direction with speed $\frac{\beta}{w_2}$. Taking $a_2 = 1$ then, $\ln a_2 = 0$. So the solution u_2 can be rewritten as follows

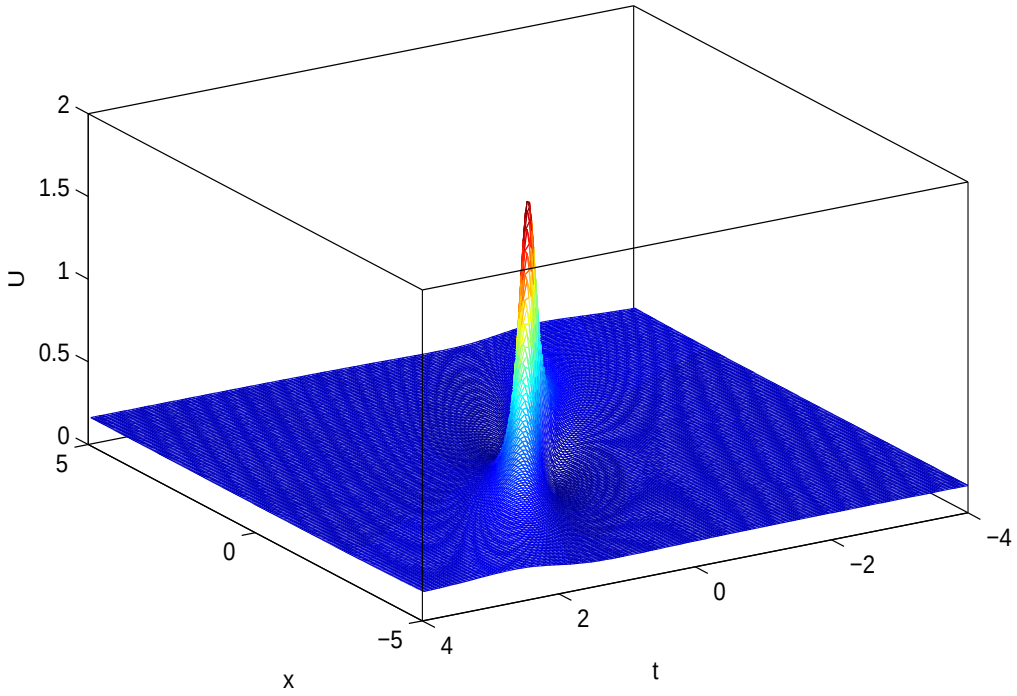

Figure 73: The figure of $U_B(x,t)$ as $u_0 = 1/6$, $w_1 = w_2$, $w_2 = 3/4$.

$$u_2^{(1)} = u_0 + 2p_1^2 \frac{b_2 - 2b_1 \sinh\left(p_1\left(x + \frac{\beta}{w_2}t\right)\right)\sin(p_1(x + w_2 t))}{\left(2\cosh\left(p_1\left(x + \frac{\beta}{w_2}t\right)\right) - b_1\cos(p_1(x + w_2 t))\right)^2}, \tag{3.129}$$

Where $b_2 = \frac{2(w_2^2 - w_1^2) + 6p_1^2}{2w_2^2 + \beta + 2p_1^2}$. Now, we consider a limit behavior of $u_2^{(1)}$ as the period $2\pi/p1$ of periodic wave $\cos(p_1(x + w_2 t))$ goes to infinite, i.e. $p_1 \to 0$.

By computing, we obtain the following result

$$U_{roguewave} = u_0 + \frac{16(6R - (x + \frac{\beta}{w_2}t)(x + w_2 t))}{\left(\left(x + \frac{\beta}{w_2}\right)^2 + (x + w_2 t)^2 + 8R\right)^2}, \tag{3.130}$$

where $R = \frac{1}{2w_2^2 + \beta}$; here we have used $b_1 \to 0$ and $w_1 = w_2$ as $p \to 0$, U contains two waves with different velocities and directions. It is easy to verify that $U_{roguewave}$ is a rational solution of Eq.3.119. Moreover, we can show that $U_{roguewave}$ is also a breather-type solution. In fact, $U \to 0$ for fixed x and $t \to \pm\infty$. So, U is not only a rational breather solution but also a rogue wave solution which has two to three times amplitude higher than its surrounding waves and generally forms in a short time Figure 73 . One

may think that whether the energy collection and superposition of breather solitary wave in many periods in many periods lead to a rogue wave or not.

3.7 Homoclinic rogue waves in a barothropic relaxing media

Rogue waves are a kind of wave which originally referred to a huge wave responsible of many marine disasters. But many efforts have been paid to study and understand the nature of this mysterious phenomenon, and the outcome is that, the rogue wave appears not only in oceanic condition but also in nonlinear physical systems such as plasma, the Bose-Einstein condensates, nonlinear optics, hydrodynamics just to name a few. It resorts also from the study that, rogue wave appears from nowhere and disappears without a trace; their amplitude is two or more times larger than the known common waves. The expressions of rogue wave solution are rational functions localized both in space and time, that is what imply their unpredictability. The simplest rogue wave solution was firstly obtained by Peregrin; more after, the first-order rogue wave solution for the nonlinear Schrödinger equation (NLSE) was calculated by Akhmediev and coworkers [19]. Analytical rogue wave solution has been also obtained for various physical models. Recently, we have made a study on a system modeling the propagation of waves in nonlinear fiber optics, and from the results it resort that the rogue wave can interact with solition-like wave without the destruction and the modification of the soliton wave [124].

Vakhnenko has recently investigated the wave propagation of high-frequency perturbations within a relaxing barothropic media and has derived a model equation known as Vakhnenko equation [170]. Indeed, the dynamic state equation of such relaxing barothropic media is given by [171]

$$(\partial_{xx}^2 - c_f^{-2}\partial_{tt}^2 + \alpha c_f^2 p^{'}\partial_{xx}^2 + \beta_f \partial_x + \gamma_f)p^{'} = 0, \tag{3.131}$$

where

$$\beta_f = \frac{c_f^2 + c_e^2}{\tau_p c_f c_e^2}, \qquad \gamma_f = \frac{c_f^4 - c_e^4}{2\tau_p^2 c_f^2 c_e^4}.$$

The physical quantity $p^{'}$ represents a pressure-valued perturbation ($p^{'} \ll p_0$) p_0 being the pressure at equilibrium. The independent variables x and t may stand for space-

and time-valued coordinates, respectively. Subscripts x and t appended to p_0 denote the partial differentiation. The quantities c_f and c_e denote the velocities for fast and slow processes, respectively. And a α_f is a characteristic quantity referring to fast processes. In this regime, the following accuracy may be necessary

$$\partial_{xx}^2 - c_f^2\partial_{tt}^2 \approx 2\partial_x(\partial_x + c_f^{-1}\partial_t),$$

such that equation (3.131) becomes

$$\partial_{\tilde{x}}(\partial_{\tilde{t}} + \tilde{u}\partial_{\tilde{x}})\tilde{u} + \tilde{\alpha}\partial_{\tilde{x}}\tilde{u} + \tilde{u} = 0,$$

provided the following transformations

$$\tilde{x} = \sqrt{\frac{\gamma_f}{2}}(x - c_f t), \quad \tilde{t} = \sqrt{\frac{\gamma_f}{2}}c_f t, \quad \tilde{u} = \alpha_f c_f^2 p', \quad \tilde{\alpha} = \frac{\beta_f}{\sqrt{2\gamma_f}},$$

hold for the dimensionless quantities $\tilde{u}$, $\tilde{x}$, $\tilde{t}$ and $\tilde{\alpha}$. Thus, setting $\beta_f = 0$, we have the following

$$\partial_{\tilde{x}}(\partial_{\tilde{t}} + \tilde{u}\partial_{\tilde{x}})\tilde{u} + \tilde{u} = 0, \tag{3.132}$$

which is known as the Vakhnenko equation.

In Ref. [122] this nonlinear evolution equation was discussed

$$\partial_x(\partial_t + u\partial_x)u + u = 0. \tag{3.133}$$

This equation model the propagation of waves in a relaxing medium [123]. The aim of this section is to construct the rogue wave solution to this equation, using the homoclinic test approach (HTA). For this end, we need to follow the procedure given in previous section for the Boussinesq equation.

First of all we need to give the bilinear form of equation (3.133). We then introduce the following variables X and T defined by

$$x = \phi(X, T) := T + \int_{-\infty}^{X} U(X', T)dX' + x_0 \qquad t = X, \tag{3.134}$$

where $u(x, t) = U(X, T)$ and x_0 is a constant. From equation (3.134), it come the following

$$\partial_X = \partial_t + u\partial_x, \qquad \partial_T = \theta\partial_x, \tag{3.135}$$

where

$$\theta(X,T) = 1 + \int_{-\infty}^{X} U_T dX^{'}, \quad so \quad that \quad \theta_X = U_T. \tag{3.136}$$

Combining the equations (3.133) and (3.135), we obtain the following one

$$U_{XT} + \theta U = 0. \tag{3.137}$$

The transformed form of the VE is obtain by eliminating the quantity θ between (3.136) and (3.137), namely

$$UU_{XXT} - U_X U_{XT} + U^2 U_T = 0. \tag{3.138}$$

Introducing the quantity W defined by $W_X = U$ and assuming that W and its derivatives vanish as $X \to -\infty$, then $\theta = 1 + W_T$ and (3.137) becomes

$$W_{XXT} + W_X W_T + W_X = 0. \tag{3.139}$$

Then, taking

$$W = 6(\ln f)_X, \tag{3.140}$$

the bilinear form of equation (3.139) is given as follows

$$(D_T D_X^3 + D_X^2) f.f = 0 \tag{3.141}$$

where the quantity D is the Hirota operator defined as follows

$$D_t^m D_x^n f(t,x).g(t,x) = \left(\frac{\partial}{\partial t} - \frac{\partial}{\partial t'}\right)^m \left(\frac{\partial}{\partial x} - \frac{\partial}{\partial x'}\right)^n f(t,x) g(t^{'}, x^{'})|_{t'=t, x'=x}.$$

We choose the homoclinic test function as follows

$$f(x,t) = e^{-p_1(x-w_1 t)} + c_1 \cos(p_2(x + w_2 t)) + c_2 e^{p_1(x-w_1 t)}. \tag{3.142}$$

Inserting the above test function in the bilinear form given in equation (3.141), we obtain the following set of equations

$$\begin{cases} p_2^2 - p_1^2 + p_1^4 w_1 - p_2^4 w_2 + 3p_1^2 p_2^2 w_2 - p_2^2 p_1^2 w_1 = 0, \\ -2 - p_1^2 w_2 - p_2^2 w_1 + 3p_1^2 w_1 + 3p_2^2 w_2 = 0, \\ -2c_1^2 p_2^2 + 8c_1^2 p_1^4 w_2 + 8p_1^2 c_2 - 32 p_1^4 w_1 c_2 = 0. \end{cases} \tag{3.143}$$

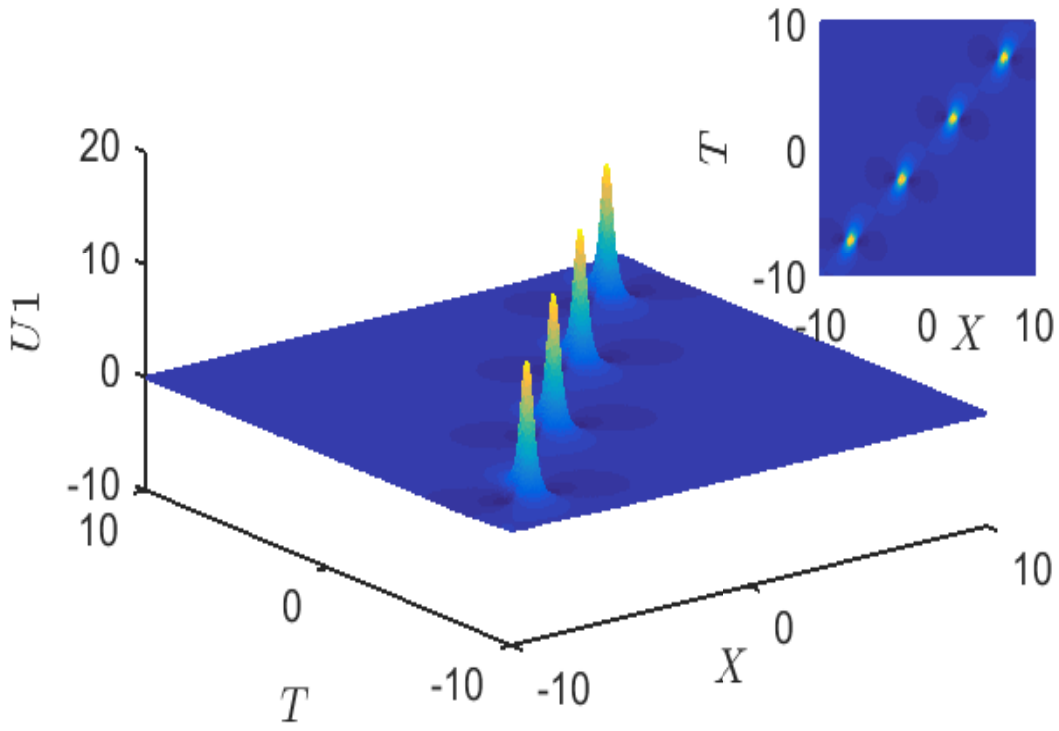

Figure 74: Figure of U_1 for $w_1 = 1$ and $c_2 = 1$.

Solving this set of equation, making the restriction $w_1 = w_2$ (without lost of generality), yields

$$c_1 = \pm 2\sqrt{\frac{(4w_1p_1^2 - 1)p_1^2}{4p_1^4w_1 - p_2^2}c_2}, \quad p_1 = \sqrt{\frac{4 + w_1}{w_1(3w_1 + 4)}}, \quad p_2 = \sqrt{\frac{4 - w_1}{w_1(3w_1 + 4)}}, \quad w_1 < 4. \tag{3.144}$$

Inserting the expressions given in equation (3.144) into the homoclinic test function given in (3.142), we obtain the following

$$f_1 = 2\sqrt{c_2}\cosh\left[p_1(x - w_1t) + \ln\sqrt{c_2}\right] + k_1\cos[p_2(x + w_1t)], \tag{3.145}$$

$$f_1 = 2\sqrt{c_2}\cosh\left[p_1(x - w_1t) + \ln\sqrt{c_2}\right] - k_1\cos[p_2(x + w_1t)], \tag{3.146}$$

where $k_1 = 2\sqrt{\frac{(4w_1p_1^2-1)p_1^2}{4p_1^4w_1-p_2^2}c_2}$.

From the expressions of the test function given above, we derive the solution of equation

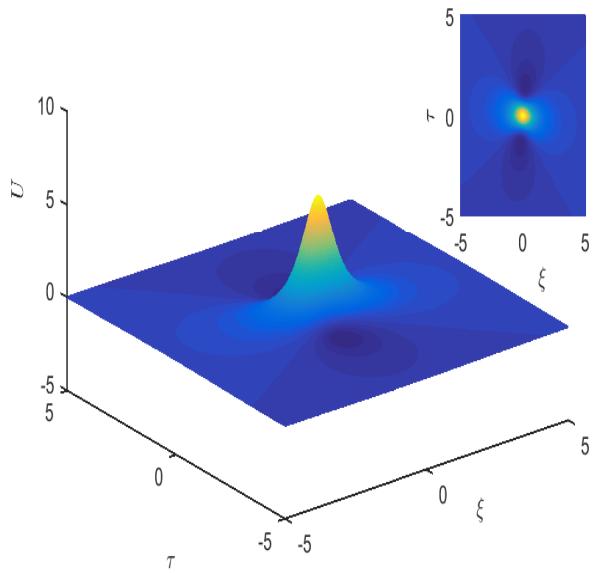

Figure 75: Depiction of U for $w_1 = 1$ and $c_2 = 1$.

(3.138) as follows

$$U_1 = \frac{2k_1\sqrt{c_2}(p_1^2 - p_2^2)\cosh(\zeta)\cos(\chi) + 4\sqrt{c_2}p_1p_2\sinh(\zeta)\sin(\chi) + 4c_2^2p_1^2 - k_1^2p_2^2}{\left[2\sqrt{c_2}\cosh(\zeta) + k_1\cos(\chi)\right]^2}, \quad (3.147)$$

$$U_2 = \frac{2k_1\sqrt{c_2}(p_1^2 - p_2^2)\cosh(\zeta)\cos(\chi) + 4\sqrt{c_2}p_1p_2\sinh(\zeta)\sin(\chi) + 4c_2^2p_1^2 + k_1^2p_2^2}{\left[2\sqrt{c_2}\cosh(\zeta) - k_1\cos(\chi)\right]^2}, \quad (3.148)$$

with $\zeta = p_1(x - w_1t) + \ln\sqrt{c_2}$ and $\chi = p_2(x + w_1t)$.

The figure corresponding to the solution U_1 is given in Figure (74).

Now, we consider a limit behavior of U_1 as the period $2\pi/p_1$ of periodic wave $\cos(p_2(x + w_1t))$ goes to infinite, i.e. $p_2 \to 0$. Hence we obtain the following expression

$$U = \frac{4\left(\frac{4}{3wt+4}(1 - 2xwt) + 2(x^2 - w^2t^2) + 1\right)}{(wt - x)^2 + (wt + x)^2 + 2} \quad (3.149)$$

U is the rational homoclinic rogue wave solution to equation (1.9). The corresponding feature is given in Figure (75).

Conclusion

Throughout this chapter, we have constructed rogue wave solutions to some nonlinear systems, by applying first the generalized Darboux transformation and secondly the homoclinic test approach. It resorts from our results that, the rogue waves can interact with other kind of wave without the destruction and the modification of the structure of that wave. It resorts also that the higher-order nonlinearity can modify the profile of the rogue waves during their dynamics. We have also shown that rogue waves can appear also in materials such as the ferrites. We have applied the homoclinic test approach on a nonlinear equation that models the dynamics of waves in the barothropic relaxing media, and it resorts that rogue waves can also exist in this media.

General Conclusion

At the starting of this dissertation, we proposed to study the rogue waves dynamics in nonlinear systems and particularly in the barothropic relaxing media. During our work, we have derived rogue wave solutions to nonlinear wave equation modeling nonlinear behavior in a wide variety of sophisticated fields such as spin chain, ferrites, monomode birefringent fiber, plasma, optics, deep water field and barothropic relaxing media. To derive these solutions, we have used two powerful mathematical tools such as the generalized Darboux transformation and the Extended Homoclinic Test Approach (EHTA). The generalized Darboux transformation originally comes from the classic Darboux matrix method. This last one unfortunately, is not appropriate to construct higher-order solution to a nonlinear system; that is why it has been modified in Ref. ([94]) to give born the most appropriated one, namely the Generalized Darboux Transformation (GDT). The GDT opere on the lax-pairs of the system under consideration. It consists of starting from a seed solution and grows like a ladder. Its particularity is that, it uses only one eigenvalue for all the procedure. The EHTA consists of starting from a test function with unknown coefficients, which is inserted in the original equation and the unknown coefficients are determined. After that, breather waves are obtained and by a Taylor expansion, the periodicity is omitted and the resulting wave is just a rogue wave.

In this thesis, we presented in detail a procedure of the construction of a generalized DT for the Manakov system. The construction is divided into two steps. First, a brief introduction of the DT for the Manakov system is given by the Darboux matrix method. Then a detailed derivation of the generalized DT for this system is discussed through the Taylor expansion and a limit procedure. The generalized DT allows us to calculate the higher-order rogue wave solution for the Manakov system in a unified way. In particular, some higher-order rogue wave solutions to the Manakov system are constructed by means

of the generalized DT with seed solutions $u[0] = e^{i\beta t}$ and $v[0] = e^{i\beta t}$. It is important to point out that the rogue wave solutions obtained in this paper are non-singular. The profiles of the higher-order rogue wave solutions for the Manakov system depend on the values of their free parameters c_j d_j $(j = 1, 2, 3...)$. We hope our result will be realized by physical experiments in the future, which is useful to understand the generation mechanism and to find possible applications of the rogue wave.

We have constructed localized waves solutions for a coupled nonlinear Schrödinger system with four wave mixing effects, self-phase modulation and cross-phase modulation effects. In this case, we have shown that the rogue wave can interact with soliton wave and breather wave elastically. From the results In fact, it ressort that rogue waves and solitons can coexist in a same medium and the information contained in the soliton cannot be destroyed during the interaction with rogue wave. During the interaction process, the fact that the rogue wave appears from nowhere and disappears without a trace can be related to the modulation instability. Indeed, the instability created by the plane wave solution on his top induces an increase of perturbation up to his highest amplitude and a decay. The mathematical tool used is the classical DT.

Higher-order rogue wave solutions to another coupled nonlinear Schrödinger equation with fifth-order nonlinearity have been constructed in this work. Up to second-order expansion rogue wave solution to this system has been provided using the GDT. It resort from the result that, increasing the value of the parameter close the higher-order nonlinearity, the wave is compressed along the x and t axis and its shape increases. Hence, the higher-order nonlinearity increases the nonlinear behavior of the wave in the medium. The effects of the parameter close to the higher-order nonlinearity on the rogue wave can be that, for the small values of this parameter, the modulation instability can be modified so that the wave lives very shortly and for the big values the wave live more longer due the increase of his amplitude. The results obtained in this work show that the profile of the rogue wave can be modified so that it can propagate in sophisticated nonlinear physical systems such as Spin chain. The rogue wave can also be controlled during its propagation by changing the values of the parameter β. The second-order rogue wave possesses two free parameters c_1 and d_1 responsible of the triplet and triangular arrangement on the rogue wave structure.

we have made an investigation on a system of generalized NLSE by mean of Darboux transformation, as a result higher-order rogue solutions has been obtained. We have studied the effects of the higher-order terms on the structure of rogue waves during their dynamics. Since the traditional DT is difficult to construct higher-order rogue wave solution, we have constructed the generalized DT for the system under consideration. Starting from seed solutions $u[0] = e^{i(4\beta^2-2)t}$ and $v[0] = e^{-i(4\beta^2-2)t}$ to the above system, we have given explicit first-order rogue wave solution. We have given explicit expressions to calculate second-order rogue wave solution. We have given formulae generating higher-order rogue wave solution to the system under study. We have introduced arbitrary parameters in the phase factor of the eigenfunction of the Lax-pairs responsible to triplet and triangular arrangement on the structure of the rogue waves. The second-order rogue wave solution contains two free parameters c_1 and d_1; for the values $c_1 = d_1 = 0$. When we set $c_1 = d_1 = 100$ we observe three fundamental rogue waves scattered in all directions and arraying a regular triangle. We have observed that increasing the values of the parameter β which implies the strength of higher-order nonlinearity and the SFS in the system, the rogue wave is compressed along the distance and the time direction and the amplitude increases. The results obtained in this work can explain the propagation of rogue waves in some sophisticated nonlinear physical systems such as spin chain, plasma, nonlinear optics and the theory of deep water waves. These results can also explain the propagation of rogue light pulses in nonlinear fiber optic.

Throughout this thesis, we have provided a generalized Darboux transformation of a generalized Nonlinear Schrödinger equation using Darboux matrix method. The starting block of this method is the Lax-pairs of this equation. Starting from a seed solution $u[0] = e^{i(2+6\gamma)t}$ and a generalized Darboux transformation, we have constructed rogue wave solutions from one to third-order. A general formula for generating Nth-order rogue wave solution has been proposed. We have shown that higher-order rogue wave solution to the GNLSE depends on their free parameters c_j and d_j. The second-order rogue wave solution contains two intrinsic parameters c_1 and d_1, the case where $c_1 = d_1 = 0$ gives a composite rogue wave crowded round the center $(0, 0)$ with the amplitude equal to 5, the case where $c_1 = d_1 = 30$ gives a feature in which we observe three fundamental rogue waves as well scattered in all directions. For the third-order, we have four intrinsic parameters

c_1, c_2, d_1 and d_2. When $c_1 = d_1 = 0$ and $c_2 = d_2 = 100$ we observe six fundamental rogue waves scattered in all directions and arraying a pentagon in which one sits in the center and the others are placed on the vertices, for the case where $c_1 = d_1 = 100$ and $c_2 = d_2 = 100$ we see also six fundamental rogue waves scattered in all directions and arraying a regular triangle. We have discussed in details the effect of the higher-order terms contained in this equation. It have been observed that, increasing the values of the parameter γ the rogue wave is compressed along the time coordinate. This result can be useful to explain the dynamic of rogue wave in some sophisticated nonlinear physical systems, especially in spin system. The results obtained in this work can also explain the propagation of rogue pulse light in nonlinear fiber optic.

We have also constructed rogue wave solution to a system modeling the dynamics of nonlinear behavior in the ferrites using the generalized Darboux transformation (GDT). The awesome pictures showing their dynamics have been plotted. From the results, it resort that, the waves are scattered in all directions and localized in both space and time directions. Throughout this thesis, we have extended system modeling the dynamics of ferrites in nonlinear systems, to a complex-valued one while studying its integrability properties. Then, we have used a generalized Darboux transformation to provide rogue wave solutions to this system using its Lax-pairs. One of the applications of the results in this work can be the propagation of rogue light pulses in ferrites. Since the magnetization is complex, the wave can rotate while propagating and the carried information can be more secured in micro-size devices such as hard-drive disk. Also, dashed magnetic signals can be efficiently eliminated in the ferrites.

Based on Darboux matrix method, a generalized Darboux transformation of a generalized nonlinear Schrödinger equation possessing higher-order terms which refer to a femto-second pulse propagation in a nonlinear fiber optic has been constructed. From this GDT, up to thirst-order expansion rogue wave solution to this equation has been provided. From the results it has been shown that, increasing the value of the parameter scaling the strength of linear and nonlinear terms, the rogue waves are compressed along the time axis. The second-order rogue wave possesses two free parameters c_1 and d_1 responsible to the triplet and triangular arrangement on rogue wave structure. Increasing the values of these parameters brings the second-order rogue wave to be divided into three

fundamental (first-order) rogue waves scattered in all directions. The thirst-order rogue wave possesses a part from the parameters c_1 and d_1, two other parameters c_2 and d_2. Giving the values different from zero to these parameters brings the thirst-order to be divided into six first-order rogue wave scattered in all directions.

Based on the homoclinic test approach, we derive the rogue wave solution to the Boussinesq equation.

In this thesis, we have applied the homoclinic breather limit method to the Vakhnenko equation. As a result, we have obtained solitary breather wave of the Vakhnenko equation. Meanwhile, considering a limit behavior of the breather wave, we have obtained the rogue wave solution to the equation under consideration. we aim in our future work to use other method such as the Darboux transformation and the wronskian determinant to construct higher-order rogue wave solution to the Vakhnenko equation.

We aim in our future works to go further while constructing more higher-order rogue wave solutions to the above systems. We aim also to make experiments of the solutions obtained in this work. We will also observe the behavior of these solutions using numerical simulations. All the systems that we have studied in this thesis are all (1+1)-dimensional systems, we will in our future works devote our attention to (2+1)-dimensional and (3+1)-dimensional systems.

Appendix

1. **Analytical expressions of coefficients of equation (3.43)**

$r_1^{[0]} = \frac{\sqrt{2}}{2\sqrt[4]{\beta}}\,(1-i)\,(-2\,\sqrt{\beta}x + 3\,\beta^{3/2}\alpha\,t - 4\,i\beta\,\alpha\,t - 1)$
$\mathrm{e}^{-2\,\sqrt{\beta}x+2\,\beta^{3/2}\alpha\,t-4\,it\alpha\,\beta+1/2\,i\beta\,t}$,

$s_1^{[0]} = \frac{a\sqrt{2}}{2\beta^{3/4}}\,(1-i)\,(-2\,\sqrt{\beta}x + 3\,\beta^{3/2}\alpha\,t - 4\,i\beta\,\alpha\,t + 1)$
$\mathrm{e}^{-2\,\sqrt{\beta}x+2\,\beta^{3/2}\alpha\,t-4\,it\alpha\,\beta-1/2\,i\beta\,t}$,

$w_1^{[0]} = \frac{b\sqrt{2}}{2\beta^{3/4}}\,(1-i)\,(-2\,\sqrt{\beta}x + 3\,\beta^{3/2}\alpha\,t - 4\,i\beta\,\alpha\,t + 1)$
$\mathrm{e}^{-2\,\sqrt{\beta}x+2\,\beta^{3/2}\alpha\,t-4\,it\alpha\,\beta-1/2\,i\beta\,t}$.

For simplicity, we have put $\alpha = 1$,($a = 1$, $b = 0$ for $s_1^{[j]}$),($a = 0$, $b = 1$ for $w_1^{[j]}$) (j=1,2)

$r_1^{[1]} = (-1/24 + 1/24\,i)\,\sqrt{2}\mathrm{e}^{-2\,x+2\,t-7/2\,it}(-3 + 117\,t^3 + 180\,xt + 15\,t - 42\,xt^2 + 147\,t^2$
$-18\,x - 36\,x^2 - 36\,x^2t + 24\,i\,d_1 - 240\,ixt - 36\,it + 504\,it^2 - 144\,it^2x + 48\,ix^2t + 44\,it^3 +$
$24\,c_1 + 8\,x^3)$,

$s_1^{[1]} = (1/24 - 1/24\,i)\,\sqrt{2}$
$\mathrm{e}^{-2\,x+2\,t-9/2\,it}(-3 - 117\,t^3 - 252\,xt + 129\,t + 42\,xt^2 - 189\,t^2 - 30\,x + 60\,x^2 + 36\,x^2t - 24\,i\,d_1 +$
$336\,ixt - 156\,it - 648\,it^2 + 144\,it^2x - 24\,c_1 - 8\,x^3 - 48\,ix^2t - 44\,it^3)$,

$w_1^{[1]} = (1/24 - 1/24\,i)\,\sqrt{2}$
$\mathrm{e}^{-2\,x+2\,t-9/2\,it}(-3 - 117\,t^3 - 252\,xt + 129\,t + 42\,xt^2 - 189\,t^2 - 30\,x + 60\,x^2 + 36\,x^2t - 24\,i\,d_1 +$
$336\,ixt - 156\,it - 648\,it^2 + 144\,it^2x - 24\,c_1 - 8\,x^3 - 48\,ix^2t - 44\,it^3)$.

$r_1^{[2]} = \left(\frac{1}{960} - \frac{1}{960}\,i\right)\,\sqrt{2}$
$\mathrm{e}^{-2\,x+2\,t-7/2\,it}(-45 - 210\,x - 765\,t + 11640\,x^2t - 3720\,xt + 21660\,xt^2 + 240\,x^4t + 60840\,t^3x -$
$4320\,tx^3 - 9240\,t^2x^2 + 5270\,t^4x + 560\,t^2x^3 - 4680\,t^3x^2 - 600\,x^2 + 3330\,t^2 - 1200\,x^3 - 102630\,t^3 -$
$39525\,t^4 + 560\,x^4 - 237\,t^5 - 32\,x^5 - 3840\,ixtc_1 + 960\,ixd_1 + 22880\,ixt^3 + 1680\,it^2d_1 + 1920\,it^2x^3 +$
$81120\,it^2x + 480\,ixt + 5760\,ix^3t + 5760\,itc_1 + 5760\,it^2c_1 + 2880\,xc_1t + 25200\,it^4 + 3116\,it^5 +$
$540\,it + 3840\,xd_1t - 320\,ix^4t - 31680\,it^2x^2 - 14880\,ix^2t - 4320\,itd_1 - 3360\,it^4x - 1760\,it^3x^2 -$
$960\,ix^2d_1 - 5760\,td_1 - 4320\,tc_1 - 5760\,t^2d_1$

$+960\,xc_1+1680\,t^2c_1-960\,x^2c_1-41160\,it^3-19440\,it^2-240\,id_1-960\,id_2+2880\,ixtd_1-240\,c_1-960\,c_2)$,

$s_1^{[2]}=\left(\frac{1}{960}-\frac{1}{960}\,i\right)\sqrt{2}$

$\mathrm{e}^{-2\,x+2\,t-9/2\,it}(45+270\,x+3555\,t+23160\,x^2t-19800\,xt+38460\,xt^2+240\,x^4t+70200\,t^3x-5280\,tx^3-10920\,t^2x^2+5270\,t^4x+560\,t^2x^3-4680\,t^3x^2+1560\,x^2-12450\,t^2-3120\,x^3-158790\,t^3-44795\,t^4+720\,x^4-237\,t^5-32\,x^5-30240\,ix^2t-7200\,itd_1-37440\,it^2x^2+28560\,it^4+2880\,ixd_1+20640\,ixt+9600\,itc_1+7040\,ix^3t+26400\,ixt^3+138720\,it^2x-3840\,ixtc_1+1680\,it^2d_1+1920\,it^2x^3+5760\,it^2c_1+2880\,xc_1t+3116\,it^5+3840\,xd_1t-320\,ix^4t-3360\,it^4x-1760\,it^3x^2-960\,ix^2d_1-62280\,it^3-1380\,it-80400\,it^2-9600\,td_1-7200\,tc_1-5760\,t^2d_1+2880\,xc_1+1680\,t^2c_1-960\,x^2c_1-240\,id_1-960\,id_2+2880\,ixtd_1-240\,c_1-960\,c_2)$,

$w_1^{[2]}=\left(\frac{1}{960}-\frac{1}{960}\,i\right)\sqrt{2}$

$\mathrm{e}^{-2\,x+2\,t-9/2\,it}(45+270\,x+3555\,t+23160\,x^2t-19800\,xt+38460\,xt^2+240\,x^4t+70200\,t^3x-5280\,tx^3-10920\,t^2x^2+5270\,t^4x+560\,t^2x^3-4680\,t^3x^2+1560\,x^2-12450\,t^2-3120\,x^3-158790\,t^3-44795\,t^4+720\,x^4-237\,t^5-32\,x^5-30240\,ix^2t-7200\,itd_1-37440\,it^2x^2+28560\,it^4+2880\,ixd_1+20640\,ixt+9600\,itc_1+7040\,ix^3t+26400\,ixt^3+138720\,it^2x-3840\,ixtc_1+1680\,it^2d_1+1920\,it^2x^3+5760\,it^2c_1+2880\,xc_1t$

$+3116\,it^5+3840\,xd_1t-320\,ix^4t-3360\,it^4x-1760\,it^3x^2-960\,ix^2d_1-62280\,it^3-1380\,it-80400\,it^2-9600\,td_1-7200\,tc_1-5760\,t^2d_1+2880\,xc_1+1680\,t^2c_1-960\,x^2c_1-240\,id_1-960\,id_2+2880\,ixtd_1-240\,c_1-960\,c_2)$.

2. **Analytical expressions for** $r_1[1]$, $s_1[1]$, $w_1[1]$, $r_1[2]$, $s_1[2]$ and $w_1[2]$.

$r_1[1]=\frac{(1/6-1/6\,i)\sqrt{2}}{(-8\,x^2+24\,xt-50\,t^2-2)(-2\,x+3\,t+4\,it-1)}$

$\mathrm{e}^{-2\,x+2\,t-7/2\,it}(-6+480\,itx^4+108\,t-24\,x-6100\,it^4x-1952\,it^2x^3-168\,it^2\,c_1-576\,it^2\,d_1-480\,ix^2t+384\,ix\,d_1\,t+24\,d_1-288\,ixt\,c_1+96\,ix^2\,c_1+1776\,ixt^2+384\,x\,c_1\,t+4464\,it^3x^2-1032\,it^3-64\,ix^5-12\,ix-24\,ic1+288\,xt\,d_1-3750\,t^4-48\,x^2+2900\,t^3+5000\,t^5-96\,x^4-300\,t^2-96\,x^3+3750\,it^5+64\,ix^3+66\,it+128\,tx^4+168\,t^2\,d_1-4800\,t^4x-768\,t^2x^3-1224\,xt^2-576\,t^2\,c_1+2752\,t^3x^2+240\,x^2t-2064\,x^2t^2+3600\,xt^3-96\,x^2\,d1+576\,x^3t+144\,xt)$,

$s_1[1]=\frac{(-1/6-1/6\,i)\sqrt{2}}{-8\,x^2+24\,xt-50\,t^2-2}\mathrm{e}^{-2\,x+2\,t-9/2\,it}(12\,ix+42\,t-12\,x-24\,c_1-350\,t^4-24\,x^2-366\,t^3+32\,x^4-486\,t^2+16\,x^3+204\,xt^2-168\,x^2t+432\,x^2t^2-432\,xt^3-192\,x^3t+168\,xt+128\,ix^3t+96\,itc_1+48\,ix^3+72\,tc_1-96\,td1-1200\,it^4-24\,ix^2-198\,it^2-90\,it-362\,it^3-24\,id_1-576\,it^2x^2-48\,ix\,d_1-120\,itx^2-24\,ixt+72\,it\,d_1+228\,ixt^2+1376\,it^3x-6\,i-48\,x\,c_1)$,

$w_1[1]=\frac{(-1/6-1/6\,i)\sqrt{2}}{-8\,x^2+24\,xt-50\,t^2-2}\mathrm{e}^{-2\,x+2\,t-9/2\,it}(12\,ix+42\,t-12\,x-24\,c_1-350\,t^4-24\,x^2-366\,t^3+$

$32\,x^4-486\,t^2+16\,x^3+204\,xt^2-168\,x^2t+432\,x^2t^2-432\,xt^3-192\,x^3t+168\,xt+128\,ix^3t+96\,itc_1+48\,ix^3+72\,tc_1-96\,td1-1200\,it^4-24\,ix^2-198\,it^2-90\,it-362\,it^3-24\,id_1-576\,it^2x^2-48\,ixd_1-120\,itx^2-24\,ixt+72\,itd_1+228\,ixt^2+1376\,it^3x-6\,i-48\,xc_1)$,

$r_1[2]=(-1/30-1/30\,i)$

$\sqrt{2}\mathrm{e}^{(-\frac{2}{65}+\frac{7}{130}\,i)(16\,x+28\,ix-65\,t)}(-540\,d_1+27648\,ix^5d_1\,t+540\,x-3510\,t-4860\,x^2t+14040\,xt+1890\,xt^2+9408\,x^6t-86016\,x^5t^3-12288\,x^7t+44544\,x^6t^2-71136\,x^5t^2+36720\,t^2{d_1}^2-66960\,t^2{c_1}^2+8640\,x^2{c_1}^2-350280\,t^4x^3+436068\,t^5x^2-124800\,t^7x+60672\,t^5x^3-140448\,t^6x^2-1313928\,t^5x-1694730\,t^6x+83520\,x^3t^3-10368\,x^5t-36000\,x^4t^2+48960\,t^4x^4+35280\,x^4t-437760\,t^3x-17280\,tx^3+218160\,t^2x^2-2115270\,t^4x-126000\,t^2x^3+628200\,t^3x^2+2880\,d_1\,x^4-8640\,{d_1}^2t+8640\,x^2{d1}^2+532440\,x^2t^4-234720\,t^4c_1+111852\,t^5d_1-129564\,t^5c_1-8064\,x^5c_1+432000\,c_1\,t^3-73440\,t{c_1}^2+8640\,xc{1}^2-29160\,t^2d_1+244080\,t^2c_1+8640\,x^2c_1-16740\,td_1+15660\,tc_1-3240\,xc1+29160\,t^3d_1+985140\,t^4d_1+276720\,x^4t^3+4320\,x^2d_1-145152\,x^6t^3+277440\,x^5t^4-6912\,x^8t+41472\,x^7t^2+168480\,t^3{d_1}^2-121248\,t^5x^4-878176\,t^6x^3+11520\,x^3{d_1}^2+2523600\,t^7x^2-3288750\,t^8x-123552\,t^6d_1-1078536\,t^6c1-4608\,x^6c1+1080\,xd1+8640\,x^3d_2+2160\,xd_2+1080\,c_1-1080\,d_2-1080\,x^2-53190\,t^2+2520\,x^3-170325\,t^3-84480\,t^3x^3d_1-718560\,t^4x^2c_1+311040\,t^3x^3c_1+448704\,t^5xd_1+1315872\,t^5xc_1-9216\,x^5td_1-241920\,t^4x^2d_1+69120\,x^4t^2d_1+41472\,x^5tc_1-155520\,x^4t^2c_1-51840\,td_1{}^2x^2-60480\,t^2{d_1}^2x+5760\,x^3td_1-25920\,xc_1\,t-21600\,xd_1\,t+108000\,x^2td_1-69120\,x^2tc_1+262440\,t^4xc_1+8640\,x^4td_1+48960\,x^4tc_1+538560\,c_1\,t^3x+11520\,c_1\,tx^3-190080\,c_1\,t^2x^2+8640\,t{c_1}^2x-60480\,x{d_1}^2t-943200\,xt^3d_1-438480\,xt^2d_1+73440\,x^2t^2d_1-358920\,t^4xd_1-182880\,t^3x^2c_1+31680\,t^2x^3d_1-66240\,t^2x^3c_1+27360\,t^3x^2d_1-644130\,t^4-1440\,x^4+1790073\,t^5-4320\,x^5+2688\,x^6-26250\,t^8+8682\,t^6+2125893\,t^7+1536\,x^8-384\,x^7-2160\,{d_1}^2-2160\,{c_1}^2+1828125\,t^9+512\,x^9-35640\,t^2d2-4320\,x^2c_2+2880\,x^3c_2-8640\,x^3d_1-5760\,x^5d_1-16200\,td_2+7560\,tc_2-2160\,xc_2+5760\,x^4c_2-87480\,t^2c_2-216000\,t^4d_2-65880\,t^3c_2-63000\,t^4c_2-65160\,t^3d_2-69120\,x^2tc_1\,d_1+207360\,t^2c_1\,xd_1+51840\,xtc_1\,d_1-63360\,t^3d_1\,c_1-17280\,x^2c_1\,d_1+8640\,xc_1\,d_1+12960\,tc_1\,c_2+247680\,t^3xd_2+30240\,t^2c_1\,d_1-2160\,ixc_2+23040\,x^3td_2+36720\,xt^2c_2-4320\,xtd_2-21600\,x^2td_2-34560\,x^3tc_2+30240\,xtc2-30240\,x^2tc_2-103680\,t^2x^2d_2+77760\,t^2x^2c_2-77760\,t^3xc_2+12960\,td_1\,d_2+38880\,c_1\,td_1+41040\,t^2xd_2+760320\,ix^3t^3d_1+56160\,ixtc_1+77760\,it^2x^2d_2+8640\,ixd_1\,c_2+4320\,ixtc_2+60480\,ixtd{d1}^2+21600\,ix^2tc_2+64800\,ixt^2d_1+8640\,ixc_1{}^2t+4320\,id_1{}^2x+4320\,ix^2c_2+8640\,id_1\,c_1{}^2+244800\,ic_1\,t^2x^3+79920\,it^3d_1+4320\,id_1\,c_2+228960\,it^4d_1+23760\,itc_1{}^2+62640\,id_1{}^2t+35640\,it^2c_2+5760\,ix^4d_2+216000\,it^4c_2+63360\,it^3c_1{}^2+286200\,it^2d_1+4320\,ix^2d_1+$

$$226304\,ix^6t^3 + 1582920\,it^4x^3 + 32940\,ix^2t + 315000\,it^3x^2 + 2292864\,it^5x^4 + 112608\,ix^5t^2 +$$
$$3072\,ix^8t+4795200\,it^7x^2+1102890\,it^6x+19440\,ix^4t+65160\,it^3c_2+2036400\,it^7x+89280\,it^3x+$$
$$15360\,ix^7t+832104\,it^5x+1802304\,it^5x^3+563400\,ix^2t^4+2880\,ix^3d_2+6480\,it^2x^2+16200\,itc_2+$$
$$7560\,itd_2 + 8640\,ic_1\,x^3 + 18720\,ix^4t^2 + 5760\,ix^5t + 398592\,ix^5t^3 + 1080\,ixt - 23040\,ix^3tc_2 -$$
$$315360\,ic_1\,t^2x^2-195840\,ix^4t^2d_1-168480\,it^3d_1\,c_1-207360\,it^2{c_1}^2x-8640\,ic1\,xd_2-241920\,ix^2t^4c_1-$$
$$9216\,ix^5c_1\,t-34560\,itx^3d_2-103680\,ic_1\,t^2d_1-8640\,ix^2td_1-41040\,it^2xc_2-54720\,itx^4c_1-$$
$$124920\,it^4c_1\,x-38880\,itc_1\,x^2-496440\,ixt^4d_1-280800\,ic_1\,t^3x^2-146880\,it^2x^3d_1-30240\,ix^2td_2+$$
$$8640\,ix^2{c_1}^2+5760\,ix^5c_1+149400\,ic_1\,t^3+336852\,it^5c_1+8100\,itc_1-247680\,it^3xc_2-11520\,ic_1\,x^3d_1-$$
$$64800\,itc_1\,d_1-1477440\,ix^2t^4d_1-84480\,ix^3t^3c_1-17280\,itd_1\,d_2-17280\,itc1\,c_2-155520\,ix^2t^2d_1-$$
$$12960\,ixd_1\,t - 12960\,itd_1\,c_2 - 77760\,it^3xd_2 - 65880\,it^3d_2 - 66960\,it^2{c_1}^2 - 8640\,ix^3c_2 -$$
$$95436\,it^5d_1-4320\,ixc_1{}^2-128250\,ixt^2-1392210\,it^4x-36864\,ix^7t^2-875520\,ix^5t^4-4108032\,it^6x^3-$$
$$585840\,ix^4t^3-14016\,ix^6t-1901124\,it^5x^2-43920\,it^2x^3-3240000\,it^8x-3072\,ix^6d_1-4320\,ix^2c_1-$$
$$4320\,ix^2d_2-63000\,it^4d_2-160920\,it^2c_1-2880\,ix^4c_1-774900\,ic_1\,t^4-87480\,it^2d_2-796464\,it^6d_1-$$
$$123552\,it^6c_1-36720\,it^2{d_1}^2-4320\,ic_1\,d_2-3456\,ix^5d_1-2160\,ixd_2-8640\,ix^2{d_1}^2-1080\,ic_1\,x-$$
$$1620\,itd_1-5760\,ix^3d_1-2251536\,it^6x^2-17280\,ix^3t-100608\,ix^6t^2-1013280\,ix^4t^4-348480\,ix^3t^3-$$
$$3240\,ixd_1 + 14400\,itx^4d_1 + 17280\,ic_1\,x^3t + 12960\,ic_1\,td_2 + 448704\,it^5xc_1 + 69120\,ix^2{c_1}^2t +$$
$$1080\,ic_2+8640\,i{d_1}^3+69120\,ix^4t^2c_1+384\,ix^7+540\,ic_1+1080\,id_1+30240\,ixtd_2+69120\,itc_1\,xd_1+$$
$$51840\,ix^2d_1\,tc_1-135\,i+60480\,it^2d_1\,xc_1+92880\,ic_1\,t^2x+8640\,ixc_1\,d_1-4320\,x^2d_2-4320\,c_1\,c_2-$$
$$4320\,d_1\,d_2 - 768\,ix^8 - 3960\,ix^3 - 270\,ix - 3744\,ix^5 - 1094349\,it^7 - 1261875\,it^8 - 327870\,it^4 -$$
$$2128626\,it^6 - 1152\,ix^6 - 33750\,it^2 - 1080\,ix^2 + 8640\,c_1\,{d_1}^2 + 2880\,ixt^3d_1 + 36720\,ixt^2d_2 +$$
$$687500\,it^9 + 457065\,it^3 + 1135251\,it^5 + 1485\,it + 1440\,ix^4 - 8640\,xd_1\,d_2 - 8640\,xc_1\,c_2 -$$
$$17280\,td_1\,c_2+17280\,c_1\,td_2+1236960\,ic_1\,t^3x+103680\,it^2x^2c_2+8640\,{c_1}^3+491040\,it^3x^2d_1+$$
$$1384128\,ixt^5d_1+34560\,itd_1\,x^3)/(9-612\,xt-192\,x^3c_1-22500\,t^5x-8928\,x^3t^3-576\,x^5t+$$
$$2928\,x^4t^2 + 792\,t^3x + 96\,tx^3 - 2232\,t^2x^2 + 18300\,x^2t^4 - 2808\,c_1\,t^3 + 864\,td_1 - 792\,tc_1 +$$
$$144\,xc_1-1056\,t^3d_1+108\,x^2+2835\,t^2-1152\,x^2td_1+864\,x^2tc_1+1008\,c_1\,xt^2+3456\,xt^2d_1+$$
$$10179\,t^4+48\,x^4+64\,x^6+15625\,t^6+144\,{d_1}^2+144\,{c_1}^2),$$

$$s_1[2] = (-1/30 - 1/30\,i)$$
$$\sqrt{2}\mathrm{e}^{\left(-\frac{2}{97}+\frac{9}{194}\,i\right)(16\,x+36\,ix-97\,t)}(-540\,d_1+95436\,it^5d_1+8640\,ix^3c_2+66960\,it^2{c_1}^2+65880\,it^3d_2+$$
$$3240\,ixd_1 + 348480\,ix^3t^3 + 1013280\,ix^4t^4 + 100608\,ix^6t^2 + 17280\,ix^3t + 2251536\,it^6x^2 +$$
$$5760\,ix^3d_1+1620\,itd_1+1080\,ic_1\,x+2160\,ixd_2+3456\,ix^5d_1+4320\,ic_1\,d_2+36720\,it^2{d_1}^2-$$
$$491040\,it^3x^2d_1-244800\,ic_1\,t^2x^3-92880\,ic_1\,t^2x-8640\,ixc_1{}^2t+27648\,ix^5d_1\,t+103680\,ic_1\,t^2d_1+$$

$$41040\,it^2xc_2+540\,x-3510\,t+8640\,ix^2td_1+496440\,ixt^4d_1+38880\,itc_1\,x^2+124920\,it^4c_1\,x+$$
$$54720\,itx^4c_1+30240\,ix^2td_2+146880\,it^2x^3d_1+280800\,ic_1\,t^3x^2-4860\,x^2t-14040\,xt+$$
$$1890\,xt^2+9408\,x^6t+86016\,x^5t^3+12288\,x^7t-44544\,x^6t^2-71136\,x^5t^2-36720\,t^2{d_1}^2+$$
$$66960\,t^2{c_1}^2-8640\,x^2{c_1}^2-350280\,t^4x^3+436068\,t^5x^2+124800\,t^7x-60672\,t^5x^3+140448\,t^6x^2+$$
$$1313928\,t^5x-1694730\,t^6x-83520\,x^3t^3+10368\,x^5t+36000\,x^4t^2-48960\,t^4x^4+35280\,x^4t+$$
$$437760\,t^3x+17280\,tx^3-218160\,t^2x^2-2115270\,t^4x-126000\,t^2x^3+628200\,t^3x^2+2880\,d_1\,x^4-$$
$$8640\,d1^2t-8640\,x^2{d_1}^2-532440\,x^2t^4-234720\,t^4c_1-111852\,t^5d_1+129564\,t^5c_1+8064\,x^5c_1-$$
$$432000\,c_1\,t^3-73440\,t{c_1}^2+8640\,x{c_1}^2-29160\,t^2d_1+244080\,t^2c_1+8640\,x^2c_1+16740\,td_1-$$
$$15660\,tc_1+3240\,xc_1-29160\,t^3d_1+985140\,t^4d_1+276720\,x^4t^3+4320\,x^2d_1-145152\,x^6t^3+$$
$$277440\,x^5t^4-6912\,x^8t+41472\,x^7t^2+168480\,t^3{d_1}^2-121248\,t^5x^4-878176\,t^6x^3+11520\,x^3{d_1}^2+$$
$$2523600\,t^7x^2-3288750\,t^8x-123552\,t^6d_1-1078536\,t^6c_1-4608\,x^6c_1-1080\,xd_1-8640\,x^3d_2-$$
$$2160\,xd_2+1080\,c_1-1080\,d_2+1080\,x^2+53190\,t^2+2520\,x^3-170325\,t^3-84480\,t^3x^3d_1-$$
$$718560\,t^4x^2c_1+311040\,t^3x^3c_1+448704\,t^5xd1+1315872\,t^5xc_1-9216\,x^5td_1-241920\,t^4x^2d_1+$$
$$69120\,x^4t^2d_1+41472\,x^5tc_1-155520\,x^4t^2c_1-51840\,t{d_1}^2x^2-60480\,t^2{d_1}^2x+5760\,x^3td_1-$$
$$25920\,xc_1\,t-21600\,xd_1\,t-108000\,x^2td_1+69120\,x^2tc_1-262440\,t^4xc_1-8640\,x^4td_1-$$
$$48960\,x^4tc_1+538560\,c_1\,t^3x+11520\,c_1\,tx^3-190080\,c_1\,t^2x^2-8640\,tc1^2x+60480\,xd1^2t-$$
$$943200\,xt^3d_1+438480\,xt^2d_1+73440\,x^2t^2d_1+358920\,t^4xd_1+182880\,t^3x^2c_1-31680\,t^2x^3d_1+$$
$$66240\,t^2x^3c_1-27360\,t^3x^2d_1+644130\,t^4+1440\,x^4+1790073\,t^5-4320\,x^5-2688\,x^6+26250\,t^8-$$
$$8682\,t^6+2125893\,t^7-1536\,x^8-384\,x^7+2160\,{d_1}^2+2160\,{c_1}^2+1828125\,t^9+512\,x^9-$$
$$35640\,t^2d_2-4320\,x^2c_2-2880\,x^3c_2+8640\,x^3d_1+5760\,x^5d_1+16200\,td_2-7560\,tc_2+2160\,xc_2+$$
$$5760\,x^4c_2-87480\,t^2c_2-216000\,t^4d_2+65880\,t^3c_2-63000\,t^4c_2+65160\,t^3d_2-69120\,x^2tc_1\,d_1+$$
$$207360\,t^2c_1\,xd_1-60480\,ixt{d_1}^2-51840\,xtc_1\,d_1-63360\,t^3d_1\,c_1+17280\,x^2c_1\,d_1+8640\,xc_1\,d_1+$$
$$12960\,tc_1\,c_2+247680\,t^3xd_2-30240\,t^2c_1\,d_1+8640\,ix^2{d_1}^2-8640\,ix^2{c_1}^2+23040\,x^3td_2-$$
$$36720\,xt^2c_2-4320\,xtd_2+21600\,x^2td_2-34560\,x^3tc_2+30240\,xtc_2+30240\,x^2tc_2-103680\,t^2x^2d_2+$$
$$77760\,t^2x^2c_2-77760\,t^3xc_2+12960\,td_1\,d_2+38880\,c_1\,td_1-41040\,t^2xd_2+760320\,ix^3t^3d_1-$$
$$21600\,ix^2tc_2-14400\,itx^4d_1-64800\,ixt^2d_1-36720\,ixt^2d_2+56160\,ixtc_1+77760\,it^2x^2d_2+$$
$$8640\,ixd_1\,c_2+4320\,ixtc_2-1440\,ix^4+1080\,ix^2+33750\,it^2+1152\,ix^6+2128626\,it^6+$$
$$327870\,it^4+1261875\,it^8+768\,ix^8-69120\,itc_1\,xd_1+4320\,i{d_1}^2x+4320\,ix^2c_2+8640\,id_1\,{c_1}^2+$$
$$228960\,it^4d_1+23760\,itc_1{}^2+62640\,id_1{}^2t+35640\,it^2c_2+5760\,ix^4d_2+216000\,it^4c_2+63360\,it^3c_1{}^2+$$
$$286200\,it^2d_1+4320\,ix^2d_1+226304\,ix^6t^3+1582920\,it^4x^3+32940\,ix^2t+315000\,it^3x^2+$$
$$2292864\,it^5x^4+112608\,ix^5t^2+3072\,ix^8t+4795200\,it^7x^2+1102890\,it^6x+19440\,ix^4t-$$

$$23040\,ix^3tc_2-315360\,ic_1\,t^2x^2-195840\,ix^4t^2d_1-168480\,it^3d_1\,c_1-207360\,it^2{c_1}^2x-8640\,ic_1\,xd_2-241920\,ix^2t^4c_1-9216\,ix^5c_1\,t-34560\,itx^3d_2-247680\,it^3xc_2-11520\,ic_1\,x^3d_1-64800\,itc_1\,d_1-1477440\,ix^2t^4d_1-84480\,ix^3t^3c_1-17280\,itd_1\,d_2-17280\,itc_1\,c_2-155520\,ix^2t^2d_1-12960\,ixd_1\,t-12960\,itd_1\,c_2-77760\,it^3xd_2-4320\,ixc_1{}^2-128250\,ixt^2-1392210\,it^4x-36864\,ix^7t^2-875520\,ix^5t^4-4108032\,it^6x^3-585840\,ix^4t^3-14016\,ix^6t-1901124\,it^5x^2-43920\,it^2x^3-3240000\,it^8x-3072\,ix^6d_1-4320\,ix^2c_1-4320\,ix^2d_2-63000\,it^4d_2-160920\,it^2c_1-2880\,ix^4c_1-774900\,ic_1\,t^4-87480\,it^2d_2-796464\,it^6d_1-123552\,it^6c_1+17280\,ic_1\,x^3t+12960\,ic_1\,td_2+448704\,it^5xc_1+69120\,ix^2{c_1}^2t+1080\,ic_2+8640\,id_1{}^3+69120\,ix^4t^2c_1+384\,ix^7+540\,ic_1+1080\,id_1+30240\,ixtd_2+51840\,ix^2d_1\,tc_1+60480\,it^2d_1\,xc_1+8640\,ixc_1\,d_1-4320\,x^2d_2+4320\,c_1\,c_2+4320\,d_1\,d_2-3960\,ix^3-270\,ix-3744\,ix^5-1094349\,it^7+8640\,c_1\,{d_1}^2+2160\,ixc_2+2880\,ixt^3d_1+687500\,it^9+457065\,it^3+1135251\,it^5+1485\,it+135\,i-8640\,xd_1\,d_2-8640\,xc_1\,c_2-17280\,td_1\,c_2+17280\,c_1\,td_2+1236960\,ic_1\,t^3x+103680\,it^2x^2c_2-4320\,id_1\,c_2-6480\,it^2x^2-563400\,ix^2t^4-1802304\,it^5x^3-832104\,it^5x-15360\,ix^7t-89280\,it^3x-2036400\,it^7x-1080\,ixt-398592\,ix^5t^3-5760\,ix^5t-18720\,ix^4t^2-336852\,it^5c_1-8100\,itc_1-65160\,it^3c_2-2880\,ix^3d_2-7560\,itd_2-16200\,itc_2-5760\,ix^5c_1-8640\,ic_1\,x^3-149400\,ic_1\,t^3-79920\,it^3d_1+8640\,{c_1}^3+1384128\,ixt^5d_1+34560\,itd_1\,x^3)/(9-612\,xt-192\,x^3c_1-22500\,t^5x-8928\,x^3t^3-576\,x^5t+2928\,x^4t^2+792\,t^3x+96\,tx^3-2232\,t^2x^2+18300\,x^2t^4-2808\,c_1\,t^3+864\,td_1-792\,tc_1+144\,xc_1-1056\,t^3d_1+108\,x^2+2835\,t^2-1152\,x^2td_1+864\,x^2tc_1+1008\,c_1\,xt^2+3456\,xt^2d_1+10179\,t^4+48\,x^4+64\,x^6+15625\,t^6+144\,{d_1}^2+144\,{c_1}^2),$$

$$w_1[2] = (-1/30-1/30\,i)$$

$$\sqrt{2}\mathrm{e}^{\left(-\frac{2}{97}+\frac{9}{194}\,i\right)(16\,x+36\,ix-97\,t)}(-540\,d_1+95436\,it^5d_1+8640\,ix^3c_2+66960\,it^2{c_1}^2+65880\,it^3d_2+3240\,ixd_1+348480\,ix^3t^3+1013280\,ix^4t^4+100608\,ix^6t^2+17280\,ix^3t+2251536\,it^6x^2+5760\,ix^3d_1+1620\,itd_1+1080\,ic_1\,x+2160\,ixd_2+3456\,ix^5d_1+4320\,ic_1\,d_2+36720\,it^2{d_1}^2-491040\,it^3x^2d_1-244800\,ic_1\,t^2x^3-92880\,ic_1\,t^2x-8640\,ixc_1{}^2t+27648\,ix^5d_1\,t+103680\,ic_1\,t^2d_1+41040\,it^2xc_2+540\,x-3510\,t+8640\,ix^2td_1+496440\,ixt^4d_1+38880\,itc_1\,x^2+124920\,it^4c_1\,x+54720\,itx^4c_1+30240\,ix^2td_2+146880\,it^2x^3d_1+280800\,ic_1\,t^3x^2-4860\,x^2t-14040\,xt+1890\,xt^2+9408\,x^6t+86016\,x^5t^3+12288\,x^7t-44544\,x^6t^2-71136\,x^5t^2-36720\,t^2{d_1}^2+66960\,t^2{c_1}^2-8640\,x^2{c_1}^2-350280\,t^4x^3+436068\,t^5x^2+124800\,t^7x-60672\,t^5x^3+140448\,t^6x^2+1313928\,t^5x-1694730\,t^6x-83520\,x^3t^3+10368\,x^5t+36000\,x^4t^2-48960\,t^4x^4+35280\,x^4t+437760\,t^3x+17280\,tx^3-218160\,t^2x^2-2115270\,t^4x-126000\,t^2x^3+628200\,t^3x^2+2880\,d_1\,x^4-8640\,d1^2t-8640\,x^2{d_1}^2-532440\,x^2t^4-234720\,t^4c_1-111852\,t^5d_1+129564\,t^5c_1+8064\,x^5c_1-$$

$$432000\,c_1\,t^3 - 73440\,t{c_1}^2 + 8640\,x{c_1}^2 - 29160\,t^2 d_1 + 244080\,t^2 c_1 + 8640\,x^2 c_1 + 16740\,t d_1 -$$
$$15660\,t c_1 + 3240\,x c_1 - 29160\,t^3 d_1 + 985140\,t^4 d_1 + 276720\,x^4 t^3 + 4320\,x^2 d_1 - 145152\,x^6 t^3 +$$
$$277440\,x^5 t^4 - 6912\,x^8 t + 41472\,x^7 t^2 + 168480\,t^3 {d_1}^2 - 121248\,t^5 x^4 - 878176\,t^6 x^3 + 11520\,x^3 {d_1}^2 +$$
$$2523600\,t^7 x^2 - 3288750\,t^8 x - 123552\,t^6 d_1 - 1078536\,t^6 c_1 - 4608\,x^6 c_1 - 1080\,x d_1 - 8640\,x^3 d_2 -$$
$$2160\,x d_2 + 1080\,c_1 - 1080\,d_2 + 1080\,x^2 + 53190\,t^2 + 2520\,x^3 - 170325\,t^3 - 84480\,t^3 x^3 d_1 -$$
$$718560\,t^4 x^2 c_1 + 311040\,t^3 x^3 c_1 + 448704\,t^5 x d1 + 1315872\,t^5 x c_1 - 9216\,x^5 t d_1 - 241920\,t^4 x^2 d_1 +$$
$$69120\,x^4 t^2 d_1 + 41472\,x^5 t c_1 - 155520\,x^4 t^2 c_1 - 51840\,t {d_1}^2 x^2 - 60480\,t^2 {d_1}^2 x + 5760\,x^3 t d_1 -$$
$$25920\,x c_1\,t - 21600\,x d_1\,t - 108000\,x^2 t d_1 + 69120\,x^2 t c_1 - 262440\,t^4 x c_1 - 8640\,x^4 t d_1 -$$
$$48960\,x^4 t c_1 + 538560\,c_1\,t^3 x + 11520\,c_1\,t x^3 - 190080\,c_1\,t^2 x^2 - 8640\,t c1^2 x + 60480\,x d1^2 t -$$
$$943200\,x t^3 d_1 + 438480\,x t^2 d_1 + 73440\,x^2 t^2 d_1 + 358920\,t^4 x d_1 + 182880\,t^3 x^2 c_1 - 31680\,t^2 x^3 d_1 +$$
$$66240\,t^2 x^3 c_1 - 27360\,t^3 x^2 d_1 + 644130\,t^4 + 1440\,x^4 + 1790073\,t^5 - 4320\,x^5 - 2688\,x^6 + 26250\,t^8 -$$
$$8682\,t^6 + 2125893\,t^7 - 1536\,x^8 - 384\,x^7 + 2160\,{d_1}^2 + 2160\,{c_1}^2 + 1828125\,t^9 + 512\,x^9 -$$
$$35640\,t^2 d_2 - 4320\,x^2 c_2 - 2880\,x^3 c_2 + 8640\,x^3 d_1 + 5760\,x^5 d_1 + 16200\,t d_2 - 7560\,t c_2 + 2160\,x c_2 +$$
$$5760\,x^4 c_2 - 87480\,t^2 c_2 - 216000\,t^4 d_2 + 65880\,t^3 c_2 - 63000\,t^4 c_2 + 65160\,t^3 d_2 - 69120\,x^2 t c_1\,d_1 +$$
$$207360\,t^2 c_1\,x d_1 - 60480\,ixt{d_1}^2 - 51840\,xt c_1\,d_1 - 63360\,t^3 d_1\,c_1 + 17280\,x^2 c_1\,d_1 + 8640\,x c_1\,d_1 +$$
$$12960\,t c_1\,c_2 + 247680\,t^3 x d_2 - 30240\,t^2 c_1\,d_1 + 8640\,ix^2 {d_1}^2 - 8640\,ix^2 {c_1}^2 + 23040\,x^3 t d_2 -$$
$$36720\,x t^2 c_2 - 4320\,x t d_2 + 21600\,x^2 t d_2 - 34560\,x^3 t c_2 + 30240\,x t c_2 + 30240\,x^2 t c_2 - 103680\,t^2 x^2 d_2 +$$
$$77760\,t^2 x^2 c_2 - 77760\,t^3 x c_2 + 12960\,t d_1\,d_2 + 38880\,c_1\,t d_1 - 41040\,t^2 x d_2 + 760320\,ix^3 t^3 d_1 -$$
$$21600\,ix^2 t c_2 - 14400\,itx^4 d_1 - 64800\,ixt^2 d_1 - 36720\,ixt^2 d_2 + 56160\,ixt c_1 + 77760\,it^2 x^2 d_2 +$$
$$8640\,ix d_1\,c_2 + 4320\,ixt c_2 - 1440\,ix^4 + 1080\,ix^2 + 33750\,it^2 + 1152\,ix^6 + 2128626\,it^6 +$$
$$327870\,it^4 + 1261875\,it^8 + 768\,ix^8 - 69120\,it c_1\,x d_1 + 4320\,i{d_1}^2 x + 4320\,ix^2 c_2 + 8640\,i d_1\,{c_1}^2 +$$
$$228960\,it^4 d_1 + 23760\,it{c_1}^2 + 62640\,i{d_1}^2 t + 35640\,it^2 c_2 + 5760\,ix^4 d_2 + 216000\,it^4 c_2 + 63360\,it^3 {c_1}^2 +$$
$$286200\,it^2 d_1 + 4320\,ix^2 d_1 + 226304\,ix^6 t^3 + 1582920\,it^4 x^3 + 32940\,ix^2 t + 315000\,it^3 x^2 +$$
$$2292864\,it^5 x^4 + 112608\,ix^5 t^2 + 3072\,ix^8 t + 4795200\,it^7 x^2 + 1102890\,it^6 x + 19440\,ix^4 t -$$
$$23040\,ix^3 t c_2 - 315360\,ic_1\,t^2 x^2 - 195840\,ix^4 t^2 d_1 - 168480\,it^3 d_1\,c_1 - 207360\,it^2 {c_1}^2 x - 8640\,ic_1\,x d_2 -$$
$$241920\,ix^2 t^4 c_1 - 9216\,ix^5 c_1\,t - 34560\,itx^3 d_2 - 247680\,it^3 x c_2 - 11520\,ic_1\,x^3 d_1 - 64800\,it c_1\,d_1 -$$
$$1477440\,ix^2 t^4 d_1 - 84480\,ix^3 t^3 c_1 - 17280\,it d_1\,d_2 - 17280\,it c_1\,c_2 - 155520\,ix^2 t^2 d_1 - 12960\,ix d_1\,t -$$
$$12960\,it d_1\,c_2 - 77760\,it^3 x d_2 - 4320\,ix{c_1}^2 - 128250\,ixt^2 - 1392210\,it^4 x - 36864\,ix^7 t^2 -$$
$$875520\,ix^5 t^4 - 4108032\,it^6 x^3 - 585840\,ix^4 t^3 - 14016\,ix^6 t - 1901124\,it^5 x^2 - 43920\,it^2 x^3 -$$
$$3240000\,it^8 x - 3072\,ix^6 d_1 - 4320\,ix^2 c_1 - 4320\,ix^2 d_2 - 63000\,it^4 d_2 - 160920\,it^2 c_1 - 2880\,ix^4 c_1 -$$
$$774900\,ic_1\,t^4 - 87480\,it^2 d_2 - 796464\,it^6 d_1 - 123552\,it^6 c_1 + 17280\,ic_1\,x^3 t + 12960\,ic_1\,t d_2 +$$

$$448704\,it^5xc_1 + 69120\,ix^2{c_1}^2t + 1080\,ic_2 + 8640\,i{d_1}^3 + 69120\,ix^4t^2c_1 + 384\,ix^7 + 540\,ic_1 + 1080\,id_1 + 30240\,ixtd_2 + 51840\,ix^2d_1\,tc_1 + 60480\,it^2d_1\,xc_1 + 8640\,ixc_1\,d_1 - 4320\,x^2d_2 + 4320\,c_1\,c_2 + 4320\,d_1\,d_2 - 3960\,ix^3 - 270\,ix - 3744\,ix^5 - 1094349\,it^7 + 8640\,c_1\,{d_1}^2 + 2160\,ixc_2 + 2880\,ixt^3d_1 + 687500\,it^9 + 457065\,it^3 + 1135251\,it^5 + 1485\,it + 135\,i - 8640\,xd_1\,d_2 - 8640\,xc_1\,c_2 - 17280\,td_1\,c_2 + 17280\,c_1\,td_2 + 1236960\,ic_1\,t^3x + 103680\,it^2x^2c_2 - 4320\,id_1\,c_2 - 6480\,it^2x^2 - 563400\,ix^2t^4 - 1802304\,it^5x^3 - 832104\,it^5x - 15360\,ix^7t - 89280\,it^3x - 2036400\,it^7x - 1080\,ixt - 398592\,ix^5t^3 - 5760\,ix^5t - 18720\,ix^4t^2 - 336852\,it^5c_1 - 8100\,itc_1 - 65160\,it^3c_2 - 2880\,ix^3d_2 - 7560\,itd_2 - 16200\,itc_2 - 5760\,ix^5c_1 - 8640\,ic_1\,x^3 - 149400\,ic_1\,t^3 - 79920\,it^3d_1 + 8640\,{c_1}^3 + 1384128\,ixt^5d_1 + 34560\,itd_1\,x^3)/(9 - 612\,xt - 192\,x^3c_1 - 22500\,t^5x - 8928\,x^3t^3 - 576\,x^5t + 2928\,x^4t^2 + 792\,t^3x + 96\,tx^3 - 2232\,t^2x^2 + 18300\,x^2t^4 - 2808\,c_1\,t^3 + 864\,td_1 - 792\,tc_1 + 144\,xc_1 - 1056\,t^3d_1 + 108\,x^2 + 2835\,t^2 - 1152\,x^2td_1 + 864\,x^2tc_1 + 1008\,c_1\,xt^2 + 3456\,xt^2d_1 + 10179\,t^4 + 48\,x^4 + 64\,x^6 + 15625\,t^6 + 144\,{d_1}^2 + 144\,{c_1}^2).$$

Bibliography

[1] M. Ablowitz, M. J. Ramani, A. Segur, J. Math. Phys. 21 715 (1998).

[2] A. Ramani, Dorizzi, Grammaticos, Phys. Rev. Lett. 31 1539 (1982).

[3] M. Lackshmanan, M. Sahadevau, Phys. Rev. A 31 861 (1985).

[4] J. Weiss, M. Tabor, G. Carnavale, J. Math. Phys. 17 825 (1983).

[5] J. Weiss, J. Math. Phys. 25 13 (1983).

[6] J. Weiss, J. Math. Phys. 25 2226 (1984).

[7] W. H. Steeb, M. Kloke, B. M. Spiker, J. Phys. A 17 825 (1984).

[8] J. He, L. Wang, L. Li, K. Porsezian and R. Erdelyi, Phys. Rev. E 89 062917 (2014)

[9] Js. He, H. Zhang, L. Wang, K. Porsezian and A. Fokas, Phys. Rev. E 87 052914 (2013)

[10] X. Lü and B. Tian, 2012 Phys. Rev. E 85 026117

[11] V. O. Vakhnenko and E. J. Parkes, Nonlinearity 11 (1998) 1457

[12] V. K. Kuetche, T. B. Bouetou and T. C. Kofane, Phys. Lett. A 372 4891 (2008)

[13] A. Sakovich, S. Sakovich, J. Phys. Soc. Jpn. 74 239 (2005).

[14] V. K. Kuetche, T. B. Bouetou, T. C. Kofane, A. Moubissi and K. Porsezian 2010 Phys. Rev. A 82 053619

[15] V. K. Kuetche, T. B. Bouetou and T. C. Kofane J. Phys. Soc. Jpn. 76 024004 (2007)

[16] S. Youssoufa, V. K. Kuetche and T. C. Kofane Chin. Phys. Lett 29 020202 (2012)

[17] S. Abbagari, T. B. Bouetou, V. K. Kuetche, F. Mouna, T. C. Kofane, Chn. Phys. Lett. 28 2 (2011).

[18] W. Deng-Shan, Z. Da-Jun and J. Yang J. Math. Phys. 51 023510 (2010)

[19] M. Onorato, S. Residori, U. Bortolozzo, A. Montina and F. T. Arecchi Phys. Rep. 528 47 (2013)

[20] A. Chabchoub, N. P. Hoffmann and N. Akhmediev Phys. Rev. Lett. 106 204502 (2011)

[21] A. Chabchoub, N. Hoffmann, M. Onorato and N. Akhmediev Phys. Rev. X 2 011015 (2012)

[22] A. Chabchoub, N. Hoffmann, M. Onorato, A. Slunyaev, A. Sergeeva, E. Pelinovsky and N. Akhmediev Phys. Rev. E 86 056601 (2012)

[23] M. Erkintalo, G. genty and J. M. Dudley Opt. Lett. 34 2468 (2009)

[24] A. Coillet, J. Dudley, .G Genty, L. Larger and Y. K. Chembo Phys. Rev. A 89 013835 (2014)

[25] M. Erkintalo, G. genty and J. M. Dudley Opt. Lett. 34, 2468 (2009)

[26] C. Liu, Z. Y. Yang, L. C. zhao, G. G. Xin and W. L. Yang Opt. Lett. 39 1057 (2014)

[27] D. W. Zuo, Y. T. Gao, L. Xue and Y. J. Feng Chaos, Solitons Fract. 69 217 (2014)

[28] N. Akhmediev, A. Ankiewicz, and M. Taki Phys. Lett. A 373 675 (2009)

[29] D. R. Solli, C. Ropers, P. Koonath and B. Jalali Nature 450 1054 (2007)

[30] C. Kharif, E. Pelinovsky and A. Slunyaev, Rogue Waves in the Ocean New York: Springer (2009)

[31] A. Osborne, Nonlinear Ocean Waves and the Inverse Scattering Transform New york: Elsevier (2010)

[32] M. Onorato, S. Residori, U. Bortolozzo, A. Montina and F. T. Arecchi, Phys. Rep. 528 (2013) 47

[33] B. Kibler, J. Fatome, C. Finot, G. Millot, G. Genty, B. Wetzel, N. Akhmediev, F. Dias and J. M. Dudley Sci. Rep. 2 463 (2012)

[34] S. Guoa, L. Meia and A. Sun Ann. Phys. (Amsterdam) 38 332 (2012)

[35] A. Chabchoub, N. Hoffmann, M. Onorato and N. Akhmediev Phys. Rev. X 2 011015 (2012)

[36] T. B. Benjamin and J. E. Feir J. Fluid Mech. 27 417 (1967)

[37] D. J. Benney and A. C. Newell J. Math. Phys. 46 133 (1967)

[38] V. E. Zkharov J. Appl. Mech. Tech. Phys. 9 190 (1968)

[39] E. A. Kuznetov Sov. Phys. Dokl 22 507 (1977)

[40] P. C. Liu Freaque waves. http://freaquewaves.blogspot.com/2006 07 01 archive.html. (2007)

[41] J. K. Mallory Abnormal waves on the south-east of South Africa. Inst Hydrog Rev 51:89-129 (1974)

[42] A. Torum and O. T. Gudmestad, Water Wave Kinematics. Kluwer, Dordrecht (1990)

[43] S. Haver and O. J. Andersen, Freak waves-rare realizations of a typical extreme wave population (2000) or typical realizations of a rare extreme wave population? In: Proc. 10th Int Offshore and Polar Eng Conf ISOPE, Seattle, USA, 2000, pp 123-130

[44] G. Lawton Monsters of the deep (The Perfect Wave). New Scientist 170 No 2297:28-32 (2001)

[45] O. lagnon and G. A. Athanassoulis, Rogue Waves. Ifremer, France (2001)

[46] C. Kharif and E. Pelinovsky, Physical mechanisms of the rogue wave phenomenon. Eur J Mech/B - Fluid 22:603-634 (2003)

[47] Time, Biggest tanker. Monday, 22 February, 1954. http://www.time.com/time/ print- out/0,8816,860511,00.html. (1954)

[48] Lavrenov IV, Wind waves in ocean: dynamics and numerical simulations. Springer-Verlag, Heidelberg (2003)

[49] ABS (American Bureau of Shipping),Technical analyses related to the Prestige casualty on 13 November 2002. http://www.eagle.org/news/press/prestige/ Tech Analysis final.pdf. (2003)

[50] A. Toffoli , J. M. Lefevre, Bitner-Gregersen E and Monbaliu J, Towards the identification of warn- ing criteria: Analysis of a ship accident database. Appl Ocean Res 27:281Ű291 (2005)

[51] F. Moreau, translated by Olagnon M, Chase G A,The Glorious Three. In: Olagnon M, Pre- vosto M (eds) Rogue Waves 2004. Ifremer, France. http://www.ifremer.fr/web-com/stw2004/ rw/fullpapers/glorious.pdf. (2005)

[52] S. H. Lehner, Extreme wave statistics from radar data sets. In: Proc. 14th Aha Huliko'a Winter Workshop, Honolulu, Hawaii (2005)

[53] M. Sokolovsky, http://www.kkclub.ru

[54] D. H. Peregrine, H. Bredmose, G. Bullock et al, Violent water wave impact on a wall. In: Proc. 14th Aha Huliko'a Winter Workshop, Honolulu, Hawaii, (2005)

[55] A. R. Palmer, A Rogue Wave. http://www.biology.ualberta.ca/courses.hp/biol361/ WavePics/WavePics.htm. (2002)

[56] D. Faulkner, Rogue waves - defining their characteristics for marine design. In: Olagnon M, Athanassoulis GA (eds) Rogue Waves. Ifremer, France, pp 3-18 (2001)

[57] W. J. Broad, Rogue giants at sea. The New York Times (July 11, 2006).

[58] M. Hopkin, Sea snapshots will map frequency of freak waves. Nature 430, 492 (2004)

[59] C. Kharif and E. Pelinovsky, Physical mechanisms of the rogue wave phenomenon. Eur. J. Mech. B Fluids 22, 603-634 (2003)

[60] R. G. Dean in Water Wave Kinematics (eds Tørum, A. and Gudmestad, O. T.) 609-612 (Kluwer, Amsterdam, 1990)

[61] P. Muller, C. Garrett and A. Osborne, Rogue waves. Oceanography 18, 66-75 (2005)

[62] D. A. G. Walker, P. H. Taylor and R. E. Taylor, The shape of large surface waves on the open sea and the Draupner New Year wave. Appl. Ocean. Res. 26, 73-83 (2004)

[63] K. Dysthe, H. Socquet-Juglard, K. Trulsen, H. E. Krogstad and J. Liu, "Freak" waves and large-scale simulations of surface gravity waves. Rogue Waves, Proc. 14th' Aha Huliko' a Hawaiian Winter Workshop 91-99, Univ. Hawaii, Honolulu, (2005)

[64] P. C. Liu and K. R. MacHutchon, Are there different kinds of rogue waves? Proc. OMAE2006, 25th Int. Conf. Offshore Mechanics and Arctic Engineering, Paper No. 92619, 1-6, American Society of Mechanical Engineers, New York, (2006).

[65] K. L. Henderson, K. L. Peregrine and J. W. Dold, Unsteady water wave modulations: fully nonlinear solutions and comparison with the nonlinear Schroĺdinger equation. Wave Motion 29, 341-361 (1999)

[66] M. Onorato, A. R. Osborne, M. Serio and S. Bertone, Freak waves in random oceanic sea states. Phys. Rev. Lett. 86, 5831-5834 (2001).

[67] M. Onorato, A. R. Osborne and M. Serio, Modulational instability in crossing sea states: A possible mechanism for the formation of freak waves. Phys. Rev. Lett. 96, 014503 (2006)

[68] P. K. Shukla, I. Kourakis, B. Eliasson, M. Marklund and L. Stenflo, Instability and evolution of nonlinearly interacting water waves. Phys. Rev. Lett. 97, 094501 (2006)

[69] P. A. E. M. Janssen, Nonlinear four-wave interactions and freak waves. J. Phys. Oceanogr. 33, 863-884 (2003)

[70] White, B. S. and Fornberg, B. On the chance of freak waves at sea. J. Fluid Mech. 355, 113-138 (1998)

[71] J. M. Dudley, G. Genty and S. Coen, Supercontinuum generation in photonic crystal fiber. Rev. Mod. Phys. 78, 1135-1184 (2006)

[72] J. K. Ranka, R. S. Windeler A. J. and Stentz, Visible continuum generation in air-silica microstructure optical fibers with anomalous dispersion at 800 nm. Opt. Lett. 25, 25-27 (2000).

[73] Herrmann, J. et al. Experimental evidence for supercontinuum generation by fission of higher-order solitons in photonic fibers. Phys. Rev. Lett. 88, 173901 (2002)

[74] G. P. Agrawal, Nonlinear Fiber Optics 3rd edn, Academic, San Diego (2001).

[75] H. Segur et al. Stabilizing the Benjamin-Feir instability. J. Fluid Mech. 539, 229-271 (2005)

[76] K. L. Corwin et al. Fundamental noise limitations to supercontinuum generation in microstructure fiber. Phys. Rev. Lett. 90, 113904 (2003)

[77] A. L. Gaeta, Nonlinear propagation and continuum generation in microstructured optical fibers. Opt. Lett. 27, 924-926 (2002)

[78] M. N. Islam et al., Femtosecond distributed soliton spectrum in fibers. J. Opt. Soc. Am. B 6, 1149-1158 (1989)

[79] J. N. Kutz, C.Lynga and B. J. Eggleton, Enhanced supercontinuum generation through dispersion-management. Opt. Express 13, 3989-3998 (2005)

[80] Y. Han, O. Boyraz and B. Jalali,Tera-sample per second real-time waveform digitizer. Appl. Phys. Lett. 87, 241116 (2005)

[81] X. Gu et al., Frequency-resolved optical gating and single-shot spectral measurements reveal fine structure in microstructure-fiber continuum. Opt. Lett. 27, 1174-1176 (2002)

[82] M. Nakazawa, H. Kubota and K. Tamura, Random evolution and coherence degradation of a high-order optical soliton train in the presence of noise. Opt. Lett. 24, 318-320 (1999)

[83] O. Boyraz, J. Kim, M. N. Islam, F. Coppinger and B. Jalali, 10 Gb/s multiple wavelength, coherent short pulse source based on spectral carving of supercontinuum generated in fibers. J. Lightwave Technol. 18, 2167-2175 (2000)

[84] K. Trulsen and K. B. Dysthe, A modified nonlinear Schrödinger equation for broader bandwidth gravity waves on deep water. Wave Motion 24, 281-289 (1996)

[85] Yu. V. Bludov, V. V. Konotop, and N. Akhmediev Phy. Rev. A 80, 033610 (2009)

[86] P. O. Fedichev, M. W. Reynolds, and G. V. Shlyapnikov, Phys. Rev. Lett. 77, 2921 (1996) .

[87] H. Bailung, S. K. Sharma and Y. Nakamura Phys. Rev. Lett. 107, 255005 (2011)

[88] M. Saito, S. Watanabe, and H. Tanaka, J. Phys. Soc. Jpn. 53 , 2304 (1984)

[89] H. Bailung and Y. Nakamura, J. Plasma Phys. 50 , 231 (1993)

[90] M. J. Lighthill, IMA J. Appl. Math. 1 , 269 (1965)

[91] V. E. Zakharov and A. B. Shabat, Sov. Phys. JETP 34 62 (1972)

[92] V. B. Matveev and M. A. Salle, Darbux transformation and solitons (Springer, Berlin, 1991)

[93] G. Darboux, Sur une proposition relative aux équations linéaires, Compts Rendus Hebdomadaires des Seances de l'Academie des Sciences, Paris 94, 1456 (1882).

[94] B. Guo , L. Ling , Q. P. Liu Phys. Rev. E 85 026607 (2012)

[95] Zhaqilao Phys. Scr. 87 065401 (2013)

[96] T. R. Marchant, Chaos Solitons Fractals 32 1328 (2007)

[97] Q. HanPark and H. J. Shin Phys. Rev. E 59 2373 (1999)

[98] H. Q. Zhang, J. Li, T. Xu, Y. X. Zhang, W. Hu and B. Tian Phys. Scr. 76 452 (2007)

[99] N. V. Priya and M. Senthilvelan Comm. Nonlinear Sci. Nummer. Simult. 20 401 (2015)

[100] N. Vishnu Priya and M. Senthilvelan wave motion 54 125-133 (2015)

[101] N. Vishnu Priya, M. Senthilvelan and M. Lakshmanan, Phys. Rev. E 89 062901 (2014)

[102] S. V. Manakov and Zh. Eksp Teor. Fiz. 65 1392 (1973)

[103] F. Baronio, A. Degasperis, M. Conforti and S. Wabnitz Phys. Rev. Lett. 109 044102 (2012)

[104] S. P. T. Mukam, V. K. Kuetche and T. B. Bouetou Eur. Phys. J. Plus 132 182 (2017)

[105] C. R. Menyuk IEEE J. Quantum Electron. 25 2674 (1989)

[106] M. Onorato, D. Proment and A. Toffoli Eur. Phys. J. Spec. Top. 185 45 (2010)

[107] S. Chen and D. Mihalache J. Phys. A: Math. Theor. 48 215202 (2015)

[108] TL Glbert, Phys Rev 100, 1243 (1955)

[109] R. A. Kraenkel , M. A. Manna and V. Merle, Phys Rev E 61, 976 (2000)

[110] V. K. Kuetche, F. T. Nguepjouo and T. C. Kofane, Chaos Solitons Fractals 66, 17 (2014)

[111] V. K. Kuetche, F. T. Nguepjouo and T. C. Kofane, J. Mag. Mag. Mat. 374, 1 (2015)

[112] H. T. Tchokouansi, V. K. Kuetche and T. C. Kofane, Chaos Solitons Fractals 86, 64 (2016)

[113] Geng, X., Hon-Wah, Tam.: Darboux transformation and soliton solutions for generalized nonlinear Schrödinger equations. J. Phys. Soc. Jpn. **68**, 1508 (1999)

[114] Kundu, A.: Landau-Lifshitz and higher-order nonlinear systems gauge generated from nonlinear Schrödinger-type equations. J. Math. Phys. **25**, 3433 (1984)

[115] Zhu, Y., Qin, W., Han, J.Z., Dai, C. Q., Wang, Y. Y.: Recurrence behavior for the controllable excitaion of rogue waves in two-dimensional PT-symmetry coupler. Nonlinear Dyn. 88, 1883-1889 (2017)

[116] H. P. Zhu, Nonlinear tunneling for controlable rogue waves in two dimensional graded-index waveguides. Nonlinear Dyn. 873-882 (2013)

[117] M. Lakshmanan, K. Porsezian, and M. Daniel, Phys. Lett. A 133 483 (1988)

[118] K. Porsezian, M. Daniel, and M. Lakshmanan , J. Math. Phys. 33 1807 (1992)

[119] K. Porsezian, Phys. Rev. E 55 3785 (1997)

[120] Z.D. Dai, J. Liu, D.L. Li, Applications of HTA and EHTA to YTSF Equation, Appl. Math. Comput. 207 360-364 (2009)

[121] R. Hirota, in: S. Takeno (Ed.), Fundamental Properties of the Binary Operators in Soliton Theory and Their Generalization, in: Dynamical Problem in Soliton Systems, Springer Series in Synergetiecs, 30, Springer, Berlin, (1985)

[122] V. A. Vakhnenko, J. Phys. A: Math. Gen. 25 4181 (1992)

[123] V. O. Vakhnenko, Ukr. J. Phys. 42 104 (1997)

[124] Serge P. Mukam, Victor K. Kuetche and Thomas B. Bouetou Arviv 1605.06132v1 (2016)

[125] Bruce Parker 2012. The Power of the Sea: Tsunamis, Storm Surges, Rogue Waves, and Our Quest to Predict Disasters. St. Martin's Press. ISBN 978-0-230-11224-7.

[126] Ian Jones; Joyce Jones (2008). Oceanography in the Days of Sail (PDF). Hale and Iremonger. p. 115. ISBN 978-0-9807445-1-4

[127] http://www.salon.com/2010/09/26/the wave susan casey interview

[128] Carlos Guedes Soares; T.A. Santos (3 October 2014). Maritime Technology and Engineering. CRC Press. ISBN 978-1-315-73159-9.

[129] "US Army Engineer Waterways Experimental Station: Coastal Engineering Technical Note CETN I-60". Chl.erdc.usace.army.mil. March 1995. Retrieved April 16, 2016.

[130] Draper, Lawrence (July 1964). ""Freak" Ocean Waves" (PDF). Oceanus. 10 (4): 12-15.

[131] Hugo Montgomery-Swan (2010). "Heavy Weather Powerboating". Adlard Coles Nautical: 33. ISBN 9780713688719.

[132] Michel Olagnon, Marc Prevosto (20 October 2004). "Rogue Waves 2004: Proceedings of a Workshop Organized by Ifremer and Held in Brest, France, 20-21-22 October 2004, Within the Brest Sea Tech Week 2004"

[133] "Rogue Waves". Ocean Prediction Center. National Weather Service. April 22, 2005. Retrieved May 8, 2006.

[134] Thomas A A Adcock and Paul H Taylor (14 October 2014). "The physics of anomalous ('rogue') ocean waves". Iopscience.iop.org. Retrieved April 17, 2016.

[135] "Freak Wave - programme summary". www.bbc.co.uk/. BBC. 14 November 2002. Retrieved 15 January 2016.

[136] Adrian Cho (13 May 2011). "Ship in Bottle, Meet Rogue Wave in Tub". Science Now. 332: 774. doi:10.1126/science.332.6031.774-b. Retrieved 2011-06-27.

[137] "Math explains water disasters Ű ScienceAlert". Sciencealert.com. 26 August 2010. Retrieved April 15, 2016.

[138] Phillips, Journal of Fluid Mechanics (1957)

[139] Miles, Journal of Fluid Mechanics (1957)

[140] Kibler, B.; Fatome, J.; Finot, C.; Millot, G.; Dias, F.; Genty, G.; Akhmediev, N.; Dudley, J.M. (2010). "The Peregrine soliton in nonlinear fibre optics". Nature Physics. 6 (10).

[141] "Peregrine's 'Soliton' observed at last". bris.ac.uk. Retrieved 2010-08-24.

[142] Keith McCloskey (15 July 2014). The Lighthouse: The Mystery of the Eilean Mor Lighthouse Keepers. History Press Limited. ISBN 978-0-7509-5741-0.

[143] Faulkner, Douglas (1998). An Independent Assessment of the Sinking of the M.V. Derbyshire. SNAME Transactions, Royal Institution of Naval Architects. pp. 59-103.

[144] Faulkner, Douglas (2000). Rogue Waves Ű Defining Their Characteristics for Marine Design

[145] Brown, David (1998). "The Loss of the 'DERBYSHIRE'" (Technical Report). Crown.

[146] "Inside the Lethal World of Bulk Carriers: Death Trips on the Seven Seas" (PDF). Coldtype.net. Retrieved April 17, 2016.

[147] V. I. Bespalov and V. I. Talanov, Zh. Eksp. Teor. Fiz. PisŠma Red. 3, 471 (1966).

[148] E. Fermi, J. Pasta, and S. Ulam, Los Alamos Report No. LA-1940, 1955 (unpublished) ; E. Fermi, Collected Papers, edited by E. Segré (University Chicago Press, Chicago, 1965) , Vol II, p. 978..

[149] N. Akhmediev, Nature (London) 413, 267 (2001).

[150] K. B. Dysthe and K. Trulsen, Phys. Scr. T82, 48 (1999).

[151] N. Akhmediev and V. I. Korneev, Teor. Mat. Fiz. 69, 189 (1986).

[152] N. Akhmediev, V. M. Eleonskii, and N. E. Kulagin, Teor. Mat.Fiz. 72, 183.

[153] N. Akhmediev, A. Ankiewicz, and J. M. Soto-Crespo, Phys.Rev. E 80, 026601 (2009).

[154] N. Akhmediev, A. Ankiewicz, and J. M. Soto-Crespo, Phys.Rev. A 80, 043818 (2009.

[155] N. Akhmediev and A. Ankiewicz, Solitons, Nonlinear Pulses, and Beams (Chapman and Hall, London, 1997).

[156] Ya.-C. Ma, Stud. Appl. Math. 60, 43 (1979).

[157] N. Akhmediev, J. M. Soto-Crespo, and A. Ankiewicz, Phys. Lett. A 373, 2137 (2009).

[158] D. M. Stamper-Kurn, and W. Ketterle, Phys. Rev. Lett. 82, 2422 (1999).

[159] V. V. Konotop and M. Salerno, Phys. Rev. A 65, 021602 (2002).

[160] Yu.V.Bludov, V. V. Konotop and N. Akhmediev, Eur. Phys. J. Special Topics 185 ,169-180(2010)

[161] M. R. Matthews, et al., Phys.Rev.Lett. 83, 3358(1999)

[162] L. Pitaevskii, S. Stringari, Bose-Einstein Condensation (OxfordUniversity-Press,2003)

[163] N. Akhmediev, A. Ankiewicz, M. Taki, Phys. Lett. A 373 675 (2009).

[164] N. Akhmediev, V. I. Korneev, N. V. Mitskevich, Zh. Teor. Eksp. Fiz. 94 (1988) 159, JETP 67 89 (1988).

[165] M. J. Ablowitz, D. J. Kaup, A. C. Newell and H. Segur, Nonlinear evolution equations of physical significance, Phys. Rev. Lett. 31, 125 (1973).

[166] V. B. Matveev, Theor. Math. Phys. 131, 483 (2002).

[167] L.L. Song, W. Chen, Z.H. Xu and H.L. Chen Advances in Pure Mathematics 5, 82-87 (2015) Chuanjian Wang, Zhengde Dai and Changfu Liu, Phys. Scr. 89 075206 (2014)

[168] V.O. Vakhnenko, J. Phys. A: Math. Gen. 25 4181 (1992).

[169] V.O. Vakhnenko, J. Math. Phys. 40 2011 (1999).

[170] S. Ishizaka and K Nakamura, J. Magn. Magn. Mater. 210, 15 (2000)

[171] M. C. Ciornei, J M Rubi and J E Wegrowe, Phys. Rev. B. 83, 020410 (2011)

[172] M. Fähnle, D. Steiauf and C. Illg, Phys.Rev.B 84, 172403 (2011)

[173] Y. B. Bazaliy, B. A. Jones and S. C. Zhang, Phys. Rev. B 57, 3213 (1998)

[174] R. F. Soohoo , Theory and Applications of Ferrites (Prentice-Hall, London) (1960)

List of publications

Papers

- S P T Mukam, V K Kuetche and T B Bouetou. Localized waves in a general coupled nonlinear Schrödinger equation. *Eur. Phys. J. Plus* **132**, 182 (2017)
- S P T Mukam, A Souleymanou, V K Kuetche and T B Bouetou. Generalized Darboux transformation and parameter-dependent rogue wave solutions to a nonlinear Schrödinger system. *Nonlinear Dyn.* **93**, 373 (2018)
- S P T Mukam, A Souleymanou, V K Kuetche and T B Bouetou. Rogue waves dynamics in barotropic relaxing media. *Pramana Journal of Physics.* **Accepted**